UCSF

UC San Francisco Electronic Theses and Dissertations

Title

Chemical approaches to study protein and lipid phosphorylation

Permalink

https://escholarship.org/uc/item/5110x54k

Author

Knight, Zachary A

Publication Date

2005

Peer reviewed|Thesis/dissertation

eScholarship.org Powered by the California Digital Library
University of California

Chemical approaches to study protein and lipid phosphorylation

by

Zachary A. Knight

DISSERTATION

Submitted in partial satisfaction of the requirements for the degree of

DOCTOR OF PHILOSOPHY

in

Chemistry and Chemical Biology

in the

GRADUATE DIVISION

of the

UNIVERSITY OF CALIFORNIA, SAN FRANCISCO

[redacted]

Copyright 2006

by

Zachary A. Knight

Acknowledgements

I would like to thank Kevan for his insight, encouragement, and enthusiasm.

Part of this thesis is a reproduction of material previously published, and contains contributions from collaborators listed therein. Chapter 1 is reproduced in part with permission from: Knight, Z.A. and Shokat K.M., Features of selective kinase inhibitors, *Chemistry and Biology*. 2005, June; 12:621-637. Chapter 2 is reproduced in part with permission from: Knight, Z.A., Schilling, B., Row, R.H., Gibson, B.W., Kenski, D.M., and Shokat, K.M., Phosphospecific proteolysis for mapping sites of protein phosphorylation, *Nature Biotechnology*. 2003, September;21(9):1047-54. Chapter 3 is reproduced in part with permission from: Knight, Z.A., Chang, G.C., Alaimo, P.J., Kenski, D.M., Ho, C.B., Abraham, R.T., and Shokat, K.M. Isoform-specific phosphoinositide 3-kinase inhibitors from an arylmorpholine scaffold, *Bioorganic and Medicinal Chemistry*. 2004, August 15; 12(17):4749-4759. Chapter 4 is reproduced in part with permission from: Alaimo, P.J.*, Knight Z.A.*, and Shokat K.M., Targeting the gatekeeper residue in phosphoinositide 3-kinases, *Bioorganic and Medicinal Chemistry*. 2005, April 15; 13(8):2825-2836. Chapter 5 is reproduced in part from: Knight, Z.A., Gonzalez-Perez, B., Feldman, M.E., Zunder, E., Goldenberg, D., Balla, A., Stokoe, D.T., Balla, T., Loewith, R., Weiss W.A., Williams, R.L., Shokat, K.M., A pharmacological map of the PI3-K family defines a role for p110α in insulin signaling, *Cell*, submitted

Chemical approaches to study protein and lipid phosphorylation

Zachary A. Knight

Kevan M. Shokat, Ph.D.

Abstract

Protein and lipid kinases direct signal transduction by the phosphorylation of their substrates. Elucidating kinase-mediated signaling pathways and validating specific kinases as targets for drug development are central goals of biomedical research. Chapter 1 describes the biochemical criteria that define the potency and selectivity of kinase inhibitors in cells. Chapter 2 describes a chemical strategy for targeting proteolysis to sites of protein phosphorylation. Chapter 3 describes isoform-specific inhibitors of PI3-kinase based on an arylmorpholine scaffold. Chapter 4 describes the role of the gatekeeper residue in PI3-kinases in controlling inhibitor sensitivity. Chapter 5 describes a pharmacological map of the PI3-K family and the role of PI3-K isoforms in insulin signaling.

Table of Contents

Chapter 1: Features of selective kinase inhibitors

1.1 Abstract 2

1.2 Introduction 2

1.3 The relationship between potency *in vitro* and *in vivo* 3

- 1.3.1 Biochemical activity predicts cellular activity 7
- 1.3.2 Sources of deviation from biochemical predictions 10
- 1.3.3 Phosphatases are endogenous kinase inhibitors 10
- 1.3.4 Kinase reactions *in vivo* are not linear 11
- 1.3.5 Bioavailability of kinase inhibitors 15
- 1.3.6 Kinases are low abundance proteins 17
- 1.3.7 The distribution of pharmacological variation 20

1.4 Biochemical and structural features of selective inhibitors 21

- 1.4.1 Selective inhibitors are drug-like molecules 21
- 1.4.2 Inhibitor selectivity is measured *in vitro* 24
- 1.4.3 Selectivity depends on potency 26
- 1.4.4 A new generation of allosteric kinase inhibitors 28

1.5 The intersection of pharmacology and genetics 31

- 1.5.1 Target validation with resistant and analog-sensitive alleles 31
- 1.5.2 Knockouts and inhibitors can yield different phenotypes 32

1.6 Why bother? 34

1.7 References 36

Chapter 2: A chemical strategy for targeting proteolysis to sites of protein phosphorylation

2.1 Abstract 48

2.2 Introduction 48

2.3 Aminoethylcysteine modification of model substrates 50

2.4 Mapping GRK2 phosphorylation of tubulin 60

2.5 Cleavage exclusively at phosphorylation sites 66

2.6 A solid-phase aminoethylcysteine reaction 70

2.7 Discussion 73

2.8 Experimental Procedures 74

- 2.8.1 Reagents 74
- 2.8.2 Aminoethylcysteine modification of model peptides 74
- 2.8.3 Modification for phosphoexclusive cleavage 75
- 2.8.4 Aminoethylcysteine modification of α and β-casein 76
- 2.8.5 Phosphorylation mapping of GRK2 and tubulin 77
- 2.8.6 Resin synthesis 78
- 2.8.7 Solid-phase capture and modification of phosphoserine peptides 78
- 2.8.8 Supplementary aminoethylcysteine modification protocol 79

Chapter 3: Isoform-specific phosphoinositide 3-kinase inhibitors from an arylmorpholine scaffold

3.1 Abstract 87

3.2 Introduction 87

3.3 LY294002 analogs 90

3.4 Arylmorpholine DNA-PK inhibitors 98

3.5 Discussion 102

3.6 Experimental Procedures 106

3.6.1 Lipid kinase expression 106
3.6.2 Lipid kinase assays 106
3.6.3 Protein kinase expression 107
3.6.4 Protein kinase assays 107
3.6.5 General chemical synthesis 108
3.6.6 – 3.6.24 Chemical synthesis 109
3.7 References

Chapter 4: Targeting the gatekeeper residue in phosphoinositide 3-kinases

4.1 Abstract 122
4.2 Introduction 122
4.3 The gatekeeper residue is conserved in lipid kinases 126
4.4 Effects of gatekeeper mutation on enzymatic activity 130
4.5 Effects of gatekeeper mutation on inhibitor sensitivity 134
4.6 Discussion 139
4.7 Experimental procedures 141
  4.7.1 Protein expression 141
  4.7.2 PI3-kinase enzymatic assay 142
  4.7.3 General chemical synthesis 143
  4.7.4 General procedure for the preparation of alcohols 1c-g 143
  4.7.5 General procedure for the preparation of ketones 2c-g 146
  4.7.6 General procedure for the preparation of compounds 3a-i 149
  4.7.7 Analysis of yeast expressing PI3-K mutant alleles 154
4.8 References 154

Chapter 5: A pharmacological map of the PI3-K family defines a role for p110α in insulin signaling

5.1 Abstract 160

5.2 Introduction 160

5.3 A basis set of isoform-specific inhibitors 163

5.4 Identification of structure-activity relationship (SAR) and target homology within the PI3-K family 164

5.5 Structures of isoform-specific inhibitors 171

5.6 The structure of PIK-39 reveals a conformational switch that controls inhibitor selectivity 173

5.7 Met 804 is a hot spot for selective inhibitors 180

5.8 Structures of PIK-90 and PIK-93 define features of potent, multi-targeted inhibitors 182

5.9 The role of PI3-K isoforms in insulin signaling 183

5.10 p110α is required for insulin signaling in adipocytes and myotubes 187

5.11 DNA-PK and ATM are dispensable for ATM activation 190

5.12 p110α is the primary lipid kinase in the IRS-1 complex 191

5.13 p110β/p110δ set a phenotypic threshold for p110α activity in myotubes, but not adipocytes 193

5.14 p110α inhibitors, but not p110β/p110δ inhibitors, block the acute effects of insulin on blood glucose in mice 195

5.15 Discussion 197

5.16 Summary of experimental procedures 200

5.16.1 Cell culture 200

5.16.2 Synthesis and biochemical characterization of PI3-K inhibitors 201
5.16.3 Determination of p110γ crystal structures 201
5.16.4 PI3-K pathway blotting 201
5.16.5 Glucose uptake 201
5.16.6 IRS-1 assays 202
5.16.7 Insulin tolerance tests 202
5.18 Experimental procedures 203
5.18.1 Reagents 203
5.18.2 Principle component analysis 203
5.18.3 Expression and assay of p110α/p85α, p110β/p85α, p110δ/p85α, and p110γ 204
5.18.4 Expression and assay of PI3KC2α, PI3KC2β, PI3KC2γ 205
5.18.5 Expression and assay of hsVPS34 205
5.18.6 Expression and assay of PI4KIIα PI4KIIIα, and PI4KIIIβ 205
5.18.7 Expression and assay of ATM and ATR 206
5.18.8 Expression and assay of DNA-PK 207
5.18.9 Expression and assay of mTORC1 and mTORC2 207
5.18.10 Expression and assay of PIPK1α, PIPKIβ, and PIPKIIβ 208
5.18.11 Protein kinase assays 209
5.18.12 Determination of p110γ crystal structures 219
5.18.13 Chemical synthesis 220
5.19 References for experimental procedures 238
5.20 References 238
Appendix A $K_{M,ATP}$ values for protein and lipid kinases 244

List of Figures

Figure 1.1 The cellular potency of an ATP-competitive kinase inhibitor depends on the $K_{M,ATP}$ 3

Figure 1.2 Correlation between K_i and EC_{50} for inhibitors of 3 protein kinases 7

Figure 1.3 Factors that can influence inhibitor sensitivity in cells 11

Figure 1.4 Expression level of protein kinases 17

Figure 1.5 Drug-like properties of kinase inhibitors 21

Figure 1.6 Recent examples of selective kinase inhibitors 28

Figure 2.1 Conversion of phosphoserine to aminoethylcysteine 51

Figure 2.2. HPLC traces of aminoethylcysteine reactions 53

Figure 2.3 MALDI-MS spectrum of β-methylaminoethylcysteine modified and digested peptide 57

Figure 2.4 MALDI-MS spectrum of peptides from digest of chemically modified β-casein 58

Figure 2.5 MALDI- MS and ESI-MS/MS spectra of digests of chemically modified β-casein 59

Figure 2.6 Detection limit of aminoethylcysteine modified proteins by MALDI-MS 61

Figure 2.7 Handling sensitivity of aminoethylcysteine modified proteins by MALDI-MS 62

Figure 2.8 Aminoethylcysteine modified GRK2 and MARCKs substrate 65

Figure 2.9 ESI-MS/MS spectra of aminoethylcysteine modified tubulin and GRK2 peptides 67

Figure 2.10 MALDI-MS of Lys-C cleavage of peracetylated MARCKs substrate 69

Figure 2.11 Solid-phase catch-and-release of phosphoserine peptides 71

Figure 3.1 ATP binding site conservation among the class I PI3-Ks 91

Figure 3.2 Synthesis of morpholino pyrimidinone analogs 93

Figure 3.3 Synthesis of TGX-115 94

Figure 3.4 IC_{50} values of LY294002 analogs against protein and lipid kinases 95

Figure 3.5 IC_{50} values of arylmorpholines against protein and lipid kinases 99

Figure 3.6 Synthesis of IC60211 and analogs 100

Figure 3.7 Correlation plot for inhibition of different PI3-K family members 101

Figure 3.8 Spectrum of characterized PI3-K inhibitor selectivities 104

Figure 4.1 Conservation of the ATP binding pocket in PI3-Ks 125

Figure 4.2 VPS34 and MEC1 alleles complement for the wild-type in *S. cerevisiae* knockout strains 127

Figure 4.3 Expression level and kinase activity of p110α alleles 129

Figure 4.4 Structure-based sequence alignment of the PI3-K family 131

Figure 4.5 Model of LY294002 analogs bound to p110γ 133

Figure 4.6 Structures of protein kinase inhibitors screened against p110α 135

Figure 4.7 Scheme for the synthesis of 3-substituted LY294002 analogs 136

Figure 5.1 Biochemical analysis of selected PI3-K inhibitors 166

Figure 5.2 Structures of active and inactive analogs of PI3-K inhibitors 167

Figure 5.3 Structural basis for isoform selective inhibition of PI3-K 172

Figure 5.4 p110β inhibitors access the induced pocket formed by Met 804 174

Figure 5.5 Structural rationale for selective inhibition of ATM by KU-55933 175

Figure 5.6 Resistance mutants and inhibitor analogs validate the role of the selectivity and affinity pockets 176

Figure 5.7 p110α is required for insulin signaling in adipocytes and myotubes 184

Figure 5.8 p110α is required for glucose uptake in adipocytes 186

Figure 5.9 p110α is the dominant lipid kinase activity associated with the IRS-1 complex 189

Figure 5.10 p110β sets a phenotypic threshold for p110α activity in adipocytes, but not myotubes 194

Figure 5.11 PI-103 and PIK-90, but not TGX-115, induces acute insulin resistance in mice 196

Figure 5.12 Synthetic schemes for the synthesis of representative inhibitors each chemotype 224

List of Tables

Table 1.1	Selected $K_{M,ATP}$ values for protein and lipid kinases	5
Table 1.2	Examples of chemical and genetic kinase knockouts that produce difference phenotypes	32
Table 2.1	Aminoethylcysteine modification of model peptide substrates	52
Table 2.2.	Results of aminoethylcysteine modification for protein substrates	55
Table 2.3	Results of phosphospecific cleavage following guanidylation or acetylation of MARCKs substrate	68
Table 4.1	IC_{50} values for p110α inhibition by 3-substituted LY294002 analogs	138
Table 5.1	IC_{50} values for inhibition of purified PI3-K family members	169
Table 5.2	Percentage inhibition of PI3-K inhibitors against purified protein kinases	170
Table 5.3	Crystallographic statistics	177

Chapter 1

Features of selective kinase inhibitors

1.1 Abstract

Small molecule inhibitors of protein and lipid kinases have emerged as indispensable tools for studying signal transduction. Despite the widespread use of these reagents, there is little consensus about the biochemical criteria that define their potency and selectivity in cells. This chapter discusses some of the features that determine the cellular activity of kinase inhibitors and proposes a framework for interpreting inhibitor selectivity.

1.2 Introduction

The dramatic clinical success of Imatinib has fueled an explosion in kinase inhibitor discovery research [1]. It is estimated that kinase inhibitors currently comprise up to 30% of drug discovery programs in the pharmaceutical industry and over 50 such compounds are now in clinical trials [2]. The scale of this investment has led to the discovery of compounds with properties that scarcely resemble their early predecessors – picomolar potency, isoform selectivity, and allosteric binding modes are increasingly common [3-9]. As these reagents filter into the hands of scientists engaged in basic research, they will transform the study of signal transduction.

The first kinase inhibitors were described nearly 20 years ago [2], and a small subset of these compounds have found widespread application, forming the basis for much of what we know about the physiological roles of their targets. As we anticipate a new era of molecularly targeted agents, it is fair to ask what practical lessons have been learned from the use of these early compounds. What determines the potency of an inhibitor in cells? What is required for a kinase inhibitor to be selective, and how can this be measured? How is it possible to validate pharmacological results? The aim of this review is to suggest a framework for evaluating and using kinase inhibitors, with a focus on the use of these reagents to explore signal transduction in cell culture-based model systems.

1.3 The relationship between potency *in vitro* and *in vivo*

The potency of a kinase inhibitor for its target is typically expressed as an IC_{50} value – the concentration of drug at which 50% of the kinase activity is inhibited. Most kinase inhibitors are reversible and ATP competitive, and for these reagents, the IC_{50} depends on the intrinsic affinity of the inhibitor (the dissociation constant, K_i) as well as the competition from ATP under the specific assay conditions (the [ATP] and the $K_{M,\ ATP}$). These variables are related to each other by the Cheng-Prusoff equation [10]:

$$IC_{50} = K_i\,(1 + [ATP]/\,K_{M,\ ATP}).$$

This equation captures the fact that at low ATP concentrations, there is no significant competition from substrate and the $IC_{50} \cong K_i$. As the ATP concentration exceeds the $K_{M,\ ATP}$, the IC_{50} increases at approximately the same rate (Figure 1.1A). Importantly, the IC_{50} does not plateau at a maximum value at high concentrations of ATP (in contrast to how an enzyme approaches V_{max} as the [ATP] exceeds the $K_{M,\ ATP}$).

For this reason, the potency of an inhibitor in cells (where the ATP concentration is 1 – 5 mM [11, 12]) depends critically on the $K_{M,\ ATP}$ of its target (Figure 1.1A). An inhibitor that has similar K_i values against multiple kinases will inhibit more potently in cells those kinases that have a higher $K_{M,\ ATP}$. We have assembled 238 published $K_{M,\ ATP}$ values for 111 protein and lipid kinases (Table 1.1). The majority of these values are in the low to mid-micromolar range, and for these targets, ATP competitive inhibitors should be active in cells at concentrations ~10- to 100-fold above their K_i. There are outliers, however, and these kinases will be more or less

A

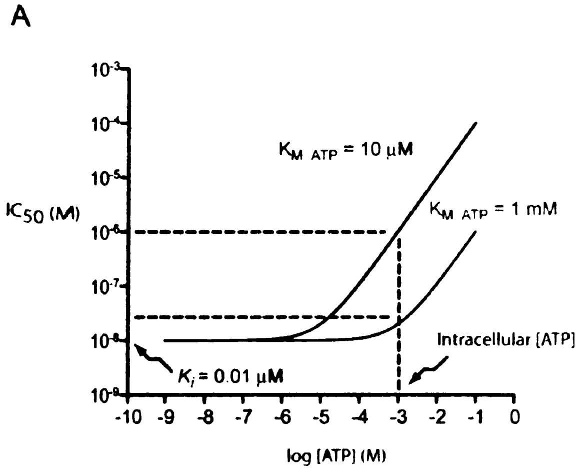

B

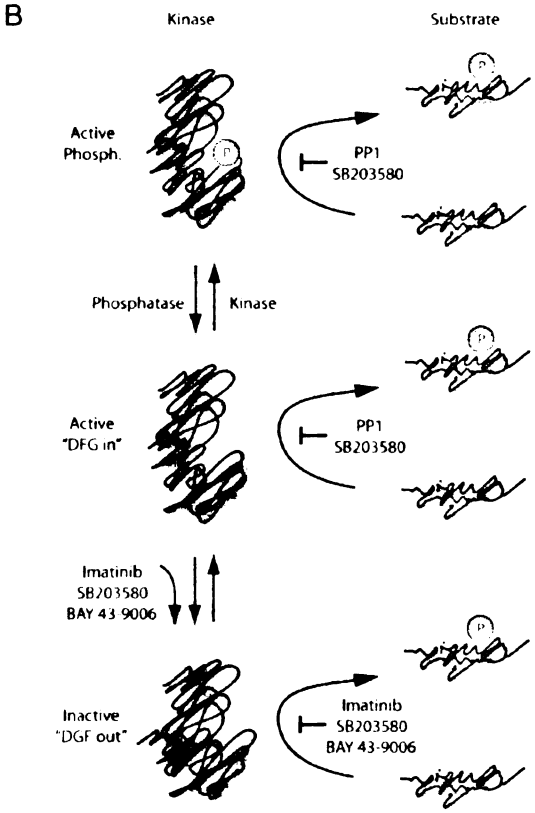
Kinase
Substrate
Active
Phosph.
PP1
SB203580
Phosphatase
Kinase
Active
"DFG in"
PP1
SB203580
Imatinib
SB203580
BAY 43 9006
Inactive
"DGF out"
Imatinib
SB203580
BAY 43-9006

C

Kinase	Active $K_{M,ATP}$	Inactive $K_{M,ATP}$
InsR	40	900
IGF1R	107	720
MuSK	380	3400
VEGF-R2	130	900
Tie2	74	366
p38α	25	>1000

Figure 1.1. The cellular potency of ATP-competitive kinase inhibitors depends on the $K_{M,\ ATP}$. (A) Theoretical relationship between $K_{M,\ ATP}$ and cellular potency for an ATP competitive inhibitor with a K_i of 10 nM. (B) A simplified schematic depicting how different classes of kinase inhibitors may block kinase activity. (C) Examples of kinases that show large differences in $K_{M,\ ATP}$ between two phosphorylated forms.

difficult to target with ATP competitive small molecules. For example, several phosphatidylinositol 4-kinases and the related protein mTOR have millimolar $K_{M,\,ATP}$ values [13-17], and we have argued that trends in IC_{50} values for LY294002 analogs against phosphatidylinositol 3-kinases (PI3-Ks) can be explained largely by differences in affinity for ATP [13].

An important caveat to the use of $K_{M,\,ATP}$ values is that they are sensitive to the specific assay conditions (such as choice of protein substrate [18] or counter-ion [19]). $K_{M,\,ATP}$ values for a single kinase measured under different conditions generally show small variation (<5-fold), and therefore likely approximate the true *in vivo* substrate affinity of these enzymes. However, for some kinases $K_{M,\,ATP}$ values are lower when measured with protein substrates versus peptides [18] or when manganese is used in place of magnesium [20], and these factors must also be considered.

Most kinases are believed to interconvert between at least two structural conformations, active and inactive, and the phosphorylation of key residues can shift the balance between these states (Figure 1.1B). These two states are characterized by movements in conformationally mobile loops which border or block the ATP binding site (for example, the DFG motif). For this reason, the $K_{M,\,ATP}$ may be significantly higher for the inactive conformation than for the active conformation (Figure 1.1C). A growing number of kinase inhibitors selectively target the inactive conformation [3, 21, 22], whereas other compounds bind to both conformations with similar affinity [23]. Inhibitors which bind to the inactive conformation will face weaker competition from cellular ATP, and this may enhance their activity *in vivo*. Indeed, even though these compounds are ATP competitive, they may act primarily by shifting equilibria between conformational states in a way that prevents kinase activation, rather than by inhibiting kinase activity directly (Figure 1.1B). For example, the p38α inhibitor SB203580, which binds to both

Tyr Kinases

c-Abl	12
v-Abl	18
Btk	29
Csk	15
EGFR	17
EphA7	30
EphB3 $^{\text{(Mn)}}$	2.7
ErbB-2	27
ErbB-4	37
FAK $^{\text{(Mn)}}$	4.3
FER	7.1
c-Fgr	20
FGFR	70
Fyn	70
IGFR	107
InsR	40
ITK	36
JAK1	15
JAK3	6
c-Kit	53.6
Lck $^{\text{(Mn)}}$	10
Lyn	35
MER	40
MuSK	380
PDGFRβ	15
c-Src	80
v-Src-cat	12
Syk	10
c-Tak	3.3
Tie-2	73.9
TrkA $^{\text{(Mn)}}$	9
VEGF-R2	130
c-Yes $^{\text{(Mn)}}$	16
Zap-70	3

Ser/Thr Kinases

Akt1	132
Akt2	254
Aurora 2	34
Cak1-*Sc*	5
CaMKI	110
CaMKIIα	19
CaMKIV	27
CaMKKα	33
CaMKKβ	33
CDK1/cyclin B	2.3
CDK2/cyclin A	23
CDK2/cyclin E	3.6
CDK4/cyclin D1	418
CDK4/cyclin D2	200
CDK5/p25	3.2
Chk1	1.4
Chk2	3.3
CK1α	19
CK1β	12
CK2α	13.9
CK2β	8.8
CLK1 $^{\text{(Mn)}}$	80
CTR1-*Ar* $^{\text{(Mn)}}$	9.1
DAPK31	2.4
DMPK	2.3
Erk2	140
GRK1	2
GRK2	60.8
GRK3	88.8
GRK5	23.8
GRK6	111
GSK3β	50.2
IKK-1/IKK-2	13
IKK-2/IKK-2	18
IKK-ι $^{\text{(Mn)}}$	3.1
IRAK4	600
JNK2	39
JNK3α1	1.9
MAPKAPK2	43
MEK1	5.6
NIMA-*As*	69
p38α	25
p38γ	27
p90Rsk-B	35
PAK2	71
PhK	200
PKA-α	25
PKA-γ	9.1
PKC-α	24.3
PKC-βI	37.2
PKC-βII	20
PKC-ε	14.5
PKC-θ	49
PKG	5.1
PLK1	2.6
Raf-1	11.6
ROCK-I	4.5
ROCK-II	4.5
Sky1p-*Sc*	235
smMLCK	71
skMLCK	101
TBK-1 $^{\text{(Mn)}}$	5.9

Lipid/PIK kinases

ATM $^{\text{(Mn)}}$	29
DNA-PK	228
mTOR	1000
p110α/p85α	62
p110γ	7.5
PI3KC2α	32
PI3KC2β	120
PI4KIIα	28
PI4KIIIα	300
PI4KIIIβ	1000
PI(4)P(5)KI	25
PI(4)P(5)KIα	27
PI(4)P(5)KIβ	33
PI(4)P(5)KIγ	39
PI(5)P(4)KII	5

Table 1.1. Selected $K_{M,\ ATP}$ values for protein and lipid kinases. When multiple values were available for a single kinase, a consensus value was selected, with preference given to values measured using magnesium, a protein substrate, and the active conformation of the kinase. A complete list, with phosphoacceptor data and references, is available online as Supplementary Figure 1.1. (Mn) indicates value was measured in the presence of manganese. Sc (*Saccharomyces cerevisiae*), Xe (*Xenopus laevis*), Ar (*Arabidopsis thaliana*), Pb (*Schizosaccharomyces pombe*), Ca (*Candida albicans*), As (*Aspergillus nidulans*).

conformations, has been proposed to act in cells by stabilizing an inactive conformation that reduces the rate of p38α phosphorylation by MAPKKs [23].

1.3.1 Biochemical activity predicts cellular activity

Biochemical affinities are measured *in vitro* in order to predict concentration ranges at which kinase inhibitors will be active in cells. To what extent does kinase inhibition in cells actually correlate with *in vitro* measurements? To address this question, we analyzed published data for 13 classes of inhibitors that target three different protein kinases: VEGF-R2, IKK-2, and Lck. Figure 1.2 plots the relationship between biochemical K_i and EC_{50} for these compounds, where EC_{50} is defined as the concentration of compound required to inhibit 50% of a cellular phenotype (different colors represent different structural classes of inhibitors, whereas different shapes represent different cellular assays). K_i values were estimated from *in vitro* IC_{50} values based on the reported assay conditions, and compounds were excluded that lacked potency *in vitro* ($K_i > 1$ μM) or had no activity at the highest concentration tested in cells (fewer than 10 compounds). These values were then compared with predictions based on the consensus $K_{M,\,ATP}$ reported for these kinases assuming an intracellular ATP concentration of 2 mM (dotted lines).

Five chemotypes of VEGF-R2 inhibitors were analyzed. There was a correlation between biochemical affinity and cellular potency for these molecules that extended across structural classes and among analogs within a series. The EC_{50} for VEGF-R2 inhibitors was, on average, 10-fold above the K_i, and most compounds fell within a five-fold window of this value (4 to 20-fold). To what extent do these values match *in vitro* predictions? The $K_{M,\,ATP}$ of the VEGF-R2 kinase domain has been measured for the phosphorylated (active) and unphosphorylated (inactive) states by at least two

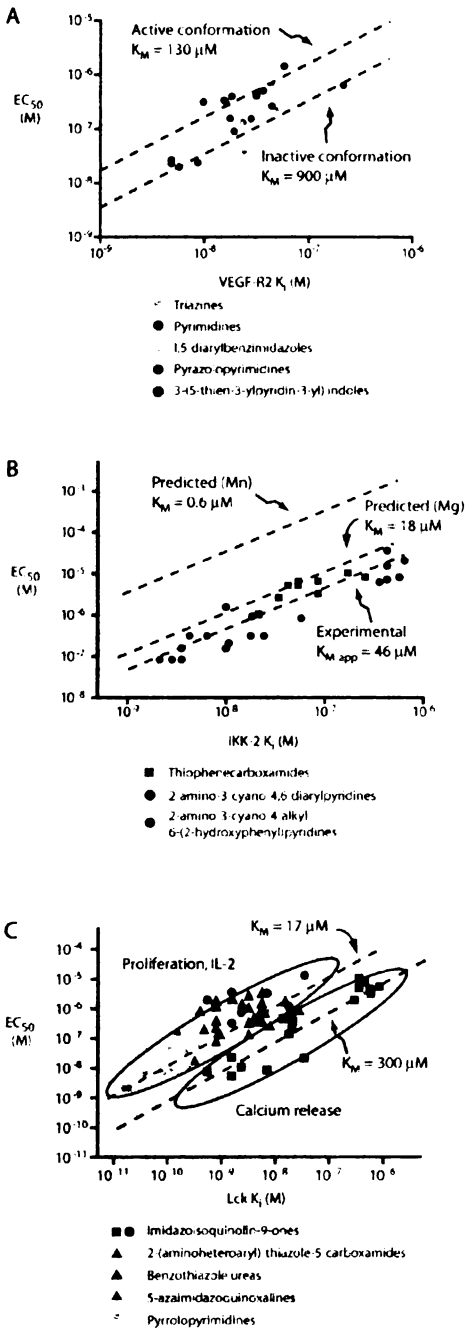

Figure 1.2. Correlation between K_i and EC_{50} for a sample of inhibitors of 3 protein kinases. (A) VEGFR2: Circles – VEGF induced mitogenesis in HUVECs [24-27]; Squares – VEGF induced p42/p44 MAPK phosphorylation in HUVECs, (B) IKK-2: Circles - RANTES induction by TNFα in A549 cells [28-30]; Squares – Production of TNFα by HUVECs stimulated with LPS [30], (C) Lck: Circles – Antibody stimulated IL-2 secretion [31, 32]; Squares - Antibody stimulated calcium release [32];Triangles – Antibody stimulated T-cell proliferation [33-35].

laboratories, and the reported values are similar (130/900 μM and 150/600 μM [36, 37]). It is not known whether these compounds target the active or inactive state, so we plotted the predicted relationship between EC_{50} and K_i for both conformations (dotted lines, Figure 1.2A). These two lines bracket most of the experimental values – suggesting that biochemical measurements predict the cellular activity of VEGF-R2 inhibitors with good accuracy.

We next analyzed data for inhibitors of IKK-2 (Figure 1.2B). IκB kinases exhibit $K_{M,\ ATP}$ values in the sub-micromolar range [38-42] – some of the lowest values reported for any protein kinase – suggesting that it may be necessary to use IKK inhibitors at high concentrations to achieve cellular activity (>1000-fold above K_i). Three classes of IKK-2 inhibitors were compared, and these compounds exhibit a strong correlation between biochemical K_i and EC_{50} across three orders of magnitude in inhibitor affinity (Figure 1.2B). Surprisingly the EC_{50} for IKK-2 inhibitors is, on average, only 44-fold above the K_i, corresponding to an effective $K_{M,\ ATP}$ of 46 μM for this kinase. What accounts for this discrepancy? One explanation is that the reported nanomolar $K_{M,\ ATP}$ values for IKK-2 (for example, 0.1, 0.14, 0.56, 0.6, and 0.65 μM [38-42]) were all measured under conditions that utilize manganese as a counterion. In the presence of only magnesium, the physiological divalent cation, the $K_{M,\ ATP}$ is 18 μM [43] – a value more consistent with the observed cellular activity of IKK-2 inhibitors. This highlights the fact that biochemical affinities measured using manganese are likely to be non-physiological and may distort calculations of inhibitor potency.

Figure 1.2C depicts data for five chemotypes of Lck inhibitors, assayed according to their ability to block calcium release, IL-2 secretion, or proliferation of T-cells. The cellular activity of these compounds falls into two classes. Calcium release is highly sensitive to Lck inhibition (mean $EC_{50} \cong 11\ K_i$, corresponding to an apparent $K_{M,\ ATP} \cong$

300 μM), whereas IL-2 production and T-cell proliferation are much less sensitive, although almost identical to each other (mean $EC_{50} \cong 440\ K_i$, corresponding to apparent $K_{M,\ ATP} \cong 17$ μM). The latter value is close to the reported $K_{M,\ ATP}$ for Lck of 10 μM [44], suggesting that the potencies against IL-2 production and T-cell proliferation are consistent with *in vitro* measurements, whereas calcium release is unexpectedly sensitive. This may reflect different thresholds for Lck activity for these two sets of processes and is consistent with the underlying differences in their kinetics – calcium release occurs in seconds, whereas cytokine production and proliferation occur over days. In general, these Lck inhibitors are also more varied in their cellular activity than IKK-2 or VEGF-R2 inhibitors. An important component of this variation is likely to be differences in the off-target activity of these inhibitors against other Src family kinases, such as Fyn, that are known to contribute to T-cell signaling.

1.3.2 Sources of deviation from biochemical predictions

The data from these three classes of inhibitors suggests that, to a first approximation, biochemical affinities predict the cellular activity of kinase inhibitors remarkably well. Still, it is clear that many kinase inhibitors are more or less potent in cells than predicted by K_i and $K_{M,\ ATP}$, and it is certainly not possible to use these values to calculate an exact EC_{50} value. For example, the widely used PI3-K inhibitor LY294002 is consistently ~10-fold more potent in cells than biochemical measurements would predict. What mechanisms can account for discrepancies between inhibitor potency *in vitro* and in cells?

1.3.3 Phosphatases are endogenous kinase inhibitors

Phosphatases reverse the action of kinases *in vivo*, and this has the effect of systematically lowering the IC_{50} values for kinase inhibitors. This is because the net flux of phosphorylated product in the cell is the difference between the kinase and phosphatase activities. If the kinase and phosphatase turn over their substrates at similar rates, then inhibiting a small fraction of the kinase activity can block the entire flux of phosphorylated product (Figure 1.3A). A prediction of this model is that phosphatase inhibitors should decrease the potency of kinase inhibitors, and indeed, inhibitors of the lipid phosphatase PTEN increase the cellular IC_{50} for LY294002 by ~5-fold [45]. Moreover, there is evidence that some signaling pathways are controlled by high levels of basal phosphatase activity. For example, treatment of lymphocytes with tyrosine phosphatase inhibitors can induce much higher phosphotyrosine levels than any physiological stimulus [46], suggesting that in these cells, the basal phosphatase activity is of the same magnitude as the stimulated kinase activity. For many signaling pathways, our understanding of the key phosphatases, their direct substrates and their modes of regulation is limited compared to our understanding of the corresponding kinases. Yet every phospho-regulated step in signal transduction reflects a dynamic equilibrium between these two activities, and the relative phosphatase activity in each step will influence its sensitivity to small molecule inhibition.

1.3.4 Kinase reactions *in vivo* are not linear

IC_{50} values are measured *in vitro* in the presence of a large excess of phosphoacceptor substrate, such that the substrate concentration does not change significantly during the course of the assay (that is, only initial rates are measured). Under these conditions, the relationship between the concentration of active kinase (the fraction of the total kinase not inhibited by drug) and the concentration of phosphorylated

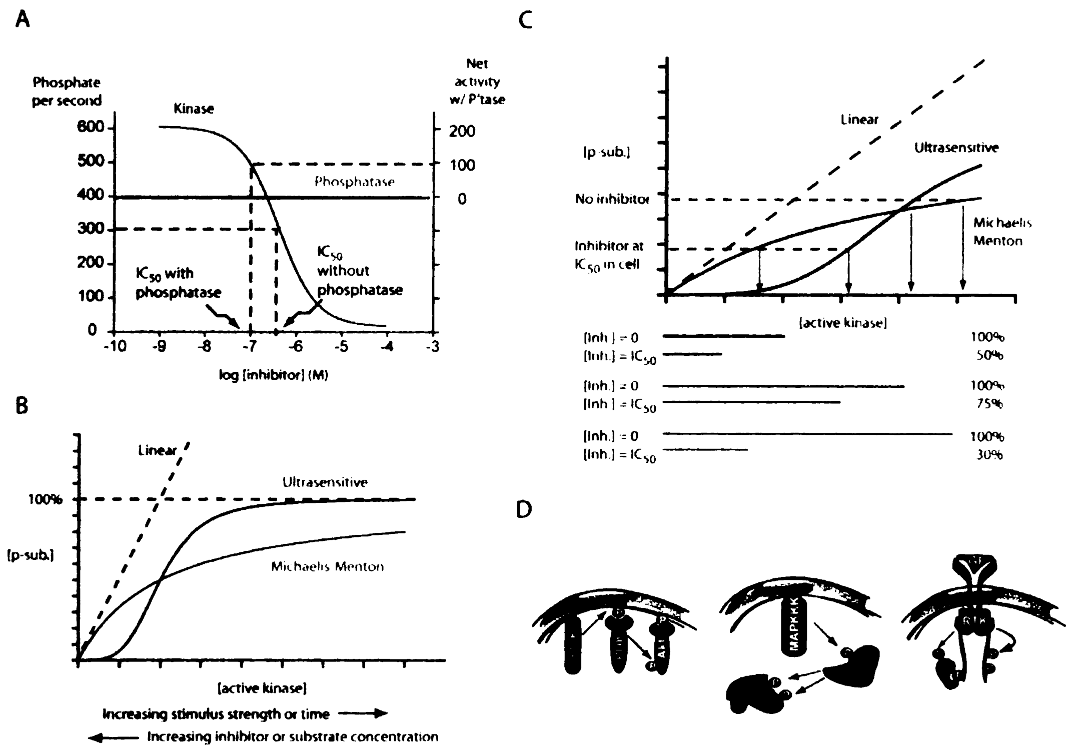

Figure 1.3. Factors that can influence inhibitor sensitivity in cells. (A) Phosphatase activity can lower IC_{50} values for kinase inhibitors. In the absence of phosphatase activity, the IC_{50} for an inhibitor is the concentration at which half the kinase activity is inhibited (here, 600/2 = 300/s). In the presence of a fixed phosphatase activity of 400/s (red line), the net flux of kinase activity is reduced to 200/s. Therefore, inhibiting only $100/600 \cong 16\%$ of the direct kinase activity will block $100/200 \cong 50\%$ of the net flux of kinase activity. This model may be realistic for early time-points, when the phosphatase activity is constant and independent of the kinase activity. (B) The concentration of phosphorylated substrate ([p-substrate]) can have differential dependence on the concentration of active kinase ([active kinase]) depending on whether the activity obeys linear (dashed), Michaelis-Menton (red), or ultrasensitive (blue) kinetics [47]. Increasing the strength of the cellular stimulus or the length of time will shift the reaction to the right along these curves, whereas increasing the concentration of inhibitor or the stoichiometry of substrate will shift the reaction to the left. (C) Detailed analysis of the effect that Michaelis-Menton or ultrasensitive kinetics can have on kinase sensitivity to inhibitors. For a linear response, the concentration of drug necessary to reduce the [p-substrate] by 50% corresponds to a 50% reduction in [active kinase] (that is, 50% of the kinase active sites are bound to drug). For Michaelis-Menton and ultrasensitive responses, reducing the [active kinase] by more or less than 50% is necessary to reduce the [p-substrate] by 50%. (D) Schematic diagram of signaling in MAP kinase, PI3-K, and receptor tyrosine kinase (RTK) pathways.

substrate is linear (Figure 1.3B, black dashed). This is not necessarily the case in the cell, where a kinase may phosphorylate a large fraction of its protein substrate; the fact that it is often possible to monitor protein phosphorylation by observing a molecular weight shift via SDS-PAGE is evidence that phosphorylation can occur at high stoichiometry in cells. Under these conditions, where phosphoacceptor substrate is significantly consumed, the concentration of active kinase and its phosphorylated substrate are related by a hyperbolic curve indicative of Michaelis-Menten kinetics (Figure 1.3B, red). In other cases, Ferrell and co-workers have shown that kinase-mediated signaling pathways, such as the MAP kinase cascade, can behave cooperatively, such that the concentration of active kinase and its phosphorylated substrate are related by a sigmoidal, rather than hyperbolic, curve [47, 48] (so-called ultrasensitivity, Figure 1.3B, blue). This ultrasensitivity has been attributed to a number of features, including multisite phosphorylation of a single substrate, the activity of a kinase at multiple steps within a pathway, or the presence of several kinases arranged in a linear cascade.

The precise nature of the relationship between kinase activity and output for any given signaling pathway has implications for the sensitivity of kinases to small molecule inhibition. Under Michaelis-Menten conditions, the biochemical IC_{50} (the concentration of drug at which half the kinase active sites are occupied by inhibitor in cells) is always lower than the EC_{50} (the concentration of drug at which half the total kinase activity is inhibited in cells) (Figure 1.3C). The magnitude of this effect can be large at very high stoichiometries of substrate consumption, and tends to make kinase inhibitors appear less potent in cell culture than would be predicted by *in vitro* measurements. As the fraction of phosphoacceptor substrate that is consumed decreases (due to a weaker stimulus, a shorter timepoint, or a more abundant substrate), the hyperbolic Michaelis-

Menten curve approaches in the limit the linear conditions observed *in vitro*, where substrate is essentially unlimited and the biochemical IC_{50} and EC_{50} are identical.

Ultrasensitive behavior can make a kinase inhibitor seem more or less potent in cells, depending on the fraction of substrate that is consumed under the given assay conditions. At low substrate consumption, it is possible to inhibit more than 50% of the net kinase activity by occupying less than 50% of the kinase active sites with inhibitor (Figure 1.3C). At high substrate consumption, the ultrasensitive response converges to the behavior of normal Michaelis-Menten kinetics.

Huang et al. have experimentally confirmed that the relationship between MAPKKK activity and the activity of its downstream effectors (MAPKK and MAPK) in *Xenopus* oocyte extracts exhibits ultrasensitivity, and this can be described by Hill coefficients of approximately 2 and 5, respectively [48]. A consequence of this fact is that a MAPKKK inhibitor that blocks 50% of MAPKK activation will inhibit less than 50% of MAPK activation, even though these enzymes are directly connected in a linear signaling cascade (Figure 1.3D). Although most signaling pathways have not been characterized at this level of detail, many common mechanisms of signal transduction contain features that may introduce cooperativity, and thereby perturb inhibitor sensitivity. For example, PI3-kinase activates the downstream kinase Akt by recruiting it and its upstream kinase PDK1 to the plasma membrane (Figure 1.3D). The quantitative relationship between PI3-K activity (PIP_3 generation) and Akt phosphorylation by PDK1 is unknown, but the simplest model is that Akt phosphorylation is a bimolecular reaction between Akt and PDK1, and therefore the rate is dependent on the concentration of each at the membrane ($v(pAkt) = k_1[Akt][PDK1]$). If the membrane concentration of each protein is proportional is to the concentration of PIP_3 ($[Akt], [PDK1] \propto [PIP_3]$), then the rate of Akt phosphorylation should increase according to the square of the PIP_3 concentration ($v(pAkt) = k_{obs}[PIP_3]^2$). Under conditions of low substrate consumption where this model may be realistic, PI3-K inhibitors should block Akt phosphorylation more potently than they block PI3-K activity directly (for example, inhibition of 50% of PI3-K activity should reduce phosphorylated Akt by 75%). A similar model would apply to a receptor tyrosine kinase, whose kinase activity both recruits its substrates via SH2 domain-phosphotyrosine interactions and subsequently activates them by direct phosphorylation (Figure 1.3D). It will be interesting to test these models experimentally in an effort to delineate the quantitative relationship between kinase inhibition and signaling output for different pathways.

1.3.5. Bioavailability of kinase inhibitors

Kinase inhibitors must enter the cell in order to inhibit their targets. The bioavailability of a kinase inhibitor in cell culture depends primarily on two factors. (1) How fast does the intracellular inhibitor concentration reach a steady-state? (2) At the steady-state, what are the relative concentrations of inhibitor inside and outside the cell? These questions depend largely on the magnitude of two rates: the rate at which the compound enters the cell by diffusion down the concentration gradient that exists across the membrane (the cell permeability), and the rate at which the compound is actively pumped out of the cell by efflux pumps.

For a given concentration gradient, the cell permeability of a compound is proportional to its lipophilicity (more lipophilic compounds will partition more readily from water into a membrane), and inversely proportional to its size. For this reason, molecules that are highly charged, have too many hydrogen bond donors and acceptors, or are very large cross cellular membranes slowly. However, molecules that are extremely hydrophobic also have poor effective permeability, either because they lack aqueous solubility, fail to partition out of the plasma membrane, or bind tightly to serum proteins. “Drug-like” kinase inhibitors tend to lack these structural defects, and these molecules often have very high rates of cell permeation. For example, levels of PIP_3 in insulin stimulated 3T3-L1 cells sharply decline within ~1 minute of LY294002 addition [49]. Actin rearrangements can be observed in T-cells within 3-5 minutes of addition of the Lck inhibitor PP2 at a low dose (20 nM) [50]. Since it is customary to preincubate kinase inhibitors for 30 – 90 minutes prior to stimulation of the cell, it is safe to assume that most drug-like kinase inhibitors approach their steady-state within the experimental time scale.

Inhibitors are also pumped out of the cell by drug efflux pumps. The rate of efflux depends on the intracellular inhibitor concentration, the K_M of a specific inhibitor for a given pump, and the overall level of pump activity. In some cases, the activity of efflux pumps can significantly lower the steady state concentration of a drug. *S. cerevisiae*, for example, is resistant to many small molecule inhibitors that are active in mammalian cells. Deletion of specific drug pumps renders yeast sensitive to most of these same compounds [51]. This is also the case for some tumor cells that overexpress transporters such as p-glycoprotein; expression of these transporters has been shown to reduce the steady-state intracellular drug concentration by up to 50-fold [52]. By contrast, most mammalian cells in culture appear to have less efflux activity

There is little published data that directly compares the bioavailability of different classes of kinase inhibitors in cell culture (bioavailability in animals is beyond the scope of this review). For drug-like kinase inhibitors with characteristically high rates of cell permeation, it seems likely that differences in steady-state intracellular drug concentration are the major source of experimental variation due to bioavailability. If this were not the case, then the potency of kinase inhibitors in cells would be highly sensitive to the length of preincubation; but this is not generally observed. An upper limit to the differences in steady-state bioavailability can be estimated indirectly by analyzing the scatter in plots such as Figure 1.2. Part of the deviation of this data from a straight line reflects differences in bioavailability across compounds (other factors include experimental error in measuring the *in vitro* and cellular IC_{50} values, as well as differences in how these assays are conducted across different laboratories). For most of the compounds analyzed here, the cellular activity deviates from the mean within a 10-fold window for any given phenotypic endpoint. This represents an upper bound on the typical differences in bioavailability for potent, drug-like kinase inhibitors. Given that there are other significant sources of uncontrolled error in this analysis, this suggests that differences in bioavailability for kinase inhibitors in cell culture may be smaller than generally believed.

1.3.6 Kinases are low abundance proteins

The lowest IC_{50} value that can be measured *in vitro* is the determined by the concentration of kinase used in the assay. An IC_{50} value cannot be lower than one-half the concentration of kinase, because it is not possible to inactivate more than one kinase per molecule of drug (assuming a normal reversible binding mechanism). By extending this reasoning, it is sometimes argued that the potency of an inhibitor in cells depends on the intracellular concentration of its kinase target. A very abundant kinase will titrate a small molecule inhibitor out of solution, such that the concentration of the kinase places a lower limit on the cellular IC_{50} for the inhibitor.

In most experimental settings, this reasoning is incorrect: the potency of a kinase inhibitor in cells should be independent of the concentration of its target (here, the concentration of kinase is distinguished from the amount of kinase activity). This is because kinase inhibitors are typically supplied in a large reservoir that can exchange matter with the cell, and the presence of a high affinity receptor within the cell will increase the steady-state intracellular drug concentration. For example, for most experiments in tissue culture, kinase inhibitors are added to the media and enter the cell

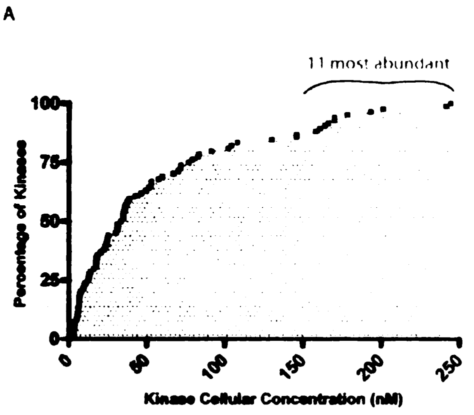

B

	ORF	Gene	Human Ortholog
1	YPL204W	HRR25	CK1δ
2	YMR291W	unnamed	KIAA1765 CaMKs
3	YBL016W	FUS3	MAPKs
4	YGL019W	CKB1	CK2β
5	YOL016C	CMK2	CaMKs
6	YIL035C	CKA1	CK2α
7	YOR039W	CKB2	CK2β
8	YMR139W	RIM11	GSK3α/GSK3β
9	YPL153C	RAD53	CHK2
10	YLR113W	HOG1	MAPKs
11	YBR160W	CDC28	CDKs

Figure 1.4. (A) The fraction of kinases that are expressed at less than a given cellular concentration in *S. cerevisiae*. (B) The 11 most highly expressed protein kinases in *S. cerevisiae*.

through passive diffusion. Standard conditions for the growth of tissue culture cells – 10^6 cells growing in a 10 cm dish bathed in 10 mL of media – correspond to a volume of cell culture media 10,000-fold greater than the volume of cells. In this regime, no change in the concentration of inhibitor within the cell can significantly alter the concentration of inhibitor in the media. For a potent inhibitor of an abundant kinase (K_i << [kinase]), the binding of the inhibitor to the kinase will therefore increase the total intracellular concentration of inhibitor, because the driving force for diffusion across the membrane is primarily the concentration gradient of unbound inhibitor.

Natural variation in the expression levels of kinases can affect inhibitor sensitivity indirectly, by changing the level of total kinase activity and thereby the number of turnovers needed to consume substrate or overcome a phenotypic threshold. For example, cell lines that overexpress Bcr-Abl can be made 3-fold more sensitive to Imatinib by reduction of Bcr-Abl levels via RNAi [53]. Limited data is available on the absolute expression level of most proteins in mammalian cells, but the expression of 80% of the predicted genes in yeast has been measured using an epitope-tag library [54]. This data set includes absolute expression levels for 84 of the 116 protein kinases predicted by the yeast genome, and we converted these values to protein concentrations by assuming a volume of 70 μm^3 for haploid *S. cerevisiae* [55] (Figure 1.4A). By this calculation, 63% of protein kinases are expressed at a concentration between 1 and 50 nM, and only 11 kinases (13%) are expressed at higher than 150 nM, with a maximum concentration of ~240 nM. By comparison, the median protein concentration in *S. cerevisiae* is ~54 nM, and the most abundant protein is expressed at ~38 μM. These calculations do not include values for the 38% of kinases for which expression data is unavailable, although the absence of data likely reflects the extremely low abundance of many of these proteins. Available data from mammalian cells and *Xenopus* oocytes is generally consistent with these concentrations, although some highly abundant kinases such as MAPKs and CDKs can be expressed as high as 1 – 2 μM [47, 56, 57]. These values provide some insight into the abundance of specific kinases within the protein kinase superfamily and relative to other cellular proteins; however, it remains necessary to empirically determine the relationship between expression levels and inhibitor sensitivity for any specific kinase.

1.3.7 The distribution of pharmacological variation

We have highlighted some of the reasons why the potency of kinase inhibitors in cells may deviate from biochemical predictions. This is not to suggest it is possible to predict these deviations in any specific case. The important fact is that kinase inhibitors have been successfully used to dissect signaling pathways, and this implies that the sources of variation in inhibitor potency must be small in magnitude and poorly correlated, such that their net effect causes modest overall deviations from *in vitro* predictions. This result was not guaranteed. Indeed, the effectiveness of kinase inhibitors in cells is entirely contingent on the fact that evolution has tuned the biochemical activities of kinases to phosphorylate a significant fraction of their substrates, but not much more, during the time course of an ordinary stimulus. If kinases were endowed with significant excess catalytic capacity – for example, 100-fold more activity than needed to phosphorylate 90% of their available substrate – then it would be, for all practical purposes, impossible to make a kinase inhibitor.

The identification of different sources of pharmacological variation has implications for kinase inhibitor selectivity, even if it is not possible to predict the magnitude of these effects. Highly related kinases (for example, isoforms within a family) are more likely to share many sources of variation – such as a common phosphatase, similar levels of specific activity relative to substrate abundance, and downstream effectors with similar kinetics and thresholds of activation. The presence of these shared signaling components reduces the number of potential sources of deviation for the *in vivo* activity of different small molecule inhibitors of these targets. This argues, counterintuitively, that closely related kinases should be easier to selectively inhibit in cells, given a fixed level of biochemical selectivity of a small molecule inhibitor.

1.4 Biochemical and structural features of selective inhibitors

1.4.1 Selective inhibitors are drug-like molecules

Most selective kinase inhibitors are drug-like molecules. Even though a kinase inhibitor can be a useful research tool without the functional properties of a drug (for example, oral bioavailability), drug-like compounds strike an appropriate balance between aqueous solubility and cell permeability [58], both of which are necessary for activity in cells. Furthermore, non-drug-like molecules often have structural properties that compromise their selectivity. In the words of Lipinski and Hopkins, "chemical features associated with failure in drug discovery tend to cause compounds to have 'promiscuous' effects in biological systems" [59].

Several approaches have been advanced to define "drug-likeness" by identifying the chemical features shared by orally active drugs. Lipinski's rule-of-five identifies upper limits on the molecular weight (< 500 Da), hydrophobicity (ClogP ≤ 5), and the number of hydrogen bond donors (≤ 5) and acceptors (≤ 10) that most drugs possess [60]. An alternative proposal by Veber has emphasized the fact that oral absorption is favored by low polar surface area (less than 140 Å^2) and decreased ligand flexibility (10 or fewer freely rotatable bonds) [61].

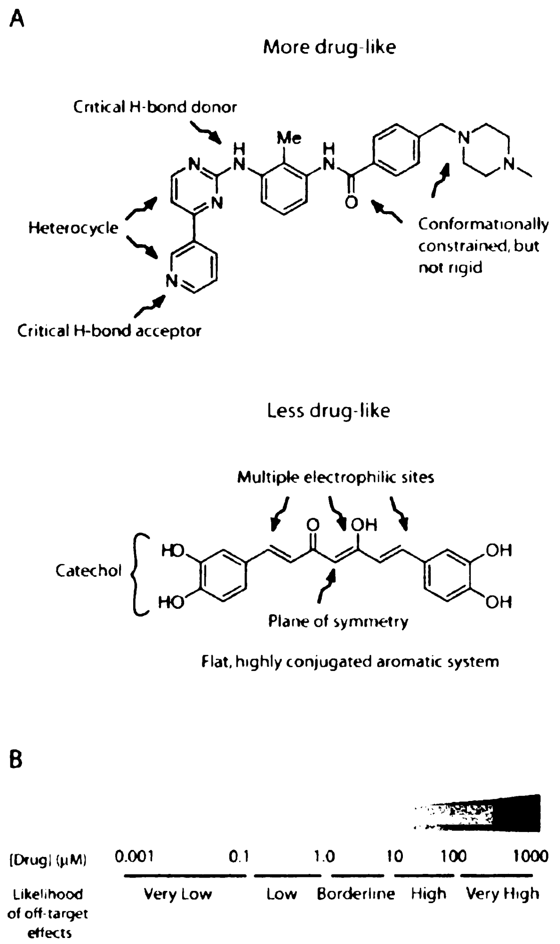
A
More drug-like
Critical H-bond donor
Me
Heterocycle
Conformationally constrained, but not rigid
Critical H-bond acceptor
Less drug-like
Multiple electrophilic sites
Catechol
HO
HO
OH
OH
Plane of symmetry
Flat, highly conjugated aromatic system
B
[Drug] (μM)
0.001
0.1
1.0
10
100
1000
Likelihood of off-target effects
Very Low
Low
Borderline
High
Very High

Figure 1.5. (A) Comparison of drug-like properties of Imatinib and a curcumin derivative. (B) Proposed general guidelines for estimating the likelihood of off-target (non-kinase) effects at different concentration ranges of inhibitor applied to cells.

Beyond specific drug-like properties, selective kinase inhibitors are almost always heterocycles, rather than peptides, lipids, or other substrate analogs (for example, see Figure 1.5A). They are typically entropic ally constrained, with four or fewer freely rotatable bonds connecting any two ring systems. Most importantly, they exhibit dramatic structure-activity relationships (SARs). For example, almost all ATP competitive kinase inhibitors satisfy at least one of the hydrogen bonds that is made between the adenine ring of ATP and the kinase [62]. Substitution of this hydrogen bonding atom can result in a ~1000-fold loss in affinity.

Many non-specific kinase inhibitors share a distinct set of structural features (Figure 1.5A). Promiscuous compounds often have dye-like structures – flat, highly conjugated polyaromatic systems. These compounds tend to be hydrophobic, bind proteins non-specifically, and aggregate at high concentrations [63]. Certain chemical moieties, such as catechols, are commonly found in low specificity inhibitors such as many flavones and tyrphostins. Catechols have been shown to undergo cellular oxidation to generate more reactive species that probably account for some of the *in vivo* activity of these molecules [64, 65]. This oxidation can also be catalyzed *in vitro* by manganese, a common component of many kinase assay buffers, and this has been shown to contribute to the biochemical potency of catechols from four different scaffold classes [66]. Another feature common to low specificity kinase inhibitors is a plane or axis of symmetry. Although symmetric molecules are prevalent in screening libraries, kinase active sites are asymmetric. For this reason, symmetry is usually an indication that a molecule has not undergone target-directed chemical optimization.

Shoichet and co-workers have defined a mechanism for non-specific inhibition *in vitro* that involves the formation of submicrometer aggregates [63, 67]. This aggregate formation is time-dependent, sensitive to protein concentration, and reversible by detergents, and may form the basis for the *in vitro* activity of low specificity kinase inhibitors such as quercetin and rottlerin [67]. However, it is important to emphasize that this type of aggregation has been observed only at micromolar concentrations. For an ATP competitive kinase inhibitor, a micromolar K_i alone is compelling evidence that the compound is not selective.

Kinase inhibitors containing electrophiles, such as Michael acceptors or α-haloketones, generally exhibit poor stability and increased off-target effects. For example, the electrophilic natural product wortmannin has a half-life in tissue culture media of ~10 minutes [68], whereas vinyl nitriles, such as those found in U0126, can undergo rearrangements on storage in DMSO [69]. While electrophiles are frequent hits from screening libraries, it is generally not possible to optimize these leads, as their activity is based on more chemical reactivity rather than target-specific contacts [70]. Nonetheless, recent examples of selective electrophilic inhibitors have been reported [71, 72]. An essential feature of these compounds is that they possess a core scaffold that binds reversibly to the kinase with moderately high affinity ($K_i < 1\ \mu M$). This scaffold then positions a relatively deactivated electrophile in proximity to a nucleophilic residue found in a subset of targets in the kinase superfamily. Absent this tight binding, reversible core structure, it is not possible to attain a high degree of selectivity with an irreversible inhibitor.

1.4.2 Inhibitor selectivity is measured *in vitro*

The target selectivity of a kinase inhibitor is typically measured by profiling its activity against a panel of kinases *in vitro*. Kinases most closely related in primary sequence are most likely to share inhibitor sensitivity [73] and these are the most important targets to test. In some cases, impressive selectivity against a panel of closely related kinases can suggest a high degree of selectivity against the remainder of the kinome. For example, BAY 61-3606 inhibits Syk with a K_i of 7.5 nM, and exhibits ≥1000-fold selectivity against the related tyrosine kinases Src, Fyn, Lck, Btk, and Itk, suggestive of a high degree of selectivity against less similar kinases [74]. In most cases, it is important to sample a broad range of kinases from different kinase subfamilies. Two valuable studies have profiled many of the most commonly used kinase inhibitors against 28 protein kinases in this way [75, 76].

The limitation of this approach is that even the largest kinase panels test only ~20% of the kinome, and therefore may miss important targets (although for smaller families, such as the lipid kinases, near-exhaustive coverage is feasible [13]). Despite this limitation, specific features beyond sequence homology have been identified that predict kinase inhibition, and these can be used to select the best targets for testing. For example, the size of a single amino acid in the ATP binding pocket – termed the gatekeeper residue – has been shown to be a critical determinant of inhibitor sensitivity [77, 78]. Kinases with a threonine at this position are sensitive to a range of inhibitors, whereas those with a larger residue are broadly resistant. Approximately 50% of tyrosine kinases contain a threonine gatekeeper, compared to 10% of serine-threonine kinases. For this reason, serine-threonine kinases that possess a threonine gatekeeper (for example, Raf and p38α) are often sensitive to tyrosine kinase inhibitors, and vice versa [77, 79]. In the same way, certain pairs of kinases are known to exhibit similar pharmacological profiles (so-called SAR homology [80]). For example, GSK3β inhibitors often inhibit CDKs and TGFβ-R inhibitors frequently inhibit p38α, even though these pairs of kinases possess limited sequence homology. Likewise, there is growing appreciation that PI3-K inhibitors tend to inhibit the related protein kinase DNA-PK much more frequently than other PI3-K related kinases (PIKKs) such as ATM and ATR [13, 81].

Affinity chromatography offers a way of identifying inhibitor targets that is complementary to *in vitro* measurements. In this approach, the inhibitor is linked to solid support and used to enrich for cellular binding proteins, which are then identified by mass spectrometry. This approach has been successfully used to identify unexpected cellular targets of kinase inhibitors such as SB203580, which was shown to inhibit RICK more potently than its known target, p38α [79]. Improvements in methodology have made this an increasingly viable strategy for target identification; immobilized pyrido[2,3-d]pyrimidines have recently been used to enrich for over 20 kinases from cell lysates [82]. A limitation of affinity chromatography, however, is that it is biased toward more abundant proteins. Four kinase families – CDKs [83-87], CK1 isoforms [79, 83], MAP kinases [79, 83-85, 88], and GSK3β [79, 84, 87, 89] – account for a disproportionate fraction of the kinase targets that have been identified by affinity-based approaches. This reflects, in part, the relative cellular abundance of these proteins, each of which is an ortholog of one of the most highly expressed kinases in yeast (Figure 1.4B). Consistent with this view, subsequent biochemical analysis often reveals that the bait compound inhibits these kinases weakly in solution [79, 83, 85, 87, 88]. For this reason, affinity chromatography may identify new targets of an inhibitor, but does not validate inhibitor specificity.

1.4.3 Selectivity depends on potency

There are on the order of 20,000 unique protein receptors in the cell, and it is impossible to test any significant fraction of these targets. At high compound concentrations, it becomes increasingly likely that an inhibitor will bind to these off-target sites. For this reason, the practical selectivity of a compound depends on its potency – more potent compounds are more selective, because they can be used at a lower dose. This is also true within the protein kinase family, where there is a strong correlation between inhibitor potency and selectivity [80]. An important corollary of this fact is that there is a minimum threshold of potency without which a molecule *cannot* be selective, irrespective of any *in vitro* data.

The PI3-K inhibitors LY294002 and wortmannin illustrate this point. Both have been extensively profiled *in vitro*, and show similar specificity profiles at their respective concentration ranges. These two compounds inhibit the class I PI3K's most potently, with mixed activity against the other PI3-K family members [13] and an off-target activity against two protein kinases: CK2 (LY294002), sMLCK (wortmannin), and PLK1 (both) [90]. Yet these compounds are not equally selective in cells, because wortmannin is used at 1000-fold lower concentrations. Several new targets of LY294002 have recently been identified, including calcium channels, potassium channels, phosphodiesterases, and the estrogen receptor [91-94], and these are inhibited in the concentration range that is commonly used to inhibit PI3-Ks. A similar spectrum of targets has not been identified for wortmannin *at the low nanomolar concentrations* at which it inhibits PI3-Ks.

We have proposed guidelines for estimating the likelihood of off-target effects across different concentration ranges (Figure 1.5B). This estimation is based in part on the observation that the fraction of small molecules that bind to a protein *in vitro* is generally low at nanomolar concentrations, but increases dramatically above ~10 μM. This is structure-dependent – certain compound classes are more promiscuous than others [95, 96]. Most selective kinase inhibitors have low nanomolar K_i values, and so are applied to cells at concentrations less than 10 μM, reducing the likelihood of off-target effects. Unfortunately, many of earliest and most commonly used kinase inhibitors are significantly less potent, and conclusions based on the use of these reagents are suspect. Compounds used at concentrations above 100 μM (for example, the PIKK inhibitor caffeine) are unlikely to have any significant selectivity.

1.4.4 A new generation of allosteric kinase inhibitors

Most kinase inhibitors are ATP competitive, which reflects the fact that ATP binding pocket presents a large hydrophobic surface that can bind small molecules with high affinity. It is much more difficult to find compounds that bind to other regions of protein kinases. However, in some cases it has been possible to identify such molecules, and, once identified, they possess advantages over their ATP competitive counterparts. As these inhibitors do not compete with cellular ATP, they can typically be used at concentrations closer to their biochemical K_i. Also, residues outside the ATP binding pocket tend to be less conserved, opening the possibility for greater selectivity. In certain cases non-competitive inhibitors can be substrate selective, inhibiting the activity of a kinase against only a subset of its targets.

The first non-competitive kinase inhibitor to be discovered was rapamycin, a cyclic macrolide natural product that inhibits the protein kinase mTOR. Rapamycin acts by binding to the ubiquitously expressed protein FKBP [97], and it is this rapamycin-FKBP complex that binds to the FRB domain of mTOR [98, 99]. The FRB domain is N-terminal to the mTOR kinase domain, and it is not understood how this binding event inhibits mTOR activity [100]. In cells, mTOR resides as part of two large (~ 2 MDa) protein complexes, termed mTORC1 and mTORC2 [101, 102]. Remarkably, only the first of these complexes is rapamycin sensitive. mTORC1 signals to increase translation in response to nutrients and growth factors, and this complex can be isolated by immobilized rapamycin-FKBP [101, 102]. mTORC2 signals to the actin cytoskeleton in response to the same stimuli, and this complex is rapamycin insensitive [101, 102].

Compound	Primary Target	Selectivity	Cellular Activity/Binding Mode
BAY 61-3606	Syk: $K_i = 7.5$ nM	700 to >1000-fold for Src, Lyn, Fyn, Itk, and Btk	Blocks cytokine release from mast cells at low nanomolar concentrations
BMS-509744	Itk: $K_i = 16$ nM	50-100-fold for IR, Fyn, Lck, Btk; ≥ 1000-fold for 14 other kinases	Blocks IL-2, proliferation in T-cells at mid-nanomolar concentations
CP-690550	JAK3: $K_i \sim 1$ nM	20 and 100-fold for JAK2 and JAK1; >3000-fold for other 30 kinases	Blocks IL-2 induced T-cell proliferation at 11 nM
BIRB-796	p38α: $K_i = 0.097$ nM	>1000-fold against 13 other kinases	Blocks TNFα release in THP-1 cells at 18 nM; binds inactive conformation
BMS-243117	Lck: $K_i \cong 4$ nM	32, 60, and 84-fold for Fyn, Fgr, and Blk; >150-fold for other Src family kinases, >6000-fold for other PKs	Blocks T-cell proliferation at 1.1 μM
BMS-345541	IKK-2: $K_i \cong 300$ nM	10-fold for IKK-1; >300-fold for 15 other kinases	Allosteric, non-ATP competitive; blocks IκBα phosphorylation in cells at 4 μM
Pyrazinone 13b	Akt1: $K_i \cong 760$ nM	30-fold against Akt2; >100-fold against other AGC kinases	Allosteric, non-ATP competitive; pro-apoptotic in A2780 cells at 12 μM
Pyrazinone 14f	Akt2: $K_i \cong 325$ nM	65-fold against Akt1; >100-fold against other AGC kinases	Allosteric, non-ATP competitive; pro-apoptotic in A2780 cells at 12 μM
Naphthyridine 19	ALK5: $K_i \cong 4$ nM	>4000-fold against 9 other kinases including p38α	Blocks TGFβ induced reporter gene transcription at 18 nM
STI-571 (Imatinib, Gleevec)	Bcr-Abl: $K_i = 14$ nM	Inhibits PDGFR and c-Kit at similar concentrations; >1000-fold for many other kinases	Binds to the inactive conformation; active in cells at ~ 1 μM
ZD1839 (Gefitinib, Iressa)	EGFR: $K_i \cong 0.4$ nM	>50-fold selectivity against ErbB-2 and ErbB-4; >1000-fold for many other kinases	Similar in structure and selectivity to OSI-774 (Tarceva)
BAY 43-9006	B-Raf: $K_i = 22$ nM	Inhibits PDGFR, c-Kit, Flt-3, and VEGFR at similar concentrations; >1000-fold for many other kinases	Binds to the inactive conformation; active in cells at 0.1 to 1 μM
KU-55933	ATM: $K_i = 2.2$ nM	>100-fold selectivity against other PI3-Ks; >1000-fold selectivity against 60 protein kinases	Blocks p53 phosphorylation induced by ionizing radition at ~ 300 nM; radiosensitizes cells at ~ 10 μM
IC87114	p110δ: $K_i \cong 20$ nM	≥ 100-fold selectivity against all other PI3-Ks and many protein kinases	Active in cells at 0.1 to 5 μM

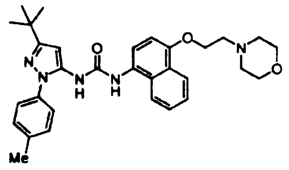

BIRB-796

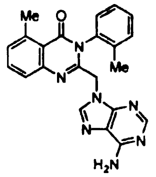

IC87114

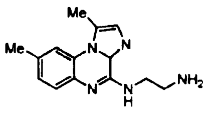

BMS-345541

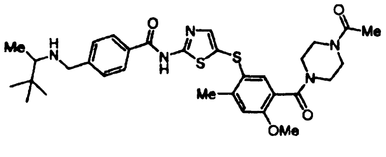

BMS-509744

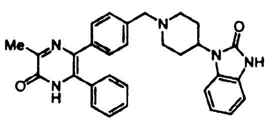

Pyrazinone 13b

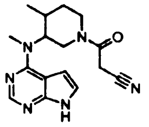

CP-690550

Figure 1.6. Recent examples of selective kinase inhibitors.

Potent, ATP competitive inhibitors of mTOR have not been reported, but such compounds will be an important tool for elucidating signaling through mTORC2.

The MEK1 inhibitor PD098059 was the first synthetic non-competitive kinase inhibitor to be described [103]. This compound acts by binding to inactive MEK1 and preventing its phosphorylation by the upstream kinase Raf [104]. The key to the discovery of this compound was the use of a biochemical screen based on reconstitution of the MAP kinase cascade *in vitro*; since this screen utilized a low activity form of MEK1, it was possible to identify a non-competitive inhibitor of MEK1 activation [104]. Several subsequent allosteric inhibitors of MEK1 and MEK2 have been described, including U0126 and PD184352 [105, 106]. The recent crystal structure of a PD184352 analog in complex with MEK1 confirms that these compounds bind to a site adjacent to, but not overlapping with, the ATP binding pocket [107]. Moreover, the low degree of sequence conservation in this region of the kinase explains the high selectivity of these compounds [107].

For many years, the MEK inhibitors were an isolated example of potent, synthetic kinase inhibitors that bind to an allosteric site. Recently, however, several new allosteric inhibitors have been described. Scientists from Merck have reported several classes of compounds, including a series of pyrazinones (Figure 1.6), which are allosteric inhibitors of Akt. These compounds are non-competitive with ATP, show selectivity between the isoforms Akt1 and Akt2, and bind to a region that includes the Akt PH domain [4]. BMS-345541 has been reported as an allosteric inhibitor of IKK-2 that displays potent activity in an animal model of inflammation [5] (Figure 1.6). Several classes of nanomolar non-competitive inhibitors of p38α have recently been described, along with extensive structural and biophysical characterization of their binding sites [3, 108]. Remarkably, at least one of these compounds is substrate selective, blocking p38α phosphorylation of MAPKAP2 but not ATF-2 [108].

1.5 The intersection of pharmacology and genetics

1.5.1 Target validation with resistant and analog-sensitive alleles

The classic way to confirm the phenotypically relevant target of a small molecule is to use a mutant allele of the kinase that has altered sensitivity to the inhibitor. For example, the TOR proteins were identified as the target of rapamycin through a screen for yeast mutants resistant to rapamycin [98]. Ecoptic expression of inhibitor-resistant allele of p38α has been used to confirm that p38α is the target of SB203580-mediated blockade of certain inflammatory responses [109]. Most recently, the identification of Bcr-Abl mutations that block Imatinib binding from CML patients refractory to Imatinib treatment confirms that Bcr-Abl is a clinically relevant target of this molecule [110].

A related approach is to use a kinase allele that is sensitive to a small molecule inhibitor that does not inhibit any wild-type kinase. For protein kinases, mutation of the gatekeeper residue to alanine or glycine can generate such analog-sensitive (as) kinase alleles [111]. By replacing the endogenous copy of the kinase with the as-allele, the effects of inhibiting that kinase in a model system can be studied using a highly specific inhibitor. A key feature of this approach is that it is possible to directly confirm that the phenotype is due to inhibition of the as-kinase by performing a control experiment in which cells expressing the wild-type kinase are treated with the same inhibitor.

Resistant and analog-sensitive alleles are complementary approaches to studying kinase function. The former asks whether inhibition of a kinase is necessary for a phenotype, whereas the latter asks if it is sufficient. Resistance mutations are typically used in the last stages of target validation, after an inhibitor, phenotype, and putative kinase target have been identified. By contrast, analog-sensitive alleles can be used in a discovery setting to identify new biological processes that are sensitive to inhibition of a specific kinase.

1.5.2 Knockouts and inhibitors can yield different phenotypes

Genetic techniques such as RNAi and knockout animals offer an alternative to small molecule inhibitors to study kinase function. RNAi in particular has great utility because it can be used to rapidly inactivate specific genes in cell culture. It is frequently proposed that RNAi might be used to validate targets for small molecule inhibition or confirm results from pharmacological experiments. Is this reasonable? Setting aside the fact that RNAi is itself a pharmacological intervention – with its own dose-dependent specificity limitations [112] – this belief reflects an underlying assumption that genetic knock-down of a kinase should phenocopy small molecule inhibition [113].

There are many reasons to conclude this is incorrect [114]. Most kinases are multi-domain proteins, and these other domains often possess kinase-independent functions [115, 116]. In some cases, the kinase domain itself has non-catalytic activity [117, 118]. It would be difficult to construct an accurate genetic model for an inhibitor such as rapamycin, which blocks a subset of mTOR's cellular functions by a complex mechanism, yet this compound was the first small molecule kinase inhibitor approved for clinical use [119]. Most importantly, knockout mice for many kinases have surprisingly few detectable phenotypes [120] – indicating that other kinases may be able to mask the function of the knocked-out gene through compensation [121, 122].

Chemical inhibition of as-kinase alleles makes it possible to directly compare phenotypes of chemical and genetic kinase knockouts, using inhibitors that have validated "single-target" specificity. These experiments indicate that small molecule kinase inhibitors rarely, if ever, precisely phenocopy the corresponding gene knockout

Kinase	Knockout phenotype	Inhibition phenotype	Proposed explanation
CDC28	CDC28-ts allele arrests in G1 at restrictive temperature	Inhibition of the CDC28-as1 allele induces arrest at G2/M at low doses, and G1 at high doses	The mitotic checkpoint is more sensitive to CDK activity than the G1 checkpoint
Ire1	Ire1Δ or Ire1-kd cells have defective unfolded protein response (UPR)	Inhibition of an Ire1-as allele that also contains a kd mutation permits the UPR	An ATP competitive inhibitor of Ire1 permits activation of its RNAse domain during the UPR
Apg1	Apg1Δ cells are defective in cytoplasm to vacuole targeting (Cvt) as well as autophagy	Inhibition of Apg1-as allele or expression of Apg1-kd blocks Cvt, but not autophagy	Cvt requires the catalytic activity of Apg1, whereas autophagy requires a scaffolding function
Cla4	Cla4Δ cells have defective septin localization to the bud neck	Inhibition of Cla4-as allele has no effect on septin localization	Septin localization may depend on a scaffolding function of Cla4
Elm1	Elm1Δ cells undergo G_2/M delay	Inhibition of elm1-as allele results in G1 delay in bud emergence and Cln2 synthesis, as well as G_2/M defect	Compensation for G1 defect in elm1Δ cells by accummulation of suppressors during culture
p110γ	p110γ -/- mice show increased cardiac contractility and tissue damage	p110γ-kd mice have normal cardiac function	p110γ interacts with PDE3B and regulates heart contractility independent of kinase activity

Table 1.2. Examples of chemical and genetic kinase knockouts that produce different phenotypes [111, 116, 117, 123-125].

(Table 1.2). The knockout frequently elicits phenotypes not observed with the inhibitor [123, 125] (likely due to non-catalytic, scaffolding functions of the kinase); the inhibitor induces phenotypes not observed in the knockout [111, 124] (likely due to compensation for the knockout by a homologous kinase); and, in at least one case, the inhibitor elicits the exact opposite phenotype as the knockout [117] (due to a non-catalytic, allosteric role of the kinase domain in signal propagation). These observations mirror studies comparing knockout mice and with mice expressing a kinase-dead allele (which better mimics the effects of a small molecule inhibitor). In many cases, the phenotypes are quite different [116, 126-128].

An additional layer of complexity arises from the fact that very few inhibitors target a single protein kinase, and the biological activity of these molecules may depend on a complex balance of inhibition of multiple targets. For example, CML, as a disease characterized by the chromosomal translocation that generates the Bcr-Abl oncogene, may define the simplest link between genotype and kinase inhibition phenotype. Yet it is clear that Imatinib's activity requires more than Bcr-Abl inhibition in some settings. The Imatinib sensitivity of murine myeloid leukemia cells that express both Bcr-Abl and c-Kit is dependent on Imatinib's ability to inhibit c-Kit [129]. Inhibition of Bcr-Abl is necessary, but not sufficient, to induce apoptosis in these cells. In this case, the Imatinib activity against c-Kit was an unintended by-product of the drug discovery process, and this sort of multi-targeted activity would be challenging to engineer into a compound based on predictive genetic models. Similarly, combined inhibition of Kin28 and Srb10 as-alleles yields a synergistic inhibition of RNA-polymerase II mediated gene transcription that cannot be predicted by single gene inactivation [130].

1.6 Why bother?

It is not easy to use kinase inhibitors to dissect signaling pathways with high selectivity. A great deal of focused, target-driven chemistry is required to find a single potent compound. The scale of this task is such that the best compounds today are developed largely by the pharmaceutical industry. Once a potent compound is identified, its selectivity must be extensively characterized *in vitro* for it to have any real usefulness – and even then, it is impossible to test all of the potential targets. We have proposed guidelines for evaluating kinase inhibitor selectivity, but, even in the best case, the possibility of confounding off-target effects cannot be eliminated.

Is there any good reason to use small molecule kinase inhibitors rather than competing genetic approaches, such as RNAi? We have emphasized that these two types of reagents perturb signaling pathways in different ways and therefore can give different outcomes. Small molecules can inhibit catalytic activity without affecting other protein domains that might be disrupted by a knockout. Small molecules are also fast-acting and reversible, and thereby can escape cellular compensation that might mask a relevant phenotype.

Perhaps the best reason to use kinase inhibitors to study signal transduction is so that we might understand the inhibitors themselves. The major barrier to developing new drugs is target validation [114, 131] – the challenge of predicting how inhibition of a target will translate into phenotype in a physiological setting. Different types of approaches can contribute to solving this problem, but pharmacology occupies a privileged position because it is the ultimate mode of intervention. No disease can be treated with a mutation (yet), and no genetic experiment can reliably predict the outcome of targeting a pathway with a small molecule. For this reason, it is critical to understand how potent and selective kinase inhibitors function in physiologically relevant model systems, even if the specific molecules themselves are not destined to be drugs. The emergence of a new generation of kinase inhibitors presents a unique opportunity to do this – by using these reagents to systematically re-define signaling pathways according to their pharmacological properties.

1.7 References

1. Druker, B.J. (2004). Molecularly targeted therapy: have the floodgates opened? Oncologist *9*, 357-360.

2. Cohen, P. (1999). The development and therapeutic potential of protein kinase inhibitors. Curr Opin Chem Biol *3*, 459-465.

3. Pargellis, C., Tong, L., Churchill, L., Cirillo, P.F., Gilmore, T., Graham, A.G., Grob, P.M., Hickey, E.R., Moss, N., Pav, S., and Regan, J. (2002). Inhibition of p38 MAP kinase by utilizing a novel allosteric binding site. Nat Struct Biol *9*, 268-272.

4. Barnett, S.F., Defeo-Jones, D., Fu, S., Hancock, P.J., Haskell, K.M., Jones, R.E., Kahana, J.A., Kral, A.M., Leander, K., Lee, L.L., Malinowski, J., McAvoy, E.M., Nahas, D.D., Robinson, R.G., and Huber, H.E. (2004). Identification and characterization of pleckstrin homology domain dependent and isozyme specific Akt inhibitors. Biochem J *Pt*.

5. Burke, J.R., Pattoli, M.A., Gregor, K.R., Brassil, P.J., MacMaster, J.F., McIntyre, K.W., Yang, X., Iotzova, V.S., Clarke, W., Strnad, J., Qiu, Y., and Zusi, F.C. (2003). BMS-345541 is a highly selective inhibitor of I kappa B kinase that binds at an allosteric site of the enzyme and blocks NF-kappa B-dependent transcription in mice. J Biol Chem *278*, 1450-1456.

6. Arnold, L.D., Calderwood, D.J., Dixon, R.W., Johnston, D.N., Kamens, J.S., Munschauer, R., Rafferty, P., and Ratnofsky, S.E. (2000). Pyrrolo[2,3-d]pyrimidines containing an extended 5-substituent as potent and selective inhibitors of lck I. Bioorg Med Chem Lett *10*, 2167-2170.

7. Sadhu, C., Dick, K., Tino, W.T., and Staunton, D.E. (2003). Selective role of PI3K delta in neutrophil inflammatory responses. Biochem Biophys Res Commun *308*, 764-769.

8. Changelian, P.S., Flanagan, M.E., Ball, D.J., Kent, C.R., Magnuson, K.S., Martin, W.H., Rizzuti, B.J., Sawyer, P.S., Perry, B.D., Brissette, W.H., McCurdy, S.P., Kudlacz, E.M., Conklyn, M.J., Elliott, E.A., Koslov, E.R., Fisher, M.B., Strelevitz, T.J., Yoon, K., Whipple, D.A., Sun, J., Munchhof, M.J., Doty, J.L., Casavant, J.M., Blumenkopf, T.A., Hines, M., Brown, M.F., Lillie, B.M., Subramanyam, C., Shang-Poa, C., Milici, A.J., Beckius, G.E., Moyer, J.D., Su, C., Woodworth, T.G., Gaweco, A.S., Beals, C.R., Littman, B.H., Fisher, D.A., Smith, J.F., Zagouras, P., Magna, H.A., Saltarelli, M.J., Johnson, K.S., Nelms, L.F., Des Etages, S.G., Hayes, L.S., Kawabata, T.T., Finco-Kent, D., Baker, D.L., Larson, M., Si, M.S., Paniagua, R., Higgins, J., Holm, B., Reitz, B., Zhou, Y.J., Morris, R.E., O'Shea,

J.J., and Borie, D.C. (2003). Prevention of organ allograft rejection by a specific Janus kinase 3 inhibitor. Science *302*, 875-878.

9. Lin, T.A., McIntyre, K.W., Das, J., Liu, C., O'Day, K.D., Penhallow, B., Hung, C.Y., Whitney, G.S., Shuster, D.J., Yang, X., Townsend, R., Postelnek, J., Spergel, S.H., Lin, J., Moquin, R.V., Furch, J.A., Kamath, A.V., Zhang, H., Marathe, P.H., Perez-Villar, J.J., Doweyko, A., Killar, L., Dodd, J.H., Barrish, J.C., Wityak, J., and Kanner, S.B. (2004). Selective Itk inhibitors block T-cell activation and murine lung inflammation. Biochemistry *43*, 11056-11062.

10. Cheng, Y., and Prusoff, W.H. (1973). Relationship between the inhibition constant (K1) and the concentration of inhibitor which causes 50 per cent inhibition (I50) of an enzymatic reaction. Biochem Pharmacol *22*, 3099-3108.

11. Traut, T.W. (1994). Physiological concentrations of purines and pyrimidines. Mol Cell Biochem *140*, 1-22.

12. Gribble, F.M., Loussouarn, G., Tucker, S.J., Zhao, C., Nichols, C.G., and Ashcroft, F.M. (2000). A novel method for measurement of submembrane ATP concentration. J Biol Chem *275*, 30046-30049.

13. Knight, Z.A., Chiang, G.G., Alaimo, P.J., Kenski, D.M., Ho, C.B., Coan, K., Abraham, R.T., and Shokat, K.M. (2004). Isoform-specific phosphoinositide 3-kinase inhibitors from an arylmorpholine scaffold. Bioorg Med Chem *12*, 4749-4759.

14. Dennis, P.B., Jaeschke, A., Saitoh, M., Fowler, B., Kozma, S.C., and Thomas, G. (2001). Mammalian TOR: a homeostatic ATP sensor. Science *294*, 1102-1105.

15. Downing, G.J., Kim, S., Nakanishi, S., Catt, K.J., and Balla, T. (1996). Characterization of a soluble adrenal phosphatidylinositol 4-kinase reveals wortmannin sensitivity of type III phosphatidylinositol kinases. Biochemistry *35*, 3587-3594.

16. Zhao, X.H., Bondeva, T., and Balla, T. (2000). Characterization of recombinant phosphatidylinositol 4-kinase beta reveals auto- and heterophosphorylation of the enzyme. J Biol Chem *275*, 14642-14648.

17. Suer, S., Sickmann, A., Meyer, H.E., Herberg, F.W., and Heilmeyer, L.M., Jr. (2001). Human phosphatidylinositol 4-kinase isoform PI4K92. Expression of the recombinant enzyme and determination of multiple phosphorylation sites. Eur J Biochem *268*, 2099-2106.

18. Hawkins, J., Zheng, S., Frantz, B., and LoGrasso, P. (2000). p38 map kinase substrate specificity differs greatly for protein and peptide substrates. Arch Biochem Biophys *382*, 310-313.

19. Tian, G., Kane, L.S., Holmes, W.D., and Davis, S.T. (2002). Modulation of cyclin-dependent kinase 4 by binding of magnesium (II) and manganese (II). Biophys Chem *95*, 79-90.

20. Sondhi, D., Xu, W., Songyang, Z., Eck, M.J., and Cole, P.A. (1998). Peptide and protein phosphorylation by protein tyrosine kinase Csk: insights into specificity and mechanism. Biochemistry *37*, 165-172.

21. Schindler, T., Bornmann, W., Pellicena, P., Miller, W.T., Clarkson, B., and Kuriyan, J. (2000). Structural mechanism for STI-571 inhibition of abelson tyrosine kinase. Science *289*, 1938-1942.

22. Wan, P.T., Garnett, M.J., Roe, S.M., Lee, S., Niculescu-Duvaz, D., Good, V.M., Jones, C.M., Marshall, C.J., Springer, C.J., Barford, D., and Marais, R. (2004). Mechanism of activation of the RAF-ERK signaling pathway by oncogenic mutations of B-RAF. Cell *116*, 855-867.

23. Frantz, B., Klatt, T., Pang, M., Parsons, J., Rolando, A., Williams, H., Tocci, M.J., O'Keefe, S.J., and O'Neill, E.A. (1998). The activation state of p38 mitogen-activated protein kinase determines the efficiency of ATP competition for pyridinylimidazole inhibitor binding. Biochemistry *37*, 13846-13853.

24. Fraley, M.E., Hoffman, W.F., Rubino, R.S., Hungate, R.W., Tebben, A.J., Rutledge, R.Z., McFall, R.C., Huckle, W.R., Kendall, R.L., Coll, K.E., and Thomas, K.A. (2002). Synthesis and initial SAR studies of 3,6-disubstituted pyrazolo[1,5-a]pyrimidines: a new class of KDR kinase inhibitors. Bioorg Med Chem Lett *12*, 2767-2770.

25. Bilodeau, M.T., Cunningham, A.M., Koester, T.J., Ciecko, P.A., Coll, K.E., Huckle, W.R., Hungate, R.W., Kendall, R.L., McFall, R.C., Mao, X., Rutledge, R.Z., and Thomas, K.A. (2003). Design and synthesis of 1,5-diarylbenzimidazoles as inhibitors of the VEGF-receptor KDR. Bioorg Med Chem Lett *13*, 2485-2488.

26. Fraley, M.E., Arrington, K.L., Hambaugh, S.R., Hoffman, W.F., Cunningham, A.M., Young, M.B., Hungate, R.W., Tebben, A.J., Rutledge, R.Z., Kendall, R.L., Huckle, W.R., McFall, R.C., Coll, K.E., and Thomas, K.A. (2003). Discovery and evaluation of 3-(5-thien-3-ylpyridin-3-yl)-1H-indoles as a novel class of KDR kinase inhibitors. Bioorg Med Chem Lett *13*, 2973-2976.

27. Manley, P.J., Balitza, A.E., Bilodeau, M.T., Coll, K.E., Hartman, G.D., McFall, R.C., Rickert, K.W., Rodman, L.D., and Thomas, K.A. (2003). 2,4-disubstituted pyrimidines: a novel class of KDR kinase inhibitors. Bioorg Med Chem Lett *13*, 1673-1677.

28. Murata, T., Shimada, M., Sakakibara, S., Yoshino, T., Kadono, H., Masuda, T., Shimazaki, M., Shintani, T., Fuchikami, K., Sakai, K., Inbe, H., Takeshita, K., Niki, T., Umeda, M., Bacon, K.B., Ziegelbauer, K.B., and Lowinger, T.B. (2003). Discovery of novel and selective IKK-beta serine-threonine protein kinase inhibitors. Part 1. Bioorg Med Chem Lett *13*, 913-918.

29. Murata, T., Shimada, M., Sakakibara, S., Yoshino, T., Masuda, T., Shintani, T., Sato, H., Koriyama, Y., Fukushima, K., Nunami, N., Yamauchi, M., Fuchikami, K., Komura, H., Watanabe, A., Ziegelbauer, K.B., Bacon, K.B., and Lowinger, T.B. (2004). Synthesis and structure-activity relationships of novel IKK-beta inhibitors.

Part 3: Orally active anti-inflammatory agents. Bioorg Med Chem Lett *14*, 4019-4022.

30. Baxter, A., Brough, S., Cooper, A., Floettmann, E., Foster, S., Harding, C., Kettle, J., McInally, T., Martin, C., Mobbs, M., Needham, M., Newham, P., Paine, S., St-Gallay, S., Salter, S., Unitt, J., and Xue, Y. (2004). Hit-to-lead studies: the discovery of potent, orally active, thiophenecarboxamide IKK-2 inhibitors. Bioorg Med Chem Lett *14*, 2817-2822.

31. Burchat, A.F., Calderwood, D.J., Friedman, M.M., Hirst, G.C., Li, B., Rafferty, P., Ritter, K., and Skinner, B.S. (2002). Pyrazolo[3,4-d]pyrimidines containing an extended 3-substituent as potent inhibitors of Lck -- a selectivity insight. Bioorg Med Chem Lett *12*, 1687-1690.

32. Goldberg, D.R., Butz, T., Cardozo, M.G., Eckner, R.J., Hammach, A., Huang, J., Jakes, S., Kapadia, S., Kashem, M., Lukas, S., Morwick, T.M., Panzenbeck, M., Patel, U., Pav, S., Peet, G.W., Peterson, J.D., Prokopowicz, A.S., 3rd, Snow, R.J., Sellati, R., Takahashi, H., Tan, J., Tschantz, M.A., Wang, X.J., Wang, Y., Wolak, J., Xiong, P., and Moss, N. (2003). Optimization of 2-phenylaminoimidazo[4,5-h]isoquinolin-9-ones: orally active inhibitors of lck kinase. J Med Chem *46*, 1337-1349.

33. Chen, P., Doweyko, A.M., Norris, D., Gu, H.H., Spergel, S.H., Das, J., Moquin, R.V., Lin, J., Wityak, J., Iwanowicz, E.J., McIntyre, K.W., Shuster, D.J., Behnia, K., Chong, S., de Fex, H., Pang, S., Pitt, S., Shen, D.R., Thrall, S., Stanley, P., Kocy, O.R., Witmer, M.R., Kanner, S.B., Schieven, G.L., and Barrish, J.C. (2004). Imidazoquinoxaline Src-family kinase p56Lck inhibitors: SAR, QSAR, and the discovery of (S)-N-(2-chloro-6-methylphenyl)-2-(3-methyl-1-piperazinyl)imidazo- [1,5-a]pyrido[3,2-e]pyrazin-6-amine (BMS-279700) as a potent and orally active inhibitor with excellent in vivo antiinflammatory activity. J Med Chem *47*, 4517-4529.

34. Das, J., Lin, J., Moquin, R.V., Shen, Z., Spergel, S.H., Wityak, J., Doweyko, A.M., DeFex, H.F., Fang, Q., Pang, S., Pitt, S., Shen, D.R., Schieven, G.L., and Barrish, J.C. (2003). Molecular design, synthesis, and structure-Activity relationships leading to the potent and selective p56(lck) inhibitor BMS-243117. Bioorg Med Chem Lett *13*, 2145-2149.

35. Chen, P., Norris, D., Das, J., Spergel, S.H., Wityak, J., Leith, L., Zhao, R., Chen, B.C., Pitt, S., Pang, S., Shen, D.R., Zhang, R., De Fex, H.F., Doweyko, A.M., McIntyre, K.W., Shuster, D.J., Behnia, K., Schieven, G.L., and Barrish, J.C. (2004). Discovery of novel 2-(aminoheteroaryl)-thiazole-5-carboxamides as potent and orally active Src-family kinase p56(Lck) inhibitors. Bioorg Med Chem Lett *14*, 6061-6066.

36. Kendall, R.L., Rutledge, R.Z., Mao, X., Tebben, A.J., Hungate, R.W., and Thomas, K.A. (1999). Vascular endothelial growth factor receptor KDR tyrosine kinase activity is increased by autophosphorylation of two activation loop tyrosine residues. J Biol Chem *274*, 6453-6460.

37. Parast, C.V., Mroczkowski, B., Pinko, C., Misialek, S., Khambatta, G., and Appelt, K. (1998). Characterization and kinetic mechanism of catalytic domain of human vascular endothelial growth factor receptor-2 tyrosine kinase (VEGFR2 TK), a key enzyme in angiogenesis. Biochemistry *37*, 16788-16801.

38. Sadler, T.M., Achilleos, M., Ragunathan, S., Pitkin, A., LaRocque, J., Morin, J., Annable, R., Greenberger, L.M., Frost, P., and Zhang, Y. (2004). Development and comparison of two nonradioactive kinase assays for I kappa B kinase. Anal Biochem *326*, 106-113.

39. Li, J., Peet, G.W., Pullen, S.S., Schembri-King, J., Warren, T.C., Marcu, K.B., Kehry, M.R., Barton, R., and Jakes, S. (1998). Recombinant IkappaB kinases alpha and beta are direct kinases of Ikappa Balpha. J Biol Chem *273*, 30736-30741.

40. Mercurio, F., Murray, B.W., Shevchenko, A., Bennett, B.L., Young, D.B., Li, J.W., Pascual, G., Motiwala, A., Zhu, H., Mann, M., and Manning, A.M. (1999). IkappaB kinase (IKK)-associated protein 1, a common component of the heterogeneous IKK complex. Mol Cell Biol *19*, 1526-1538.

41. Kishore, N., Huynh, Q.K., Mathialagan, S., Hall, T., Rouw, S., Creely, D., Lange, G., Caroll, J., Reitz, B., Donnelly, A., Boddupalli, H., Combs, R.G., Kretzmer, K., and Tripp, C.S. (2002). IKK-i and TBK-1 are enzymatically distinct from the homologous enzyme IKK-2: comparative analysis of recombinant human IKK-i, TBK-1, and IKK-2. J Biol Chem *277*, 13840-13847.

42. Huynh, Q.K., Boddupalli, H., Rouw, S.A., Koboldt, C.M., Hall, T., Sommers, C., Hauser, S.D., Pierce, J.L., Combs, R.G., Reitz, B.A., Diaz-Collier, J.A., Weinberg, R.A., Hood, B.L., Kilpatrick, B.F., and Tripp, C.S. (2000). Characterization of the recombinant IKK1/IKK2 heterodimer. Mechanisms regulating kinase activity. J Biol Chem *275*, 25883-25891.

43. Wisniewski, D., LoGrasso, P., Calaycay, J., and Marcy, A. (1999). Assay for IkappaB kinases using an in vivo biotinylated IkappaB protein substrate. Anal Biochem *274*, 220-228.

44. Flint, N.A., Amrein, K.E., Jascur, T., and Burn, P. (1994). Purification and characterization of an activated form of the protein tyrosine kinase Lck from an Escherichia coli expression system. J Cell Biochem *55*, 389-397.

45. Schmid, A.C., Byrne, R.D., Vilar, R., and Woscholski, R. (2004). Bisperoxovanadium compounds are potent PTEN inhibitors. FEBS Lett *566*, 35-38.

46. Mustelin, T., Alonso, A., Bottini, N., Huynh, H., Rahmouni, S., Nika, K., Louis-dit-Sully, C., Tautz, L., Togo, S.H., Bruckner, S., Mena-Duran, A.V., and al-Khouri, A.M. (2004). Protein tyrosine phosphatases in T cell physiology. Mol Immunol *41*, 687-700.

47. Ferrell, J.E., Jr. (1996). Tripping the switch fantastic: how a protein kinase cascade can convert graded inputs into switch-like outputs. Trends Biochem Sci *21*, 460-466.

48. Huang, C.Y., and Ferrell, J.E., Jr. (1996). Ultrasensitivity in the mitogen-activated protein kinase cascade. Proc Natl Acad Sci U S A *93*, 10078-10083.

49. Tengholm, A., and Meyer, T. (2002). A PI3-kinase signaling code for insulin-triggered insertion of glucose transporters into the plasma membrane. Curr Biol *12*, 1871-1876.

50. Kohler, K., Lellouch, A.C., Vollmer, S., Stoevesandt, O., Hoff, A., Peters, L., Rogl, H., Malissen, B., and Brock, R. (2005). Chemical inhibitors when timing is critical: a pharmacological concept for the maturation of T cell contacts. Chembiochem *6*, 152-161.

51. Rogers, B., Decottignies, A., Kolaczkowski, M., Carvajal, E., Balzi, E., and Goffeau, A. (2001). The pleitropic drug ABC transporters from Saccharomyces cerevisiae. J Mol Microbiol Biotechnol *3*, 207-214.

52. Stein, W.D. (1998). Kinetics of the P-glycoprotein, the multidrug transporter. Exp Physiol *83*, 221-232.

53. Wohlbold, L., van der Kuip, H., Miething, C., Vornlocher, H.P., Knabbe, C., Duyster, J., and Aulitzky, W.E. (2003). Inhibition of bcr-abl gene expression by small interfering RNA sensitizes for imatinib mesylate (STI571). Blood *102*, 2236-2239.

54. Ghaemmaghami, S., Huh, W.K., Bower, K., Howson, R.W., Belle, A., Dephoure, N., O'Shea, E.K., and Weissman, J.S. (2003). Global analysis of protein expression in yeast. Nature *425*, 737-741.

55. Sherman, F. (1991). Guide to Yeast Genetics and Molecular Biology, Volume 194 (San Diego: Academic Press).

56. Bhatt, R.R., and Ferrell, J.E., Jr. (2000). Cloning and characterization of Xenopus Rsk2, the predominant p90 Rsk isozyme in oocytes and eggs. J Biol Chem *275*, 32983-32990.

57. Arooz, T., Yam, C.H., Siu, W.Y., Lau, A., Li, K.K., and Poon, R.Y. (2000). On the concentrations of cyclins and cyclin-dependent kinases in extracts of cultured human cells. Biochemistry *39*, 9494-9501.

58. Lipinski, C.A. (2000). Drug-like properties and the causes of poor solubility and poor permeability. J Pharmacol Toxicol Methods *44*, 235-249.

59. Lipinski, C., and Hopkins, A. (2004). Navigating chemical space for biology and medicine. Nature *432*, 855-861.

60. Lipinski, C.A., Lombardo, F., Dominy, B.W., and Feeny, P.J. (1997). Experimental and computational approaches to estimate solubility and

permeability in drug discovery and development settings. Advanced Drug Delivery Reviews *23*, 3-25.

61. Veber, D.F., Johnson, S.R., Cheng, H.Y., Smith, B.R., Ward, K.W., and Kopple, K.D. (2002). Molecular properties that influence the oral bioavailability of drug candidates. J Med Chem *45*, 2615-2623.

62. Noble, M.E., Endicott, J.A., and Johnson, L.N. (2004). Protein kinase inhibitors: insights into drug design from structure. Science *303*, 1800-1805.

63. McGovern, S.L., Helfand, B.T., Feng, B., and Shoichet, B.K. (2003). A specific mechanism of nonspecific inhibition. J Med Chem *46*, 4265-4272.

64. Ramdas, L., McMurray, J.S., and Budde, R.J. (1994). The degree of inhibition of protein tyrosine kinase activity by tyrphostin 23 and 25 is related to their instability. Cancer Res *54*, 867-869.

65. Ramdas, L., Obeyesekere, N.U., McMurray, J.S., Gallick, G.E., Seifert, W.E., Jr., and Budde, R.J. (1995). A tyrphostin-derived inhibitor of protein tyrosine kinases: isolation and characterization. Arch Biochem Biophys *323*, 237-242.

66. Ramdas, L., and Budde, R.J. (1998). The instability of polyhydroxylated aromatic protein tyrosine kinase inhibitors in the presence of manganese. Cancer Biochem Biophys *16*, 375-385.

67. McGovern, S.L., and Shoichet, B.K. (2003). Kinase inhibitors: not just for kinases anymore. J Med Chem *46*, 1478-1483.

68. Holleran, J.L., Egorin, M.J., Zuhowski, E.G., Parise, R.A., Musser, S.M., and Pan, S.S. (2003). Use of high-performance liquid chromatography to characterize the rapid decomposition of wortmannin in tissue culture media. Anal Biochem *323*, 19-25.

69. Duncia, J.V., Santella, J.B., 3rd, Higley, C.A., Pitts, W.J., Wityak, J., Frietze, W.E., Rankin, F.W., Sun, J.H., Earl, R.A., Tabaka, A.C., Teleha, C.A., Blom, K.F., Favata, M.F., Manos, E.J., Daulerio, A.J., Stradley, D.A., Horiuchi, K., Copeland, R.A., Scherle, P.A., Trzaskos, J.M., Magolda, R.L., Trainor, G.L., Wexler, R.R., Hobbs, F.W., and Olson, R.E. (1998). MEK inhibitors: the chemistry and biological activity of U0126, its analogs, and cyclization products. Bioorg Med Chem Lett *8*, 2839-2844.

70. Rishton, G.M. (2003). Nonleadlikeness and leadlikeness in biochemical screening. Drug Discov Today *8*, 86-96.

71. Fry, D.W., Bridges, A.J., Denny, W.A., Doherty, A., Greis, K.D., Hicks, J.L., Hook, K.E., Keller, P.R., Leopold, W.R., Loo, J.A., McNamara, D.J., Nelson, J.M., Sherwood, V., Smaill, J.B., Trumpp-Kallmeyer, S., and Dobrusin, E.M. (1998). Specific, irreversible inactivation of the epidermal growth factor receptor and erbB2, by a new class of tyrosine kinase inhibitor. Proc Natl Acad Sci U S A *95*, 12022-12027.

72. Cohen, M., Zhang, C., Shokat, K., and Taunton, J. (2004). submitted.

73. Vieth, M., Higgs, R.E., Robertson, D.H., Shapiro, M., Gragg, E.A., and Hemmerle, H. (2004). Kinomics-structural biology and chemogenomics of kinase inhibitors and targets. Biochim Biophys Acta *1697*, 243-257.

74. Yamamoto, N., Takeshita, K., Shichijo, M., Kokubo, T., Sato, M., Nakashima, K., Ishimori, M., Nagai, H., Li, Y.F., Yura, T., and Bacon, K.B. (2003). The orally available spleen tyrosine kinase inhibitor 2-[7-(3,4-dimethoxyphenyl)-imidazo[1,2-c]pyrimidin-5-ylamino]nicotinamide dihydrochloride (BAY 61-3606) blocks antigen-induced airway inflammation in rodents. J Pharmacol Exp Ther *306*, 1174-1181.

75. Bain, J., McLauchlan, H., Elliott, M., and Cohen, P. (2003). The specificities of protein kinase inhibitors: an update. Biochem J *371*, 199-204.

76. Davies, S.P., Reddy, H., Caivano, M., and Cohen, P. (2000). Specificity and mechanism of action of some commonly used protein kinase inhibitors. Biochem J *351*, 95-105.

77. Liu, Y., Bishop, A., Witucki, L., Kraybill, B., Shimizu, E., Tsien, J., Ubersax, J., Blethrow, J., Morgan, D.O., and Shokat, K.M. (1999). Structural basis for selective inhibition of Src family kinases by PP1. Chem Biol *6*, 671-678.

78. Blencke, S., Zech, B., Engkvist, O., Greff, Z., Orfi, L., Horvath, Z., Keri, G., Ullrich, A., and Daub, H. (2004). Characterization of a conserved structural determinant controlling protein kinase sensitivity to selective inhibitors. Chem Biol *11*, 691-701.

79. Godl, K., Wissing, J., Kurtenbach, A., Habenberger, P., Blencke, S., Gutbrod, H., Salassidis, K., Stein-Gerlach, M., Missio, A., Cotten, M., and Daub, H. (2003). An efficient proteomics method to identify the cellular targets of protein kinase inhibitors. Proc Natl Acad Sci U S A *100*, 15434-15439.

80. Frye, S.V. (1999). Structure-activity relationship homology (SARAH): a conceptual framework for drug discovery in the genomic era. Chem Biol *6*, R3-7.

81. Leahy, J.J., Golding, B.T., Griffin, R.J., Hardcastle, I.R., Richardson, C., Rigoreau, L., and Smith, G.C. (2004). Identification of a highly potent and selective DNA-dependent protein kinase (DNA-PK) inhibitor (NU7441) by screening of chromenone libraries. Bioorg Med Chem Lett *14*, 6083-6087.

82. Wissing, J., Godl, K., Brehmer, D., Blencke, S., Weber, M., Habenberger, P., Stein-Gerlach, M., Missio, A., Cotten, M., Muller, S., and Daub, H. (2004). Chemical proteomic analysis reveals alternative modes of action for pyrido[2,3-d]pyrimidine kinase inhibitors. Mol Cell Proteomics.

83. Knockaert, M., Gray, N., Damiens, E., Chang, Y.T., Grellier, P., Grant, K., Fergusson, D., Mottram, J., Soete, M., Dubremetz, J.F., Le Roch, K., Doerig, C., Schultz, P., and Meijer, L. (2000). Intracellular targets of cyclin-dependent kinase

inhibitors: identification by affinity chromatography using immobilised inhibitors. Chem Biol *7*, 411-422.

84. Knockaert, M., Wieking, K., Schmitt, S., Leost, M., Grant, K.M., Mottram, J.C., Kunick, C., and Meijer, L. (2002). Intracellular Targets of Paullones. Identification following affinity purification on immobilized inhibitor. J Biol Chem *277*, 25493-25501.

85. Knockaert, M., Lenormand, P., Gray, N., Schultz, P., Pouyssegur, J., and Meijer, L. (2002). p42/p44 MAPKs are intracellular targets of the CDK inhibitor purvalanol. Oncogene *21*, 6413-6424.

86. Rosania, G.R., Merlie, J., Jr., Gray, N., Chang, Y.T., Schultz, P.G., and Heald, R. (1999). A cyclin-dependent kinase inhibitor inducing cancer cell differentiation: biochemical identification using Xenopus egg extracts. Proc Natl Acad Sci U S A *96*, 4797-4802.

87. Brehmer, D., Godl, K., Zech, B., Wissing, J., and Daub, H. (2004). Proteome-wide identification of cellular targets affected by bisindolylmaleimide-type protein kinase C inhibitors. Mol Cell Proteomics *3*, 490-500.

88. Wissing, J., Godl, K., Brehmer, D., Blencke, S., Weber, M., Habenberger, P., Stein-Gerlach, M., Missio, A., Cotten, M., Muller, S., and Daub, H. (2004). Chemical Proteomic Analysis Reveals Alternative Modes of Action for Pyrido[2,3-d]pyrimidine Kinase Inhibitors. Mol Cell Proteomics *3*, 1181-1193.

89. Ding, S., Wu, T.Y., Brinker, A., Peters, E.C., Hur, W., Gray, N.S., and Schultz, P.G. (2003). Synthetic small molecules that control stem cell fate. Proc Natl Acad Sci U S A *100*, 7632-7637.

90. Liu, Y., Shreder, K.R., Gai, W., Corral, S., Ferris, D.K., and Rosenblum, J.S. (2005). Wortmannin, a Widely Used Phosphoinositide 3-Kinase Inhibitor, also Potently Inhibits Mammalian Polo-like Kinase. Chem Biol *12*, 99-107.

91. Abbott, B.M., and Thompson, P.E. (2004). PDE2 inhibition by the PI3 kinase inhibitor LY294002 and analogues. Bioorg Med Chem Lett *14*, 2847-2851.

92. Welling, A., Hofmann, F., and Wegener, J.W. (2004). Inhibition of L-type Cav1.2 Ca2+ channels by LY294002 and Go6983. Mol Pharmacol.

93. Sun, H., Oudit, G.Y., Ramirez, R.J., Costantini, D., and Backx, P.H. (2004). The phosphoinositide 3-kinase inhibitor LY294002 enhances cardiac myocyte contractility via a direct inhibition of Ik,slow currents. Cardiovasc Res *62*, 509-520.

94. Pasapera Limon, A.M., Herrera-Munoz, J., Gutierrez-Sagal, R., and Ulloa-Aguirre, A. (2003). The phosphatidylinositol 3-kinase inhibitor LY294002 binds the estrogen receptor and inhibits 17beta-estradiol-induced transcriptional activity of an estrogen sensitive reporter gene. Mol Cell Endocrinol *200*, 199-202.

95. Hajduk, P.J., Bures, M., Praestgaard, J., and Fesik, S.W. (2000). Privileged molecules for protein binding identified from NMR-based screening. J Med Chem *43*, 3443-3447.

96. Aronov, A.M., and Murcko, M.A. (2004). Toward a pharmacophore for kinase frequent hitters. J Med Chem *47*, 5616-5619.

97. Schreiber, S.L. (1991). Chemistry and biology of the immunophilins and their immunosuppressive ligands. Science *251*, 283-287.

98. Heitman, J., Movva, N.R., and Hall, M.N. (1991). Targets for cell cycle arrest by the immunosuppressant rapamycin in yeast. Science *253*, 905-909.

99. Choi, J., Chen, J., Schreiber, S.L., and Clardy, J. (1996). Structure of the FKBP12-rapamycin complex interacting with the binding domain of human FRAP. Science *273*, 239-242.

100. Zheng, X.F., Florentino, D., Chen, J., Crabtree, G.R., and Schreiber, S.L. (1995). TOR kinase domains are required for two distinct functions, only one of which is inhibited by rapamycin. Cell *82*, 121-130.

101. Jacinto, E., Loewith, R., Schmidt, A., Lin, S., Ruegg, M.A., Hall, A., and Hall, M.N. (2004). Mammalian TOR complex 2 controls the actin cytoskeleton and is rapamycin insensitive. Nat Cell Biol *6*, 1122-1128.

102. Loewith, R., Jacinto, E., Wullschleger, S., Lorberg, A., Crespo, J.L., Bonenfant, D., Oppliger, W., Jenoe, P., and Hall, M.N. (2002). Two TOR complexes, only one of which is rapamycin sensitive, have distinct roles in cell growth control. Mol Cell *10*, 457-468.

103. Dudley, D.T., Pang, L., Decker, S.J., Bridges, A.J., and Saltiel, A.R. (1995). A synthetic inhibitor of the mitogen-activated protein kinase cascade. Proc Natl Acad Sci U S A *92*, 7686-7689.

104. Alessi, D.R., Cuenda, A., Cohen, P., Dudley, D.T., and Saltiel, A.R. (1995). PD 098059 is a specific inhibitor of the activation of mitogen-activated protein kinase kinase in vitro and in vivo. J Biol Chem *270*, 27489-27494.

105. Favata, M.F., Horiuchi, K.Y., Manos, E.J., Daulerio, A.J., Stradley, D.A., Feeser, W.S., Van Dyk, D.E., Pitts, W.J., Earl, R.A., Hobbs, F., Copeland, R.A., Magolda, R.L., Scherle, P.A., and Trzaskos, J.M. (1998). Identification of a novel inhibitor of mitogen-activated protein kinase kinase. J Biol Chem *273*, 18623-18632.

106. Sebolt-Leopold, J.S., Dudley, D.T., Herrera, R., Van Becelaere, K., Wiland, A., Gowan, R.C., Tecle, H., Barrett, S.D., Bridges, A., Przybranowski, S., Leopold, W.R., and Saltiel, A.R. (1999). Blockade of the MAP kinase pathway suppresses growth of colon tumors in vivo. Nat Med *5*, 810-816.

107. Ohren, J.F., Chen, H., Pavlovsky, A., Whitehead, C., Zhang, E., Kuffa, P., Yan, C., McConnell, P., Spessard, C., Banotai, C., Mueller, W.T., Delaney, A., Omer, C., Sebolt-Leopold, J., Dudley, D.T., Leung, I.K., Flamme, C., Warmus, J.,

Kaufman, M., Barrett, S., Tecle, H., and Hasemann, C.A. (2004). Structures of human MAP kinase kinase 1 (MEK1) and MEK2 describe novel noncompetitive kinase inhibition. Nat Struct Mol Biol *11*, 1192-1197.

108. Davidson, W., Frego, L., Peet, G.W., Kroe, R.R., Labadia, M.E., Lukas, S.M., Snow, R.J., Jakes, S., Grygon, C.A., Pargellis, C., and Werneburg, B.G. (2004). Discovery and characterization of a substrate selective p38alpha inhibitor. Biochemistry *43*, 11658-11671.

109. Martin, J.L., Avkiran, M., Quinlan, R.A., Cohen, P., and Marber, M.S. (2001). Antiischemic effects of SB203580 are mediated through the inhibition of p38alpha mitogen-activated protein kinase: Evidence from ectopic expression of an inhibition-resistant kinase. Circ Res *89*, 750-752.

110. Gorre, M.E., Mohammed, M., Ellwood, K., Hsu, N., Paquette, R., Rao, P.N., and Sawyers, C.L. (2001). Clinical resistance to STI-571 cancer therapy caused by BCR-ABL gene mutation or amplification. Science *293*, 876-880.

111. Bishop, A.C., Ubersax, J.A., Petsch, D.T., Matheos, D.P., Gray, N.S., Blethrow, J., Shimizu, E., Tsien, J.Z., Schultz, P.G., Rose, M.D., Wood, J.L., Morgan, D.O., and Shokat, K.M. (2000). A chemical switch for inhibitor-sensitive alleles of any protein kinase. Nature *407*, 395-401.

112. Jackson, A.L., and Linsley, P.S. (2004). Noise amidst the silence: off-target effects of siRNAs? Trends Genet *20*, 521-524.

113. Zambrowicz, B.P., and Sands, A.T. (2003). Knockouts model the 100 best-selling drugs--will they model the next 100? Nat Rev Drug Discov *2*, 38-51.

114. Hardy, L.W., and Peet, N.P. (2004). The multiple orthogonal tools approach to define molecular causation in the validation of druggable targets. Drug Discov Today *9*, 117-126.

115. Chong, Y.P., Mulhern, T.D., Zhu, H.J., Fujita, D.J., Bjorge, J.D., Tantiongco, J.P., Sotirellis, N., Lio, D.S., Scholz, G., and Cheng, H.C. (2004). A novel non-catalytic mechanism employed by the C-terminal Src-homologous kinase to inhibit Src-family kinase activity. J Biol Chem *279*, 20752-20766.

116. Patrucco, E., Notte, A., Barberis, L., Selvetella, G., Maffei, A., Brancaccio, M., Marengo, S., Russo, G., Azzolino, O., Rybalkin, S.D., Silengo, L., Altruda, F., Wetzker, R., Wymann, M.P., Lembo, G., and Hirsch, E. (2004). PI3Kgamma modulates the cardiac response to chronic pressure overload by distinct kinase-dependent and -independent effects. Cell *118*, 375-387.

117. Papa, F.R., Zhang, C., Shokat, K., and Walter, P. (2003). Bypassing a kinase activity with an ATP-competitive drug. Science *302*, 1533-1537.

118. Yu, V.P., Baskerville, C., Grunenfelder, B., and Reed, S.I. (2005). A kinase-independent function of Cks1 and Cdk1 in regulation of transcription. Mol Cell *17*, 145-151.

119. Cohen, P. (2002). Protein kinases--the major drug targets of the twenty-first century? Nat Rev Drug Discov *1*, 309-315.

120. Ortega, S., Prieto, I., Odajima, J., Martin, A., Dubus, P., Sotillo, R., Barbero, J.L., Malumbres, M., and Barbacid, M. (2003). Cyclin-dependent kinase 2 is essential for meiosis but not for mitotic cell division in mice. Nat Genet *35*, 25-31.

121. Lowell, C.A., Soriano, P., and Varmus, H.E. (1994). Functional overlap in the src gene family: inactivation of hck and fgr impairs natural immunity. Genes Dev *8*, 387-398.

122. Lowell, C.A., Niwa, M., Soriano, P., and Varmus, H.E. (1996). Deficiency of the Hck and Src tyrosine kinases results in extreme levels of extramedullary hematopoiesis. Blood *87*, 1780-1792.

123. Abeliovich, H., Zhang, C., Dunn, W.A., Jr., Shokat, K.M., and Klionsky, D.J. (2003). Chemical genetic analysis of Apg1 reveals a non-kinase role in the induction of autophagy. Mol Biol Cell *14*, 477-490.

124. Sreenivasan, A., Bishop, A.C., Shokat, K.M., and Kellogg, D.R. (2003). Specific inhibition of Elm1 kinase activity reveals functions required for early G1 events. Mol Cell Biol *23*, 6327-6337.

125. Weiss, E.L., Bishop, A.C., Shokat, K.M., and Drubin, D.G. (2000). Chemical genetic analysis of the budding-yeast p21-activated kinase Cla4p. Nat Cell Biol *2*, 677-685.

126. Vanhaesebroeck, B., Rohn, J.L., and Waterfield, M.D. (2004). Gene targeting: attention to detail. Cell *118*, 274-276.

127. Okkenhaug, K., Bilancio, A., Farjot, G., Priddle, H., Sancho, S., Peskett, E., Pearce, W., Meek, S.E., Salpekar, A., Waterfield, M.D., Smith, A.J., and Vanhaesebroeck, B. (2002). Impaired B and T cell antigen receptor signaling in p110delta PI 3-kinase mutant mice. Science *297*, 1031-1034.

128. Jou, S.T., Carpino, N., Takahashi, Y., Piekorz, R., Chao, J.R., Carpino, N., Wang, D., and Ihle, J.N. (2002). Essential, nonredundant role for the phosphoinositide 3-kinase p110delta in signaling by the B-cell receptor complex. Mol Cell Biol *22*, 8580-8591.

129. Wong, S., McLaughlin, J., Cheng, D., Zhang, C., Shokat, K.M., and Witte, O.N. (2004). Sole BCR-ABL inhibition is insufficient to eliminate all myeloproliferative disorder cell populations. Proc Natl Acad Sci U S A.

130. Liu, Y., Kung, C., Fishburn, J., Ansari, A.Z., Shokat, K.M., and Hahn, S. (2004). Two cyclin-dependent kinases promote RNA polymerase II transcription and formation of the scaffold complex. Mol Cell Biol *24*, 1721-1735.

131. Williams, M. (2003). Target validation. Curr Opin Pharmacol *3*, 571-577.

Chapter 2

A chemical strategy for targeting proteolysis to sites of protein phosphorylation

2.1 Abstract

Protein phosphorylation is a dominant mechanism of information transfer in cells, and a major goal of current proteomic efforts is to generate a system-level map describing all the sites of protein phosphorylation. Recent efforts have focused on developing technologies for enriching and quantitating phosphopeptides. By contrast, identification of the sites of phosphorylation typically relies on the use of tandem mass spectrometry to sequence individual peptides. Herein is described a novel approach for phosphopeptide mapping that makes it possible to interrogate a protein sequence directly with a protease that recognizes sites of phosphorylation. The key to this approach is the selective chemical transformation of phosphoserine and phosphothreonine residues into lysine analogs (aminoethylcysteine and β-methylaminoethylcysteine, respectively). Aminoethylcysteine-modified peptides are then selectively cleaved with a lysine-specific protease to map sites of phosphorylation. A blocking step enables single-site cleavage when desired, and adaptation of this reaction to the solid phase facilitates phosphopeptide enrichment and modification in one step.

2.2 Introduction

Much of the complexity of higher organisms is believed to reside in the specific post-translational modification of proteins [1]. Protein phosphorylation is the most ubiquitous such modification; almost 2% of the human genome encodes protein kinases and an estimated one-third of all proteins are phosphorylated [2]. Due to the importance of protein phosphorylation in regulating cellular signaling, there is intense interest in developing technologies for mapping phosphorylation events [3, 4].

Existing approaches for phosphorylation site mapping rely largely on the use of tandem mass spectrometry (MS/MS) to sequence individual peptides. Despite the power of this approach, MS/MS of phosphopeptides remains challenging [5-10] due to (i) the signal suppression of phosphate containing molecules in the commonly used positive detection mode, (ii) the inherent lability of the phosphate group on collision induced dissociation (CID), and (iii) the difficulty in achieving full sequence coverage, especially for long peptides, peptides present in low abundance, and peptides phosphorylated at substoichiometric levels– all of which are common for phosphopeptides. The challenge of mapping phosphorylation sites is highlighted by recent efforts to enrich phosphopeptides from complex mixtures. While these strategies have provided powerful tools for purifying phosphopeptides, the next step – identifying the precise site of phosphorylation – often fails for many of the peptides that are recovered [7, 8].

Currently, the first step in mapping the phosphorylation sites of a protein is to digest the phosphoprotein with a protease (e.g., trypsin) that generates smaller peptide fragments for sequencing. We reasoned that this process would be more informative if a protease that specifically cleaves its substrates at the site of phosphorylation were used. Such a digestion would selectively hydrolyze the amide bond adjacent to each phosphorylated residue, facilitating identification of the phosphorylation site directly from the cleavage pattern without sequencing any individual peptide (e.g., from an MS fingerprint specifying the exact masses of the cleavage products). Phosphospecific cleavage would also facilitate the interpretation of MS/MS spectra, since the C-terminal residue would always be the phosphorylated residue, resulting in a unique y_1 ion. In this regard, it is often possible to obtain tandem mass spectra of a phosphopeptide, but still fail to localize the phosphoamino acid within that sequence [7, 8]. Unfortunately, no protease is known that selectively recognizes a phosphorylated amino acid, or any other post-translational modification.

To address this problem, a strategy for specific proteolysis at sites of serine and threonine phosphorylation has been developed. This approach relies on the well-established β-elimination of phosphoserine residues to generate dehydroalanine under basic conditions (phosphothreonine is converted to β-methyldehydroalanine). Similar chemistry has been used to enrich and quantitate phosphoproteins for traditional trypsin digestion and MS/MS sequencing [8, 11-15]. In the next step, dehydroalanine acts as a Michael acceptor for cysteamine, generating an aminoethylcysteine (Aec) residue (for phosphothreonine, β-methylaminoethylcysteine is generated) (Figure 2.1a). Since aminoethylcysteine is isosteric with lysine, proteases that recognize lysine (e.g. trypsin, Lys-C, and lysyl endopeptidase) will cleave proteins at this residue.

2.3 Aminoethylcysteine modification of model substrates

A panel of seven phosphoserine and two phosphothreonine peptides was chosen to demonstrate the feasibility of this approach. Extensive peptide degradation was found to result when standard β-elimination conditions (~1M hydroxide, 42-55 °C, >1 hour) were applied [8, 15, 16]. To achieve nearly quantitative β-elimination without peptide hydrolysis, several parameters were critical, including reaction temperature, length, basicity, and order of addition [13, 14] (see Supplementary Methods section). By this means, each peptide was cleanly converted into its aminoethylcysteine or β-methylaminoethylcysteine analogue (Figure 2.1, Table 2.1 and Figure 2.2). Digestion of the aminoethylcysteine modified peptides with Lys-C or trypsin liberated peptide fragments corresponding to selective cleavage at the site of serine phosphorylation (Table 2.1). Surprisingly, β-methylaminoethylcysteine was also found to be an efficient substrate for Lys-C and lysyl endopeptidase, generating peptide fragments corresponding to specific cleavage at the former site of threonine phosphorylation (Table 2.1 and Figure 2.3); trypsin cleaved at this residue

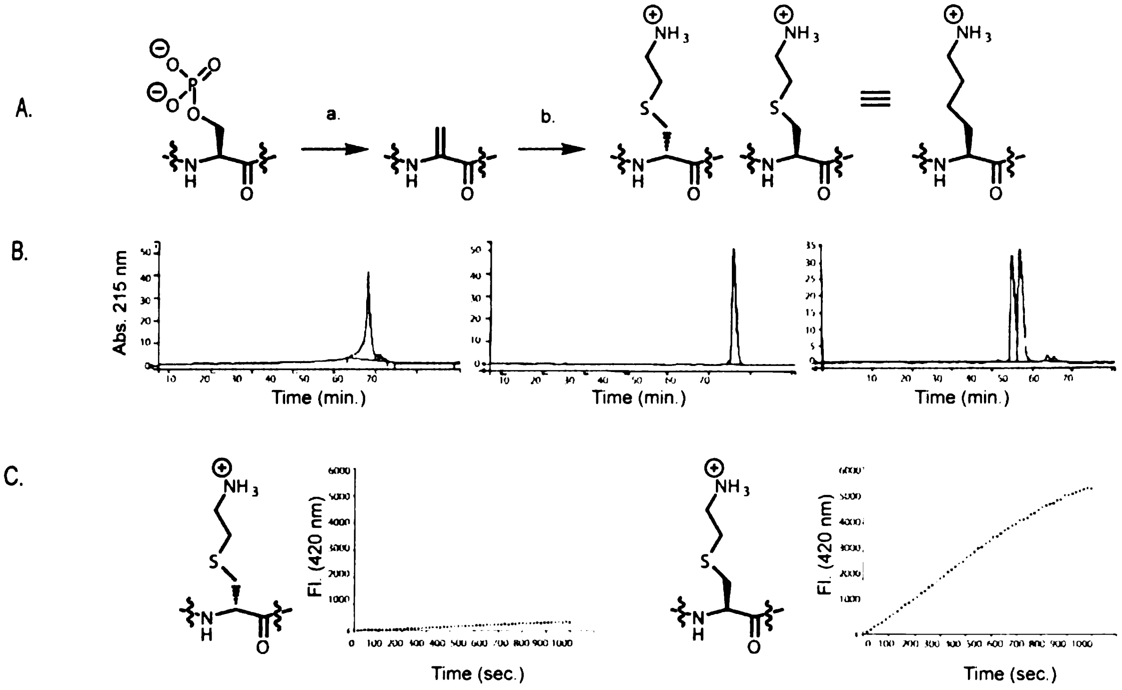
A.
a.
b.
NH3
S
N
H
O
B.
Abs. 215 nm
Time (min.)
Time (min.)
Time (min.)
C.
FI. (420 nm)
Time (sec.)
FI. (420 nm)
Time (sec.)

Figure 2.1. (A) Scheme for transformation of phosphoserine residues to dehydroalanine, then aminoethylcysteine. (B) HPLC traces of crude reactions cleanly converting phosphoserine peptide ZFRPpSGFY*D (left) to dehydroalanine (middle) then aminoethylcysteine (right). (C) Reaction progress curve for the hydrolysis of (S)-aminoethylcysteine (left) and (R)-aminoethylcysteine derivatives of peptide ZFRPpSGFY*D by trypsin as monitored by FRET.

	Experimental Mass **M** (Calculated Mass **M**)		
Sequence	Dehydroalanine	Aminoethylcysteine	Lys-C Digest
GRTGRRN**pS**IHDIL	1,475.4 (1,476.6)	1,554.6 (1,553.8)	609.4 (609.7)
DLDVPIPGRFDRRV**pS**VAAE	2,093.0 (2,094.4)	2,170.6 (2,171.5)	1,800.0 (1,801.1)
SLRRS**pS**C*FGGRIDRIGAQSGLGC*NSFRY	3,140.4 (3,142.4)	3,218.2 (3,219.5)	2,471.8 (2,473.6)
KRP**pS**QRHGSKY-NH_2	1,324.4 (1,324.5)	1,402.2 (1,401.6)	711.6 (711.8)
LRRA**pS**LG	753.6 (753.9)	830.6 (831.0)	660.4 (660.8)
ZFRP**pS**GFY*D	1,133.7 (1,134.2)	1,210.7 (1,211.3)	684.6 (683.8)
ZFRP**pT**GFY*D	1,147.52 (1,147.47)	**1,224.54** (1,224.50)	**697.35** (697.34)
RRA**pS**PVA	737.43 (737.43)	**814.53** (814.46)	547.32 (547.22)
KR**pT**IRR	810.56 (810.53)	887.62 (887.56)	n/a

Table 2.1. Results of aminoethylcysteine modification for model peptide substrates. Molecular weights were determined by ESI-MS on a Waters Micromass ZQ instrument, and exact masses by LC-ESI-MS recorded on a QSTAR Pulsar i instrument or by MALDI-MS recorded on a Voyager DESTR plus instrument. All masses listed in bold letters were additionally confirmed by LC-MS/MS. Abbreviations: K*: aminoethylcysteine; M*: methionine sulphone; C*: cysteic acid; Y*: 3-nitrotyrosine; Z: 2-aminobenzoic acid.

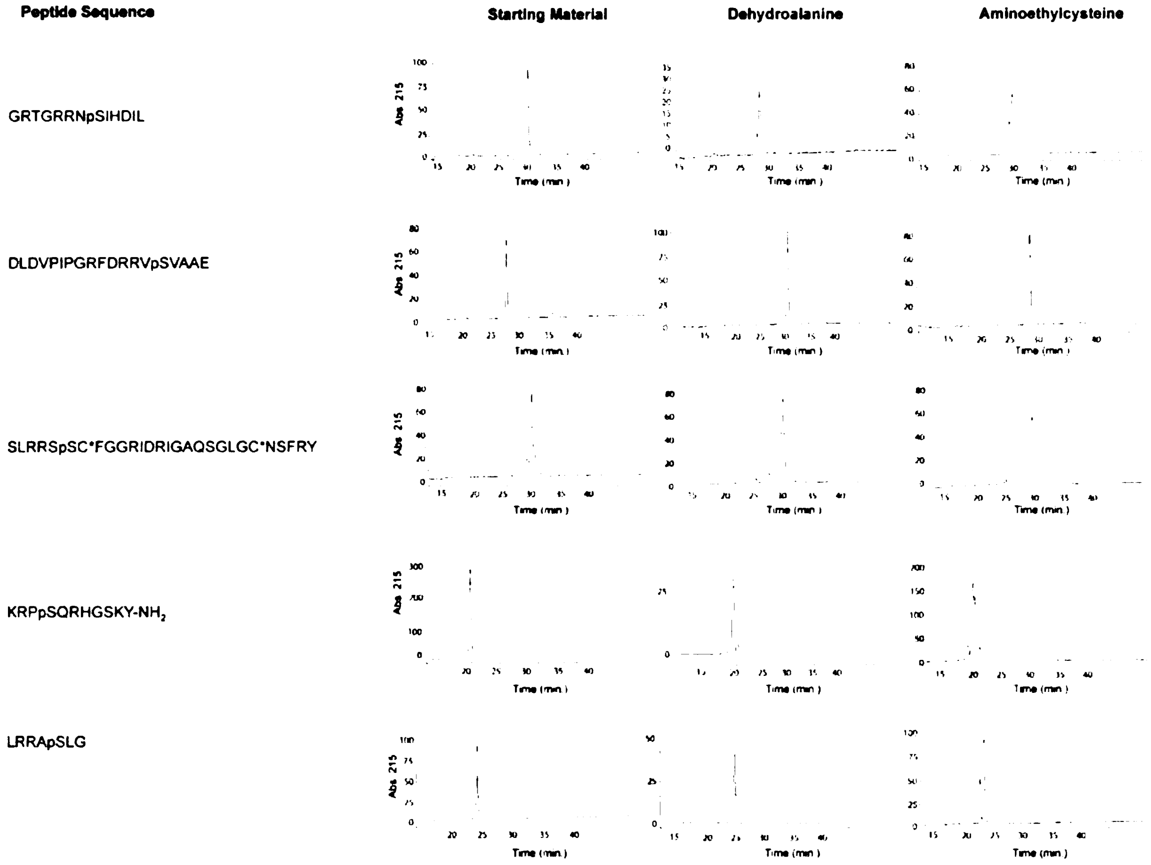

Figure 2.2: HPLC traces of crude reactions converting starting phosphoserine peptide (left) to the corresponding dehydroalanine (middle) and then aminoethylcysteine (right) modified peptide. In some cases, aminoethylcysteine peptide diastereomers were separable under the HPLC conditions used.

less efficiently. In this way, site-specific modification combined with proteolytic digestion allows for the unambiguous identification of serine and threonine phosphorylation sites from the exact masses of the liberated fragments.

To further explore the potential of this strategy for mapping phosphorylation sites, two model proteins (α- and β-casein) were selected that contain three and five sites of phosphorylation, respectively. Each protein was subjected to aminoethylcysteine modification followed by digestion with trypsin. One pmol of each digested protein was separated by nanoflow liquid chromatography on a nano-C18 column and then directly analyzed by online LC-MS, and MS/MS on a quadrupole orthogonal TOF spectrometer. Eight peptides were identified by mass fingerprinting (ESI-MS) corresponding to direct cleavage at all eight predicted phosphorylation sites of the two proteins (Table 2.2). For example, for β-casein, phosphorylation is described for serine residues in positions 15, 17, 18, 19 and 35. Accordingly, after aminoethylcysteine modification and digestion, peptides were observed containing C-terminal Aec residues corresponding Arg1-Aec15, Arg1-Aec17, Arg1-Aec18, and Arg1-Aec19. The phosphorylation site at position 35 was assigned from the presence of the peptide Glu36-Lys48, whose N terminus can be attributed to cleavage at the adjacent Aec35 residue.

The identity of many of these aminoethylcysteine-containing peptides was confirmed by LC-MS/MS sequencing as listed in Table 2.2. Peptides containing aminoethylcysteine were found to produce typical peptide MS/MS fragmentation patterns that were readily interpretable. For example, the tandem mass spectrum for the peptide containing the putative phosphorylation site at position 15 in β-casein is shown in Figure 2a. Importantly, the characteristic y_1 ion at *m/z* 165.1 that results from a loss of a C-terminal aminoethylcysteine residue appears as a highly abundant product ion in this MS/MS spectrum and other CID spectra of peptides containing this C-terminal residue.

Protein	Residues	Peptide Sequence	Mr Obs. (Calcd.)
α_{s1}-casein	43-58	DIGK^*EK^*TEDQAM*EDIK	**1,916.74** (1,916.78)
α_{s1}-casein	47-58	(K^*)EK^*TEDQAM*EDIK	**1,485.53** (1,485.59)
α_{s1}-casein	49-58	(K^*)TEDQAM*EDIK	**1,210.48** (1,210.50)
α_{s1}-casein	106-119	VPQLEIVPNK^*AEER	**1,638.84** (1,638.84)
α_{s1}-casein	106-115	VPQLEIVPNK^*	**1,153.58** (1,153.61)
α_{s2}-casein	153-164	TVDM*EK^*TEVFTK	1,476.60 (1,476.66)
α_{s2}-casein	159-164	(K^*)TEVFTK	**723.36** (723.38)
β-casein	1-25	RELEELNVPGEIVEK^*L$K^*K^*K^*$EESITR	**3,037.39** (3,037.47)
β-casein	1-19	RELEELNVPGEIVEK^*L$K^*K^*K^*$	**2,322.11** (2,322.12)
β-casein	1-18	RELEELNVPGEIVEK^*LK^*K^*	2,176.03 (2,176.07)
β-casein	1-17	RELEELNVPGEIVEK^*LK^*	**2,029.92** (2,030.01)
β-casein	1-15	RELEELNVPGEIVEK^*	**1,770.78** (1,770.88)
β-casein	33-48	FQK^*EEQQQTEDELQDK	**2,039.80** (2,039.87)
β-casein	36-48	(K^*)EEQQQTEDELQDK	1,618.65 (1,618.69)
GRK2	666-677	NKPRK^*PVVELSK	**1,411.78** (1,411.80)
GRK2	668-677	PRK^*PVVELSK	**1,169.62** (1,169.66)
GRK2	671-677	(K^*) PVVELSK	**771.40** (771.45)
β-Tubulin	404-416	DEMEFK_T^*EAESNMN	**1,604.52** (1,604.58)
β-Tubulin	404-416	DEM**EFK_T^*EAESNMN	**1,620.60** (1,620.57)
β-Tubulin	404-409	DEMEFK_T^*	829.34 (829.30)
β-Tubulin	404-409	DEM**EFK_T^*	845.38 (845.30)
β-Tubulin	417-426	DLVK^*EYQQYQ	**1,330.51** (1,330.58)
β-Tubulin	421-426	(K^*) EYQQYQ	857.32 (857.36)
β-Tubulin	417-420	DLVK^*	491.26 (491.24)

Table 2.2. Results of aminoethylcysteine modification and proteolytic digestion for α-casein, β-casein, β-tubulin and GRK2. Molecular weights were determined by LC-ESI-MS recorded on a QSTAR instrument. All masses listed in bold letters were additionally confirmed by LC-MS/MS. Abbreviations: K^*: aminoethylcysteine; K_T^*: β-methylaminoethylcysteine; M*: methionine sulphone; C*: cysteic acid.

Since the mass of this y_1-ion (165.07) is unique and does not overlap with other fragment ions resulting from naturally occurring amino acids, we suggest that this ion may also be used for precursor ion scanning in order to increase the sensitivity of phosphopeptide detection in complex peptide mixtures [9, 17]. Unlike existing precursor ion scanning approaches, the detection of this y_1 ion is not only indicative of the presence of a phosphoserine containing peptide, but also positively identifies its precise position in the sequence (i.e., at the C terminus).

During aminoethylcysteine modification, epimerization occurs at C_α of the formerly phosphorylated amino acid, generating diastereomeric aminoethylcysteine peptides (R, S) in an approximately 1:1 mixture (Figure 2.1b). The peptides containing the R stereochemistry at C_α are substrates for lysine-specific proteases, whereas those with the S stereochemistry are not (Figure 2.1c). As a consequence, cleavage occurs at approximately 50% of the sites for any given phosphopeptide under complete proteolysis conditions. For a single tryptic peptide containing multiple phosphorylation sites, this partial digestion generates a ladder of peptides corresponding to successive single cleavage at each of the phosphorylation sites (Table 2.2). This effect is illustrated dramatically for β-casein tryptic peptide Arg1-Arg25, which contains four phosphorylation sites within a five amino acid sequence. In practice, this obligatory partial digestion is advantageous for phosphopeptide mapping, by providing staggered and redundant mass information for multiply phosphorylated peptides.

While introducing new cleavage sites can provide more information about phosphorylation sites, it can also increase the complexity of the resulting mass spectra. Several experiments were performed to investigate the trade-off between these effects. First, two equivalent samples of β-casein, one of which was aminoethylcysteine modified

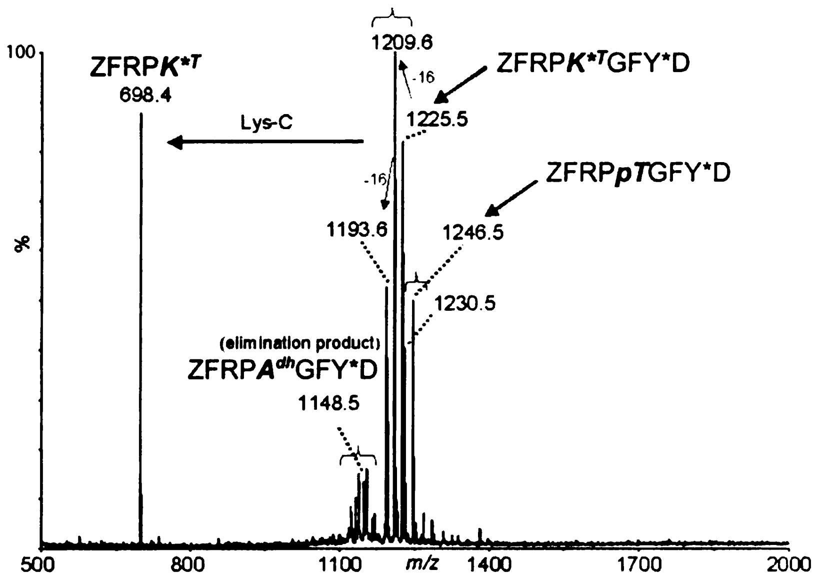

Figure 2.3: MALDI-MS spectrum of peptide ZFRPK^{*T}GFY*E (*m/z* 1225.5) obtained after β-methylaminoethylcysteine modification of phosphothreonine residue and its cleavage product ZFRPK^{*T} (*m/z* 698.4) after digestion with Lys-C. A mixture of some nonreacted phosphothreonine containing peptide (starting material) with MH at *m/z* 1246.5, modified β-methylaminoethylcysteine containing peptide (*m/z* 1225.5) and traces of β-elimination product (*m/z* 1148.5) show side products due to oxygen loss (-16 Da) resulting from the nitrotyrosine residue (Y*) as previously reported[18]. Abbreviations: K^{*T}: β-methylaminoethylcysteine; pT: phosphotyrosine; A^{dh}: dehydroalanine (β-elimination product of pT); Y*: 3-nitrotyrosine; Z: 2-aminobenzoic acid.

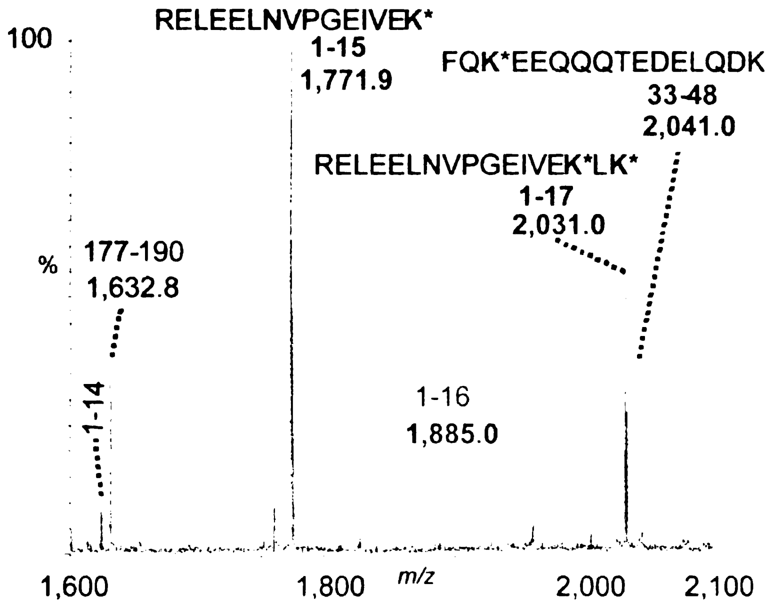

Figure 2.4. MALDI-MS peptide mass fingerprint spectrum showing peptides obtained after digestion of chemically modified β-casein with trypsin under less stringent conditions. The mass range of interest from *m/z* 1600-2100 displays several abundant aminoethylcysteine (K*) modified containing peptides indicated in red color. Relative to these aminoethylcysteine peptides in similar spectra (e.g. Figure 2), peaks corresponding to peptides that resulted from unexpected "chymotryptic-like" cleavages from Roche trypsin (e.g. residues 1-14, *m/z* 1625.9 and residues 1-16, *m/z* 1885.0) are suppressed.

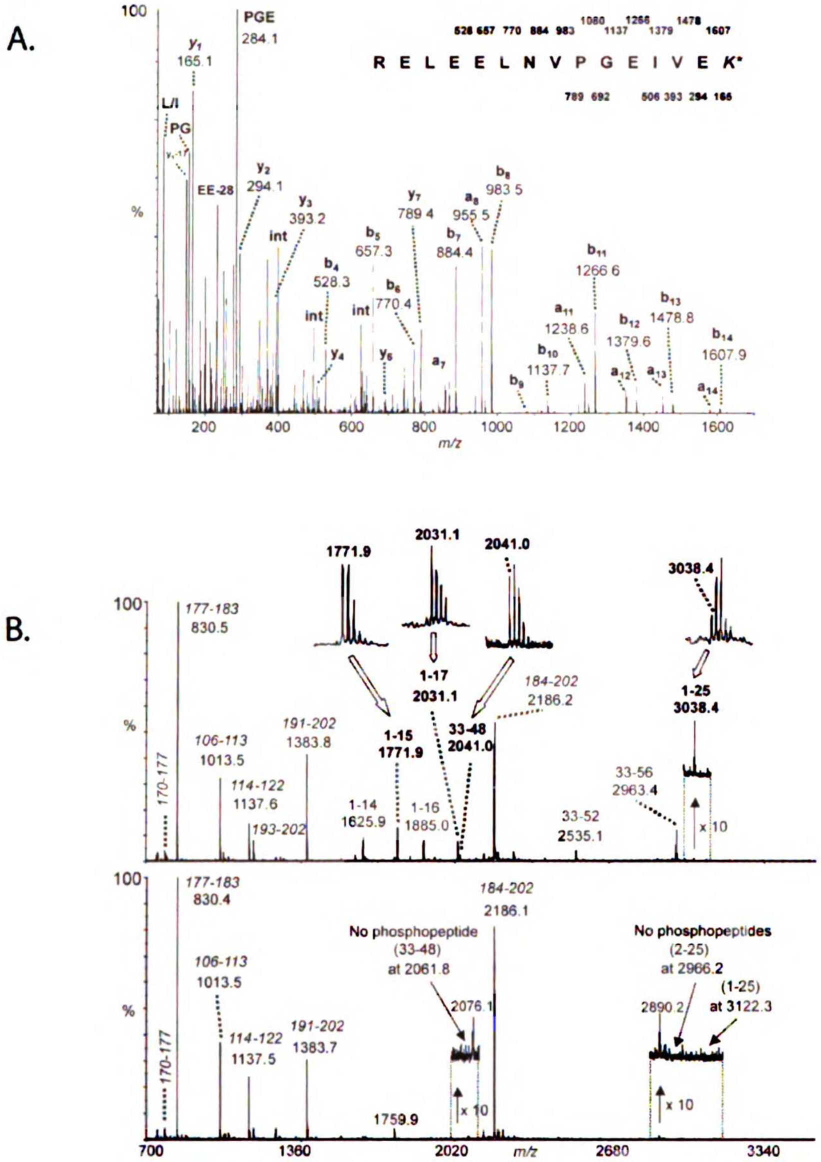

Figure 2.5. (A) ESI-MS/MS spectrum of peptide RELEELNVPGEIVK* [residues Arg(1)-Lys*(15)] obtained after aminoethylcysteine modification of phosphoserine residues and digestion of β-casein with trypsin/Lys-C. The $[M + 2H]^{2+}$ at *m/z* 886.40^{2+} (M = 1770.79) was selected for CID. K* is aminoethylcysteine. (B) Top panel: β-casein (2 μg) was modified as aminoethylcysteine, digested with trypsin, and ca. 1 pmol analyzed by MALDI-MS. Masses in bold and magnified indicate aminoethylcysteine modified peptides. Bottom panel: Unmodified β-casein (2 μg) was digested with trypsin, and ca. 1 pmol analyzed by MALDI-MS. Insets indicate that unmodified phosphoserine containing peptides, predicted at *m/z* 2,061.8 (Phe33 -- Lys48) and at *m/z* 2,966.2 (Glu2 -- Arg25) or 3,122.3 (Arg1 -- Arg25) could not be detected in this spectrum.

and one of which was untreated, were subjected to trypsin digestion and analyzed by MALDI-MS (Figure 2.4 and Figure 2.5b). In the MALDI spectrum from the aminoethylcysteine derivatized sample, four modified phosphopeptides are detected as prominent ions at *m/z* 1771.9, 2031.1, 2041.0, and 3038.4 (residues 1-15, 1-17, 33-48, and 1-25, respectively). Three aminoethylcysteine peptides detected by LC-MS are not observed by MALDI-MS, and we believe this reflects their lesser susceptibility as trypsin cleavage sites (e.g., two of the three peptides contain X-EE motifs that are known to slow trypsin cleavage). In the MALDI-MS spectrum from the untreated control sample, tryptic peptides containing the phosphorylation sites are not detected (Figure 2.5b, inset). Thus, in the absence of AEC modification, none of the phosphopeptides are observed by MALDI-MS under the standard conditions used for most proteomic work (positive-ion reflectron mode with α-cyano-4-hydroxycinnamic acid (HCCA) as the matrix), whereas with chemical modification, four of these peptides are prominent ions in the digest mixture. Otherwise, the spectra are very similar in both the distribution of ions and their relative abundance (Figure 2.5). While experimental conditions are known that can enhance the detection of phosphopeptides by MALDI-MS [19], we believe that aminoethylcysteine modification selectively enhances the positive-ion mode mass spectrometric response of formerly phosphorylated peptides [9]. Indeed, dilution experiments with these samples indicated that aminoethylcysteine modified peptides could be identified from as little as 25 fmol of an unseparated tryptic digest by MALDI-MS (Figure 2.6).

2.4 Mapping GRK2 phosphorylation of tubulin

In contrast to model phosphoproteins such as caseins, many cellular phosphoproteins contain features that make their direct analysis by mass spectrometry

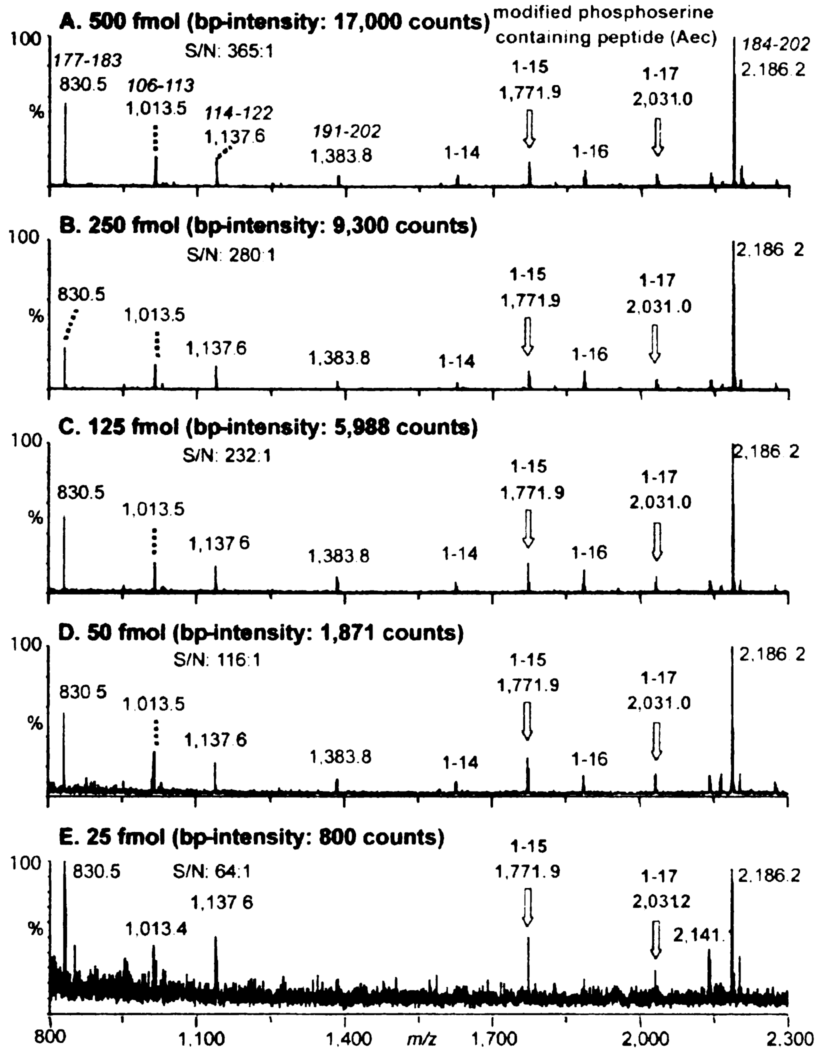

Figure 2.6. MALDI-MS peptide mass fingerprint spectra showing peptides obtained from tryptic digestion of aminoethylcysteine modified β-casein. 4 µg of β-casein was chemically modified, digested and then diluted into a series of samples with different protein concentrations. Total amounts of digested protein ranging between 500 fmol and 25 fmol were loaded and analyzed by MALDI mass spectrometry, as shown in panels (A) 500 fmol, (B) 250 fmol, (C) 125 fmol, (D) 50 fmol, and (E) 25 fmol of modified β-casein. The observed masses are labeled and annotated with starting and ending amino acids. Masses in red indicate peptides that are specific to chemical modification of phosphoserine to aminoethylcysteine amino acid residues. The basepeak (bp) intensity and the signal to noise ratio (S/N) are listed for each panel as a measure for the quality of the spectra.

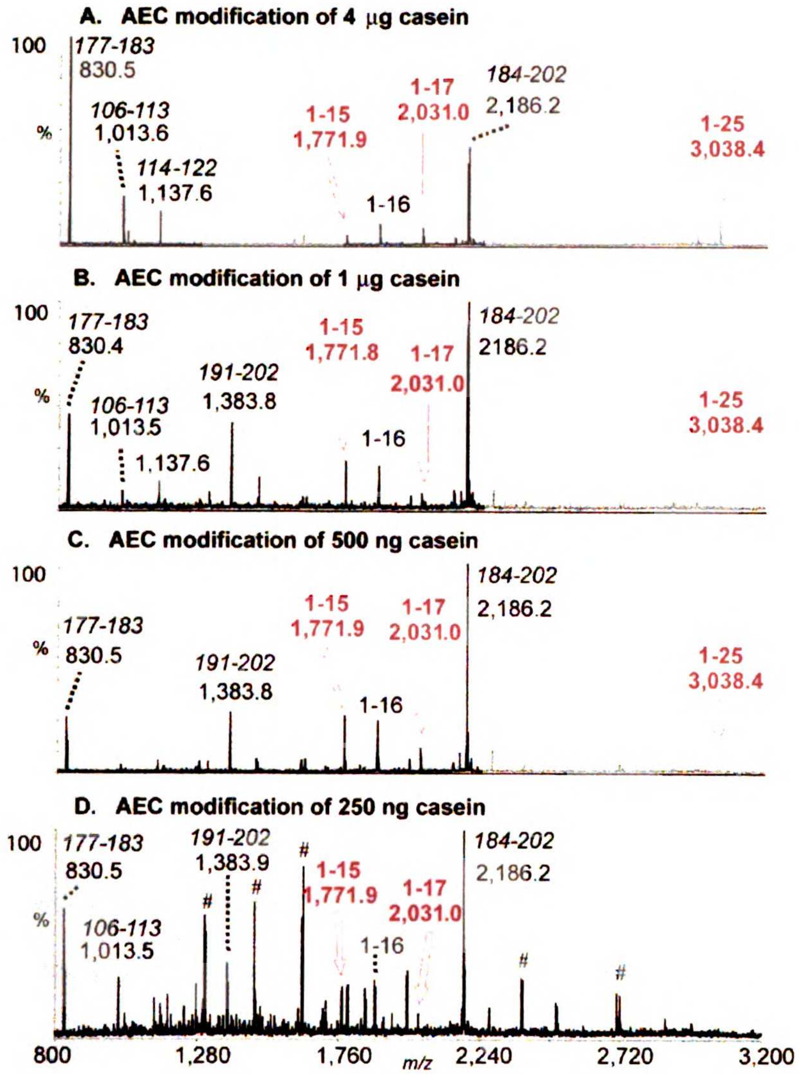

Figure 2.7. MALDI-MS peptide mass fingerprint spectra of several chemically modified β-casein preparations are shown. The chemical modification was performed independently with different amounts of β-casein starting material, as shown in panels (A) 4 µg, (B) 1 µg, (C) 500 ng, (D) 250 ng of β-casein. Subsequent to the chemical modification, samples were digested with trypsin and a total amount of 1 pmol of material was loaded and analyzed for each sample (A-D). The observed masses are labeled and annotated with starting and ending amino acids. Masses in red indicate peptides that are specific to chemical modification of phosphoserine to aminoethylcysteine.

more challenging itself may represent only one component of a more complex mixture [6]. In addition, such samples are often phosphorylated substoichoimetrically, and the phosphoprotein unrelated post-translational modifications as well as sequence variations can contribute to sample complexity. To investigate the applicability of our approach toward samples of greater complexity, we chose to analyze the phosphorylation of the cytoskeletal component tubulin by the G protein-coupled receptor kinase 2 (GRK2). While microtubules have been implicated in playing a role in GPCR endocytosis [20], their post-translational modifications and consequent functional roles in this process have only begun to be elucidated. GRK2 has recently been shown to associate with tubulin *in vitro*, co-localize with tubulin *in vivo*, and phosphorylate tubulin heterodimers in an agonist dependent fashion [21-23].

Bovine tubulin copurifies as a mixture of 21 charge variants of the approximately 12 genetic sub-isoforms of the major α– and β-tubulin isoforms [24, 25]. Tubulin purified from bovine brain was phosphorylated by recombinant GRK2 *in vitro*. As the precise amino acid sequence of bovine tubulins is not known, we chose to look for phosphopeptides based on the known porcine sequences, reasoning that there would be few sequence differences between the two organisms. The mixture of phosphorylated and nonphosphorylated α- and β- tubulin isoforms in the presence of the GRK2 kinase was subjected to aminoethylcysteine modification, and then digested with different combinations of proteases to generate fragments suitable for mass spectrometry. We then searched the mass spectra for signature ions indicating aminoethylcysteine formation and cleavage after aminoethylcysteine sites. Co-digestion with Lys-C and Asp-N yielded two peptides with masses of 1330.51 and 1604.52, corresponding to peptides that span residues 417-426 and 404-416 of β-tubulin and that contain one aminoethylcysteine or one β-methylaminoethylcysteine residue, respectively (Table 2.2).

Additional fragments corresponding to cleavage of these peptides directly at the two sites of phosphorylation were observed, and these fragment masses were sufficient to identify serine 420 and threonine 409 in β-tubulin as the phosphorylated residues. These assignments were confirmed by MS/MS sequencing of the derivatized peptides (Figure 2.9a), and none of these peptides were detected in control experiments lacking GRK2 treatment, confirming that GRK2 is the kinase responsible for this phosphorylation event. Interestingly, these phosphorylation sites occur near the C-terminus of β-tubulin, within a highly acidic 6-7 kDa region that has been shown to undergo multiple post-translational modifications [24, 25] and which does not contain any basic residues (except for a lysine at the extreme C-terminus in β_{III}-tubulin). Lastly, we note that while this manuscript was in preparation, Yoshida et al. reported the identification of the analogous sites in porcine tubulin as targets of GRK2 [26]. That study required a combination of radiolabelling, phosphoaminoacid TLC analysis, Edman degradation and the construction of chimeric substrates to pinpoint these sites.

Since GRK2 itself is known to be a phosphoprotein [26], we looked for GRK2 phosphopeptides that might be present in our *in vitro* kinase reactions. Following aminoethylcysteine modification and Lys-C digestion, we identified a peptide at *m/z* 1412.78, which corresponds to a Lys-C fragment spanning residues 666 to 677 of GRK2 and contains one aminoethylcysteine residue (Table 2.2, Figure 2.8a, and Figure 2.9b). Additional fragments were observed corresponding direct cleavage at the site of phosphorylation, identifying serine 670 as the site of modification. These results are consistent with earlier reports based on site-directed mutagenesis data that the S670A mutant is not phosphorylated in SF9 cells during protein expression [27].

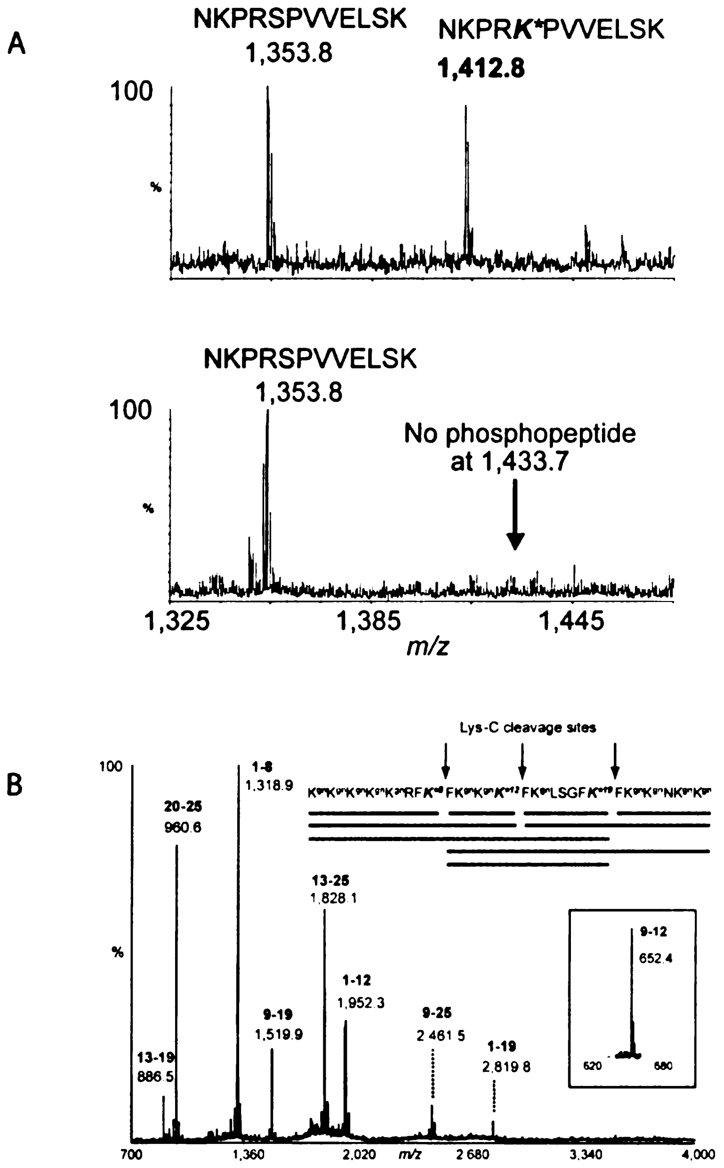

Figure 2.8. (A) Top Panel: The MALDI-MS spectrum displays molecular ions of peptides obtained after chemical modification of GRK2 and digestion with endoprotease Lys-C. The nonphosphorylated peptide observed at *m/z* 1353.8 (residues 666-677) is in approximately equal abundance to the corresponding aminoethylcysteine modified peptide at *m/z* 1412.8. Bottom Panel: MALDI-MS of Lys-C digest of GRK-2 without chemical modification. The unmodified phosphopeptide (residues 666-677, containing phosphoserine 670) with an expected molecular ion at *m/z* 1433.8 is not observed. (B) MALDI-MS spectrum following Lys-C cleavage of perguanidinated MARCKS substrate – a 25 residue peptide, $K^{gn}K^{gn}K^{gn}K^{gn}K^{gn}RFK^{*8}FK^{gn}K^{gn}K^{*12}FK^{gn}LSGFK^{*19}FK^{gn}K^{gn}NK^{gn}K^{gn}$ (K^{gn}: homoarginine; K^{*}: aminoethylcysteine). An inset showing a mass range from *m/z* 620-680 reveals a cleavage product at m/z 652.4 (peptide Phe9 – Lys*12) that was observed by MALDI-MS in a similar experiment after extended digestion with Lys-C.

In the kinase reactions used in this study, GRK2 is present at ~10% stoichiometry relative to the tubulin substrate. Moreover, inspection of the MALDI-MS spectrum of a GRK2 digest indicates that the phosphorylation of serine 670 itself is further substoichiometric, as the aminoethylcysteine modified and nonphosphorylated (unmodified) peptides spanning residues 666-677 are equally abundant (Figure 2.8a). To explore the sensitivity of this approach for identification of phosphorylation sites within a moderately complex and substoichiometric mixture, we carried out dilution experiments to determine the amount of starting protein from a kinase reaction that can be carried through the aminoethylcysteine chemistry. Aminoethylcysteine modified peptides spanning GRK2 residues 666-677 and 668-677 were identified by LC-MS from 375 fmol of starting material; the peptide spanning residues 671-677 was detected at a level of 750 fmol. The tubulin phosphorylation sites could be identified at a level of 1.2 pmol of β-tubulin starting material. Lower starting amounts of tubulin were not tested, and the precise distribution of modified and cleaved peptides was dependent on the specific digest conditions used. However, this suggests that moderately substoichiometric and low abundance phosphorylation events can be analyzed via aminoethylcysteine modification in the absense of any pre-enrichment for phosphopeptides, although such enrichment would undoubtedly yield further improvements in sensitivity [6]. Lastly, similar titration experiments were performed with β-casein and the unfractionated digests were analyzed by MALDI-MS, yielding somewhat lower sensitivity (Figure 2.7).

2.5 Cleavage exclusively at phosphorylation sites

In some cases, it may be desirable to obtain cleavage exclusively at the phosphorylation site (not at lysine residues), generating larger fragments that might

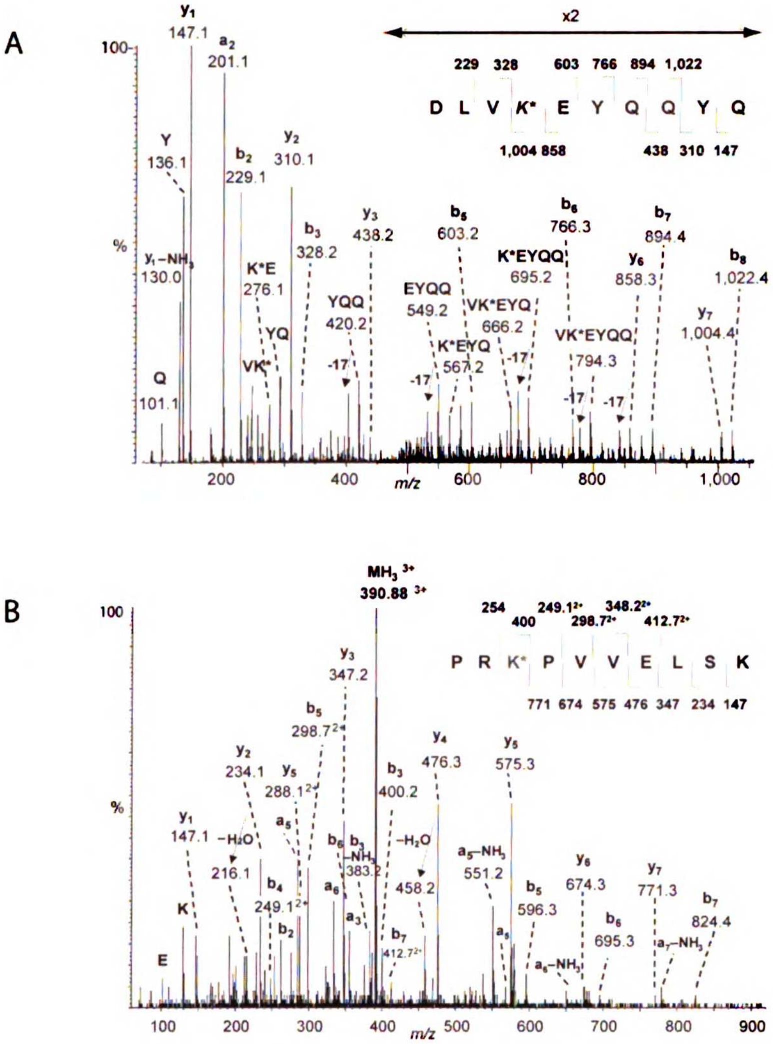

Figure 2.9. (A) ESI-MS/MS spectrum of peptide DLVK*EYQQYQ [residues Asp417-Gln426] obtained after aminoethylcysteine modification of phosphoserine residues and digestion of tubulin with Lys-C/Asp-N. The molecular ion $[M + 2H]^{2+}$ at m/z 666.26^{2+} ($M = 1330.51$) was selected for CID. (B) ESI-MS/MS spectrum of peptide PRK*PVVELSK [residues Pro668-Lys677] obtained after aminoethylcysteine modification of phosphoserine residues and digestion of GRK2 with Lys-C. The molecular ion $[M + 3H]^{3+}$ at m/z 390.88^{3+} ($M = 1169.62$) was selected for CID.

Peptide	Residues	Peptide Sequence	Mr Obs. (Calcd.)
MARCKS-guanil	1-25	KKKKKRFK*FKKK*FKLSGFK*FKKNKK	3,763.4$^{\#}$ (3,764.2$^{\#}$)
MARCKS-ac	1-25		3,802.33 (3,802.07)
MARCKS-guanil	1-19	KKKKKRFK*FKKK*FKLSGFK*	2,818.75 (2,818.61)
MARCKS-ac	1-19		**2,860.75** (2,860.53)
MARCKS-guanil	1-12	KKKKKRFK*FKKK*	1,951.24 (1,951.17)
MARCKS-ac	1-12		**1,993.27** (1,993.10)
MARCKS-guanil	1-8	KKKKKRFK*	1,317.86 (1,317.81)
MARCKS-ac	1-8		**1,359.90** (1,359.77)
MARCKS-guanil	9-25	(K*)FKKK*FKLSGFK*FKKNKK	2,460.44 (2,460.38)
MARCKS-ac	9-25		2,460.50 (2,460.31)
MARCKS-guanil	9-19	(K*)FKKK*FKLSGFK*	1,518.85 (1,518.80)
MARCKS-ac	9-19		1,518.92 (1,518.77)
MARCKS-guanil	9-12	(K*)FKKK*	651.39 (651.34)**
MARCKS-ac	9-12		651.37 (651.34)**
MARCKS-guanil	13-25	(K*)FKLSGFK*FKKNKK	1,827.08 (1,827.03)
MARCKS-ac	13-25		**1,827.12** (1,826.98)
MARCKS-guanil	13-19	(K*)FKLSGFK*	885.53 (885.45)
MARCKS-ac	13-19		**885.57** (885.44)
MARCKS-guanil	20-25	(K*)FKKNKK	959.63 (959.59)
MARCKS-ac	20-25		**959.54** (959.54)

Table 2.3. Results of aminoethylcysteine modification and proteolytic digestion for the guanidinated or acetylated MARCKS substrate. Molecular weights were determined by LC-ESI-MS and MALDI-MS. All masses are exact monoisotopic masses except for one average mass marked with “#” (measured in linear mode). All masses listed in bold letters were additionally confirmed by LC-MS/MS. Abbreviations: *K**: aminoethylcysteine; ac-: acetylated N-terminus. For MARCKS-guanil substrate masses, all lysine residues are guanidinated at the □-amino group yielding a homoarginine residue (the N-terminus is free) (see Figure 2B). For MARCKS-ac substrate masses, all lysine residues are acetylated at the ε-amino group, in addition, the N-terminus is acetylated. ** MARCKS-ac peptide Phe9 – Lys*12 was observed by MALDI after extended digestion with Lys-C beyond that shown in Figure 2.10.

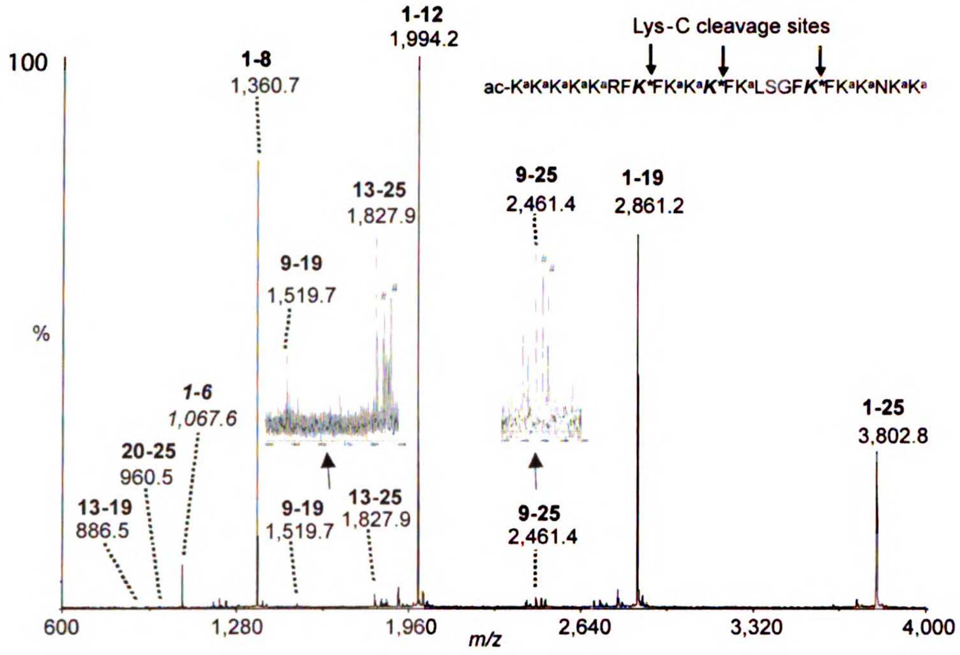

Figure 2.10. MALDI-MS spectrum following Lys-C cleavage of peracetylated MARCKS substrate – a 25 residue peptide, ac-K^{a}K^{a}K^{a}K^{a}K^{a}RFK*FK^{a}K^{a}K*FK^{a}LSGFK*FK^{a}K^{a}NK^{a}K^a Abbreviations: ac-: acetylated N-terminus; K^a: lysine with acetylated ε-amino side chain; K*: aminoethylcysteine. Lys-C cleavages were observed at Lys* residues 8, 12, and 19 resulting in various combinations of cleaved peptides. Insets zoom into ranges of the full mass spectrum magnifying mass ranges from *m/z* 1450-1900 and 2360-2600, respectively in order to detect low abundant proteolytic cleavage products.

provide information about the gross topology of phosphorylation. The MARCKs substrate, a 25 residue peptide containing 12 lysine and three phosphoserine residues, was selected to explore the feasibility of achieving phosphoexclusive cleavage. To do this, lysine residues were first converted to homoarginine using o-methylisourea in order to block digestion at those sites with Lys-C. In addition to blocking proteolytic digestion, this modification has several practical advantages, including the enhancement of the ionization of homoarginine containing peptides in MALDI [28-30] and reaction conditions that can facilitate the nearly quantitative (90-99%) guanidination of the lysine residues in full-length proteins [31, 32].

Following guanidination, the MARCKS substrate was modified as aminoethylcysteine, digested with Lys-C, and subjected to mass analysis by MALDI (Figure 2.8b). The MALDI mass spectrum from the digest exhibits eight prominent peaks corresponding to eight of nine possible combinations of cleavage at the three phosphorylation sites (Table 2.3). The smallest fragment, corresponding to cleavage at aminoethylcysteine residues 8 and 12 ($m/z = 652.4$), required longer digestion times and higher concentrations of protease to detect and is shown inset. No other major products are observed, confirming that homoarginine is not a substrate for Lys-C. Alternative chemistries are known for efficiently blocking lysine residues, and we have obtained similar results by acetylation (Table 2.3 and Figure 2.10), although this modification may be less practical for full-length proteins.

2.6 A solid-phase aminoethylcysteine reaction

Although phosphorylation is among the most common post-translational modifications, phosphoproteins are often present at low abundance and phosphorylated

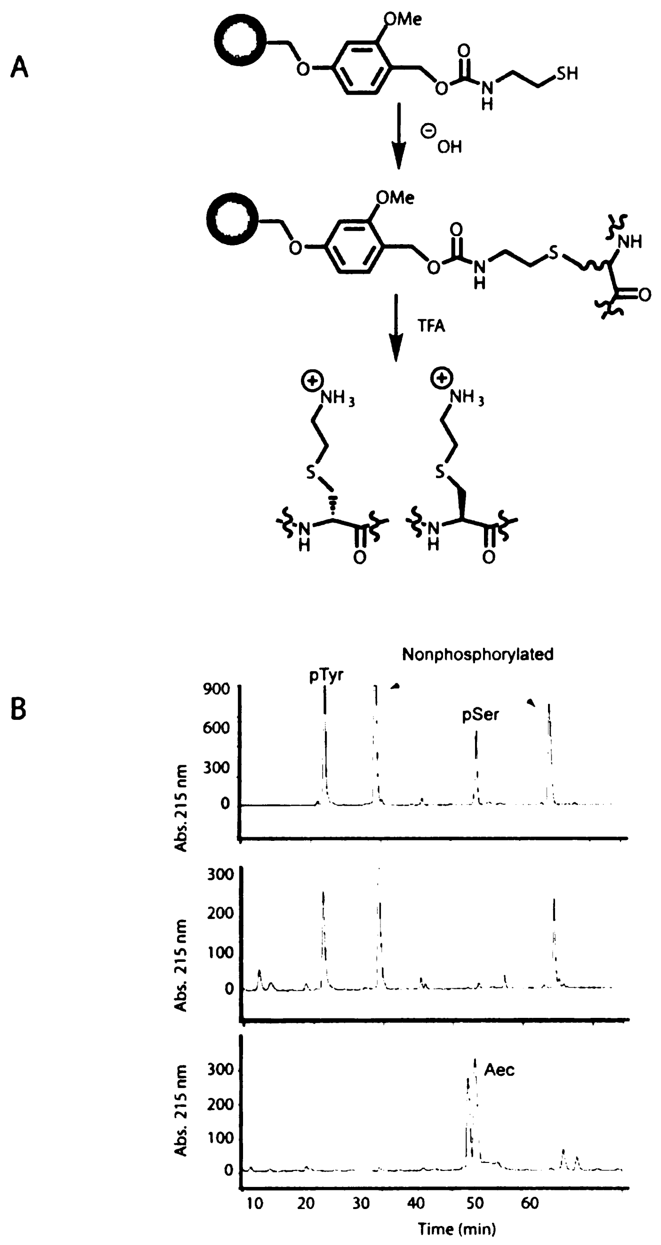
A
OMe
O
O
N
H
SH
OH
OMe
O
O
N
H
S
NH
O
TFA
NH3
S
N
H
O
NH3
S
N
H
O
B
Nonphosphorylated
pTyr
pSer
900
600
300
0
Abs. 215 nm
300
200
100
0
Abs. 215 nm
Aec
300
200
100
0
Abs. 215 nm
10
20
30
40
50
60
Time (min)

Figure 2.11. (A) Scheme for the capture and modification of phosphoserine peptides using a solid-phase reagent. (B) Selective capture and modification of phosphoserine peptides using the cysteamine resin. Top, starting material; middle, flow-through; bottom, released aminoethylcysteine peptides. Peptide sequences (left to right, top panel): ZAAPpYGGY*D, ZAAPYGGY*D, ZFRPpSGFY*D, ZFRPFGFY*D. Z: 2-aminobenzoic acid; Y*: 3-nitrotyrosine.

sub-stoichiometrically, making genome wide phosphorylation analysis an analytical challenge. Several approaches have been proposed for the selective enrichment of phosphopeptides from complex mixtures [7, 8, 10], and the aminoethylcysteine derivatization described here should be compatible with the use of many of these strategies as a first step to enrich for phosphorylated peptides. However, we sought to investigate whether it would be possible to couple aminoethylcysteine modification directly to an approach for phosphopeptide enrichment. For this purpose, we adapted the aminoethylcysteine reaction to a solid phase catch and release strategy to provide one step modification and enrichment of phosphopeptides.

To prepare an appropriate solid phase cysteamine equivalent, a polyethyleneglycol-polystyrene (PEG-PS) copolymer base resin was loaded with cystamine as the benzyl carbamate (Figure 2.11a). This design incorporates two important features that facilitate aminoethylcysteine modification. First, the PEG-PS resin swells in both organic and aqueous solvents, allowing resin capture to be performed under conditions that have been optimized for the solution phase chemistry. Secondly, the methoxybenzyl carbamate linkage is stable to the basic conditions of the β-elimination reaction, allowing for efficient peptide capture, but highly acid labile, facilitating aminoethylcysteine peptide release by brief treatment with trifluoroacetic acid (TFA).

We tested the ability of this reagent to selectively capture and modify phosphopeptides by incubating the resin with an approximately equimolar mixture of two nonphosphorylated peptides, one phosphotyrosine peptide, and one phosphoserine peptide under β-elimination conditions for one hour (Figure 2.11b, panel 1). Following incubation, HPLC analysis of the flow through indicated that the nonphosphorylated and phosphotyrosine peptides remained intact, but the phosphoserine peak was absent, consistent with selective capture of the phosphoserine peptide (Figure 2.11b, panel 2). Brief treatment with TFA released the phosphoserine peptide as the aminoethylcysteine modified diastereomer pair (Figure 2.11b, panel 3), suitable for enzymatic phosphorylation mapping. This type of approach has the potential to allow proteolytic phosphorylation site-mapping to be directly coupled to phosphopeptide enrichment from complex mixtures. The optimization and application of this solid-phase reaction is currently being explored.

2.7 Discussion

We describe here an approach for mapping protein phosphorylation by direct enzymatic cleavage of polypeptides at the site of post-translational modification. Despite the large number of unique protease specificities found in nature, this reaction is to our knowledge the first example of selective proteolysis at any site of protein post-translational modification. We believe that this type of approach will be a valuable complement to traditional MS/MS sequencing as a strategy for phosphorylation site mapping. In this regard, we have recently designed a protease that shows selectivity for phosphotyrosine substrates (Z.A.K. & K.M.S., unpublished observations). As O-glycosylated residues also undergo β-elimination under basic conditions [33], it may be possible to extend this strategy to map protein glycosylation in an analogous fashion; in this regard, it will be important to investigate ways to distinguish between phosphorylation and glycosylation [33-35], such as pretreatment with an appropriate glycosidase or phosphatase. We envision a rapid expansion of enzyme tools for selective interrogation of the proteome, with tailor-made sequence specificity for all natural post-translational modifications.

2.8 Experimental Procedures

2.8.1 Reagents

Sequencing grade Trypsin, Lys-C, and Asp-N were from Roche Diagnostics. Lysyl Endopeptidase was from Wako. Tentagel AC resin was from Advanced Chemtech. All peptides were from Anaspec or synthesized using standard Fmoc solid-phase chemistry. All other reagents were from Sigma unless otherwise noted and were of the highest grade commercially available.

2.8.2 Aminoethylcysteine modification of model peptides

The model phosphoserine peptides were dissolved in a 4:3:1 solution of H_2O:DMSO:EtOH (50 μL). The β-elimination solution (saturated $Ba(OH)_2$ solution (23 μL) and 5M NaOH (1 μL)) was added, and the reaction was incubated at room temperature. After 1 hour, a 1M solution of cysteamine in H_2O (50 μL) was added directly to this reaction and the reaction was incubated 3 – 6 hours at room temperature. For peptides containing pSer-Pro sequences and pThr residues, the β-elimination reaction was allowed to proceed for two hours at 37° C. Reactions were analyzed by dilution into 1 ml H_2O/0.1% TFA and separation of the reaction products by reverse phase HPLC on a Dynamax SD-200 solvent delivery system (Rainin) equipped with a Zorbax 300 C-18 9.4 mm x 25 cm column. Individual fractions were analyzed by ESI-MS offline using a Micromass ZQ (Waters) or by MALDI-MS and ESI-MS/MS. (below).

For site-mapping, modified peptides were reconstituted in either 10 mM Tris, pH 8.5 (Trypsin) or 10 mM Tris, pH 8.5, 1 mM EDTA (Lys-C) and digested overnight at 37° C. Reactions were analyzed as above. For FRET monitoring of the Lys-C digestion of diastereomeric aminoethylcysteine peptides, peptide diastereomers (~ 5 μg) were separated by HPLC, and digested with 5 μg Trypsin. Reaction progress was monitored as emission at 420 nm following excitation at 320 nm in a SpectraMax GeminiXS fluorescence plate reader (Molecular Devices) as described[36].

2.8.3 Modification for Phosphoexclusive Cleavage

For guanidination reactions, the MARCKS substrate or β-casein was dissolved in 0.5 M O-methylisourea, pH 10.5 and incubated overnight at 37° C essentially as described[29, 30, 37]. For acetylation reactions, the MARCKS substrate was dissolved in 100 mM $NaHCO_3$, pH 8.5 and treated with approximately 100 equivalents of sulphosuccinimidyl acetate (Pierce) for 2 hours at room temperature to quantitatively acetylate lysine residues. Reactions were desalted by HPLC or dialysis and subjected to aminoethylcysteine modification and Lys-C digestion as above.

Mass spectra were obtained by matrix-assisted laser desorption ionization time-of-flight (MALDI-TOF) mass spectrometry on a Voyager DESTR plus (Applied Biosystems). All mass spectra were acquired in positive-ionization mode with reflectron optics. The instrument was equipped with a 337 nm nitrogen laser and operated under delayed extraction conditions in reflectron mode; a delay time of 190 nsec, and grid voltage 66-70% of full acceleration voltage (20-25 kV). For linear mode experiments, the delay time was 100 nsec and the grid voltage 93.4% of the acceleration voltage. Prior to MALDI-MS analysis, the proteolytic reaction mixtures were desalted with reversed-phase Zip Tips$_{C18}$ (C-18 resin, Millipore). All peptide samples were prepared using a matrix solution consisting of 33 mM HCCA in acetonitrile/methanol (1/1; v/v); 1 μL of analyte (0.1-1 pmol of material) was mixed with 1 μL of matrix solution, and then air-dried at room temperature on a stainless steel target. Typically, 50 laser shots were used to record each spectrum. The obtained mass spectra were externally calibrated with an equimolar mixture of angiotensin I, ACTH 1-17, ACTH 18-39, and ACTH 7-38.

2.8.4 Aminoethylcysteine modification of α and β–casein

α-casein was pretreated with performic acid for 2 hours to quantitatively oxidize cysteine residues[8]; β-casein, which contains no cysteine residues, was used as provided by the manufacturer. Proteins (ca. 2 μg) were modified in 0.5 mL microcentrifuge tubes using the same conditions as described for peptides, except that the sample volume was adjusted to maintain a protein concentration greater than or equal to 0.01 μg/μL. When the reaction was complete, reagents were removed by dialysis overnight against 1 liter of 20 mM Tris, pH 8.0 using 10000 MWCO Slide-A-Lyzer Mini Dialysis units (Pierce). Other methods for reaction solvent exchange (e.g. gel filtration) led to unacceptable sample losses. Dialyzed samples were transferred to a new 0.5 mL microcentrifuge tube, and the dialysis membrane was washed three times with 10 μL of 20 mM Tris, pH 8.0. Samples were concentrated to ~ 5 μL by Speedvac and 5 μL of acetonitrile was added as a denaturant. The sample mixture was heated to 65° C for 10 minutes and then the digestion was initiated by the addition of 15 μL of 10 mM Tris, pH 8.0 containing trypsin or Lys-C at 1/10 enzyme to substrate by weight. Reactions were allowed to proceed approximately 6 hours at 37° C.

The proteolytic peptide mixtures (ca. 1 pmol) were analyzed by MALDI-MS as described or by reversed-phase HPLC-MS/MS. Briefly, peptides were separated on an Ultimate nanocapillary HPLC system equipped with a PepMap™ C18 nano-column (75 μm I.D. x 15 cm) (LC Packings) and CapTrap Micro guard column (0.5 μL bed volume, Michrom). Peptide mixtures were loaded onto the guard column and washed with the loading solvent (H_2O/0.05 % formic acid, flow rate: 20 μL/min) for 5 min to remove salts and denaturing reagents, then transferred onto the analytical C18-nanocapillary HPLC column and eluted at a flow rate of 300 nL/min using the following gradient: 2% B (from 0-5 min), and 2-70% B (from 5-55 min). Solvent A consisted of 0.05 % formic acid in 98% H_2O/2 % ACN and solvent B consisted of 0.05% formic acid in 98% ACN/2% H_2O. The column eluant was directly coupled to QSTAR quadrupole orthogonal TOF mass spectrometer (MDS Sciex) equipped with a Protana nanospray ion source. The nanospray needle voltage was typically 2300 V in the HPLC-MS mode. Mass spectra (ESI-MS) and tandem mass spectra (ESI-MS/MS) were recorded in positive-ion mode with a resolution of 12000-15000 FWHM. For collision induced dissociation tandem mass spectrometry (CID-MS/MS), the mass window for precursor ion selection of the quadrupole mass analyzer was set to ± 1 mass unit. The precursor ions were fragmented in a collision cell using nitrogen as the collision gas. The LC-MS runs on the QSTAR instrument were acquired in “Information Dependent Acquisition” mode (advanced IDA), which allows the user to acquire MS/MS spectra based on an inclusion mass list and dysnamic assessment of relative ion. Spectra were calibrated in static nanospray mode using MS/MS fragment-ions of a renin peptide standard (His immonium-ion with *m/z* at 110.0713, and b_8-ion with *m/z* at 1028.5312) providing a mass accuracy of ≤50 ppm.

2.8.5 Phosphorylation mapping of GRK2 and tubulin

N-terminal His6-tagged GRK2 was expressed in SF9 insect cells and purified using Ni-NTA beads (Qiagen) as described [38]. Bovine tubulin was a gift from Ron Vale. Tubulin (5 μM) and GRK2 (0.6 μM) were incubated in 100 *μ*l of 20 mM HEPES, pH 7.4, 2.0 mM EDTA, 10 mM $MgCl_2$ containing 1 mM ATP. Kinase reactions were performed at 25 °C for 3 hours [23], after which the reactions were desalted by microdialysis, subjected to aminoethylcysteine modification, digested with either Lys-C/Trypsin or Lys-C/Asp-N, and finally analyzed by LC-MS/MS and MALDI-MS as described above. In a similar fashion, purified GRK2 (~5 ug) was subjected to aminoethylcysteine modification, digested with Lys-C, and then analyzed by mass spectrometry as described.

2.8.6 Resin Synthesis

Resin was loaded using a modification of the procedure of Dorff [39]. Briefly, Tentagel AC resin (5 g) was swelled in anhydrous THF (75 mL) at room temperature under an inert atmosphere. 1,1 carbonyldiimidazole (2.5 g) was added and stirred for 3 hours. The resin was filtered, washed with THF, Et_2O, and dried *in vacuo* overnight.

Before use, cystamine HCl salt (5 g) was dissolved in H_20 (45 mL), the pH was adjusted to 12 with NaOH, and the cystamine was extracted with CH_2Cl_2. The organic phase was dried with $MgSO_4$, filtered, and the solvent removed *in vacuo* to give a clear oil. This oil (ca. 1 g) was added to the activated resin (2 g) swelled in THF (25 mL). N-methylmorpholine (2 mL) was added and the resin was heated to 60° C for 4 – 6 hours under an inert atmosphere.

The resin was filtered, washed with THF, Et_2O, dried in vacuo, and stored at –20° C. Immediately before use, the resin was deprotected by brief treatment (15 min.) with 100 mM DTT in H_2O to expose the cysteamine thiol. Quantitation of resin loading with Ellman's reagent typically demonstrated 60 – 80% loading (0.20 to 0.25 mmol/g).

2.8.7 Solid-Phase Capture and Modification of Phosphoserine Peptides

Following deprotection, the resin was washed with 5 times with H_2O and 5 times with 4:3:1 H_2O:DMSO:EtOH. Peptides were dissolved in 4:3:1 H_2O:DMSO:EtOH (250

µl) and added to 80 mg of resin swollen in the same. Sat. $Ba(OH)_2$ (225 µL) and 5M NaOH (10 µL) were added and the reaction was incubated for one hour at room temperature. The resin was then rinsed successively with H_2O, DMF, CH_2Cl_2 and Et_2O and dried overnight *in vacuo*. To release the peptides, the dried resin was suspended in 95:2.5:2.5 TFA:Me_2S:H_2O (1 mL) for 15 minutes at room temperature. The resin was then filtered, washed 3 times with TFA (1 mL), and the filtrate was concentrated *in vacuo*. The released peptides were taken up in H_2O/0.1% TFA and analyzed by HPLC and MS as described.

2.8.8 Supplementary Aminoethylcysteine Modification Protocol

Several parameters were found to be critical for successful aminoethylcysteine modification: (1) Limiting hydroxide concentration to ~150 mM, (2) adding barium as a specific catalyst for phosphate elimination [13], (3) carrying out reactions in a previously optimized mixture of DMSO, water, and ethanol [14], (4) carefully limiting the reaction length and temperature (one hour at room temperature was sufficient for most phosphoserine peptides; two hours at 37° C was required for peptides containing phosphothreonine and phosphoserine residues N-terminal to proline), (5) performing the β-elimination and Michael addition steps consecutively, such that the addition of cysteamine to the basic reaction mixture in the second step reduces the pH of the reaction to ~ 8, and (6) allowing the Michael addition step to proceed for up to 6 hours for full modification of phosphothreonine peptides.

Protein samples for aminoethylcysteine modification are first desalted overnight by microdialysis against 2 liters water using 10000 MWCO Slide-A-Lyzer Mini Dialysis units. Before use, dialysis units are rinsed extensively to remove any polymeric material that remains from the manufacturing process. Following dialysis, dialyzed samples are

transferred to 0.5 mL eppendorf tubes, and the dialysis membrane is washed three times with 20 μL water. The combined dialyate is then concentrated by Speed-Vac to reduce volume to ~5 μL, with care not to concentrate to dryness. 5 μL of a 3:1 mixture of DMSO:EtOH is added directly to this sample. β-elimination is initiated by the addition of 4.6 μL sat. $Ba(OH)_2$ and 1 μL 500 mM NaOH. For most proteins, a 2 hour incubation in a 37° C water bath is recommended. At this stage, solutions of some full-length proteins may appear somewhat heterogeneous; this has no effect on the efficiency of the reaction, but gentle vortexing every 20 or 30 minutes is recommended to prevent excessive aggregation. After two hours, the sample is placed at room temperature. While the sample is cooling (5 – 10 minutes), a 1 M solution of cysteamine HCl is freshly prepared, and 10 μL of this solution is added directly to the β-elimination reaction. This reaction is allowed to proceed 3 to 6 hours at room temperature.

When the Michael addition reaction is complete, the protein solution is transferred to a rinsed mini-dialysis unit and dialyzed overnight against 2 liters of 20 mM Tris, pH 8.0. The eppendorf tube from the β-elimination reaction is rinsed three times with 15 ml of 20 mM Tris, pH 8.0 to ensure complete protein transfer. Following dialysis, the protein is transferred to a new 0.5 mL eppendorf tube, with careful rinsing of the dialysis membrane. This protein solution is then concentrated by Speed-Vac. This concentrated protein sample is then ready for digestion with appropriate proteases (e.g., trypsin or Lys-C) and analysis by LC-MS/MS or MALDI-MS. In general, we find that Lys-C cleaves at modified sites somewhat more efficiently than trypsin, and that it is advisable to use slightly higher concentrations of protease than would be recommended for an ordinary trypsin digestion, although optimal digestion conditions vary significantly between samples.

2.9 References

1. Venter, J.C., Adams, M.D., Myers, E.W., Li, P.W., Mural, R.J., Sutton, G.G., Smith, H.O., Yandell, M., Evans, C.A., Holt, R.A., Gocayne, J.D., Amanatides, P., Ballew, R.M., Huson, D.H., Wortman, J.R., Zhang, Q., Kodira, C.D., Zheng, X.H., Chen, L., Skupski, M., Subramanian, G., Thomas, P.D., Zhang, J., Gabor Miklos, G.L., Nelson, C., Broder, S., Clark, A.G., Nadeau, J., McKusick, V.A., Zinder, N., Levine, A.J., Roberts, R.J., Simon, M., Slayman, C., Hunkapiller, M., Bolanos, R., Delcher, A., Dew, I., Fasulo, D., Flanigan, M., Florea, L., Halpern, A., Hannenhalli, S., Kravitz, S., Levy, S., Mobarry, C., Reinert, K., Remington, K., Abu-Threideh, J., Beasley, E., Biddick, K., Bonazzi, V., Brandon, R., Cargill, M., Chandramouliswaran, I., Charlab, R., Chaturvedi, K., Deng, Z., Di Francesco, V., Dunn, P., Eilbeck, K., Evangelista, C., Gabrielian, A.E., Gan, W., Ge, W., Gong, F., Gu, Z., Guan, P., Heiman, T.J., Higgins, M.E., Ji, R.R., Ke, Z., Ketchum, K.A., Lai, Z., Lei, Y., Li, Z., Li, J., Liang, Y., Lin, X., Lu, F., Merkulov, G.V., Milshina, N., Moore, H.M., Naik, A.K., Narayan, V.A., Neelam, B., Nusskern, D., Rusch, D.B., Salzberg, S., Shao, W., Shue, B., Sun, J., Wang, Z., Wang, A., Wang, X., Wang, J., Wei, M., Wides, R., Xiao, C., Yan, C., Yao, A., Ye, J., Zhan, M., Zhang, W., Zhang, H., Zhao, Q., Zheng, L., Zhong, F., Zhong, W., Zhu, S., Zhao, S., Gilbert, D., Baumhueter, S., Spier, G., Carter, C., Cravchik, A., Woodage, T., Ali, F., An, H., Awe, A., Baldwin, D., Baden, H., Barnstead, M., Barrow, I., Beeson, K., Busam, D., Carver, A., Center, A., Cheng, M.L., Curry, L., Danaher, S., Davenport, L., Desilets, R., Dietz, S., Dodson, K., Doup, L., Ferriera, S., Garg, N., Gluecksmann, A., Hart, B., Haynes, J., Haynes, C., Heiner, C., Hladun, S., Hostin, D., Houck, J., Howland, T., Ibegwam, C., Johnson, J., Kalush, F., Kline, L., Koduru, S., Love, A., Mann, F., May, D., McCawley, S., McIntosh, T., McMullen, I., Moy, M., Moy, L., Murphy, B., Nelson, K., Pfannkoch, C., Pratts, E., Puri, V., Qureshi, H., Reardon, M., Rodriguez, R., Rogers, Y.H., Romblad, D., Ruhfel, B., Scott, R., Sitter, C., Smallwood, M., Stewart, E., Strong, R., Suh, E., Thomas, R., Tint, N.N., Tse, S., Vech, C., Wang, G., Wetter, J., Williams, S., Williams, M., Windsor, S., Winn-Deen, E., Wolfe, K., Zaveri, J., Zaveri, K., Abril, J.F., Guigo, R., Campbell, M.J., Sjolander, K.V., Karlak, B., Kejariwal, A., Mi, H., Lazareva, B., Hatton, T., Narechania, A., Diemer, K., Muruganujan, A., Guo, N., Sato, S., Bafna, V., Istrail, S., Lippert, R., Schwartz, R., Walenz, B., Yooseph, S., Allen, D., Basu, A., Baxendale, J., Blick, L., Caminha, M., Carnes-Stine, J., Caulk, P., Chiang, Y.H., Coyne, M., Dahlke, C., Mays, A., Dombroski, M., Donnelly, M., Ely, D., Esparham, S., Fosler, C., Gire, H., Glanowski, S., Glasser, K., Glodek, A., Gorokhov, M., Graham, K., Gropman, B., Harris, M., Heil, J., Henderson, S., Hoover, J., Jennings, D., Jordan, C., Jordan, J., Kasha, J., Kagan, L., Kraft, C., Levitsky, A., Lewis, M., Liu, X., Lopez, J., Ma, D., Majoros, W., McDaniel, J., Murphy, S., Newman, M., Nguyen, T., Nguyen, N., Nodell, M., Pan, S., Peck, J., Peterson, M., Rowe, W., Sanders, R., Scott, J., Simpson, M., Smith, T., Sprague, A., Stockwell, T., Turner, R., Venter, E., Wang, M., Wen, M., Wu, D., Wu, M., Xia, A., Zandieh, A., and Zhu, X. (2001). The sequence of the human genome. Science *291*, 1304-1351.

2. Manning, G., Whyte, D.B., Martinez, R., Hunter, T., and Sudarsanam, S. (2002). The protein kinase complement of the human genome. Science *298*, 1912-1934.

3. Shah, K., and Shokat, K.M. (2002). A chemical genetic screen for direct v-Src substrates reveals ordered assembly of a retrograde signaling pathway. Chem Biol *9*, 35-47.

4. Bishop, A.C., Ubersax, J.A., Petsch, D.T., Matheos, D.P., Gray, N.S., Blethrow, J., Shimizu, E., Tsien, J.Z., Schultz, P.G., Rose, M.D., Wood, J.L., Morgan, D.O., and Shokat, K.M. (2000). A chemical switch for inhibitor-sensitive alleles of any protein kinase. Nature *407*, 395-401.

5. McLachlin, D.T., and Chait, B.T. (2001). Analysis of phosphorylated proteins and peptides by mass spectrometry. Curr Opin Chem Biol *5*, 591-602.

6. Mann, M., Ong, S.E., Gronborg, M., Steen, H., Jensen, O.N., and Pandey, A. (2002). Analysis of protein phosphorylation using mass spectrometry: deciphering the phosphoproteome. Trends Biotechnol *20*, 261-268.

7. Zhou, H., Watts, J.D., and Aebersold, R. (2001). A systematic approach to the analysis of protein phosphorylation. Nat Biotechnol *19*, 375-378.

8. Oda, Y., Nagasu, T., and Chait, B.T. (2001). Enrichment analysis of phosphorylated proteins as a tool for probing the phosphoproteome. Nat Biotechnol *19*, 379-382.

9. Steen, H., and Mann, M. (2002). A new derivatization strategy for the analysis of phosphopeptides by precursor ion scanning in positive ion mode. J Am Soc Mass Spectrom *13*, 996-1003.

10. Ficarro, S.B., McCleland, M.L., Stukenberg, P.T., Burke, D.J., Ross, M.M., Shabanowitz, J., Hunt, D.F., and White, F.M. (2002). Phosphoproteome analysis by mass spectrometry and its application to Saccharomyces cerevisiae. Nat Biotechnol *20*, 301-305.

11. Meyer, H.E., Hoffmann-Posorske, E., Korte, H., and Heilmeyer, L.M., Jr. (1986). Sequence analysis of phosphoserine-containing peptides. Modification for picomolar sensitivity. FEBS Lett *204*, 61-66.

12. Simpson, D.L., Hranisavljevic, J., and Davidson, E.A. (1972). Elimination and sulfite addition as a means of localization and identification of substituted seryl and threonyl residues in proteins and proteoglycans. Biochemistry *11*, 1849-1856.

13. Byford, M.F. (1991). Rapid and selective modification of phosphoserine residues catalysed by Ba2+ ions for their detection during peptide microsequencing. Biochem J *280 (Pt 1)*, 261-265.

14. Adamczyk, M., Gebler, J.C., and Wu, J. (2001). Selective analysis of phosphopeptides within a protein mixture by chemical modification, reversible biotinylation and mass spectrometry. Rapid Commun Mass Spectrom *15*, 1481-1488.

15. Goshe, M.B., Conrads, T.P., Panisko, E.A., Angell, N.H., Veenstra, T.D., and Smith, R.D. (2001). Phosphoprotein isotope-coded affinity tag approach for isolating and quantitating phosphopeptides in proteome-wide analyses. Anal Chem *73*, 2578-2586.

16. Jaffe, H., Veeranna, and Pant, H.C. (1998). Characterization of serine and threonine phosphorylation sites in beta-elimination/ethanethiol addition-modified proteins by electrospray tandem mass spectrometry and database searching. Biochemistry *37*, 16211-16224.

17. Annan, R.S., Huddleston, M.J., Verma, R., Deshaies, R.J., and Carr, S.A. (2001). A multidimensional electrospray MS-based approach to phosphopeptide mapping. Anal Chem *73*, 393-404.

18. Sarver, A., Scheffler, N.K., Shetlar, M.D., and Gibson, B.W. (2001). Analysis of peptides and proteins containing nitrotyrosine by matrix-assisted laser desorption/ionization mass spectrometry. J Am Soc Mass Spectrom *12*, 439-448.

19. Janek, K., Wenschuh, H., Bienert, M., and Krause, E. (2001). Phosphopeptide analysis by positive and negative ion matrix-assisted laser desorption/ionization mass spectrometry. Rapid Commun Mass Spectrom *15*, 1593-1599.

20. Limas, C.J., and Limas, C. (1983). Involvement of microtubules in the isoproterenol-induced 'down'-regulation of myocardial beta-adrenergic receptors. Biochim Biophys Acta *735*, 181-184.

21. Haga, K., Ogawa, H., Haga, T., and Murofushi, H. (1998). GTP-binding-protein-coupled receptor kinase 2 (GRK2) binds and phosphorylates tubulin. Eur J Biochem *255*, 363-368.

22. Pitcher, J.A., Hall, R.A., Daaka, Y., Zhang, J., Ferguson, S.S., Hester, S., Miller, S., Caron, M.G., Lefkowitz, R.J., and Barak, L.S. (1998). The G protein-coupled receptor kinase 2 is a microtubule-associated protein kinase that phosphorylates tubulin. J Biol Chem *273*, 12316-12324.

23. Carman, C.V., Som, T., Kim, C.M., and Benovic, J.L. (1998). Binding and phosphorylation of tubulin by G protein-coupled receptor kinases. J Biol Chem *273*, 20308-20316.

24. Banerjee, A. (2002). Coordination of posttranslational modifications of bovine brain alpha-tubulin. Polyglycylation of delta2 tubulin. J Biol Chem *277*, 46140-46144.

25. Alexander, J.E., Hunt, D.F., Lee, M.K., Shabanowitz, J., Michel, H., Berlin, S.C., MacDonald, T.L., Sundberg, R.J., Rebhun, L.I., and Frankfurter, A. (1991). Characterization of posttranslational modifications in neuron-specific class III beta-tubulin by mass spectrometry. Proc Natl Acad Sci U S A *88*, 4685-4689.

26. Yoshida, N., Haga, K., and Haga, T. (2003). Identification of sites of phosphorylation by G-protein-coupled receptor kinase 2 in beta-tubulin. Eur J Biochem *270*, 1154-1163.

27. Pitcher, J.A., Tesmer, J.J., Freeman, J.L., Capel, W.D., Stone, W.C., and Lefkowitz, R.J. (1999). Feedback inhibition of G protein-coupled receptor kinase 2 (GRK2) activity by extracellular signal-regulated kinases. J Biol Chem *274*, 34531-34534.

28. Beardsley, R.L., Karty, J.A., and Reilly, J.P. (2000). Enhancing the intensities of lysine-terminated tryptic peptide ions in matrix-assisted laser desorption/ionization mass spectrometry. Rapid Commun Mass Spectrom *14*, 2147-2153.

29. Beardsley, R.L., and Reilly, J.P. (2002). Optimization of guanidination procedures for MALDI mass mapping. Anal Chem *74*, 1884-1890.

30. Brancia, F.L., Oliver, S.G., and Gaskell, S.J. (2000). Improved matrix-assisted laser desorption/ionization mass spectrometric analysis of tryptic hydrolysates of proteins following guanidination of lysine-containing peptides. Rapid Commun Mass Spectrom *14*, 2070-2073.

31. Cupo, P., El-Deiry, W., Whitney, P.L., and Awad, W.M., Jr. (1980). Stabilization of proteins by guanidination. J Biol Chem *255*, 10828-10833.

32. Kimmel, J.R. (1967). Guanidination of Proteins. Methods Enzymol *11*, 584-589.

33. Mega, T., Nakamura, N., and Ikenaka, T. (1990). Modifications of substituted seryl and threonyl residues in phosphopeptides and a polysialoglycoprotein by beta-elimination and nucleophile additions. J Biochem (Tokyo) *107*, 68-72.

34. Wells, L.V., Keith; Cole, Robert N.; Cronshaw, Janet M., Matunis, Michael J., Hart, Gerald W. (2002). Mapping Sites of O-GlcNAc Modification Using Affinity Tags for Serine and Threonine Post-translational Modifications. Molecular and Cellular Proteomics *1*, 791-804.

35. Greis, K.D., Hayes, B.K., Comer, F.I., Kirk, M., Barnes, S., Lowary, T.L., and Hart, G.W. (1996). Selective detection and site-analysis of O-GlcNAc-modified glycopeptides by beta-elimination and tandem electrospray mass spectrometry. Anal Biochem *234*, 38-49.

36. Meldal, M., and Breddam, K. (1991). Anthranilamide and nitrotyrosine as a donor-acceptor pair in internally quenched fluorescent substrates for endopeptidases: multicolumn peptide synthesis of enzyme substrates for subtilisin Carlsberg and pepsin. Anal Biochem *195*, 141-147.

37. Bonetto, V., Bergman, A.C., Jornvall, H., and Sillard, R. (1997). C-terminal sequence analysis of peptides and proteins using carboxypeptidases and mass spectrometry after derivatization of Lys and Cys residues. Anal Chem *69*, 1315-1319.

38. Kim, C.M., Dion, S.B., Onorato, J.J., and Benovic, J.L. (1993). Expression and characterization of two beta-adrenergic receptor kinase isoforms using the baculovirus expression system. Receptor *3*, 39-55.

39. Dorff, P.a.H., J.R. (1995). A Solid Phase CBZ Chloride Equivalent - A New Matrix Specific Linker. Tetrahedron Letters *36*, 1589-1592.

Chapter 3

Isoform-specific phosphoinositide 3-kinase inhibitors from an arylmorpholine scaffold

3.1 Abstract

Phosphoinositide 3-kinases (PI3-Ks) are a ubiquitous class of signaling enzymes that regulate diverse cellular processes including growth, differentiation, and motility. Physiological roles of PI3-Ks have traditionally been assigned using two pharmacological inhibitors, LY294002 and wortmannin. Although these compounds are broadly specific for the PI3-K family, they show little selectivity among family members, and the development of isoform-specific inhibitors of these enzymes has been long anticipated. Herein, we prepare compounds from two classes of arylmorpholine PI3-K inhibitors and characterize their specificity against a comprehensive panel of targets within the PI3-K family. We identify multiplex inhibitors that potently inhibit distinct subsets of PI3-K isoforms, including the first selective inhibitor of p110β/p110δ (IC_{50} p110β = 0.13 μM, p110δ = 0.63 μM). We also identify trends that suggest certain PI3-K isoforms may be more sensitive to potent inhibition by arylmorpholines, thereby guiding future drug design based on this pharmacophore.

3.2 Introduction

Phosphatidylinositol 3-kinases are activiated by a wide range of cell surface receptors to generate the lipid second messengers phosphatidylinositol 3,4-bisphosphate (PIP_2) and phosphatidylinositol 3,4,5-trisphosphate (PIP_3). In the appropropriate cellular context, these two lipids can regulate a remarkably diverse array of physiological processes, including glucose homeostasis, cell growth, differentiation and motility [1]. These distinct functions are carried out by a family of eight related PI3-Ks in vertebrates that possess unique substrate specificities, localization, and modes of regulation [1]. These include the class IA PI3-Ks (p110α, p110β, p110δ), which are activated by receptor tyrosine kinases, the class IB PI3-K (p110γ), which is activated by

heterotrimeric G-proteins, and the class II PI3-Ks (PI3KC2α, PI3KC2β, PI3KC2γ) whose regulation remains poorly understood. Despite these known differences in upstream activation, the physiological roles of individual PI3-K isoforms remain largely unassigned, and dissecting the unique functions of members of this family is a major focus of ongoing research [2].

In addition to sequence homology within their catalytic domain, PI3-Ks share sensitivity to two small molecule inhibitors, wortmannin and LY294002. Wortmannin is a fungal natural product that irreversibly inhibits PI3-Ks at low nanomolar concentrations [3, 4], whereas LY294002 is a synthetic chromone that reversibly inhibits most PI3-Ks at low micromolar concentrations [5]. Together, these two compounds have served as powerful probes for implicating PI3-Ks in a wide range of physiological processes, and much of our understanding of PI3-K action in cells derives from the use of these two reagents.

Although wortmannin and LY294002 are broadly active against the PI3-K family, they show little specificity among PI3-K family members. Since these compounds do not pharmacologically discriminate between PI3-K isoforms, comparatively little is known about the specific signalling functions of individual PI3-Ks. Knockout mice have defined essential roles for p110γ and p110δ in leukocyte function, including signaling from the B and T cell receptors [6, 7] (p110δ) as well as chemotaxis of neutrophils and macrophages [8, 9] (p110γ). Furthermore, microinjection of isoform-specific inhibitory antibodies has demonstrated that individual class I PI3-Ks can relay unique downstream signals following activation of a common upstream receptor. For example, colony-stimulating factor-1 treatment of macrophages induces DNA synthesis through p110α, whereas actin cytoskeleton rearrangement and cell migration require p110β and p110δ [10]. These studies suggest that PI3-K isoforms likely possess non-redundant

functions downstream of the wide range of receptors that are known to activate PI3-Ks. In general, however, the systematic analysis of PI3-K isoform action in cells awaits the discovery of small molecule inhibitors that can selectively target PI3-K family members. For this reason, the development of isoform-specific inhibitors of PI3-Ks has been long anticipated [2, 11-13].

Recently, patent disclosures have described new inhibitors based on the LY294002 arylmorpholine pharmacophore [11, 12, 14], although the detailed isoform selectivity of these compounds has not been reported. Since these compounds are potentially useful probes for PI3-K isoform activity in cells, we sought to determine their target specificity by characterizing their activity against a comprehensive panel of PI3-Ks. In this regard, a recent characterization of 28 common protein kinase inhibitors against a panel of 24 protein kinases has significantly challenged many preconceptions about the true selectivity of protein kinase inhibitors [15]. The analysis we report here identifies several compounds that inhibit distinct subsets of the PI3-K family, including the first selective inhibitors of the p110δ/p110β isoforms.

We also sought to explore the potential of the morpholino chromone scaffold as a starting point for PI3-K inhibitor optimization. LY294002 has been shown to be quite selective for lipid kinases relative to protein kinases [15] and to possess broad activity within the PI3-K family. Indeed, until very recently, LY294002 was the only reversible inhibitor that had been reported to target the PI3-K family – even though this compound was originally described ten years ago [5]. Given the importance of PI3-Ks in signal transduction, it is remarkable that there has not been a single subsequent structure-activity study published investigating compounds of this class. Our comprehensive selectivity analysis of a panel of arylmorpholines identifies PI3-K isoforms that tend to be sensitive to this pharmacophore, as well as others that are more resistant. This

information should prove useful in guiding future drug design based on this core structure.

3.3 LY294002 analogs

Thrombogenix has disclosed a series of LY294002 analogs that differ in the substitution pattern of heteroatoms within the chromone core [14], as well as through replacement of the phenyl group at the eight position of LY294002 with more extended aromatic substituents (Figure 3.1). Comparison of the co-crystal structures of p110γ bound to LY294002 [16] and ATP [17] suggests that the adenine ring of ATP and the morpholino-chromone core of LY294002 occupy essentially the same space in the interior of the ATP binding pocket, with both rings anchored by a hydrogen bond to the backbone amide of V882 (Figure 3.1A). Likewise, the 8-phenyl moiety of LY294002 and the ribose sugar of ATP occupy a similar space at the entrance to the pocket and project outward toward solvent. To understand how LY294002 analogs with extended substitutents at C8 might interact differentially with PI3-K isoforms, we identified all of the residues in p110γ whose side chains possess a rotamer that can extend within 4 Å of either the adenine/LY294002 chromone core (Figure 3.1, red) or the ATP ribose/8-phenyl of LY294002 (Figure 3.1, yellow). This first set of residues defines the interior of the ATP binding pocket, while the second set mark the entrance to that pocket (Figure 3.1C). We then aligned these residues with the corresponding residues from each of the class I PI3-Ks, and shaded them according to their physiochemical properties (hydrophobicity, size, and charge) (Figure 3.1B). This alignment reveals that the interior of the ATP binding pocket is highly conserved within the class I PI3-Ks; the only differences are two conservative substitutions that distinguish p110γ from the class IA

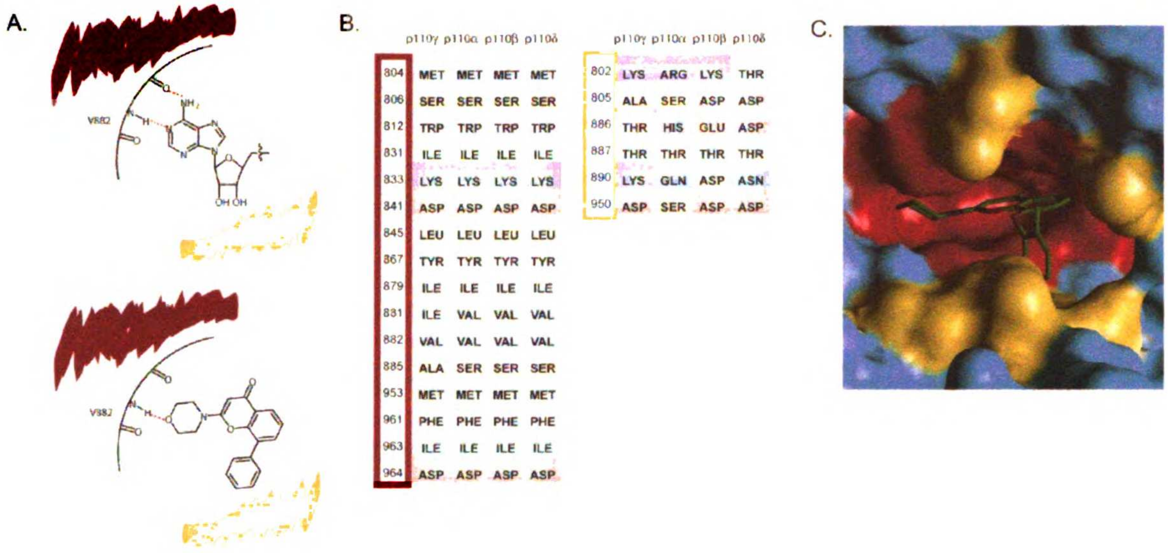

	p110γ	p110α	p110β	p110δ
804	MET	MET	MET	MET
806	SER	SER	SER	SER
812	TRP	TRP	TRP	TRP
831	ILE	ILE	ILE	ILE
833	LYS	LYS	LYS	LYS
841	ASP	ASP	ASP	ASP
845	LEU	LEU	LEU	LEU
867	TYR	TYR	TYR	TYR
879	ILE	ILE	ILE	ILE
881	ILE	VAL	VAL	VAL
882	VAL	VAL	VAL	VAL
885	ALA	SER	SER	SER
953	MET	MET	MET	MET
961	PHE	PHE	PHE	PHE
963	ILE	ILE	ILE	ILE
964	ASP	ASP	ASP	ASP

	p110γ	p110α	p110β	p110δ
802	LYS	ARG	LYS	THR
805	ALA	SER	ASP	ASP
886	THR	HIS	GLU	ASP
887	THR	THR	THR	THR
890	LYS	GLN	ASP	ASN
950	ASP	SER	ASP	ASP

Figure 3.1. ATP binding site conservation among the class I PI3-Ks. A. Schematic of the hydrogen bonds made by ATP (top) and LY294002 (bottom) in the active site of p110γ. Pocket interior (red) and entrance (yellow) are marked for reference. B. Sequence of alignment residues in the interior (left) and exterior (right) of the ATP binding pocket. Residue coloring: hydrophobic aliphatic (green), hydrophobic aromatic (light blue), small (yellow), polar uncharged (dark blue), basic (purple), and acidic (orange). Residue number is for porcine p110γ. C. Model of TGX115 bound to p110γ, based on the LY294002-p110γ co-crystal structure [16].

PI3-Ks (Figure 3.1B, left). By contrast, the residues that line the entrance to the ATP binding pocket are divergent, with major differences between isoforms in their size and charge (Figure 3.1B, right). LY294002 analogs with larger substituents at C8 would be expected to extend outside the ATP binding pocket and potentially make extensive contacts with these less conserved residues (Figure 3.1C). This suggests that it may be possible for such extended analogs to target specific PI3-K isoforms, although it is not immediately apparent how to design compounds that would exploit these differences.

We initially prepared (Figures 3.2 and 3.3) and tested two compounds from this series (TGX115 and TGX126) as well as a synthetic intermediate lacking the aromatic substituent at C8 (TGX066) and compared these compounds to LY294002 and the related LY292223 (which lacks the C8 phenyl group). To obtain a detailed picture of the target specificity of these compounds, we determined IC_{50} values *in vitro* against a panel of 14 enzymes selected to span the most relevant targets for these molecules. These include seven mammalian PI3-Ks (p110α, p110β, p110δ, p110γ, PI3KC2α, PI3KC2β, and PI3KC2γ), four protein kinases in the PI3-K family (DNA-PK, ATM, ATR, mTOR), PI4-kinase β (a PI3-K family member reported to be weakly inhibited by LY294002[18]), casein kinase II (the only protein kinase family member known to be inhibited by LY294002 [15]), and the unrelated serine-threonine kinase G-protein coupled receptor kinase 2 (GRK2). These 14 proteins include all of the known targets of LY294002 and most of the proteins that contain sequence homology to the PI3-K catalytic domain. To facilitate comparison of IC_{50} values across kinases with different substrate affinities, all assays were carried out in the presence of 100 μM ATP.

As has been previously reported, LY29002 exhibits a very broad specificity profile, inhibiting the class I PI3-Ks, PI3KC2β, PI3KC2γ, mTOR, casein kinase 2 and DNA-PK all with IC_{50} values in the low micromolar range. Within the class I PI3-Ks,

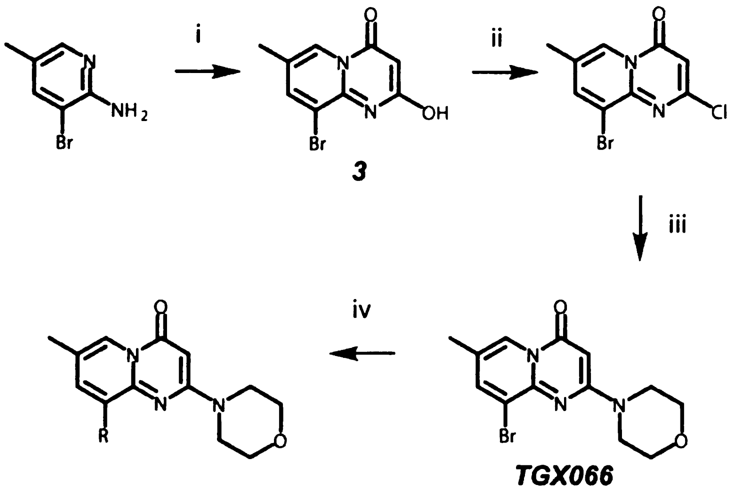
i
ii
iii
iv
NH2
Br
N
O
OH
Cl
R
3
TGX066

Figure 3.2. Synthesis of morpholino-pyrimidinone analogs. The reagents used are: (i) Diethylmalonate, 200 °C, (ii) $POCl_3$, reflux, (iii) morpholine, EtOH, reflux, (iv) substituted benzylamine or aniline, $PdCl_2$(dppf), potassium *tert*-butoxide, THF, reflux.

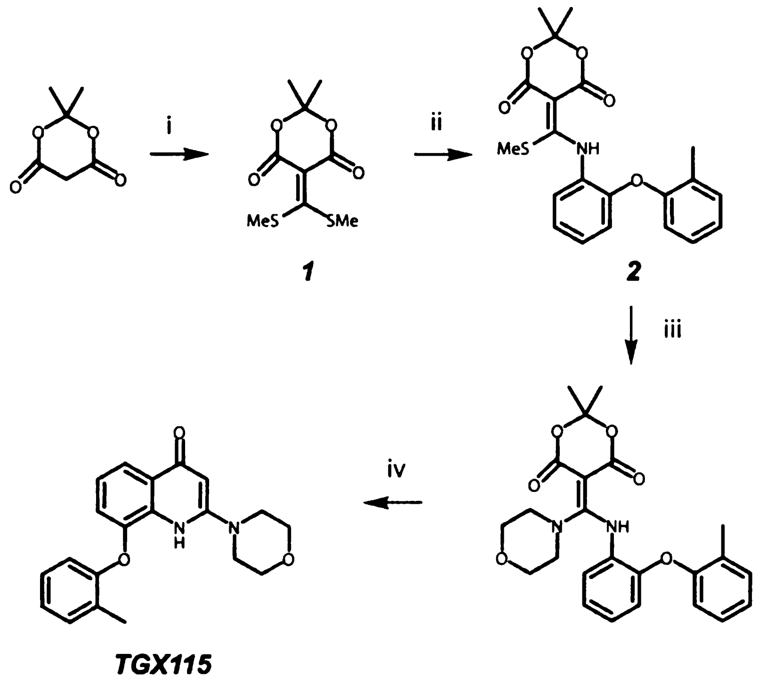
i
ii
iii
iv
MeS
SMe
NH
N
H
O
1
2
TGX115

Figure 3.3. Synthesis of TGX115. The reagents used are: (i) TEA, CS_2, DMSO, MeI, rt, (ii) 2-amino-2'-methyldiphenylether, EtOH, reflux (iii) morpholine, THF, reflux (iv) Ph_2O, 265 °C.

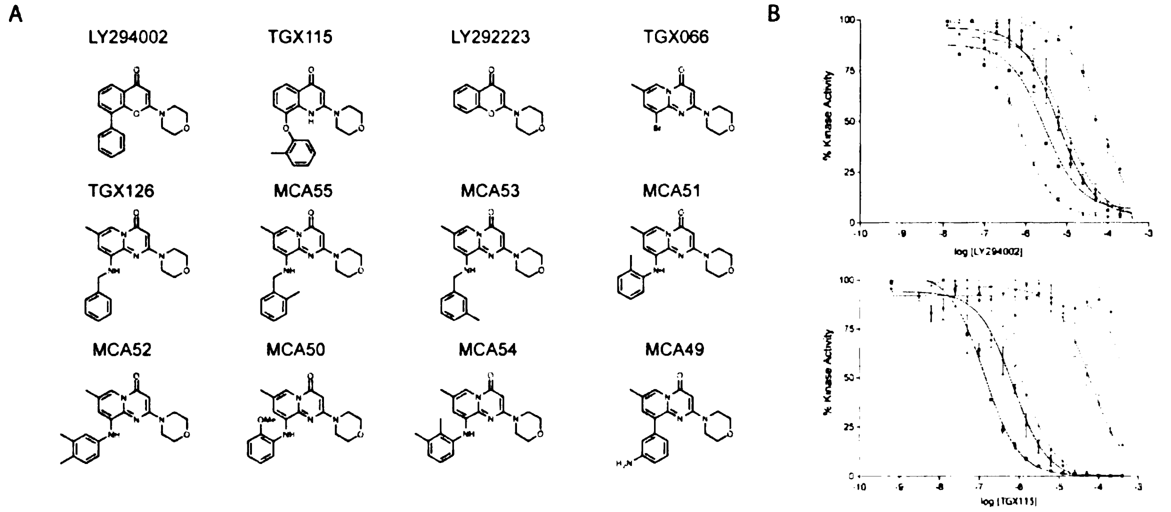
A
LY294002
TGX115
LY292223
TGX066
TGX126
MCA55
MCA53
MCA51
MCA52
MCA50
MCA54
MCA49
B
% Kinase Activity
100
75
50
25
0
-10
-9
-8
-7
-6
-5
-4
-3
log [LY294002]
log [TGX115]

C

	p110α	p110β	p110δ	p110γ	PIKC2α	PIKC2β	PIKC2γ	PI4Kβ	DNA-PK	ATM	ATR	mTOR	CK2	GRK2
TGX115	61	0.13	0.63	~100	>100	~50	~100	>100	1.2	>100	>100	>100	>100	>100
TGX126	8.1	0.16	0.15	~10	ND	ND	ND	>100	0.28	ND	ND	ND	>100	>100
TGX066	58	9.9	8.5	>100	ND	ND	ND	>100	1.3	>100	ND	>100	>100	>100
MCA49	14	18	6.9	38	ND	>100	ND	ND	7.1	ND	ND	ND	ND	ND
MCA50	~50	~20	~10	>100	>100	>100	>100	>100	0.19	>100	ND	>100	>100	>100
MCA51	~9	3.3	3.8	>100	>100	>100	~50	>100	0.15	>100	ND	>100	>100	>100
MCA52	~10	14	~5	>100	>100	ND	~50	>100	0.55	>100	ND	>100	>100	>100
MCA53	1.8	0.99	0.39	~25	>100	~10	>100	>100	0.38	>100	ND	>100	>100	>100
MCA54	6.2	3.5	3.3	~100	>100	ND	~50	>100	0.36	>100	ND	>100	>100	>100
MCA55	1.1	0.11	0.87	~100	>100	2.8	~50	>100	0.27	>100	>100	>100	>100	>100
LY292223	45	7.5	13	~100	ND	~100	~20	>100	0.42	ND	ND	ND	>100	>100
LY294002	9.3	2.9	6.0	38	~100	5.7	40	~100	0.66	>100	>100	8.9	12.2	>100

Figure 3.4. IC$_{50}$ values of LY294002 analogs against protein and lipid kinases. A. Structures of LY294002 analogs. B. Dose response curves for LY294002 (top) and TGX115 (bottom) against different PI3-K family members. DNA-PK (purple), p110α (red), p110β (blue), p110γ (green), p110δ (black), and CK2 (yellow). C. IC$_{50}$ values (μM) measured in the presence of 100 μM ATP.

LY294002 exhibits a maximum of approximately 10-fold selectivity between any two isoforms, with p110β being most sensitive (2.9 μM) and p110γ the least sensitive (38 μM). Interestingly, LY294002 did not show activity at 100 μM against the PI3-K related protein kinases ATM and ATR. Although we are not aware of any reports that LY294002 inhibits these two enzymes at micromolar concentrations[19], the effects of LY294002 treatment of cells has been interpreted to imply a requirement for ATM or ATR kinase activity in several studies [20, 21] .

In contrast to LY294002, TGX115 and TGX126 were signficantly more potent and selective. Surprisingly, we find that TGX115 inhibits p110β and p110δ at nanomolar concentrations, but p110α and p110γ only at concentrations more than 100-fold higher (Figure 3.4). TGX126 showed a more modest specificity profile, although this compound was still ~50 fold more potent against p110β/ p110δ than against p110α/p110γ. Against the other 10 enzymes in this panel, TGX115 and TGX126 showed significant activity only against DNA-PK, with high nanomolar IC_{50} values. Thus, within the lipid kinases, these two compounds represent the first selective inhibitors of the p110β/p110δ isoforms. By contrast, the unsubstituted analogs TGX066 and LY292223 were significantly less potent against all PI3-Ks, although they retained strong activity against DNA-PK (Figure 3.4). This suggests that presence of an aromatic substituent at C8 plays an essential role in achieving binding affinity for PI3-Ks, but may be dispensable for DNA-PK inhibition.

On the basis of this initial data, seven additional compounds were prepared by palladium catalyzed coupling of different aromatic substituents to TGX066 (Figure 3.2) to explore the chemical space surrounding TGX115 and TGX126. These compounds, termed morpholino chromone analogs 49-55 (MCA049-MCA055), all contain the pyrimidone heterocycle scaffold of TGX126 and differ in their aromatic substitution at the

position analagous to C8 in LY294002. They include compounds that substitute the pyrimidone core with anilines (MCA50-MCA52, MCA54), benzylamines (MCA53 and MCA55), and a biaryl linkage (MCA49) that mimics LY294002 in this new scaffold, and were prepared

The specificity profile of these compounds was determined, and several structure-activity trends were identified (Figure 3.4). Compounds containing a benzylamine substitution to the pyrimidone core exhibit potent activity against the class IA PI3-Ks p110$\alpha/\beta/\delta$ ($IC_{50} = 0.1 - 2\ \mu M$), but display comparatively less activity against the class IB PI3-K p110γ ($IC_{50} = 25 - 100\ \mu M$). Compared to the closely related TGX126, these methyl-substituted compounds possess modestly enhanced activity toward p110α and diminished activity against p110γ. MCA55 showed the largest selectivity between p110α and p110γ of any compound in our panel (~50 fold) and this compound can be regarded as a multiplex inhibitor of the growth factor regulated class IA PI3-Ks with little activity against the G-protein regulated class IB enzyme, p110γ.

In contrast, compounds containing an aniline substitution on the pyrimidone scaffold all showed a 10 – 100 fold loss of activity against the PI3-K isoforms p110δ and p110β relative to the parent compounds TGX115 and TGX126, while retaining potent DNA-PK inhibition. This trend includes MCA51, a compound that is isosteric to TGX115 within the pyrimidone scaffold. Compared to TGX115, this compound is ~20 fold less potent against p110δ/p110β and ~10 fold more potent against DNA-PK. This effect appears to be a consequence of the aniline substitution, rather than the pyrimidone core itself, because TGX126 and related compounds containing a benzylamine substitution remain highly potent against p110δ/p110β. This suggests that very subtle changes to the aromatic substituent can significantly shift inhibitor specificity among PI3-K family members. Indeed, we find that several anilino-pyrimidones inhibit DNA-PK at nanomolar

concentrations and display significant selectivity (~10 – 100 fold) relative to all other members of the PI3-K family. These compounds may prove useful as selective inhibitors of DNA-PK, or as lead structures for the development of more highly specific compounds.

3.4 Arymorpholine DNA-PK inhibitors

ICOS has recently disclosed a set of arylmorpholines[22, 23] that are potent inhibitors of DNA-PK (Figure 3.5). These compounds are trisubstituted benzene derivatives with hydroxy and carbonyl moieties meta and para to the morpholine ring, respectively. As these molecules are structurally reminiscent of LY294002, we prepared a small set of eight arylmorpholines (Figure 3.6) and determined their specificity profile against our enzyme panel.

We find that IC60211 and IC86621 are high nanomolar inhibitors of DNA-PK, with IC_{50} values against class I PI3-Ks in the low to mid-micromolar range, consistent with an earlier report [22]. In this regard, these compounds exhibit a specificity profile that mirrors LY294002, with modestly enhanced DNA-PK activity (1.5 - 5 fold). Nonetheless, we find that these compounds are more selective than LY294002 in that they show no activity against the secondary targets mTOR, casein kinase II or any of the class II PI3-Ks. Thus, within the lipid kinases, this structural class is selective for the class I PI3-Ks. Arylmorpholine analog 37 (AMA37) is the most DNA-PK selective of these compounds, with ~10-fold specificity relative to p110β and ~100 fold specificity relative to the other class I PI3Ks. This potency and selectivity is comparable to the most DNA-PK selective compounds identified from our panel of anilino pyrimidones.

We tested a series of analogs of these compounds to probe the requirements for DNA-PK inhibition, and confirm that both the hydrogen bond acceptor at the 1-position and the donor at the 2-position are required for potent DNA-PK inhibition (Figure 3.5).

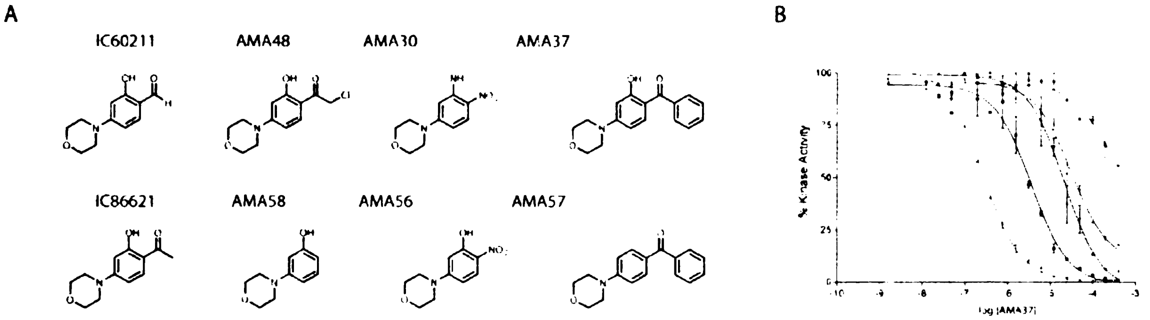
A
IC60211
AMA48
AMA30
AMA37
IC86621
AMA58
AMA56
AMA57
B
% Kinase Activity
100
75
50
25
0
-10
-9
-8
-7
-6
-5
-4
-3
log [AMA37]

C

	p110α	p110β	p110δ	p110γ	PIKC2α	PIKC2β	PIKC2γ	PI4Kβ	DNA-PK	ATM	ATR	mTOR	CK2	GRK2
AMA30	~100	23	24	~100	ND	ND	ND	>100	2.3	>100	ND	>100	>100	>100
IC60211	~10	2.8	5.1	37	>100	>200	~50	>100	0.43	>100	ND	>100	>100	>100
IC86621	16	0.99	3.8	10	ND	~200	>100	>100	0.17	>100	ND	>100	>100	>100
AMA37	32	3.7	22	~100	>100	~200	~50	>100	0.27	>100	>100	>100	>100	>100
AMA48	30	ND	4.8	~70	ND	ND	ND	>100	1.1	>100	ND	>100	>100	>100
AMA56	ND	ND	ND	ND	ND	ND	ND	ND	1.2	ND	ND	ND	ND	ND
AMA57	ND	ND	ND	ND	ND	ND	ND	ND	14.7	ND	ND	ND	ND	ND
AMA58	ND	ND	ND	ND	ND	ND	ND	ND	~100	ND	ND	ND	ND	ND

Figure 3.5. IC_{50} values of arylmorpholines against protein and lipid kinases. A. Structures of arylmorpholine analogs. B. Dose response curves for AMA37 against different PI3-K family members (color coded as in Figure 3.4.) C. IC_{50} values (μM) measured in the presence of 100 μM ATP.

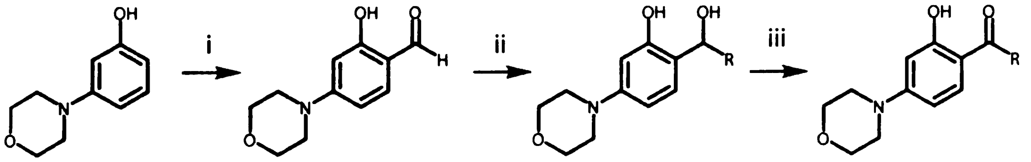
OH
i
OH
H
ii
OH
OH
R
iii
OH
R
N
O

Figure 3.6. Synthesis of IC60211 and analogs. The reagents used are: (i) $POCl_3$, DMF, reflux, (ii) RLi, THF, -78 °C, and (iii) MnO_2, MeCN, rt.

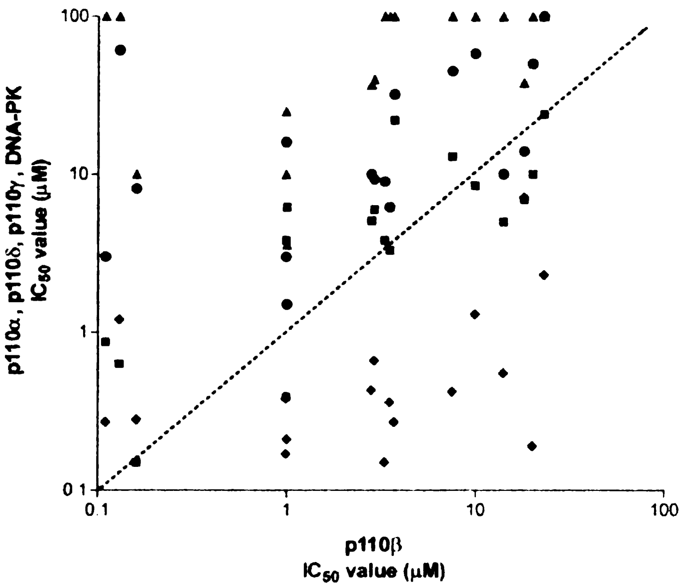

Figure 3.7. Correlation plot for inhibition of different PI3-K isoforms. IC_{50} values (μM) for p110β (x-axis) plotted against IC_{50} values for DNA-PK (purple), p110α (red), p110γ (green), and p110δ (black).

[illegible] [illegible]

For example, AMA57, which differs from AMA37 by the substitution of a hydrogen for the 2-hydroxyl, is ~80 fold less potent, whereas AMA58, which differs from IC60211 by removal of the aldehyde moiety, is ~200 fold less potent. However, the specific identity of hydrogen bond donor and acceptor is not a requirement for potent DNA-PK inhibition. For example, AMA56, which differs from IC60211 by the replacement of the aldehyde with a nitro group, is only ~3 fold less potent. Likewise, AMA30, which differs from AMA56 by the further substitution of the 2-hydroxyl group with an amine, is only ~2 fold less potent.

3.5 Discussion

We have measured the activity of a panel of compounds that share the arylmorpholine pharmacophore first identified in LY294002 against a comprehensive set of targets within the PI3-K family. Analysis of this data suggests several trends in selectivity among different PI3-K family members. First, while we confirm that LY294002 inhibits three protein kinases at low micromolar concentrations (DNA-PK, mTOR, CK2), we find that two of these kinases (mTOR and CK2) are resistant to all other arylmorpholines in our panel. DNA-PK, by contrast, is potently inhibited by almost every compound tested, and shows very broad SAR with respect different analogs in the same series. In part, we believe these differences reflect the fact that DNA-PK binds with high affinity to the core arylmorpholine pharmacophore, whereas the other protein kinases (and to a lesser extent, the PI3-Ks) require more extensive interactions with other regions of the molecule for high affinity binding. Consistent with this view, the most structurally simple compounds in our panel (TGX066, LY292223, and IC60211) all exhibit potent inhibition of DNA-PK, even though their PI3-K activity is significantly reduced compared to more substituted analogs. Moreover, a third class of DNA-PK inhibitors based on a limited arylmorpholine scaffold have recently been reported[24],

suggesting that diverse compounds containing this core structure can exhibit potent and selective DNA-PK inhibition.

Selectivity trends were also observed within the class I PI3-Ks. To visualize these differences, we plotted the IC_{50} values of all of the compounds for inhibition of p110β (x-axis) against the IC_{50} values for inhibition of the other class I PI3-Ks and DNA-PK (y-axis), such that each data point represents the intersection of IC_{50} values for the same compound against two different enzymes (Figure 3.7). In this representation, compounds that lie along the diagonal show equipotent inhibition of p110β and the second kinase, whereas those that lie above or below the diagonal are more or less potent, respectively, against the second enzyme than p110β. Virtually all of the DNA-PK IC_{50} values (purple) occupy the lower section of the plot, reflecting the fact that DNA-PK is more sensitive to arylmorpholines than the class I PI3Ks. p110δ IC_{50} values (black) cluster around the diagonal as few compounds within this series show differential activity against p110δ and p110β, whereas p110α (red) tends to be inhibited less potently. p110γ (green) was unexpectedly resistant to inhibition by a large number of arylmorpholines, although this insensitivity is consistent with p110γ's underlying poor sensitivity to LY294002 relative to the other class I isoforms.

While we have not been able to rationalize these differences in inhibitor sensitivity in terms of specific residues that differ between PI3-K isoforms, several observations are consistent with these IC_{50} trends. First, the similarity in the sensitivity of p110δ and p110β to diverse compounds is likely a reflection of the fact that these two kinases are more closely related in primary sequence than any other members of the PI3-K family. For this reason, it may be challenging to find analogs of potent p110β/p110δ inhibitors such as TGX115 containing the arylmorpholine core that can distinguish between these two isoforms. Second, we find that the overall trend in

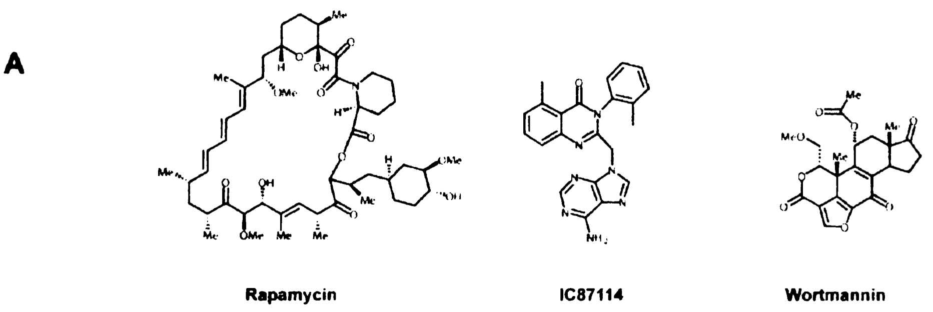

B

	p110α	p110β	p110δ	p110γ	C2α	C2β	C2γ	DPK	ATM	ATR	TOR
Wortmannin (mid µM)	X	X	X	X	X	X	X	X	X		X
Wortmannin (mid nM)	X	X	X	X		X	X				
LY294002	X	X	X	X		X	X	X			X
IC60211	X	X	X	X				X			
MCA055	X	X	X				X		X		
TGX115		X	X					X			
IC87114, others			X								
AMA037, others								X			
Rapamycin											X

Figure 3.8. Spectrum of characterized PI3-K inhibitor selectivities. A. Structures of reported inhibitors of PI3-K family members. B. Selectivity profile of well-characterized PI3-K inhibitors. Data for wortmannin, IC87114, and rapamycin is drawn from published reports. Compounds characterized in this study are highlighted in red.

inhibitor sensitivity among these targets (p110γ < p110α < p110β, p110δ < DNA-PK) roughly mirrors the K_M for ATP of these proteins. That is, we have found that p110γ has the lowest K_M for ATP among these enzymes (7.4 μM), whereas DNA-PK has the highest (192 μM), and the class IA PI3-Ks exhibit intermediate values. While this alone cannot explain the potency and isoform selectivity of compounds such as TGX115, it does suggest that smaller differences between the class I isoforms (*e.g.*, as observed for LY294002) likely reflect differential competition from ATP substrate between isoforms. This suggests that the PI3-K family members for which selective inhibitors have been identified to date (DNA-PK, and, to a lesser extent, p110β and p110δ) may be inherently easier to target with ATP competitive small molecules than other isoforms.

It has long been anticipated that the development of isoform-specific PI3-K inhibitors would make it possible to dissect the unique contributions of individual PI3-K isoforms in well-characterized signaling pathways [2, 11-13]. Recently, Sadhu et al. described the first isoform selective PI3-K inhibitor [25], IC87114, which targets p110δ, and this compound has found rapid use in identifying essential roles for p110δ in chemotaxis and inflammatory responses of neutrophils [25-27], spontaneous tone of arteries [28] and EGF driven migration of cancer cell lines [29]. TGX115, when used either in conjunction with IC87114 or in cells that do not express p110δ, should prove equally effective in elucidating physiological roles for p110β, and we have begun to use this compound to explore p110β mediated signaling in several systems (Z.A.K. and K.M.S., unpublished results). As other mutliplex inhibitors we describe in this report also possess activity against unique combinations of PI3-K family members (Figure 3.8), it may be possible to use these compounds in combination in order to interogate additional PI3-K isoforms. In this way, we envision a route to begin to pharmacalogically dissect the distinct contributions of members of this important family of signaling enzymes.

3.6 Experimental Procedures

3.6.1 Lipid kinase expression

Epitope tagged p110α, p110β, p110δ, PI3KC2α, PI3KC2β, and PI3KC2γ were expressed by transient transfection of cos-1 cells. Cells were lysed in lysis buffer (50 mM Tris (pH 7.4), 300 mM NaCl, 5 mM EDTA, 0.02% NaN$_3$, 1% Triton X-100, and protease inhibitors) and the kinase immunoprecipitated with the appropriate antibody-protein G complex. Immunoprecipitates were washed twice with buffer A (PBS, 1 mM EDTA, 1% Triton X-100), twice with buffer B (100 mM Tris (pH 7.4), 500 mM LiCl, 1 mM EDTA), and twice with buffer C (50 mM Tris (pH 7.4), 100 mM NaCl). GST-PI4Kβ was expressed in BL21 *E. coli* and purified by glutathione chromatography essentially as described [18]. Recombinant p110γ was obtained from Sigma. In control experiments, no differences in inhibitor sensitivity were observed between p110α immunoprecipitated from cos-1 cells and protein expressed in Sf9 cells using a baculovirus system.

3.6.2 Lipid kinase assays

All kinase assays were conducted at a final concentration of 100 μM ATP and 2% DMSO. PI3-K and PI4-K assays were carried out essentially as described[18]. Briefly, a reaction mixture was prepared containing kinase, inhibitor, buffer (25 mM HEPES (pH 7.4), 10 mM MgCl$_2$), and freshly sonicated phosphatidylinositol (200 μg/mL). Reactions were initiated by the addition of ATP containing 10 μCi of γ-^{32}P-ATP to a final concentration 100 μM. Reactions were incubated 15 min at rt and then terminated by the addition of 105 μL1N HCl followed by 160 μL CHCl$_3$:MeOH (1:1). The biphasic mixture was then vortexed, briefly centrifuged, and the organic phase transferred to a new tube using a gel loading pipette tip precoated with CHCl$_3$. This extract was spotted

on TLC plates and developed for 3 – 4 h in a 65:35 solution of *n*-propanol:2M AcOH. The TLC plates were then dried and quantitated using a PhosphorImager (Molecular Dynamics). For each compound, kinase activity was measured at 12 – 15 inhibitor concentrations representing two-fold dilutions from the highest concentration tested (typically, 200 μM). For compounds showing significant activity, IC_{50} determinations were repeated two to six times, and the reported value is the average of these independent measurements.

3.6.3 Protein kinase expression

HA-ATM, FLAG-ATR, and AU-1 mTOR were expressed by transient transfection of HEK293 cells. The cells were lysed in lysis buffer (50 mM Tris-Cl (pH 7.4), 100 mM NaCl, 50 mM β-glycerophosphate, 10% glycerol (w/v), 1% Tween-20, 1 mM EDTA, 25 mM NaF, and protease inhibitors), and lysates were subjected to immunoprecipitation with the appropriate epitope-tag antibody. Immune complexes were collected on rabbit anti-mouse Sepharose (Sigma) and washed three times in lysis buffer, once in high salt buffer (100 mM Tris-Cl (pH 7.4), 500 mM LiCl), and once in kinase wash buffer (10 mM HEPES (pH 7.4), 50 mM NaCl, 50 mM β-glycerophosphate, 10% glycerol). N-terminal His6-tagged GRK2 was expressed in Sf9 insect cells and purified using Ni-NTA beads (Qiagen) as described[30]. Casein kinase 2 was obtained from Upstate Biotechnology, and DNA-PK was obtained from Promega.

3.6.4 Protein kinase assays

ATM, ATR, and mTOR immunoprecipitates were resuspended in kinase assay buffer (10 mM HEPES (pH 7.4), 50 mM NaCl, 50 mM β-glycerophosphate, 10% glycerol, 10 mM $MnCl_2$, 1 mM DTT) and incubated with inhibitor for 30 min prior to the kinase reaction.

Kinase reactions were initiated by the addition of 100 μM ATP, 10 μCi (γ-^{32}P)-ATP and 1 μg of either a GST-p70S6K fragment (amino acids 332-414) for mTOR, or 1 μg of a GST-p53 fragment (amino acids 1-70) for ATM or ATR. Reactions were incubated at 30 $^\circ$C for 20 min and terminated by the addition of 2X SDS-PAGE sample buffer. Samples were resolved by SDS-PAGE and transferred to PVDF membranes. The portion of the membrane containing the ^{32}P-labeled substrate was quantitated by PhosphorImager, while the portion of the membrane containing ATM, ATR, or mTOR was subjected to Western blotting with anti-HA, anti-FLAG, or anti-AU1 antibody, respectively.

The amount of ^{32}P incorporation in the substrate was normalized to the amount of ATM or mTOR present. GRK2 assays were carried out using tubulin as substrate in 20 mM HEPES, pH 7.4, 2 mM EDTA, 10 mM $MgCl_2$ containing 100 μM ATP essentially as described[30]. DNA-PK assays were carried out using the DNA-PK assay system (Promega) as directed by the manufacturer. Casein kinase 2 assays were carried out using the casein kinase 2 assay kit (Upstate Biotechnology) as directed by the manufacturer.

3.6.5 General Chemical Synthesis

The following reagents were obtained commercially: 2-amino-2'-methyldiphenyl ether (TCI America), 3-morpholinophenol (Avacado Research), 4-morpholinobenzophenone (Sigma), 5-morpholino-2-nitrophenol (Alfa Aesar), LY294002 (Calbiochem), and MnO_2 and $PdCl_2(dppf)$ (Strem Chemicals). All other reagents were from Aldrich, were of the highest grade commercially available, and were used as supplied by the manufacturer without further purification. Reversed phase high performance liquid chromatography (RP-HPLC) was performed on a Ranin SD-200

solvent delivery system equipped with a Zorbax 300-SB C18 column using a $MeCN/H_2O$/0.1% TFA gradient (0-100%) as the mobile phase.

3.6.6 5-(Bis-methylsulfanyl-methylene)-2,2-dimethyl-(1,3)dioxane-4,6-dione (1)

Triethylamine (9.6 mL, 69 mmol) and CS_2 (2.05 mL, 34.7 mmol) were added consecutively to a stirred solution of Meldrum's acid (5.0 g, 35 mmol) in DMSO (50 mL) at rt [31]. After 1 h, the reaction was cooled on ice, MeI (4.3 mL, 69 mmol) was added, and the reaction was allowed to proceed overnight at rt. After 18 h, the reaction was terminated by adding ice water, and the precipitate was chromatographed on silica gel (50% EtOAc/hexanes) to yield 1.962 g (23%) of a yellow solid. ^{1}H NMR (400 MHz, $CDCl_3$) δ 2.45 (6H, s), 1.53 (6H, s).

3.6.7 2,2-Dimethyl-5-(1-methylsulfanyl-2-(2-*o*-tolyloxy-phenyl)-ethylidene)-(1,3)dioxane-4,6-dione (2)

2-amino-2'-methyldiphenyl ether (802 mg, 4.03 mmol) was added to a solution of **2** (1.0 g, 4.0 mmol) in EtOH (9 mL) and stirred at reflux for 9 h essentially as described [14, 32]. When the reaction was complete, the solvent was removed *in vacuo* and the product chromatographed twice on silica (10% EtOAc/hexanes followed by 50% EtOAc/hexanes) to yield 1.54 g (95.8%). ^{1}H NMR (400 MHz, $CDCl_3$) δ 7.39 (1H, d, $J = 8$ Hz), 7.00 – 7.24 (5H, m), 6.78 – 6.81 (2H, m), 5.24 (1H, s), 2.27 (3H, s), 2.21 (3H, s), 1.66 (6H, s); ^{13}C NMR (100 MHz, $CDCl_3$) δ 178.5, 153.8, 151.3, 131.8, 129.8, 129.5, 128.0, 127.7, 127.3, 124.7, 123.1, 118.9, 117.9, 117.1, 103.2, 86.8, 26.5, 19.0, 16.3.

3.6.8 2-Morpholin-4-yl-8-*o*-tolyloxy-1H-quinolin-4-one (TGX115)

Morpholine (0.44 mL, 5.0 mmol) was added to a solution of **2** (900 mg, 2.25 mmol) in THF (12 mL) [14]. The reaction was heated to reflux for 24 h. After cooling to rt, the solvent was removed *in vacuo*, the solid washed with Et_2O, and then dissolved in Ph_2O (10 mL). The reaction was heated to 265 °C for 15 min, and then cooled to rt. The product was purified by chromatography on silica gel twice (50% EtOAc/hexanes followed by 10% MeOH/EtOAc) to yield 227 mg (33%) of a white solid. ^1H NMR (400 MHz, $CDCl_3$) δ 8.51 (1H, s), 7.88 (1H, d, $J = 8$ Hz), 7.11 – 7.27 (3H, m), 7.05 (1H, t, $J = 16$ Hz), 6.94 (1H, d, $J = 8$ Hz), 6.67 (1H, d, $J = 8$ Hz) 5.73 (1H, s), 3.81 (4H, s), 3.29 (4H, t, $J = 4$ Hz), 2.18 (3H, s); ^{13}C NMR (100 MHz, DMSO-d_6) δ 161.6, 157.7, 157.0, 149.7, 140.9, 130.6, 126.8, 126.6, 121.7, 120.6, 119.6, 118.9, 117.6, 115.9, 91.1, 65.8, 44.8, 16.1; HR-EI MS $(M)^+$ *m/z* calcd for $C_{20}H_{20}N_2O_3$ 336.1474, found 336.1457.

3.6.9 9-Bromo-2-hydroxy-7-methyl-pyrido(1,2-*a*)pyrimidin-4-one (3)

A stirred solution of 2-amino-3-bromo-5-methylpyridine (9.85 g, 52.7 mmol) in diethylmalonate (20 mL, 130 mmol) was heated to 200 °C for 3.5 h [14]. The heat was then removed and the diethylmalonate was removed under a stream of argon as the reaction was allowed to cool to rt. The solid product was purified by chromatography on silica gel twice (50% EtOAc/hexanes, followed by 5% MeOH/CH_2Cl_2) to yield 1.7 g (12.7%) of a yellow solid. ^1H NMR (400 MHz, DMSO-d_6) δ 11.71 (1H, br), 8.69 (1H, s), 8.25 (1H, s), 5.46 (1H, s), 2.30 (3H, s); HR-EI MS $(M)^+$ *m/z* calcd for $C_9H_7BrN_2O_2$ 253.9691, found 253.9674.

3.6.10 9-Bromo-7-methyl-2-morpholin-4-yl-pyrido(1,2-*a*)pyrimidin-4-one (TGX66)

A stirred solution of **3** (1.7 g, 6.7 mmol) in $POCl_3$ (20.0 mL, 215 mmol) was heated to reflux overnight [14]. After 18 h, the reaction was quenched by pouring onto ice. The aqueous phase was extracted three times with CH_2Cl_2, concentrated to dryness *in vacuo*, and dissolved in EtOH (25 mL). Morpholine (1.5 mL, 17 mmol) was added to this solution and the reaction was heated to reflux for 1 h. After 1 h, the reaction was allowed to cool to rt, yielding a white precipitate. The precipitate was collected by filtration and rinsed with cold EtOH to yield 737 mg (38.8%) of a white solid. ^{1}H NMR (400 MHz, DMSO-d_6) δ 8.56 (1H, s), 8.14 (1H, s), 5.57 (1H, s), 3.63 (4H, s), 3.60 (4H, s), 2.26 (3H, s); ^{13}C NMR (100 MHz, $CDCl_3$) δ 160.6, 159.0, 142.4, 125.2, 122.3, 119.2, 118.9, 81.1, 65.8, 65.7, 44.8, 44.7, 18.0; HR-EI MS $(M)^+$ *m/z* calcd for $C_{13}H_{14}BrN_3O_2$ 323.0269, found 323.0259.

3.6.11 Benzylamino-7-methyl-2-morpholin-4-yl-pyrido(1,2-*a*)pyrimidin-4-one (TGX126)

A stirred solution of TGX66 (15 mg, 0.046 mmol), $PdCl_2$(dppf) (1.9 mg, 0.0023 mmol), potassium *tert*-butoxide (10.4 mg, 0.0928 mmol), and benzylamine (4.97 mg, 0.0464) in THF (1 mL) was heated to reflux for 24 h [14]. The product was purified by chromatography on silica gel (5% MeOH/CH_2Cl_2), followed by RP-HPLC, to yield 10 mg (61%) of a white solid. ^{1}H NMR (400 MHz, $CDCl_3$) δ 8.10 (1H, s), 7.22 – 7.31 (m), 6.35 (1H, s), 5.73 (1H, s), 4.47 (2H, s), 3.78 (4H, t, J = 4 Hz), 3.59 (4H, t, J = 4 Hz), 2.22 (3H, s); HR-EI MS $(M)^+$ *m/z* calcd for $C_{20}H_{22}N_4O_2$ 350.1743, found 350.1749.

3.6.12 9-(3-Amino-phenyl)-7-methyl-2-morpholin-4-yl-pyrido[1,2-*a*]pyrimidin-4-one (MCA49)

Prepared following the general procedure for TGX126, using TGX66 (50 mg, 0.16 mmol), 3-aminophenylboronic acid (96 mg, 0.62 mmol), and Na_2CO_3 (164 mg, 1.55 mmol) in place of potassium *tert*-butoxide. The product was purified by chromatography on silica gel (5% MeOH/EtOAc) to yield 30 mg (58%) of a white solid. LR-ESI MS $(M+H)^+$ *m/z* calcd for $C_{20}H_{22}N_4O_3$ 337.2, found 337.0.

3.6.13 9-(2-Methoxy-phenylamino)-7-methyl-2-morpholin-4-yl-pyrido(1,2-*a*)pyrimidin-4-one (MCA50)

Prepared following the general procedure for TGX126, using TGX66 (50 mg, 0.16 mmol) and *o*-anisidine (0.017 mL, 0.155 mmol). The product was purified by chromatography on silica gel (2% MeOH/hexanes) followed by RP-HPLC to yield 3.8 mg (6.7%) of a white solid. ^{1}H NMR (400 MHz, DMSO-d_6) δ 8.37 (1H, s), 8.04 (1H, s), 7.52 (1H, d, *J* = 8 Hz), 7.17 (1H, s), 6.98 – 7.09 (4H, m), 3.83 (3H, s), 3.70 (4H, t, *J* = 4 Hz), 3.62 (4H, t, *J* = 4 Hz), 2.23 (3H, s); HR-EI MS $(M)^+$ *m/z* calcd for $C_{20}H_{22}N_4O_3$ 366.1692, found 366.1701.

3.6.14 7-Methyl-2-morpholin-4-yl-9-*o*-tolylamino-pyrido(1,2-*a*)pyrimidin-4-one (MCA51)

Prepared following the general procedure for TGX126, using TGX66 (50 mg, 0.16 mmol) and *o*-toluidine (0.017 mL, 0.16 mmol). The product was purified by chromatography on silica gel (2% MeOH/hexanes) followed by RP-HPLC to yield 6.8 mg (12.6%) of an off-white solid. ^{1}H NMR (400 MHz, DMSO-d_6) δ 7.99 (1H, s), 7.82 (1H, s), 7.23 – 7.34 (3H, m), 7.12 (1H, t, *J* = 7.2 Hz), 6.48 (1H, s), 5.59 (1H, s), 3.64 (8H, br),

2.18 (3H, s), 2.15 (3H, s); HR-EI MS $(M)^+$ *m/z* calcd for $C_{20}H_{22}N_4O_2$ 350.1743, found 350.1754.

3.6.15 9-(3,4-Dimethyl-phenylamino)-7-methyl-2-morpholin-4-yl-pyrido(1,2-*a*)pyrimidin-4-one (MCA52)

Prepared following the general procedure for TGX126, using TGX66 (50 mg, 0.16 mmol) and 3,4-dimethylaniline (18.8 mg, 0.155 mmol). The product was purified by chromatography on silica gel (2% MeOH/hexanes) followed by RP-HPLC to yield 13.4 mg (23.9%) of a yellow solid. ^{1}H NMR (400 MHz, DMSO-d_6) δ 8.00 (1H, s), 7.85 (1H, br), 7.05 – 7.13 (3H, m), 6.94 (1H, s), 5.58 (1H, s), 3.64 (8H, br), 2.18 – 2.21 (9H, m); HR-EI MS $(M)^+$ *m/z* calcd for $C_{21}H_{24}N_4O_2$ 364.1899, found 364.1909.

3.6.16 7-Methyl-9-(3-methyl-benzylamino)-2-morpholin-4-yl-pyrido(1,2-*a*)pyrimidin-4-one (MCA53)

Prepared following the general procedure for TGX126, using TGX66 (50 mg, 0.16 mmol) and 3-methylbenzylamine (0.019 mL, 0.16 mmol). The product was purified by chromatography on silica gel (2% MeOH/hexanes) followed by RP-HPLC to yield12.3 mg (22%) of an off-white solid. ^{1}H NMR (400 MHz, DMSO-d_6) δ 7.85 (1H, s), 7.09 – 7.19 (3H, m), 7.01 (1H, d, $J = 8$ Hz), 6.92 (1H, br), 6.32 (1H, s), 5.54 (1H, s), 4.43 (2H, s), 3.65 (4H, t, $J = 5$ Hz), 3.61 (4H, t, $J = 5$ Hz), 2.25 (3H, s), 2.11 (3H, s); HR-EI MS $(M)^+$ *m/z* calcd for $C_{21}H_{24}N_4O_2$ 364.1899, found 364.1904.

3.6.17 9-(2,3-Dimethyl-phenylamino)-7-methyl-2-morpholin-4-yl-pyrido(1,2-*a*)pyrimidin-4-one (MCA54)

Prepared following the general procedure for TGX126, using TGX66 (50 mg, 0.16 mmol) and 2,3-dimethylaniline (19 mg, 0.16 mmol). The product was purified by chromatography on silica gel (2% MeOH/hexanes) followed by RP-HPLC to yield 12.3 mg (22%). ^{1}H NMR (400 MHz, DMSO-d_6) δ 7.96 (1H, s), 7.83 (1H, s), 7.05 – 7.14 (3H, m), 6.30 (1H, s), 5.58 (1H, s), 3.64 (8H, br), 2.27 (3H, s), 2.13 (3H, s), 2.06 (3H, s); HR-EI MS $(M)^+$ *m/z* calcd for $C_{21}H_{24}N_4O_2$ 364.1899, found 364.1910.

3.6.18 7-Methyl-9-(2-methyl-benzylamino)-2-morpholin-4-yl-pyrido(1,2-*a*)pyrimidin-4-one (MCA55)

Prepared following the general procedure for TGX126, using TGX66 (50 mg, 0.16 mmol) and 2-methylbenzylamine (0.019 mL, 0.16 mmol). The product was purified by chromatography on silica gel (2% MeOH/hexanes) followed by RP-HPLC to yield 12.9 mg (23%) of an off-white solid. ^{1}H NMR (400 MHz, DMSO-d_6) δ 7.87 (1H, s), 7.09 – 7.17 (4H, m), 6.76 (1H, br), 6.31 (1H, s), 5.55 (1H, s), 4.44 (2H, s), 3.64 (4H, t, *J* = 5 Hz), 3.60 (4H, t, *J* = 5 Hz), 2.32 (3H, s), 2.11 (3H, s); HR-EI MS $(M)^+$ *m/z* calcd for $C_{21}H_{24}N_4O_2$ 364.1899, found 364.1905.

3.6.19 5-Morpholin-4-yl-2-nitro-phenylamine (AMA30)

Morpholine (2.03 mL, 23.2 mmol) was added to a stirred solution of 5-chloro-2-nitroaniline (2.0 g, 12 mmol) in DMSO (10 mL) and heated to 90 °C for 18 h[23]. When the reaction was complete, the product was precipitated by pouring into H_2O(150 mL), and then purified by chromatography on silica gel (50% EtOAc/hexanes) to yield 660 mg (25.4%) of a yellow solid. ^{1}H NMR (400 MHz, DMSO-d_6) δ 7.79 (1H, d, *J* = 8 Hz), 7.25

(2H, s), 6.34 (1H, d, $J = 10$ Hz), 6.18 (1H, s), 3.67 (4H, t, $J = 5$ Hz), 3.23 (4H, t, $J = 5$ Hz); ^{13}C NMR (100 MHz, DMSO-d_6) δ 155.9, 148.9, 127.8, 123.9, 105.8, 98.3, 66.4, 44.1; HR-EI MS $(M)^+$ *m/z* calcd for $C_{10}H_{13}N_3O_3$ 223.0957, found 223.0954.

3.6.20 2-Hydroxy-4-morpholin-4-yl-benzaldehyde (IC60211)

DMF (10 mL) was cooled on ice and $POCl_3$ (1.4 mL, 15 mmol) was added dropwise. 3-morpholinophenol (2.5 g, 14 mmol) was slowly added to the stirred solution at rt, incubated at rt for an additional 40 min, and then heated to 100 °C for 9 h essentially as described[23]. The reaction was terminated by dumping into 1M NaOAc (40 mL). The solid was filtered, rinsed three times with H_2O, and purified by chromatography on silica gel (25% EtOAc/hexanes) to yield 802 mg (28%) of an off-white solid. ^{1}H NMR (400 MHz, DMSO-d_6) δ 11.07 (1H, s), 9.72 (1H, s), 7.46 (1H, d, $J = 8$ Hz), 6.55 (1H, dd, $J = 9$ Hz, 2.4 Hz), 6.28 (1H, d, $J = 2.4$ Hz), 3.66 (4H, t, $J = 5$ Hz), 3.30 (4H, t, $J = 5$ Hz); ^{13}C NMR (100 MHz, DMSO-d_6) δ 192.0, 163.7, 157.2, 133.9, 113.8, 106.8, 99.5, 66.4, 47.1; HR-EI MS $(M)^+$ *m/z* calcd for $C_{11}H_{13}NO_3$ 207.0895, found 207.0893.

3.6.21 1-(2-Hydroxy-4-morpholin-4-yl-phenyl)-ethanone (IC86621)

MeLi (2.4 mL of 1.6M solution in Et_2O, 3.9 mmol) was added dropwise to a solution of IC60211 (200 mg, 0.996 mmol) in THF (4 mL) at –78 °C[23]. The reaction was allowed to warm to rt and proceed overnight, at which point the reagent was quenched with sat. NH_4Cl (1 mL), extracted six times with Et_2O, and concentrated *in vacuo*. The product was chromatographed on silica gel (25% EtOAc/hexanes) to yield a white solid. The solid was dissolved in 10 mL MeCN, MnO_2 (391 mg, 4.5 mmol) was added, and the reaction was allowed to proceed for three days at rt under an inert

atmosphere. The product was chromatographed on silica gel (50% EtOAc/hexanes) to yield17.8 mg (18%) of a white solid. ^{1}H NMR (400 MHz, $CDCl_3$) δ 12.71 (1H, s), 7.55 (1H, d, $J = 9$ Hz), 6.35 (1H, d, $J = 9$ Hz), 6.26 (1H, s), 3.79 (4H, t, $J = 5$ Hz), 3.30 (4H, t, $J = 5$ Hz), 2.50 (3H, s); ^{13}C NMR (100 MHz, $CDCl_3$) δ 201.7, 165.0, 156.7, 132.5, 105.5, 100.6, 66.6, 47.2; HR-EI MS $(M)^+$ *m/z* calcd for $C_{12}H_{15}NO_3$ 221.1052, found 221.1049.

3.6.22 1-(2-Hydroxy-4-morpholin-4-yl-phenyl)-phenyl-methanone (AMA37)

Prepared according to the general procedure of IC86621 using PhMgBr (1.1 mL, 3.4 mmol) and IC60211 (150 mg, 0.724 mmol), except that the product of PhMgBr addition was taken on for oxidation by MnO_2 (249 mg, 3.38 mmol) without intervening chromatographic purification. Chromatography of the final product on silica gel (50% EtOAc/hexanes) yielded (28.9 mg, 14.1%) of a yellow solid. ^{1}H NMR (400 MHz, $CDCl_3$) δ 12.73 (1H, s), 7.41 – 7.61 (5H, m), 6.35 (1H, d, $J = 2.4$ Hz), 6.31 (1H, dd, $J = 9$ Hz, 2.8 Hz), 3.81 (4H, t, $J = 8$ Hz), 3.31(4H, t, $J = 8$ Hz); ^{13}C NMR (100 MHz, $CDCl_3$) δ 199.1, 166.1, 156.6, 138.8, 135.5, 131.4, 129.0, 128.4, 119.2, 111.3, 105.3, 100.6, 66.7, 47.1; HR-EI MS $(M)^+$ *m/z* calcd for $C_{17}H_{17}NO_3$ 283.1208, found 283.1195.

3.6.23 2-Chloro-1-(2-hydroxy-4-morpholin-4-yl-phenyl)-ethanone (AMA48)

A solution of 3-morpholinophenol (5.0 g, 28 mmol) and chloroacetonitrile (2.1 mL, 34 mmol) in chloroethane (150 mL) in a 3-neck flask was cooled in a ice bath, and BCl_3 (100 mL, 1M in CH_2Cl_2) was slowly added by an addition funnel essentially as described[23]. $AlCl_3$ (1.9 g, 14 mmol) was then added to this solution, the flask was equipped with a reflux condensor, and the reaction was heated to 60 °C for 24 h. The reaction was then cooled to 0 °C and 100 mL 2N HCl was added by addition funnel. Following acidification, the organic phase was collected and rinsed twice with 2N HCl

(100 mL) and once with H_2O (100 mL). The organic phase was concentrated in vacuo and the product purified by chromatography on silica gel (30% EtOAc/hexanes) to yield 775 mg (10.9%). ^1H NMR (400 MHz, DMSO-d_6) δ 11.91 (1H, s), 7.66 (1H, d, $J = 9$ Hz), 6.53 (1H, dd, $J = 9$ Hz, 2.4 Hz), 4.93 (2H, s), 3.66 (4H, t, $J = 5$ Hz), 3.31 (4H, t, $J = 5$ Hz); ^{13}C NMR (100 MHz, DMSO-d_6) δ 193.0, 163.6, 156.5, 132.1, 109.1, 105.8, 99.1, 65.7, 46.4, 46.3; HR-EI MS $(M)^+$ m/z calcd for $C_{12}H_{14}ClNO_3$ 255.0662, found 255.0670.

3.6.24 LY292223

Prepared according to the general procedure described for the synthesis of 2-aminochromones [33]. 2'-hydroxyacetophenone (0.50 mL, 4.2 mmol) was dissolved in 11 mL CH_2Cl_2, cooled to –78 °C and $TiCl_4$ (6.5 mL, 1M solution in THF, 6.5 mmol) was added. After 1 h, DIPEA (2.7 mL, 16 mmol) was added at –78 °C and the reaction was allowed to proceed for an additional 1 h. 4-dichloromethylenemorpholin-4-ium[34] (1.2 g, 5.0 mmol) was then added and the reaction was allowed to proceed at –78 °C for 20 min. The reaction was warmed to 0 °C, MeOH (30 mL) was added, and the reaction was allowed to warm to rt overnight. The reaction was then concentrated *in vacuo*, washed once with sat. $NaHCO_3$, and the $NaHCO_3$ was extracted three times with CH_2Cl_2. The combined organic phase was dried over MgSO4, filtered, and solvent removed *in vacuo*. The product was purified by chromatography on silica gel (10% MeOH/EtOAc) to yield 344 mg of a white powder (36%). ^1H NMR (400 MHz, $CDCl_3$) δ 7.95 (1H, s), 7.35 (1H, s), 7.14 (1H, s), 7.08 (1H, s), 5.27 (1H, s), 3.63 (4H, t, $J = 5$ Hz), 3.30 (4H, t, $J = 5$ Hz); ^{13}C NMR (100 MHz, $CDCl_3$) δ 176.8, 162.5, 153.5, 132.2, 125.2, 124.6, 122.8, 116.3, 87.0, 65.8, 44.5; IR: 1616, 1555, 1418, 1300, 1251, 1117, 985, 766; HR-EI MS $(M)^+$ m/z calcd for $C_{13}H_{13}NO_3$ 231.0895, found 231.0887.

3.7 References

1. Katso, R., Okkenhaug, K., Ahmadi, K., White, S., Timms, J., and Waterfield, M.D. (2001). Cellular function of phosphoinositide 3-kinases: implications for development, homeostasis, and cancer. Annu Rev Cell Dev Biol *17*, 615-675.

2. Anderson, K.E., and Jackson, S.P. (2003). Class I phosphoinositide 3-kinases. Int J Biochem Cell Biol *35*, 1028-1033.

3. Arcaro, A., and Wymann, M.P. (1993). Wortmannin is a potent phosphatidylinositol 3-kinase inhibitor: the role of phosphatidylinositol 3,4,5-trisphosphate in neutrophil responses. Biochem J *296 (Pt 2)*, 297-301.

4. Wymann, M.P., Bulgarelli-Leva, G., Zvelebil, M.J., Pirola, L., Vanhaesebroeck, B., Waterfield, M.D., and Panayotou, G. (1996). Wortmannin inactivates phosphoinositide 3-kinase by covalent modification of Lys-802, a residue involved in the phosphate transfer reaction. Mol Cell Biol *16*, 1722-1733.

5. Vlahos, C.J., Matter, W.F., Hui, K.Y., and Brown, R.F. (1994). A specific inhibitor of phosphatidylinositol 3-kinase, 2-(4-morpholinyl)-8-phenyl-4H-1-benzopyran-4-one (LY294002). J Biol Chem *269*, 5241-5248.

6. Okkenhaug, K., Bilancio, A., Farjot, G., Priddle, H., Sancho, S., Peskett, E., Pearce, W., Meek, S.E., Salpekar, A., Waterfield, M.D., Smith, A.J., and Vanhaesebroeck, B. (2002). Impaired B and T cell antigen receptor signaling in p110delta PI 3-kinase mutant mice. Science *297*, 1031-1034.

7. Jou, S.T., Carpino, N., Takahashi, Y., Piekorz, R., Chao, J.R., Wang, D., and Ihle, J.N. (2002). Essential, nonredundant role for the phosphoinositide 3-kinase p110delta in signaling by the B-cell receptor complex. Mol Cell Biol *22*, 8580-8591.

8. Sasaki, T., Irie-Sasaki, J., Jones, R.G., Oliveira-dos-Santos, A.J., Stanford, W.L., Bolon, B., Wakeham, A., Itie, A., Bouchard, D., Kozieradzki, I., Joza, N., Mak, T.W., Ohashi, P.S., Suzuki, A., and Penninger, J.M. (2000). Function of PI3Kgamma in thymocyte development, T cell activation, and neutrophil migration. Science *287*, 1040-1046.

9. Hirsch, E., Katanaev, V.L., Garlanda, C., Azzolino, O., Pirola, L., Silengo, L., Sozzani, S., Mantovani, A., Altruda, F., and Wymann, M.P. (2000). Central role for G protein-coupled phosphoinositide 3-kinase gamma in inflammation. Science *287*, 1049-1053.

10. Vanhaesebroeck, B., Jones, G.E., Allen, W.E., Zicha, D., Hooshmand-Rad, R., Sawyer, C., Wells, C., Waterfield, M.D., and Ridley, A.J. (1999). Distinct PI(3)Ks mediate mitogenic signalling and cell migration in macrophages. Nat Cell Biol *1*, 69-71.

11. Ward, S.G., and Finan, P. (2003). Isoform-specific phosphoinositide 3-kinase inhibitors as therapeutic agents. Curr Opin Pharmacol *3*, 426-434.

12. Ward, S., Sotsios, Y., Dowden, J., Bruce, I., and Finan, P. (2003). Therapeutic potential of phosphoinositide 3-kinase inhibitors. Chem Biol *10*, 207-213.

13. Wymann, M.P., Zvelebil, M., and Laffargue, M. (2003). Phosphoinositide 3-kinase signalling--which way to target? Trends Pharmacol Sci *24*, 366-376.

14. Roberson, A., Jackson S, Kenche, V, Yaip,C, Parbaharan, H, Thompson, P (2001). Therapeutic Morpholino-Substituted Compounds, vol. WO 01/53266, Thrombogenix.

15. Davies, S.P., Reddy, H., Caivano, M., and Cohen, P. (2000). Specificity and mechanism of action of some commonly used protein kinase inhibitors. Biochem J *351*, 95-105.

16. Walker, E.H., Pacold, M.E., Perisic, O., Stephens, L., Hawkins, P.T., Wymann, M.P., and Williams, R.L. (2000). Structural determinants of phosphoinositide 3-kinase inhibition by wortmannin, LY294002, quercetin, myricetin, and staurosporine. Mol Cell *6*, 909-919.

17. Walker, E.H., Perisic, O., Ried, C., Stephens, L., and Williams, R.L. (1999). Structural insights into phosphoinositide 3-kinase catalysis and signalling. Nature *402*, 313-320.

18. Zhao, X.H., Bondeva, T., and Balla, T. (2000). Characterization of recombinant phosphatidylinositol 4-kinase beta reveals auto- and heterophosphorylation of the enzyme. J Biol Chem *275*, 14642-14648.

19. Hall-Jackson, C.A., Cross, D.A., Morrice, N., and Smythe, C. (1999). ATR is a caffeine-sensitive, DNA-activated protein kinase with a substrate specificity distinct from DNA-PK. Oncogene *18*, 6707-6713.

20. Fukuchi, K., Watanabe, H., Tomoyasu, S., Ichimura, S., Tatsumi, K., and Gomi, K. (2000). Phosphatidylinositol 3-kinase inhibitors, Wortmannin or LY294002, inhibited accumulation of p21 protein after gamma-irradiation by stabilization of the protein. Biochim Biophys Acta *1496*, 207-220.

21. Roshal, M., Kim, B., Zhu, Y., Nghiem, P., and Planelles, V. (2003). Activation of the ATR-mediated DNA damage response by the HIV-1 viral protein R. J Biol Chem *278*, 25879-25886.

22. Kashishian, A., Douangpanya, H., Clark, D., Schlachter, S.T., Eary, C.T., Schiro, J.G., Huang, H., Burgess, L.E., Kesicki, E.A., and Halbrook, J. (2003). DNA-dependent protein kinase inhibitors as drug candidates for the treatment of cancer. Mol Cancer Ther *2*, 1257-1264.

23. Halbrook, J., Kesicki, E., Burgess, L.E., Schlachter S.T., Eary, C.T., Schiro, J.S., Huang, H., Evans, M., Han, Y. (2002). Materials and Methods to Potentiate Cancer Treatment, vol. WO 02/20500 A2, ICOS Corporation.

24. Hollick, J.J., Golding, B.T., Hardcastle, I.R., Martin, N., Richardson, C., Rigoreau, L.J., Smith, G.C., and Griffin, R.J. (2003). 2,6-disubstituted pyran-4-one and

thiopyran-4-one inhibitors of DNA-Dependent protein kinase (DNA-PK). Bioorg Med Chem Lett *13*, 3083-3086.

25. Sadhu, C., Masinovsky, B., Dick, K., Sowell, C.G., and Staunton, D.E. (2003). Essential role of phosphoinositide 3-kinase delta in neutrophil directional movement. J Immunol *170*, 2647-2654.

26. Puri, K.D., Doggett, T.A., Douangpanya, J., Hou, Y., Tino, W.T., Wilson, T., Graf, T., Clayton, E., Turner, M., Hayflick, J.S., and Diacovo, T.G. (2004). Mechanisms and implications of phosphoinositide 3-kinase {delta} in promoting neutrophil trafficking into inflamed tissue. Blood.

27. Sadhu, C., Dick, K., Tino, W.T., and Staunton, D.E. (2003). Selective role of PI3K delta in neutrophil inflammatory responses. Biochem Biophys Res Commun *308*, 764-769.

28. Northcott, C.A., Hayflick, J.S., and Watts, S.W. (2004). PI3-kinase upregulation and involvement in spontaneous tone in arteries from DOCA-salt rats: is p110delta the culprit? Hypertension *43*, 885-890.

29. Sawyer, C., Sturge, J., Bennett, D.C., O'Hare, M.J., Allen, W.E., Bain, J., Jones, G.E., and Vanhaesebroeck, B. (2003). Regulation of breast cancer cell chemotaxis by the phosphoinositide 3-kinase p110delta. Cancer Res *63*, 1667-1675.

30. Kim, C.M., Dion, S.B., Onorato, J.J., and Benovic, J.L. (1993). Expression and characterization of two beta-adrenergic receptor kinase isoforms using the baculovirus expression system. Receptor *3*, 39-55.

31. Huang, X., and Chen, B.C. (1986). Synthesis of Bisalkylthiolydine Derivatives of Meldrums Acid and Barbituric-Acid. Synthesis-Stuttgart, 967-968.

32. Ye, F.C., Chen, B.C., and Huang, X. (1989). Synthesis of 7-Substituted 5-Oxo-5h-Thiazolo[3,2-a]Pyrimidine-6-Carboxylic Acids, 2-Substituted 4-Oxo-4h-Pyrido[1,2-a]Pyrimidine-3-Carboxylic Acids, and 2,6-Disubstituted 4-Quinolones from Meldrum Acid-Derivatives. Synthesis-Stuttgart, 317-320.

33. Morris, J., Luke, G.P., and Wishka, D.G. (1996). Reaction of phosgeniminium salts with enolates derived from Lewis acid complexes of 2'-hydroxypropiophenones and related beta-diketones. J. Org. Chem. *61*, 3218-3220.

34. Morris, J., Wishka, D.G., and Fang, Y. (1992). A Novel Synthesis of 2-Aminochromones Via Phosgeniminium Salts. J. Org. Chem. *57*, 6502-6508.

HRC Library

Chapter 4

Targeting the gatekeeper residue in phosphoinositide 3-kinases

IDRC Library

4.1 Abstract

A single residue in the ATP binding pocket of protein kinases – termed the gatekeeper – has been shown to control sensitivity to a wide range of small molecule inhibitors [1, 2]. Kinases that possess a small side chain at this position (Thr, Ala, or Gly) are readily targeted by structurally diverse classes of inhibitors, whereas kinases that possess a larger residue at this position are broadly resistant. Recently, lipid kinases of the phosphoinositide 3-kinase (PI3-K) family have become the focus of intense interest as potential drug targets [3, 4]. In this study, we identify the residue that corresponds structurally to the gatekeeper in PI3-Ks, and explore its importance in controlling enzyme activity and small molecule sensitivity. Isoleucine 848 of p110α was mutated to alanine and glycine, but the mutated kinase was found to have severely impaired enzymatic activity. A structural bioinformatic comparison of this kinase with its yeast orthologs identified second site mutations that rescued the enzymatic activity of the I848A kinase. To probe the dimensions of the gatekeeper pocket, a focused panel of analogs of the PI3-K inhibitor LY294002 were synthesized and their activity against gatekeeper mutated and wild-type p110α was assessed.

4.2 Introduction

In the past decade protein kinases have emerged as one of the most important new classes of drug targets. Protein kinases play a central role in many signaling pathways disregulated in disease, and these enzymes can be readily targeted with cell permeable, small molecule inhibitors [5]. These facts have led to the hope that inhibitors of individual protein kinases might be tailored to specific diseases based on an understanding of their molecular etiology [6]. Recently, this concept has been dramatically validated by the clinical success of Gleevec, an inhibitor of the Abl tyrosine

kinase [7], in the treatment of chronic mylogenous leukemia, a disease driven by the activity of the BCR-ABL oncogene.

The search for protein kinase inhibitors has led to the realization that not all kinases are equally amenable to targeting with potent, ATP competitive small molecules. In this regard, a single residue in the ATP binding pocket (corresponding to threonine 338 in Hck) has been shown to control kinase sensitivity to a wide range of structurally unrelated compounds, including pyridinylimidazoles [8], pyrazolopyrimidines [2], purines [9], quinazolines [10], phenylaminopyrimidines [11], and staurosporines [12]. This residue is conserved as a threonine or larger amino acid in the human kinome (no wild-type protein kinases contain an alanine or glycine at this position), and structural analysis has shown that the size of this gatekeeper residue restricts access to a pre-existing cavity within the ATP binding pocket [13]. Kinases that possess a threonine at this position are readily targeted by diverse classes of small molecule inhibitors that can access this nascent pocket. Moreover, mutation of the gatekeeper residue to a smaller amino acid, such as alanine or glycine, has been shown to induce sensitivity to pyrazolopyrimidine inhibitors at low nanomolar concentrations in over 30 protein kinases – even though in many cases the wild-type kinase is completely insensitive to compounds of this class [12].

The importance of the gatekeeper in controlling inhibitor sensitivity is underscored by the fact that most kinase inhibitors in clinical use target kinases that contain a threonine at this position, even though threonine is found in only ~ 20% of the human kinome (e.g., Iressa: EGFR; Gleevec: Abl, PDGFR, and c-Kit; BAY43-9006: Raf and VEGFR). Indeed, analysis of mutations in BCR-Abl that confer drug resistance has shown that mutation of the gatekeeper to a larger amino acid (T315I) is one of the most common mechanisms of resistance to Gleevec [11]. Remarkably, second generation BCR-Abl inhibitors designed to target resistant alleles have been shown to effectively

inhibit every naturally occuring mutant of this kinase except those mutated at the gatekeeper residue [14, 15].

Recently, lipid kinases of the phosphoinositide 3-kinase family have attracted considerable interest as a new class of drug targets [3, 4]. These enzymes act by generating the lipid second messengers phosphatidylinositol-3,4-bisphosphate ($PI(3,4)P_2$) and phosphatidylinositol-3,4,5-trisphosphate ($PI(3,4,5)P_3$), which in turn activate downstream enzymes in a wide-range of signaling pathways involved in cell growth, survival, differentiation, and motility [16]. Activating mutations in the PI3-K isoform p110α have recently been identified at high frequency in several types of cancer [17], and PTEN, the lipid phosphatase that reverses the PI3-K reaction, has been identified as one of the most commonly inactivated tumor suppressors in the human genome [18]. Moreover, the clinical efficacy of recently approved agents that target the epidermal growth factor receptor in breast [19] and lung [20, 21] cancers has been demonstrated to correlate with the dependence of those cancers on aberrant PI3-K signaling and the ability of these agents to suppress that pathway. For these reasons, considerable effort has been directed toward the development of selective inhibitors of these enzymes as potential cancer therapeutics [22].

Although PI3-Ks possess very low overall sequence homology to protein kinases, they possess the same overall fold, share several consensus sequences (e.g., the DFG motif that is responsible for coordination of Mg^{2+}), and are sensitive to two pan-specific protein kinase inhibitors (staurosporine [23] and quercetin [24]). Due to the importance of these enzymes as an emerging class of drug targets, we sought identify the residue analogous to the gatekeeper in lipid kinases and explore how the size of this residue might affect the active site structure and inhibitor sensitivity of this class of enzymes.

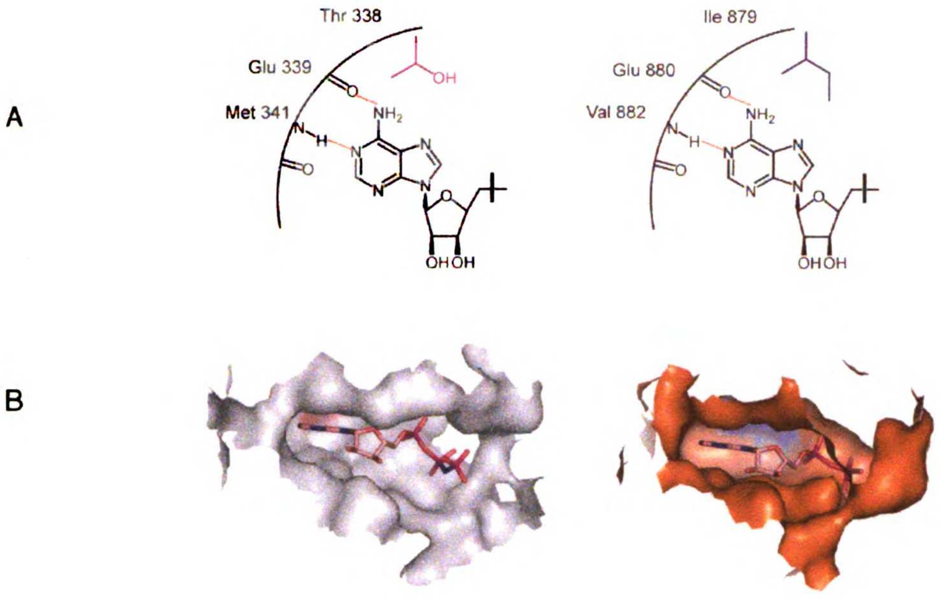
A
Thr 338
Glu 339
Met 341
OH
NH2
N
H
O
OHOH
Ile 879
Glu 880
Val 882
B

C

		338			
Hck	V	**T**	E	Y	M
		879			
p110γ	M	**I**	E	I	V
p110α	L	**I**	E	V	V
PI3KC2α	M	**V**	E	L	V
VSP34	A	**I**	E	F	I
MEC1	I	**L**	E	M	V

Figure 4.1. Conservation in the ATP binding pocket of PI3Ks. (A) Schematic illustrating the hydrogen bonding contacts to ATP. (B) Surface representation of the interior face of the ATP binding pocket of Hck (gray) and p110γ (orange), from published crystal structure data. (C) Structure-based sequence analysis of several residues lining the ATP binding pockets of Hck and several PI3Ks.

4.3 The gatekeeper residue is conserved in lipid kinases

The crystal structure of the PI3-K p110γ bound to ATP has been solved [25], and the catalytic domain was found to share several features with reported protein kinase structures. These similarities include a two-lobed structure consisting of a N-terminal lobe containing a 5 to 7-stranded β-sheet, a loop connecting two of these strands that interacts with the phosphate groups of ATP, a conserved lysine residue that positions the α and β phosphate groups of ATP for the phosphotransfer reaction, and a primarily α-helical C-terminal lobe that binds the phosphoacceptor. In protein kinases, conserved hydrogen bonds to the N6 and N1 of positions of the adenine ring of ATP are made by the backbone amides of two conserved residues (corresponding to Glu 339 and Met 341 of Hck, respectively). The gatekeeper residue immediately precedes Glu 339, and forms the hydrophobic interior face of the ATP binding pocket, with Cβ of the gatekeeper typically positioned 4 to 7 Å from the N6 and N7 residues of adenine. Inspection of the ATP binding pocket of p110γ reveals a similar set of contacts. Hydrogen bonds to ATP are made by backbone amides from two residues – Glu 880 and Val 882 – and these residues are immediately preceded by a large hydrophobic residue (Ile 879 in p110γ) that is positioned approximately 5 Å from N6 and N7 of adenine (Figure 4.1A). To directly compare the orientation of these two residues (Ile 879 in p110γ and Thr 338 in Hck), we aligned the crystal structures of Hck and p110γ with respect to the adenine ring of ATP. This structural alignment indicates that these two residues occupy a largely overlapping, but not identical, space within the interior of the ATP binding pocket, forming the innermost face that contacts the adenine ring of ATP (Figure 4.1B). The most important difference between the p110γ and Hck structures in this region is that Cα of Ile 879 in p110γ is shifted slightly perpendicular to the plane of the adenine ring (~ 2

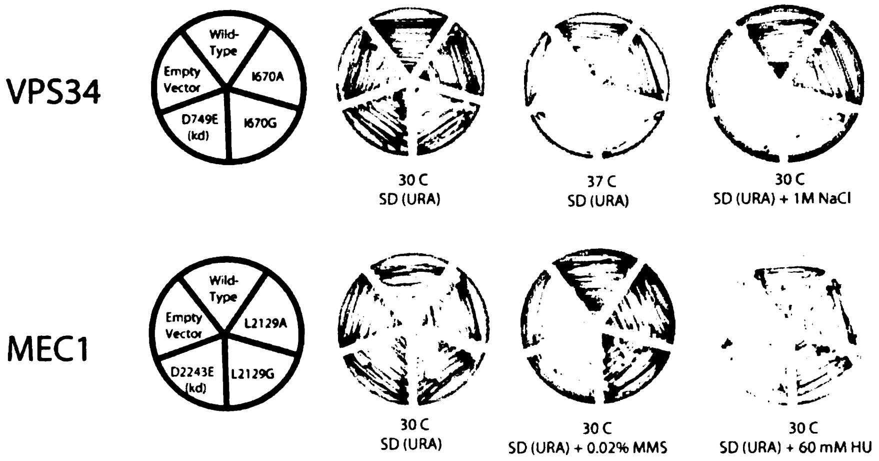
VPS34
Wild-Type
Empty Vector
I670A
D749E (kd)
I670G
30 C SD (URA)
37 C SD (URA)
30 C SD (URA) + 1M NaCl
MEC1
Wild-Type
Empty Vector
L2129A
D2243E (kd)
L2129G
30 C SD (URA)
30 C SD (URA) + 0.02% MMS
30 C SD (URA) + 60 mM HU

Figure 4.2. Growth of yeast expressing various alleles of VPS34 and MEC1 under nonselective and selective growth conditions. *S. cerevisiae* expressing VPS34 alleles (wild type, empty vector, kinase dead (kd; D749E), I670G, or I670A) were plated on nonselective media (SD(URA)) or selective media (SD(URA), 1 M NaCl). *S. cerevisiae* expressing MEC1 alleles (wild type, empty vector, kinase dead (kd; D2243E), L2129G, or L2129A) were plated on media (SD(URA)) or selective media (SD(URA), 0.02% (MMS); or SD(URA), 60 mM hydroxyurea (HU)).

Å) relative to Thr 338 in Hck, such that Ile 879 also participates in forming the interior roof of the ATPbinding pocket, whereas Thr 338 is more completely fixed within the plane of the adenine ring.

To compare this region of primary sequence between PI3-Ks and protein kinases, a structure based sequence alignment was generated. This analysis reveals that the gatekeeper residue is situated within a small region of sequence homology between lipid and protein kinases (Figure 4.1C). As observed for the gatekeeper residue in protein kinases, Ile 879 is conserved as a large hydrophobic residue in all PI3-Ks (isoleucine, leucine, methionine, or valine, although no PI3-Ks contain threonine at this position). The residue immediately following the Ile 879 in PI3-Ks is conserved as a glutamate (83%), and this is also the most common residue at that position in protein kinases (75%). The residues at the -1 and +1/+2 positions positions relative to Ile 879 in PI3-Ks are conserved as large hydrophobic residues, and the corresponding positions in protein kinases show a similar preference (Figure 4.1C). For example, position 337 is either isoleucine, leucine, valine, or methionine in 86% of protein kinases and in 92% of human PI3-Ks. On this basis, we conclude that p110γ residue Ile 879 structurally corresponds to the gatekeeper residue in protein kinases.

As the gatekeeper residue is structurally conserved between PI3-Ks and protein kinases, we asked whether it is also functionally conserved, and in particular whether mutagenesis of this position to a smaller residue might induce inhibitor sensitivity as has been observed for protein kinases [12]. Three representative members of the PI3-K family were selected for this analysis: the yeast PI3-K VPS34, the yeast PI3-K related protein kinase MEC1, and the prototypical mammalian PI3-K p110α. The gatekeeper residue in each of these kinases was mutated to alanine and glycine, and the effect of this mutation on enzyme activity and inhibitor sensitivity was assessed.

A.

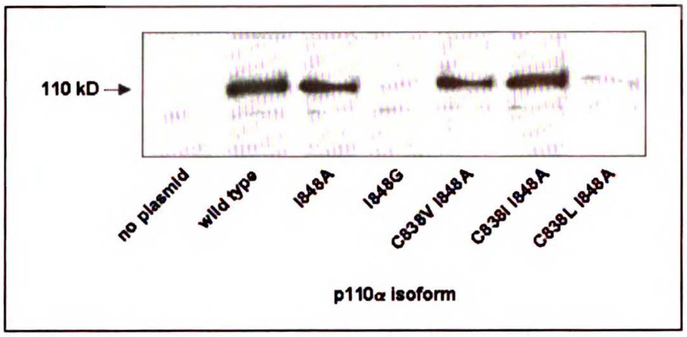
110 kD →
no plasmid
wild type
I848A
I848G
C838V I848A
C838I I848A
C838L I848A
p110α isoform

B.

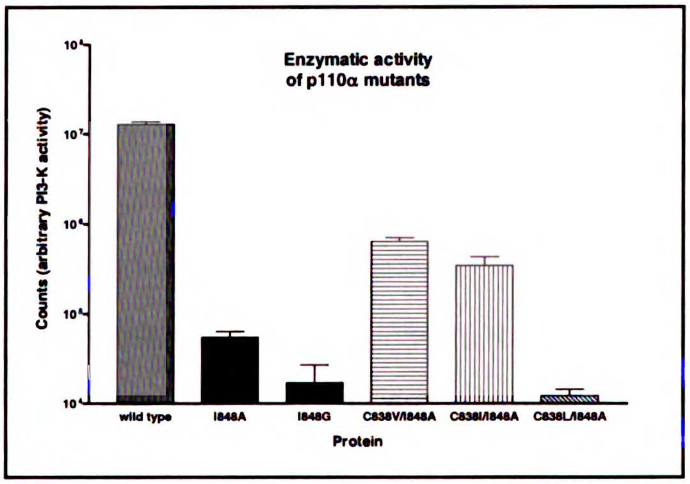

Figure 4.3. Relative expression levels and enzymatic activities of Myc-tagged p110α alleles. (A) Equal amounts of soluble protein (29 µg) from transiently transfected cos-1 cells were subjected to Western analysis (anti-Myc antibody, 9E10). (B) Relative enzymatic activities of p110α alleles. Cos-1 cells were co-transfected with equal amounts of expression vectors containing the indicated genes and p85 (a p110α adaptor protein). Protein was immunoprecipitated (anti-Myc antibody) from 950 µg of total soluble protein, and the activity assay was performed. Error bars represent the standard deviation from the mean from three independent measurements.

4.4 Effects of gatekeeper mutation on enzymatic activity

Plasmids encoding mutated VPS34 and MEC1 kinases were transformed into *S. cerevisiae* knockout strains, such that mutant allele functionally replaces the wild-type enzyme. Although yeast are viable in the absense of these proteins, specific growth conditions can induce a requirement for their catalytic activity, allowing us to examine whether the gatekeeper mutated alleles encode active kinases. The activity of VPS34 is required [26] for growth of yeast at elevated temperature (37º C) or high salt (1.0 M NaCl), whereas MEC1 activity is required [27, 28] for growth in the presence of agents that alkylate DNA (0.02% methylmethanesulphonate) or inhibit ribonucleotide reductase (60 mM hydroxylurea). Growth of the mutant strains under these conditions showed that the alanine gatekeeper mutant of VPS34 (I670A) as well as the alanine and glycine gatekeeper mutants of MEC1 (L2129A and L2129G) are able to functionally complement for the knockout at a level comparable to the wild-type enzyme (Figure 4.2). Importantly, transformation with the empty vector or a vector containing a catalytically inactive, kinase-dead mutant of each protein did not to rescue the knockout phenotype, confirming that the observed complementation is due to the catalytic activity of these proteins (Figure 4.2).

For p110α, the gatekeeper residue was mutated to alanine and glycine (I848A and I848G) and the mutant kinases were expressed by transient transfection in cos-1 cells. The myc-tagged mutated kinases were purified by immunoprecipitation and their lipid kinase activity was assessed using an *in vitro* kinase assay. The enzymatic activity of the I848A and I848G mutants was significantly impaired relative to wild-type p110α, with the gatekeeper mutants displaying approximately one-hundredth (I848A) to one-thousandth (I848G) of the wild-type activity (Figure 4A), The expression level of the wild-

	p110α	p110β	p110δ	p110γ	C2β	HsC3	ScC3	ATM	MEC1	TEL1	mTOR	DPK	ATR	STT4	PI4Kβ
1	M772	M784	M855	M804	F1057	F612	F600	A2693	F2056	G2443	I2163	M3728	L2303	K1624	R554
2	S774	S786	S857	S806	S1059	S614	S602	G2695	S2058	S2445	S2165	S3730	S2305	D1626	I556
3	P778	P790	P861	P810	P1063	P618	P606	P2699	P2062	I2449	P2169	P3734	P2309	L1631	S560
4	I800	I808	I780	I831	I1081	I634	M622	L2715	M2078	L2463	L2185	L3750	M2325	I1645	I574
5	K802	K810	K782	K833	K1083	K636	K624	K2717	K2080	K2465	K2187	K3752	K2327	K1647	K576
6	G804	G812	G784	G835	G1085	G638	G626	R2719	K2081	N2468	G2188	G3754	K2329	G1649	G578
7	D805	D813	D785	D836	D1086	D639	D627	D2720	E2082	D2469	E2190	E3755	D2340	D1650	D579
8	L807	L815	L787	L838	L1088	L641	L629	L2722	V2084	L2471	L2192	L3757	L2342	C1652	L581
9	D810	D818	D790	D841	D1091	D644	D632	D2725	D2087	D2474	D2195	D3759	D2345	D1655	E584
10	L814	L822	L794	L845	L1095	L648	V636	Q2729	M2091	E2478	M2199	E3763	M2349	L1659	F588
11	Y836	Y844	Y816	Y867	F1117	Y670	Y658	Y2755	Y2117	Y2504	Y2225	Y3789	Y2365	Y1681	Y610
12	G837	G845	G817	G868	R1118	K671	K659	K2756	S2118	K2505	A2226	S3790	A2366	R1682	K611
13	C838	C846	C818	C869	C1119	V672	I660	V2757	V2119	V2506	V2227	V3791	V2367	V1683	I612
14	S840	A848	P820	S871	S1121	A674	A662	P2759	S2121	P2508	P2229	P3793	P2369	A1685	V614
15	G846	G854	G826	G877	G1127	G680	G668	G2765	G2127	G2514	G2235	G3799	G2375	G1691	G620
16	I848	I853	I827	I879	V1129	M682	I670	L2767	L2129	I2516	I2237	I3801	I2377	I1693	I622
17	E849	E854	E828	E880	E1130	Q683	E671	E2768	E2130	E2517	G2238	E3803	E2379	D1694	E623
18	V850	V855	V829	I881	M1131	F684	F672	W2769	M2131	F2518	W2239	W3804	W2380	V1695	P624
19	V851	V856	V830	V882	I1132	I685	I673	C2770	V2132	V2519	V2240	L3805	V2381	L1696	V625
20	S854	S859	S833	A885	A1135	S687	L678	I2775	V2135	S2522	C2243	T3808	T2384	S1699	A628
21	HIS 855	E860	D834	T886	E1136	V688	A679	G2776	V2136	T2523	D2244	V3809	A2385	V1700	V629
22	T856	T861	T835	T887	T1137	P689	S680	E2777	T2137	S2524	T2245	T3810	G2386	S1701	S630
23	N920	N924	N898	N951	N1199	N738	N736	N2875	N2229	N2617	N2343	N3926	N2480	N1759	N688
24	M922	M926	M900	M953	M1201	M740	L738	L2877	L2231	L2619	M2345	M3928	L2482	M1761	L690
25	F930	F934	F908	F961	F1209	F748	F746	V2896	L2240	I2628	L2354	I3937	V2491	L1769	I697
26	I932	I936	I910	I963	I1211	I750	A748	I2898	V2242	I2630	I2356	I3939	V2493	I1771	I699
27	D933	D937	D911	D964	D1212	D751	D749	D2899	D2243	D2631	D2357	D3940	D2494	D1772	D700
28	F934	F938	F912	F965	F1213	F752	F750	L2900	F2244	L2632	F2358	F3941	F2495	F1773	F701
29	G935	G939	G913	G966	G1214	G753	G751	G2901	D2245	G2633	EMP	G3942	N2496	G1774	G702

Figure 4.4. Structure-based sequence alignment of 15 members of the PI3K family. Residue coloring: hydrophobic aliphatic (green), hydrophobic aromatic (light blue), small (yellow), polar charged (dark blue), basic (purple), and acidic (orange).

type and I848A proteins was similar by western blotting (Figure 4.3B), suggesting that the gatekeeper mutation had disrupted the integrity of the enzyme active site in this mutant without globally destabilizing the protein.

As VPS34 and MEC1 appear to tolerate the gatekeeper mutation, the impaired activity of p110α I848A was surprising, and led us to search for differences in primary sequence between these related kinases that might account for the observed differences in biochemical activity. Based on the crystal structure of p110γ, the residues that form the core of the ATP binding pocket were identified, and these residues were aligned among 15 members of the PI3-K family (Figure 4.4). We then searched for residues that are common to VPS34 and MEC1, but different in p110α, that might potentially account for the observed difference in tolerating the gatekeeper mutation. This analysis focused our attention on cysteine 838 in p110α (Position 13, Figure 4.4). Among the class I PI3-Ks such as p110α, this residue is conserved as a cysteine, whereas among the class III PI3Ks (e.g., VPS34) and PI3-K related protein kinases (e.g., MEC1), this residue is conserved as a β-branched residue (valine or isoleucine). Importantly, inspection of the crystal structure of p110γ reveals that C838 is located in β-strand 6, directly adjacent to I848 in β-strand 7 (Figure 5), suggesting that it may cooperate with the gatekeeper residue to stabilize this region of the protein. As β-branched amino acids have been shown to promote β-sheet formation [29], we reasoned that the presence of an isoleucine or valine residue at this position might stabilize that region of the protein when the gatekeeper is mutated, and thereby account for the differences in activity between MEC1/VPS34 and p110α.

To test this hypothesis, we prepared double mutants of p110α containing the I848A gatekeeper mutation in the context of second site mutations C838V, C838I and C838L. The double mutant enzymes were expressed in cos1 cells, and their expression

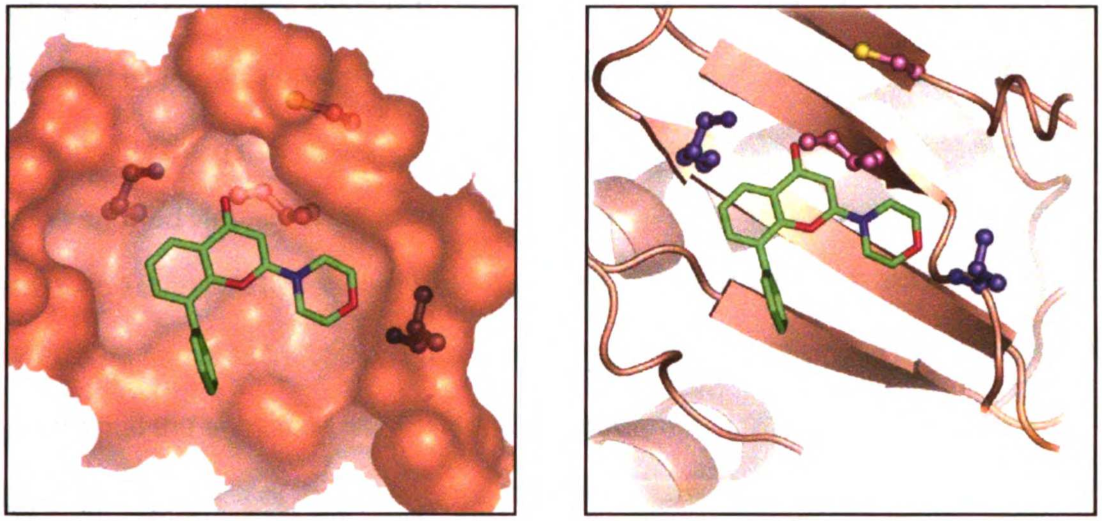

Figure 4.5. Co-crystal structure of p110γ-LY294002. (A) Surface representation and (B) ribbon representation of the protein illustrating the important hydrogen-bonding contacts and residues mutated in this study.

levels and enzymatic activity was assessed. The I848A/C838V and I848A/C838I double mutants both showed ~10-fold increased enzymatic activity relative to the I848A single mutant enzyme (Figure 4.3A). This enhancement in activity occurred without significantly changing the expression level of the protein (Figure 4.3B), and confirms that mutation of this position to a β-branched residue can restore enzymatic activity in the background of the gatekeeper mutation. Strikingly, the I848A/C838L double mutant enzyme showed virtually undetectable catalytic activity and expression of this protein could not be detected by western blotting (Figure 4.3), indicating that the isomeric I848A/C838I and I848A/C838L p110α proteins have dramatically different stability. This suggests that the enhanced activity of the isoleucine and valine mutants is likely a specific consequence of the β-branched residue at position 838 stabilizing β-strands 6 and 7, rather than a non-specific consequence of additional hydrophobic surface in the protein core.

4.5 Effects of gatekeeper mutation on inhibitor sensitivity

We next sought to assess how mutation of the gatekeeper residue to a smaller amino acid would affect inhibitor sensitivity. In protein kinases, mutation of the gatekeeper to alanine or glycine has been shown to induce sensitivity to both pyrazolopyrimidine inhibitors based on the Src-family kinase inhibitor PP1 and analogs of the natural product K252a [12]. p110γ has been shown to be sensitive to staurosporine (K_d = 0.29 μM) [23], which is structurally related to K252a, suggesting that K252a analogs may also target engineered lipid kinases. Although wild-type PI3-Ks are not sensitive to the protein kinase inhibitor PP1, mutation of the gatekeeper residue in protein kinases can induce sensitivity to this class of compounds in kinases that

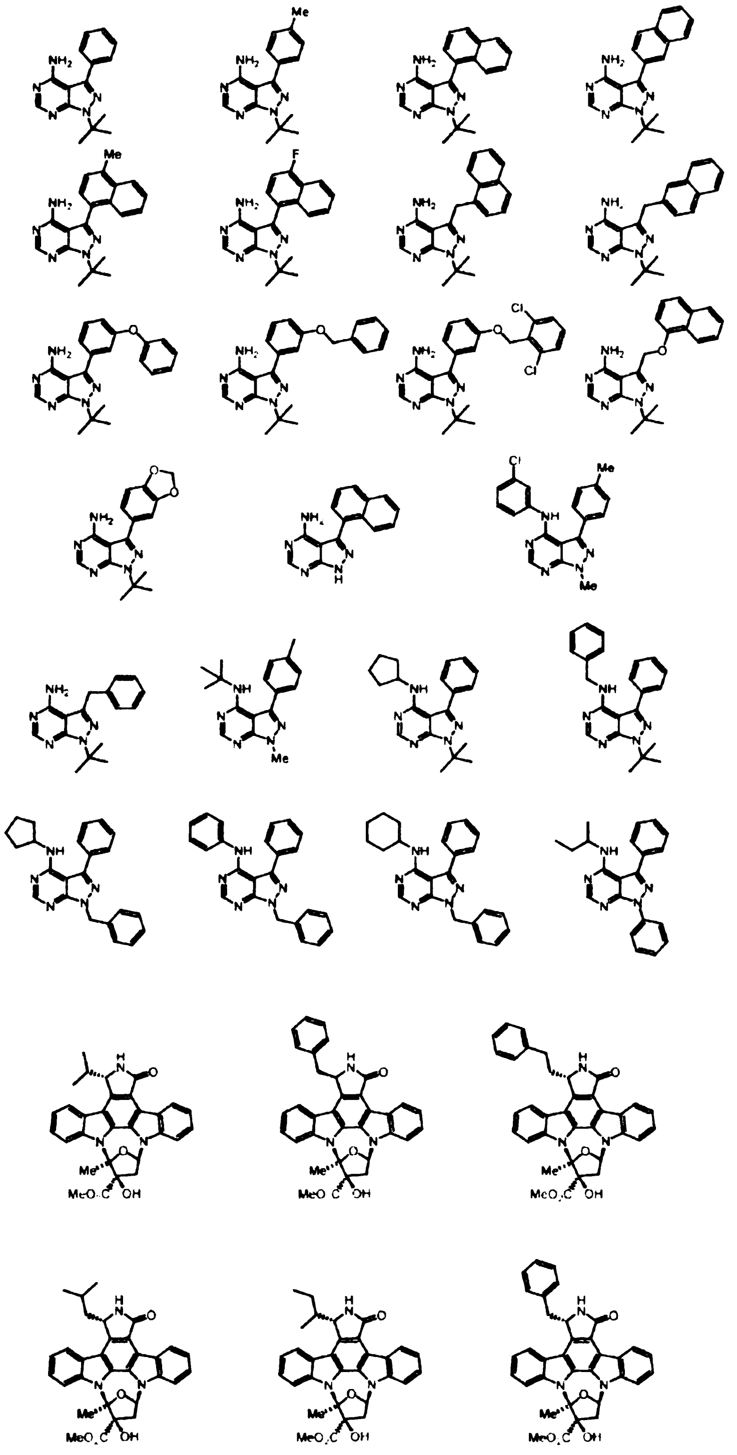

Figure 4.6 Structures of protein kinase inhibitors screened against p110α

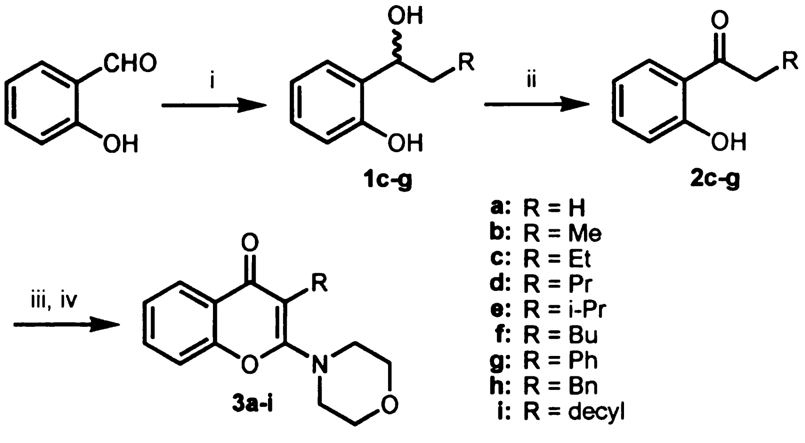
CHO
OH
i
OH
R
OH
1c-g
ii
O
R
OH
2c-g
iii, iv
O
R
O
N
O
3a-i

a: R = H
b: R = Me
c: R = Et
d: R = Pr
e: R = i-Pr
f: R = Bu
g: R = Ph
h: R = Bn
i: R = decyl

Figure 4.7 Scheme for the synthesis of 3-substituted LY292223 analogs

otherwise show no affinity for this scaffold [12]. Following this reasoning, we screened a small panel of these compounds *in vitro* against the wild-type and I848A p110α and *in vivo* against the wild-type and I670A mutant VPS34 (Figure 4.6). None of these compounds showed selective inhibition of the I848A allele of p110α at a concentration of 50 μM *in vitro* or I670A VPS34 at a concentration of 1 mM in a yeast halo assay. These results suggest that the structural differences between protein and lipid kinases may be too significant to bridge with a single inhibitor scaffold, and that new inhibitor analogs would be necessary to explore the gatekeeper pocket in lipid kinases.

To more directly probe the engineered gatekeeper pocket, we prepared a panel of analogs of the PI3-K inhibitor LY294002 [30]. LY294002 reversibly inhibits PI3-Ks with IC$_{50}$ values in the low micromolar range, but shows little selectivity among individual family members [31]. The crystal structure of LY294002 bound to p110γ has been solved [23], and reveals that the C3 position of LY294002 is positioned adjacent to the gatekeeper residue at a distance of approximately 4 Å. Molecular modelling based on this structure suggests that analogs of LY294002 containing extended substituents at C3 would access the space created by the gatekeeper mutation (Figure 4.5). A series of C3 substituted analogs of LY294002 were designed (lacking the 8-phenyl group of LY294002, as this moiety has been shown to be dispensable for binding to PI3-Ks [30]) and a panel of such analogs was prepared. This series of compounds was designed to include analogs that possess C3 substituents similar in size to the space created directly by the isoleucine to alanine mutation (e.g., Et, nPr), as well as those that contain much larger substituents (Ph, Bn). These latter compounds were included to probe whether the gatekeeper mutation would allow access to a deeper cavity within the kinase active site; in protein kinases, mutation of the gatekeeper has been shown to facilitate binding

	IC$_{50}$ (μM)	
analog	wild type	C838V/I848A
LY294002	1.1	1.1
LY292223 (**3a**)	2.6	15
3b (Me)	33	40
3c (Et)	28	4.4
3d (Pr)	31	68
3e (i-Pr)	51	>200
3f (Bu)	25	48
3g (Ph)	>200	>200
3h (Bn)	>200	>200
3i (decyl)	ND*	ND*

Table 4.1 IC50 values for LY292223 analogs against p110α wild-type and C838V/I848A

of substrate and inhibitor analogs containing bulky substituents much larger than the space created directly by the amino acid change [12, 13].

Synthesis was accomplished by addition of an excess of the appropriate Grignard reagent to salicylaldehyde to afford benzylic alcohols 1c-g (Figure 4.7). The resulting alcohols were oxidized to the corresponding ketones 2c-g using MnO_2, and the ring closing was performed using a using the morpholine phosgeniminium salt [30] to afford the desired 3-substituted analogs of LY294002 in high purity as white solids.

This panel of LY294002 analogs was tested for inhibition of the wild-type and C838V/I848A mutant of p110α in an *in vitro* PI3-K assay. Both LY294002 and the des-phenyl analog LY292223 inhibited wild-type and C838V/I848A p110α at low micromolar concentrations, although inhibition by LY292223 was modestly reduced for the double mutant (Table 4.1). As the size of the C3-moiety was increased, IC_{50} values against both the mutant and wild-type p110α increased by ~10 to >100-fold, and this increase tracked with the size of the C3 substituent, with the weakest inhibition by the compounds 3g (Ph) and 3h (Bn). Surprisingly, only compound 3c (Et) showed enhanced binding to the mutant relative to wild-type p110α, with modest selectivity for the engineered kinase (~6-fold). This compound contains an ethyl moiety at the C3 position, which is the most similar in size to the space created directly by the amino acid change (Ile to Ala) at the gatekeeper position. This suggests that mutation of this residue does create a corresponding cavity in the kinase active site, but that this cavity does not expose a preexisting pocket or allow for the binding of significantly larger inhibitor analogs with enhanced affinity, as has been observed in the protein kinase family.

4.6 Discussion

We have explored the role of the gatekeeper residue in PI3-Ks by a convergent engineering approach that combines mutagenesis of the target residue with design of inhibitor analogs to complement this mutation. This analysis suggests that mutation of the gatekeeper residue in lipid kinases can create a non-natural pocket, but that this mutation does not expose the deeper pocket that is found in protein kinases. This difference may reflect the different way that protein and lipid kinases utilize their primary sequence to construct the innermost wall of the ATP binding pocket. Crystal structures of protein kinases reveal that residues from β-strand 5, which include the gatekeeper, from the deepest face of the ATP binding pocket, and that most of the contacts that this face makes with adenine involve the side chain of the gatekeeper residue directly. By comparison, in the crystal structure of p110γ, the gatekeeper is shifted upward and away from the N6 of adenine by ~ 2 Å. To help fill this space, the side chain of Tyr 867 from β-strand 6 (which is otherwise positioned in a second sphere of residues that do not contact ATP directly) infiltrates the ATP binding pocket to make a direct contact with adenine near N6. The analogous residue in protein kinases (corresponding to Leu 325 in Hck) is positioned within a second sphere that is obstructed from accessing ATP by the gatekeeper. Thus, it appears that in lipid kinases two residues (Tyr 867 and Ile 879) collaborate to fill the space that is otherwise occupied by a single residue in protein kinases. Unfortunately, we have found that mutation of Tyr 836 in p110α (which corresponds to Tyr 867 in p110γ) to any other amino acid (glycine, alanine, threonine, aspartic acid, leucine, methionine, or histidine) results in a complete loss of catalytic activity, indicating that this region of the protein is not amenable to structural modification (Z.A.K. and K.M.S., unpublished observations). These results, as well as the nearly total conservation of Tyr 867 within the PI3-K family (Figure 4.4), suggest that a different set of residues in lipid kinases are likely responsible for controlling sensitivity to small

molecule inhibitors. Ultimately, the identification of rules guiding inhibitor sensitivity for this important family of enzymes will require the discovery of new structural classes of PI3-K inhibitors and the broad characterization of their specificity against individual PI3-K isoforms, a process that is currently underway in our laboratory [31] and others [32].

4.7 Experimental Procedures

4.7.1. Protein expression

Mutations were introduced by Quikchange (Stratagene), and confirmed using standard dideoxy-based sequencing. Myc-tagged p110α was expressed by transient transfection of cos-1 cells. Cells were lysed in lysis buffer (50 mM Tris (pH 7.4), 300 mM NaCl, 5mM EDTA, 0.02% NaN_3, 1% Triton X-100, protease inhibitors (protease inhibitor cocktail tablets (Roche); sodium orthovanadate (8 mM); PMSF (1 mM)), and 8 mM DTT. The kinase was immunoprecipitated using a Protein-G-9E10 antibody complex, and washed twice with buffer A (PBS, 1 mM EDTA, 1% Triton X-100), twice with buffer B (100 mM Tris (pH 7.4), 500 Mm LiCl, 1 mM EDTA), twice with buffer C (50 mM Tris (pH 7.4), 100 mM NaCl), and once with PBS. In control experiments, no differences in inhibitor sensitivity were observed between wild type p110α protein that was obtained from transfected cos-1 cells, Sf9 cells using a baculovirus system, or commercially available recombinant protein (Jena Bioscience).

For SDS-PAGE and Western blot analyses, protein concentrations in cell lysates were determined using a Bradford assay. Proteins were loaded onto a Tris-glycine gel (8-16% gradient; Gradipore) and separated by SDS-PAGE before being transferred onto a nitrocellulose membrane. The blot was treated with blocking reagent (5% dry milk in TBST) for 1h, then primary antibody (9E10 (anti-Myc; Santa Cruz Biotech), 1:500 in TBST) overnight at 4 °C. The blot was then rinsed (5 min each) with deionized water (1 x

20 mL) and TBST (3 x 20 mL) before treatment with secondary anti-mouse-HRP antibody (1:1000 in TBST) for 30 min at rt.

4.7.2 PI3-kinase enzymatic assay

The PI3-K assay was performed essentially as described.[33, 34] Briefly, a mixture of kinase, inhibitor, buffer (25 mM HEPES (pH 7.4), 10 mM $MgCl_2$), and freshly sonicated phosphatidylinositol (200 μg/mL) was prepared at 4 °C, and aliquotted into eppendorf tubes. The tubes were allowed to warm to rt over 5 min, and the enzymatic reaction was initiated with the addition of ATP (10 μCi γ-^{32}P-ATP; final [ATP] = 20 nM). Reactions were incubated for 20 min at rt, and quenched by addition of 1M HCl (105 μL) followed by 1:1 MeOH:$CHCl_3$ (160 μL). The resulting biphasic mixture was vortexed (ca. 5 s), briefly centrifuged (ca. 5 s), and the organic phase (~100 μL) was transferred to a new tube using a gel-loading tip pre-coated with $CHCl_3$. This extract was spotted on TCL plates (silica gel 60 F254, 250 μm) and developed for 3-4 h using 65:35 1-propanol:2M AcOH as eluent. The TLC plates were then air-dried (ca. 45 min), and the reaction products quantitated using a phosphorimager (Molecular Dynamics). For each compound, kinase activity was measured at 15 inhibitor concentrations representing two-fold dilutions from the highest concentration tested (usually 400 μM). For compounds showing significant activity, IC_{50} value determinations were repeated (2-5 times) and the value reported is the average of these independent measurements. Preincubation of the enzyme with cold ATP (1 μM, 10 min) was sometimes used to suppress the observation of radiolabeled impurities that were kinase-independent (data not shown). In control experiments, no difference was observed in inhibitor sensitivity between performing the assay in the absence or presence (1 μM) of cold ATP.

4.7.3 General chemical synthesis

All reactions were performed under argon in oven- or flame-dried glassware fitted with rubber septa, and were stirred magnetically. Thin layer chromatography was performed on Merck pre-coated silica gel F-254 plates (0.25 mm). Flash column chromatography was performed using Merck silica gel 60 (230-400 mesh).[35] Proton NMR spectra were recorded at 400 MHz and are reported in δ (ppm) as s (singlet), d (doublet), t (triplet), q (quartet), m (multiplet) or br (broad), and are referenced to the residual solvent signal: $CDCl_3$ (7.26) or C_6D_6 (7.15). Carbon NMR spectra were recorded at 100 MHz and are reported in δ (ppm), and are referenced to the solvent signal: $CDCl_3$ (77.0), C_6D_6 (128.0). Infrared spectra were recorded on a Nicolet Impact 400 spectrometer using thin films of sample and resonances are reported in wavenumbers (cm^{-1}). Mass spectra were recorded on a VG-70S mass spectrometer and are reported in units of mass/charge (*m/z*). Unless otherwise noted, all materials were obtained from commercial sources and used without further purification. In experiments involving air- or moisture-sensitive compounds, solvents and reagents were either distilled or purchased as anhydrous grade material. Dichloromethylenemorpholin-4-ium chloride[36, 37] was prepared according to literature procedures.

4.7.4 General procedure for the preparation of alcohols 1c-g

A round bottom flask charged with salicylaldehyde and THF was cooled to –78 ºC. To this mixture was added the appropriate Grignard reagent (5-10 equiv.) by syringe over 10 min, and the resulting mixture was allowed to stir at –78 ºC for 10 min. The stirred reaction mixture was allowed to warm to rt overnight. In air, this mixture was slowly added to a 0 ºC saturated NH_4Cl solution. The aqueous phase was extracted with ether and the combined organic phases were dried over Na_2SO_4, filtered, and

concentrated to give a crude oil. Further purification and characterization of each derivative is described below.

4.7.4.1. 2-(1-Hydroxybutyl)phenol (1c).

Synthesis was performed using the general procedure described above using 1.15 g salicylaldehyde (9.4 mmol), 94 mL THF, 94 mmol propylmagnesium chloride (47 mL of 2.0 M solution in ether), saturated NH_4Cl solution (75 mL), and ether (3 x 40 mL). The crude oil was purified by flash column chromatography (SiO_2, 10% EtOAc-hexanes) to give a clear, pale yellow oil (1.226 g, 7.4 mmol, 79%) ^1H NMR: ($CDCl_3$) δ 8.16 (s, 1H), 7.12 (t, $J = 8$, 1H), 6.91 (d, $J = 8$, 1H), 6.82 (m, 2H), 4.76 (t, $J = 7$, 1H), 3.35 (s, 1H), 1.83 (m, 1H), 1.74 (m, 1H), 1.43 (m, 1H), 1.30 (m, 1H), 0.91 (t, $J = 8$, 3H). $^{13}C\{^1H\}$ NMR: ($CDCl_3$) δ 155.2, 128.7, 127.8, 127.2, 119.7, 116.9, 75.5, 39.3, 18.9, 13.8. IR: 3321. HRMS: (EI) calcd for $C_{10}H_{14}O_2$ (M^+) 166.0994; found 166.0995. Anal. Calcd for $C_{10}H_{14}O_2$: C, 72.26; H, 8.49. Found: C, 72.19; H, 8.41.

4.7.4.2. 2-(1-Hydroxypentyl)phenol (1d).

Synthesis was performed using the general procedure described above using 2.29 g salicylaldehyde, 100 mL THF, 94 mmol of butylmagnesium chloride (47 mL of 2.0 M solution in THF), saturated NH_4Cl solution (75 mL), and ether (4 x 50 mL). The crude oil was purified by flash column chromatography (SiO_2, 10% EtOAc-hexanes) to give a clear colorless oil (3.37 g, 18.7 mmol, 99%) ^1H NMR: ($CDCl_3$) δ 8.32 (s, 1H), 7.12 (m, 1H), 6.93 (m, 1H), 6.82 (m, 2H), 4.74 (t, $J = 7$, 1H), 3.84 (br s, 1H), 1.90-1.71 (m, 2H), 1.44-1.22 (m, 4H), 0.90 (t, $J = 7$, 3H). Lit. [38] δ 7.93 (s, 1H), 7.4-6.7 (m, 4H), 4.82 (t, $J = 5.6$, 1H), 2.53 (br 1H), 2.0-1.1 (m, 6H), 0.90 (t, $J = 5.9$, 3H). $^{13}C\{^1H\}$ NMR: ($CDCl_3$) δ 155.2, 128.7, 128.2, 127.0, 119.8, 117.0, 73.8, 46.0, 24.5, 23.1, 22.0. IR: 3357. HRMS:

(EI) 180.1150 calcd for $C_{11}H_{16}O_2$ (M^+); found 180.1144. Lit. [38] 180.1150 calcd for $C_{11}H_{16}O_2$ (M^+); found 180.1119.

4.7.4.3. 2-(1-Hydroxy-3-methylbutyl)phenol (1e).

Synthesis was performed using the general procedure described above using 1.15 g salicylaldehyde, 95 mL THF, 94 mmol of isobutylmagnesium bromide (47 mL of 2.0 M solution), saturated NH_4Cl (75 mL), and ether (3 x 50 mL). The crude oil was purified by flash column chromatography (SiO_2, 10% EtOAc-hexanes) to give a clear, pale yellow oil (1.66 g, 9.2 mmol, 98%). ^1H NMR: ($CDCl_3$) δ 8.09 (s, 1H), 7.12 (m, 1H), 6.91 (m, 1H), 6.81 (m, 2H), 4.84 (br d, J = 3, 1H), 3.22 (s, 1H), 1.81 (m, 1H), 1.70 (m, 1H), 1.56 (m, 1H), 0.93 (m, 6H). Lit.[39] (CCl_4:C_6D_6 7:1) δ 7.76 (s, 1H), 6.50-7.20 (m, 4H), 4.50-4.90 (m, 1H), 2.55 (s, 1H), 1.00-2.00 (m 3H), 0.75-1.00 (m, 6H). $^{13}C\{^1H\}$ NMR: ($CDCl_3$) δ 155.2, 128.6, 128.1, 126.9, 119.8, 116.9, 73.7, 45.9, 24.5, 23.0, 22.0. IR: 3341. Lit.[39] 3384 (s,b), 1596 (m), 1384 (m), 1372 (m), 760 (s). HRMS: (EI) 180.1150 calcd for $C_{11}H_{16}O_2$ (M^+); found 180.1152.

4.7.4.4. 2-(1-Hydroxyhexyl)phenol (1f).

Synthesis was performed using the general procedure described above using 2.29 g salicylaldehyde, 100 mL THF, 80 mmol of pentylmagnesium bromide (40 mL of 2.0 M solution), saturated NH_4Cl (75 mL), and ether (3 x 50 mL). The crude oil was purified by flash column chromatography (SiO_2, 10% EtOAc-hexanes) to give a clear, pale yellow oil (3.6 g, 18.7 mmol, 99%). ^1H NMR: ($CDCl_3$) δ 8.44 (s, 1H), 7.12 (m, 1H), 6.96 (m, 1H), 6.83 (m, 2H), 4.76 (br m, 1H), 4.16 (br s, 1H), 1.91-1.72 (m, 2H), 1.48-1.38 (m, 1H), 1.30 (m, 5H), 0.91 (t, J = 7, 3H). $^{13}C\{^1H\}$ NMR: ($CDCl_3$) δ 155.5, 128.5, 127.9, 127.1, 119.9, 116.8, 75.5, 37.1, 31.5, 25.3, 22.5, 13.9. IR: 3348. HRMS: (EI) 194.1306

calcd for $C_{12}H_{18}O_2$ (M^+); found 194.1302. Combustion analysis was not obtained for this compound due to its similarity to **1c-g**.

4.7.4.5. 2-(1-Hydroxy-2-phenylethyl)phenol (1g).

Synthesis was performed using the general procedure described above using 1.15 g salicylaldehyde, 95 mL THF, 94 mmol of benzylmagnesium bromide (47 mL of 2.0 M solution in THF), saturated NH_4Cl (75 mL), and ether (3 x 50 mL). The crude oil was purified by flash column chromatography (SiO_2, 50% EtOAc-hexanes) to give a colorless solid (1.42 g, 6.6 mmol, 75%). ^1H NMR: ($CDCl_3$) δ 8.01 (s, 1H), 7.34-7.14 (m, 5H), 6.93-6.79 (m, 4H), 4.98 (dt, *J* = 3, *J* = 7, 1H), 3.10 (d, *J* = 7, 2H), 2.81 (d, *J* = 3, 1H). Lit.[40] (partial) δ 5.02 (t, *J* = 7, 1H), 3.11 (d, *J* = 7, 2H). $^{13}C\{^1H\}$ NMR: ($CDCl_3$) δ 151.6, 133.6, 125.8, 125.3, 125.0, 123.5, 123.3, 122.8, 116.1, 113.5, 73.0, 40.4. IR: 3327. HRMS: (EI) 214.0993 calcd for $C_{14}H_{14}O_2$ (M^+); found 214.1003.

4.7.5. General procedure for the preparation of ketones 2c-g.

A round bottom flask was charged with the appropriate diol **1**, MnO_2 and CH_2Cl_2, and stirred for 7 h at rt. The heterogeneous reaction mixture was filtered through a pad of Celite, and the solids were washed with 500 mL CH_2Cl_2. The filtrate was concentrated *in vacuo* to give a crude oil. The crude oil was purified by flash column chromatography (SiO_2, 10% EtOAc-hexanes) to give a colorless oil. Characterization of each derivative is described below.

4.7.5.1. 1-(2-Hydroxyphenyl)butan-1-one (2c).

Synthesis was performed using the general procedure described above using **1c** (2.5 g, 15.1 mmol), MnO_2 (11.5 g, 132 mmol) and CH_2Cl_2 (140 mL). Compound **2c** was

isolated as a colorless oil (1.13 g, 6.9 mmol, 46%). ^{1}H NMR: (CDCl$_3$) δ 12.38 (s, 1H), 7.68 (dd, *J* = 1, *J* = 7, 1H), 7.36 (dt, *J* = 2, *J* = 7, 1H), 6.90 (dd, *J* = 1, *J* = 7, 1H), 6.80 (dt, *J* = 2, *J* = 7, 1H), 2.87 (t, (dt, *J* = 8, 2H), 1.70 (sextet, *J* = 8, 2H), 0.96 (t, *J* = 8, 3H). Lit.[41] δ 12.40 (s, 1H), 7.82-6.80 (m, 4H), 2.96 (t, *J* = 7.4 Hz, 2H), 1.78 (sextet, *J* = 7.4 Hz, 2H), 1.02 (t, *J* = 7.4 Hz, 3H). ^{13}C{^{1}H} NMR: (CDCl$_3$) δ 206.7, 162.5, 136.1, 129.9, 119.3, 118.8, 118.4, 40.1, 17.8, 13.7. Lit.[41] □ 206.79, 162.49, 136.17, 130.00, 119.36, 118.82, 118.48, 40.17, 17.90, 13.38. IR: 1641, 1614, 1581, 1488, 1447, 1265, 1202, 1158, 754. Lit.[41] 1640, 1448, 1226, 1203. HRMS: (EI) 164.0837 calcd for $C_{10}H_{12}O_2$ (M$^+$); found 164.0840. Lit.[41] 164. Anal. Calcd for $C_{10}H_{12}O_2$: C, 73.15; H, 7.37. Found: C, 73.22; H, 7.45.

4.7.5.2. 1-(2-Hydroxyphenyl)pentan-1-one (2d).

Synthesis was performed using the general procedure described above using **1d** (2.0 g, 11.1 mmol), MnO$_2$ (9.7 g, 110 mmol) and CH$_2$Cl$_2$ (100 mL). Compound **2d** was isolated as a colorless oil (796 mg, 4.47 mmol, 40%). ^{1}H NMR: (CDCl$_3$) □ 12.38 (s, 1H), 7.71 (dd, *J* = 1, *J* = 8, 1H), 7.41 (m, 1H), 6.92 (dd, *J* = 1, *J* = 8, 1H), 6.84 (m, 1H), 2.93 (t, *J* = 7, 2H), 1.68 (m, 2H), 1.38 (m, 2H), 0.93 (t, *J* = 7, 3H). ^{13}C{^{1}H} NMR: (CDCl$_3$) □ 208.7, 162.3, 135.9, 129.8, 119.0, 118.5, 118.2, 37.8, 26.3, 22.1, 13.6. IR: 1640, 1582, 1487, 1446, 1353, 1249, 119, 1157, 753. HRMS: (EI) 178.0994 calcd for $C_{11}H_{14}O_2$ (M$^+$); found 178.0996. Combustion analysis was not obtained for this compound due to its similarity to **2c-g**.

4.7.5.3. 1-(2-Hydroxyphenyl)-3-methylbutan-1-one (2e).

Synthesis was performed using the general procedure described above using **1e** (2.0 g, 11.1 mmol), MnO$_2$ (10.0 g, 115 mmol) and CH$_2$Cl$_2$ (120 mL). Compound **2e** was

7.86 (dd, $J = 2$, $J = 8$, 1H), 7.45 (m, 1H), 7.36 (m, 2H), 7.31 (m, 3H), 6.99 (m, 1H), 6.88 (m, 1H), 4.29 (s, 2H). Lit.[42] δ 12.1 (s, 1H), 7.73-6.91 (m, 9H), 4.2 (s, 2H). $^{13}C\{^1H\}$ NMR: ($CDCl_3$) δ 203.7, 162.7, 136.4, 133.8, 130.3, 129.3, 128.6, 127.0, 118.9, 118.9, 118.5, 44.9. Lit.[42] δ 203.7, 162.7, 136.3-118.4 (11C), 44.9. IR: 1638, 1487, 1446, 1344, 1275, 1156, 754. Lit.[42] 1680. HRMS: (EI) 212.0837 calcd for $C_{14}H_{12}O_2$ (M^+); found 212.0835. Lit.[42] 213.

4.7.6. General Procedure for the Preparation of Compounds 3a-i.

A round bottom flask was charged with the appropriate 2´-hydroxyketophenol (**2**), CH_2Cl_2, and cooled to –78 ºC. $TiCl_4$ (1.0 M CH_2Cl_2 solution) was added dropwise by syringe and was stirred for 1 h at –78 ºC to produce a redish-brown-colored solution. Diisopropylethylamine was added and the reaction was stirred at –78 ºC for 1 h. 4-Dichloromethylenemorpholin-4-ium chloride was added and the reaction mixture was stirred at –78 ºC then warmed to 0 ºC for 2 h, then allowed to warm to rt and stirred overnight. The reaction was cooled to 0 ºC, and Et_3N and MeOH were added. The stirred reaction mixture was allowed to warm to rt over 3 h. The volatile materials were removed *in vacuo* to give a crude red-colored residue that was washed with $NaHCO_3$ (satd, 30 mL), then the solids were extracted with CH_2Cl_2 (3 x 15 mL). The combined organics were dried over $MgSO_4$, filtered, and concentrated *in vacuo* to give a crude oil which was purified by flash column chromatography, and lyophilized from C_6H_6 to give a flocculent white powder. Characterization of each derivative is described below.

4.7.6.1. 2-Morpholin-4-yl-chromen-4-one (LY292223) (3a).

Synthesis was performed using the general procedure described above using 2´-hydroxyacetophenone (565 mg, 4.15 mmol), CH_2Cl_2 (11 mL), $TiCl_4$ (6.5 mL of a 1.0 M

UST LIBRARY

isolated as a colorless oil (650 mg, 3.65 mmol, 33%). ^{1}H NMR: (CDCl$_3$) δ 12.45 (s, 1H), 7.69 (dd, *J* = 2, *J* = 8, 1H), 7.38 (dt, *J* = 2, *J* = 8, 1H), 6.91 (dd, *J* = 2, *J* = 8, 1H), 6.82 (dt, *J* = 2, *J* = 8, 1H), 2.77 (d, *J* = 7, 2H), 2.24 (nonet, *J* = 6, 1H), 0.96 (d, *J* = 6, 6H). Lit.[41] δ 12.47 (s, 1H), 7.81-6.82 (m, 4H), 2.85 (d, *J* = 6.9 Hz, 2H), 1.78 (nonet, *J* = 6.7 Hz, 1H), 1.02 (d, *J* = 6.6 Hz, 6H). ^{13}C{^{1}H} NMR: (CDCl$_3$) □ 206.4, 162.5, 136.0, 130.0, 119.5, 118.6, 118.3, 46.9, 25.3, 22.5. Lit.[41] δ 207.2, 163.1, 136.7, 130.6, 120.1, 119.3, 119.0, 47.6, 26.0, 23.2. IR: 1638, 1488, 1447, 1306, 1202, 1158, 753. Lit.[41] 1639, 1488, 1447, 1158. HRMS: (EI) 178.0994 calcd for $C_{11}H_{14}O_2$ (M$^+$); found 178.0999. Lit.[41] 178.

4.7.5.4. 1-(2-Hydroxyphenyl)hexan-1-one (2f).

Synthesis was performed using the general procedure described above using **1f** (2.0 g, 10.3 mmol), MnO$_2$ (8.0 g, 92 mmol) and CH$_2$Cl$_2$ (110 mL). Compound **2f** was isolated as a colorless oil (900 mg, 4.68 mmol, 46%). ^{1}H NMR: (CDCl$_3$) δ 12.38 (s, 1H), 7.70 (dd, *J* = 2, *J* = 8, 1H), 7.40 (m, 1H), 6.92 (m, 1H), 6.83 (m, 1H), 2.92 (t, *J* = 7, 2H), 1.70 (m, 2H), 1.33 (m, 4H), 0.88 (t, *J* = 7, 3H). Lit.[41] δ 12.40 (s, 1H), 7.82-6.80 (m, 4H), 2.98 (t, *J* = 7.6 Hz, 2H), 1.84-1.25 (m, 6H), 0.91 (t, *J* = 6.7 Hz, 3H). ^{13}C{^{1}H} NMR: (CDCl$_3$) δ 206.8, 162.4, 136.0, 129.9, 119.2, 118.7, 118.3, 38.1, 31.3, 24.0, 22.4, 13.8. Lit.[41] δ 207.18, 162.70, 136.36, 130.18, 119.53, 119.01, 118.70, 38.49, 31.64, 24.41, 22.67, 14.11. IR: 3426, 1639, 1487, 1447, 1197, 1156, 752. HRMS: (EI) 192.1150 calcd for $C_{12}H_{16}O_2$ (M$^+$); found 192.1145. Lit.[41] 192.

4.7.5.5. 1-(2-Hydroxyphenyl)-2-phenylethanone (2g).

Synthesis was performed using the general procedure described above using **1g** (1.5 g, 7.0 mmol), MnO$_2$ (6.0 g, 69 mmol) and CH$_2$Cl$_2$ (80 mL). Compound **2g** was isolated as a colorless oil (624 mg, 2.94 mmol, 42%). ^{1}H NMR: (CDCl$_3$) δ 12.27 (s, 1H),

CH_2Cl_2 solution, 6.5 mmol), diisopropylethylamine (2.7 mL, 15.5 mmol), 4-dichloromethylenemorpholin-4-ium chloride (1.2 g, 5.0 mmol), Et_3N (1.0 mL), and MeOH (5 mL). Column chromatography: SiO_2, 40% EtOAc-hexanes + 1% Et_3N to 90% EtOAc-MeOH + 1% Et_3N gradient. (344 mg, 1.5 mmol, 36%). ^1H NMR: ($CDCl_3$) δ 7.95, 7.35, 7.14, 7.08, 5.27 (s, 1H), 3.63 (t, *J* = 5, 4H), 3.30 (t, *J* = 5, 4H). Lit.[43] δ 8.15 (m, 1H), 7.56 (m, 1H), 7.31 (m, 2H), 5.49 (s, 1H), 3.83 (t, J = 4.7 Hz, 4H), 3.50 (t, J = 4.7 Hz, 4H). $^{13}C\{^1H\}$ NMR: ($CDCl_3$) δ 176.8, 162.5, 153.5, 132.2, 125.2, 124.6, 122.8, 116.3, 87.0, 65.8, 44.5. Lit.[43] δ 176.9, 162.4, 153.5, 132.1, 125.3, 124.6, 122.7, 116.1, 87.2, 65.8, 44.4. IR: 1616, 1555, 1418, 1300, 1251, 1117, 985, 766. Lit.[43] 1622, 1559. HRMS: (EI) 231.0895 calcd for $C_{13}H_{13}NO_3$ (M^+); found 231.0887. Anal. Calcd for $C_{13}H_{13}NO_3$: C, 67.52; H, 5.66; N, 6.00. Found: C, 67.59; H, 5.69; N, 5.97.

4.7.6.2. 3-Methyl-2-morpholin-4-yl-chromen-4-one (3b).

Synthesis was performed using the general procedure described above using 200 mg 2′-hydroxypropiophenone, 3.5 mL CH_2Cl_2, 2.0 mmol $TiCl_4$, 600 mg *i*-Pr_2EtN, 308 mg dichloromethylenemorpholin-4-ium chloride, 0.4 mL Et_3N and 2 mL MeOH. Column chromatography: SiO_2, 50% EtOAc-hexanes + 1% Et_3N. (77 mg, 0.31 mmol, 24%). ^1H NMR: (C_6D_6) δ 8.52 (d, *J* = 8, 1H), 7.07 (m, 1H), 6.93 (m, 2H), 3.31 (t, *J* = 5, 4H), 2.70 (t, *J* = 5, 4H), 2.01 (s, 3H). $^{13}C\{^1H\}$ NMR: (C_6D_6) δ 177.9, 161.5, 154.2, 132.0, 126.4, 124.6, 123.4, 116.7, 103.6, 66.5, 48.3, 11.0. IR: 1612, 1556, 1410, 1114. HRMS: (EI) 245.1051 calcd for $C_{14}H_{15}NO_3$ (M^+); found 245.1050. Combustion analysis was not obtained for this compound due to its similarity to **3a-i**.

4.7.6.3. 3-Ethyl-2-morpholin-4-yl-chromen-4-one (3c).

USF Library

Synthesis was performed using the general procedure described above using 407 mg **2c**, 30 mL CH_2Cl_2, 3.71 mmol $TiCl_4$, 3.2 g *i*-Pr_2EtN, 759 mg dichloromethylenemorpholin-4-ium chloride, 0.6 mL Et_3N and 3 mL MeOH. Column chromatography: SiO_2, 30% EtOAc-hexanes + 1% Et_3N. (364 mg, 1.40 mmol, 57%). ^1H NMR: (C_6D_6) □ 8.29 (d, *J* = 8, 1H), 7.12 (m, 1H), 6.95 (m, 2H), 3.40 (t, *J* = 5, 4H), 2.83 (t, *J* = 5, 4H), 2.48 (q, *J* = 7, 2H), 1.19 (t, *J* = 7, 3H). $^{13}C\{^1H\}$ NMR: (C_6D_6) □177.8, 161.8, 154.2, 132.3, 126.0, 124.5, 123.5, 116.9, 110.4, 66.6, 49.3, 18.6, 13.3. IR: 1615, 1556, 1467, 1401, 1361, 1264, 1223, 1116, 759. HRMS: (EI) 259.1208 calcd for $C_{15}H_{17}NO_3$ (M^+); found 259.1199. Anal. Calcd for $C_{15}H_{17}NO_3$: C, 69.48; H, 6.61; N, 5.40. Found: C, 69.43; H, 6.60; N, 5.36.

4.7.6.4. 2-Morpholin-4-yl-3-propylchromen-4-one (3d).

Synthesis was performed using the general procedure described above using 68 mg **2d**, 5 mL CH_2Cl_2, 0.57 mmol $TiCl_4$, 490 mg *i*-Pr_2EtN, 117 mg dichloromethylenemorpholin-4-ium chloride, 0.1 mL Et_3N and 0.5 mL MeOH. Column chromatography: SiO_2, 20% EtOAc-hexanes + 1% Et_3N. (58 mg, 0.21 mmol, 56%). ^1H NMR: (C_6D_6) δ 8.46 (d, *J* = 6, 1H), 7.08 (m, 1H), 6.94 (m, 2H), 3.38 (t, *J* = 5, 4H), 2.77 (t, *J* = 5, 4H), 2.57 (t, *J* = 8, 2H), 1.77 (tq, *J* = 8, 2H), 0.99 (t, *J* = 8, 3H). $^{13}C\{^1H\}$ NMR: (C_6D_6) δ 178.2, 162.0, 154.5, 132.2, 126.5, 124.6, 123.6, 116.8, 110.2, 66.6, 49.4, 27.3, 22.0, 14.7. IR: 1616, 1556, 1467, 1400, 1115, 759. HRMS: (EI) 273.1365 calcd for $C_{16}H_{19}NO_3$ (M^+); found 273.1369. Combustion analysis was not obtained for this compound due to its similarity to **3a-i**.

4.7.6.5. 3-Isopropyl-2-morpholin-4-yl-chromen-4-one (3e).

Synthesis was performed using the general procedure described above using 150 mg **2e**, 10 mL CH_2Cl_2, 1.24 mmol $TiCl_4$, 1.06 g *i*-Pr_2EtN, 253 mg dichloromethylenemorpholin-4-ium chloride, 0.2 mL Et_3N and 1.0 mL MeOH. Column chromatography: SiO_2, 20% EtOAc-hexanes + 1% Et_3N. (138 mg, 0.50 mmol, 60%). ^1H NMR: (C_6D_6) δ 8.36 (d, *J* = 8, 1H), 7.01 (m, 1H), 6.89 (m, 2H), 3.47 (t, *J* = 5, 4H), 2.96 (m, 1H), 2.72 (t, *J* = 5, 4H), 1.54 (d, *J* = 7, 6H). $^{13}C\{^1H\}$ NMR: (C_6D_6) δ 178.2, 162.1, 154.4, 132.2, 126.3, 124.5, 124.4, 116.7, 115.2, 66.4, 50.1, 27.7, 20.5. IR: 1616, 1557, 1466, 1390, 1217, 1115, 759. HRMS: (EI) 273.1364 calcd for $C_{16}H_{19}NO_3$ (M^+); found 273.1364. Combustion analysis was not obtained for this compound due to its similarity to **3a-i**.

4.7.6.6. 3-Butyl-2-morpholin-4-yl-chromen-4-one (3f).

Synthesis was performed using the general procedure described above using 375 mg **2f**, 20 mL CH_2Cl_2, 2.92 mmol $TiCl_4$, 2.51 g *i*-Pr_2EtN, 597 mg dichloromethylenemorpholin-4-ium chloride, 0.4 mL Et_3N and 2.0 mL MeOH. Column chromatography: SiO_2, 20% EtOAc-hexanes + 1% Et_3N. (296 mg, 1.03 mmol, 53%). ^1H NMR: (C_6D_6) δ 8.48 (d, *J* = 8, 1H), 7.07 (m, 1H), 6.93 (m, 2H), 3.39 (t, *J* = 5, 4H), 2.77 (t, *J* = 5, 4H), 2.61 (t, *J* = 8, 2H), 1.75 (p, *J* = 8, 2H), 1.41 (s, *J* = 8, 2H), 0.95 (t, *J* = 8, 3H). $^{13}C\{^1H\}$ NMR: (C_6D_6) δ 178.1, 162.0, 154.5, 132.2, 126.5, 124.6, 123.7, 116.8, 110.4, 66.6, 49.4, 30.8, 24.8, 23.3, 14.2. IR: 1615, 1558, 1466, 1398, 1223, 1116, 759. HRMS: (EI) 287.1521 calcd for $C_{17}H_{21}NO_3$ (M^+); found 287.1520. Combustion analysis was not obtained for this compound due to its similarity to **3a-i**.

4.7.6.7. 2-Morpholin-4-yl-3-phenylchromen-4-one (3g).

Synthesis was performed using the general procedure described above using 143 mg **2g**, 5 mL CH_2Cl_2, 1.01 mmol $TiCl_4$, 870 mg *i*-Pr_2EtN, 206 mg dichloromethylenemorpholin-4-ium chloride, 0.1 mL Et_3N and 0.5 mL MeOH. Column chromatography: SiO_2, 20% EtOAc-hexanes + 1% Et_3N. (144 mg, 0.47 mmol, 70%). ^1H NMR: (C_6D_6) δ 8.39 (d, *J* = 8, 1H), 7.47 (m, 2H), 7.20 (m, 2H), 7.11-7.02 (m, 2H), 6.96-6.90 (m, 2H), 3.11 (t, *J* = 5, 4H), 2.68 (t, *J* = 5, 4H). $^{13}C\{^1H\}$ NMR: (C_6D_6) δ 175.5, 160.9, 153.6, 134.5, 132.2, 131.3, 128.2, 126.9, 126.6, 124.7, 124.0, 116.6, 105.2, 66.1, 47.8. IR: 1614, 1550, 1417, 1340, 1232, 1116, 760. HRMS: (EI) 307.1208 calcd for $C_{19}H_{17}NO_3$ (M^+); found 307.1206. Combustion analysis was not obtained for this compound due to its similarity to **3a-i**.

4.7.6.8. 3-Benzyl-2-morpholin-4-yl-chromen-4-one (3h).

Synthesis was performed using the general procedure described above using 1.0 g 2′-hydroxy-3-phenylpropiophenone, 12 mL CH_2Cl_2, 6.63 mmol $TiCl_4$, 2.7 mL *i*-Pr_2EtN, 1.2 g dichloromethylenemorpholin-4-ium chloride, 0.2 mL Et_3N and 1.2 mL MeOH. Column chromatography: SiO_2, 35% EtOAc-hexanes + 1% Et_3N. (552 mg, 1.80 mmol, 41%). ^1H NMR: (C_6D_6) δ 8.18 (d, *J* = 8, 1H), 7.57 (t, *J* = 8, 1H), 7.34 (m, 2H), 7.19 (m, 5H), 3.94 (s, 2H), 3.67 (t, *J* = 5, 4H), 3.28 (t, *J* = 5, 4H). $^{13}C\{^1H\}$ NMR: (C_6D_6) δ 178.5, 162.8, 153.9, 140.0, 132.6, 128.4, 127.9, 126.1, 125.9, 124.7, 122.6, 116.7, 106.5, 66.6, 48.8, 30.5. IR: 1615, 1555, 1467, 1402, 1236, 1114, 759. HRMS: (EI) 321.1365 calcd for $C_{20}H_{19}NO_3$ (M^+); found 321.1368. Combustion analysis was not obtained for this compound due to its similarity to **3a-i**.

4.7.6.9. 3-Decyl-2-morpholin-4-yl-chromen-4-one (3i).

Synthesis was performed using the general procedure described above for 102 mg 2′-hydroxydodecanophenone, 3.0 mL CH_2Cl_2, 0.551 mmol $TiCl_4$, 473 mg *i*-Pr_2EtN, 113 mg dichloromethylenemorpholin-4-ium chloride, 0.06 mL Et_3N and 0.3 mL MeOH. Column chromatography: SiO_2, 20% EtOAc-hexanes + 1% Et_3N. (37 mg, 0.098 mmol, 27%). ^1H NMR: (C_6D_6) δ 8.50 (d, *J* = 8, 1H), 7.07 (m, 1H), 6.93 (m, 2H), 3.42, *J* = 5, 4H), 2.80 (t, *J* = 5, 4H), 2.66 (t, *J* = 8, 2H), 1.82 (m, 2H), 1.48-1.20 (m, 14H), 0.90 (t, *J* = 7, 3H). $^{13}C\{^1H\}$ NMR: (C_6D_6) δ 178.2, 162.0, 154.5, 132.2, 126.5, 124.6, 123.7, 116.8, 110.5, 66.6, 49.4, 32.3, 30.4, 30.11, 30.09, 29.9, 29.8, 28.7, 25.2, 23.1, 14.3. IR: 1615, 1561, 1466, 1395, 1117. HRMS: (EI) 371.2460 calcd for $C_{23}H_{33}NO_3$ (M^+); found 371.2458. Combustion analysis was not obtained for this compound due to its similarity to **3a-i**.

4.7.7 Analysis of yeast expressing PI3-K mutant alleles

The VPS34 *S. cerevisiae* knockout strain 15149 was obtained from the ATCC. The MEC1/SML1 *S. cerevisiae* knockout strain yBRT7-4b was a gift from David Toczyski (UCSF). Knockout strains were transformed with plasmids (pRS416 CEN URA3) encoding wild-type and mutant VPS34 and MEC1 and transformants were selected on SD –URA media. Cells were streaked onto plates containing SD -URA or the same media supplemented with either 1M NaCl (VPS34) or 0.02% MMS or 60 mM HU (MEC1), grown at 30º C or 37º C for 3 days, and photographed.

4.8 References

1. Blencke, S., Zech, B., Engkvist, O., Greff, Z., Orfi, L., Horvath, Z., Keri, G., Ullrich, A., and Daub, H. (2004). Characterization of a conserved structural determinant controlling protein kinase sensitivity to selective inhibitors. Chem Biol *11*, 691-701.

2. Liu, Y., Bishop, A., Witucki, L., Kraybill, B., Shimizu, E., Tsien, J., Ubersax, J., Blethrow, J., Morgan, D.O., and Shokat, K.M. (1999). Structural basis for selective inhibition of Src family kinases by PP1. Chem Biol *6*, 671-678.

3. Ward, S., Sotsios, Y., Dowden, J., Bruce, I., and Finan, P. (2003). Therapeutic potential of phosphoinositide 3-kinase inhibitors. Chem Biol *10*, 207-213.

4. Ward, S.G., and Finan, P. (2003). Isoform-specific phosphoinositide 3-kinase inhibitors as therapeutic agents. Curr Opin Pharmacol *3*, 426-434.

5. Noble, M.E., Endicott, J.A., and Johnson, L.N. (2004). Protein kinase inhibitors: insights into drug design from structure. Science *303*, 1800-1805.

6. Druker, B.J. (2004). Molecularly targeted therapy: have the floodgates opened? Oncologist *9*, 357-360.

7. Druker, B.J., Tamura, S., Buchdunger, E., Ohno, S., Segal, G.M., Fanning, S., Zimmermann, J., and Lydon, N.B. (1996). Effects of a selective inhibitor of the Abl tyrosine kinase on the growth of Bcr-Abl positive cells. Nat Med *2*, 561-566.

8. Eyers, P.A., Craxton, M., Morrice, N., Cohen, P., and Goedert, M. (1998). Conversion of SB 203580-insensitive MAP kinase family members to drug-sensitive forms by a single amino-acid substitution. Chem Biol *5*, 321-328.

9. Shah, K., Liu, Y., Deirmengian, C., and Shokat, K.M. (1997). Engineering unnatural nucleotide specificity for Rous sarcoma virus tyrosine kinase to uniquely label its direct substrates. Proc Natl Acad Sci U S A *94*, 3565-3570.

10. Blencke, S., Ullrich, A., and Daub, H. (2003). Mutation of threonine 766 in the epidermal growth factor receptor reveals a hotspot for resistance formation against selective tyrosine kinase inhibitors. J Biol Chem *278*, 15435-15440.

11. Gorre, M.E., Mohammed, M., Ellwood, K., Hsu, N., Paquette, R., Rao, P.N., and Sawyers, C.L. (2001). Clinical resistance to STI-571 cancer therapy caused by BCR-ABL gene mutation or amplification. Science *293*, 876-880.

12. Bishop, A.C., Ubersax, J.A., Petsch, D.T., Matheos, D.P., Gray, N.S., Blethrow, J., Shimizu, E., Tsien, J.Z., Schultz, P.G., Rose, M.D., Wood, J.L., Morgan, D.O., and Shokat, K.M. (2000). A chemical switch for inhibitor-sensitive alleles of any protein kinase. Nature *407*, 395-401.

13. Liu, Y., Shah, K., Yang, F., Witucki, L., and Shokat, K.M. (1998). A molecular gate which controls unnatural ATP analogue recognition by the tyrosine kinase v-Src. Bioorg Med Chem *6*, 1219-1226.

14. Shah, N.P., Tran, C., Lee, F.Y., Chen, P., Norris, D., and Sawyers, C.L. (2004). Overriding imatinib resistance with a novel ABL kinase inhibitor. Science *305*, 399-401.

15. La Rosee, P., Corbin, A.S., Stoffregen, E.P., Deininger, M.W., and Druker, B.J. (2002). Activity of the Bcr-Abl kinase inhibitor PD180970 against clinically

relevant Bcr-Abl isoforms that cause resistance to imatinib mesylate (Gleevec, STI571). Cancer Res *62*, 7149-7153.

16. Katso, R., Okkenhaug, K., Ahmadi, K., White, S., Timms, J., and Waterfield, M.D. (2001). Cellular function of phosphoinositide 3-kinases: implications for development, homeostasis, and cancer. Annu Rev Cell Dev Biol *17*, 615-675.

17. Samuels, Y., Wang, Z., Bardelli, A., Silliman, N., Ptak, J., Szabo, S., Yan, H., Gazdar, A., Powell, S.M., Riggins, G.J., Willson, J.K., Markowitz, S., Kinzler, K.W., Vogelstein, B., and Velculescu, V.E. (2004). High frequency of mutations of the PIK3CA gene in human cancers. Science *304*, 554.

18. Leslie, N.R., and Downes, C.P. (2004). PTEN function: how normal cells control it and tumour cells lose it. Biochem J *382*, 1-11.

19. Nagata, Y., Lan, K.H., Zhou, X., Tan, M., Esteva, F.J., Sahin, A.A., Klos, K.S., Li, P., Monia, B.P., Nguyen, N.T., Hortobagyi, G.N., Hung, M.C., and Yu, D. (2004). PTEN activation contributes to tumor inhibition by trastuzumab, and loss of PTEN predicts trastuzumab resistance in patients. Cancer Cell *6*, 117-127.

20. Cappuzzo, F., Magrini, E., Ceresoli, G.L., Bartolini, S., Rossi, E., Ludovini, V., Gregorc, V., Ligorio, C., Cancellieri, A., Damiani, S., Spreafico, A., Paties, C.T., Lombardo, L., Calandri, C., Bellezza, G., Tonato, M., and Crino, L. (2004). Akt phosphorylation and gefitinib efficacy in patients with advanced non-small-cell lung cancer. J Natl Cancer Inst *96*, 1133-1141.

21. Sordella, R., Bell, D.W., Haber, D.A., and Settleman, J. (2004). Gefitinib-sensitizing EGFR mutations in lung cancer activate anti-apoptotic pathways. Science *305*, 1163-1167.

22. Luo, J., Manning, B.D., and Cantley, L.C. (2003). Targeting the PI3K-Akt pathway in human cancer: rationale and promise. Cancer Cell *4*, 257-262.

23. Walker, E.H., Pacold, M.E., Perisic, O., Stephens, L., Hawkins, P.T., Wymann, M.P., and Williams, R.L. (2000). Structural determinants of phosphoinositide 3-kinase inhibition by wortmannin, LY294002, quercetin, myricetin, and staurosporine. Mol Cell *6*, 909-919.

24. Matter, W.F., Brown, R.F., and Vlahos, C.J. (1992). The inhibition of phosphatidylinositol 3-kinase by quercetin and analogs. Biochem Biophys Res Commun *186*, 624-631.

25. Walker, E.H., Perisic, O., Ried, C., Stephens, L., and Williams, R.L. (1999). Structural insights into phosphoinositide 3-kinase catalysis and signalling. Nature *402*, 313-320.

26. Herman, P.K., and Emr, S.D. (1990). Characterization of VPS34, a gene required for vacuolar protein sorting and vacuole segregation in Saccharomyces cerevisiae. Mol Cell Biol *10*, 6742-6754.

27. Kato, R., and Ogawa, H. (1994). An essential gene, ESR1, is required for mitotic cell growth, DNA repair and meiotic recombination in Saccharomyces cerevisiae. Nucleic Acids Res *22*, 3104-3112.

28. Desany, B.A., Alcasabas, A.A., Bachant, J.B., and Elledge, S.J. (1998). Recovery from DNA replicational stress is the essential function of the S-phase checkpoint pathway. Genes Dev *12*, 2956-2970.

29. Pal, D., and Chakrabarti, P. (2000). beta-sheet propensity and its correlation with parameters based on conformation. Acta Crystallogr D Biol Crystallogr *56 (Pt 5)*, 589-594.

30. Vlahos, C.J., Matter, W.F., Hui, K.Y., and Brown, R.F. (1994). A specific inhibitor of phosphatidylinositol 3-kinase, 2-(4-morpholinyl)-8-phenyl-4H-1-benzopyran-4-one (LY294002). J Biol Chem *269*, 5241-5248.

31. Knight, Z.A., Chiang, G.C., Alaimo, P.J., Kenski, D.M., Ho, C.B., Coan, K., Abraham, R.T., and Shokat, K.M. (2004). Isoform-specific phosphoinositide 3-kinase inhibitors from an arylmorpholine scaffold. Bioorg Med Chem *12*, 4749-4759.

32. Sadhu, C., Dick, K., Tino, W.T., and Staunton, D.E. (2003). Selective role of PI3K delta in neutrophil inflammatory responses. Biochem Biophys Res Commun *308*, 764-769.

33. Knight, Z.A., Chiang, G., Alaimo, P.J., Kenski, D.M., Coan, K., Abraham, R., and Shokat, K.M. (2004). Isoform-specific phosphoinositide 3-kinase inhibitors from an arylmorpholine scaffold. Bioorg. Med. Chem. *12*, 4749-4759.

34. Ward, S.G. (2000). Measurement of phosphoinositide 3-kinase activity. Methods in Molec. Biol. *138*, 163-172.

35. Still, W.C., Kahn, M., and Mitra, A. (1978). Rapid chromatographic technique for preparative separations with moderate resolution. J. Org. Chem. *43*, 2923-2925.

36. Morris, J., Wishka, D.G., and Fang, Y. (1992). A novel synthesis of 2-aminochromones via phosgeniminium salts. Journal of Organic Chemistry *57*, 6502-6508.

37. Morris, J., Luke, G.P., and Wishka, D.G. (1996). Reaction of phosgeniminium salts with enolates derived from Lewis acid complexes of 2'-hydroxypropiophenones and related beta-diketones. Journal of Organic Chemistry *61*, 3218-3220.

38. Tanque, Y., Terada, A., Seto, I., Umezu, Y., and Tsuge, O. (1988). One-pot ortho hydroxylations of 2-(1-hydroalkyl)naphthylenes and (1-hydroxyalkyl)benzenes. Bull. Chem. Soc. Jpn. *61*, 1221-1224.

39. Aniol, M., and Wawrzenczyk, C. (1997). Chromenes and chromanones. 4. The birch reduction of 2,2-dimethyl-4-chromanone and its 7-substituted analogues. Heterocycles *45*, 1069-1079.

40. Foster, K.L., Baker, S., Brousmiche, D.W., and Wan, P. (1999). o-Quinone methide formation from excited state intramolecular proton transfer (ESIPT) in an o-hydroxystyrene. Journal of Photochemistry and Photobiology a-Chemistry *129*, 157-163.

41. Cimarelli, C., and Palmieri, G. (1998). Alkylation of dianions derived from 2-(1-iminoalkyl) phenols: Synthesis of functionalized 2-acyl phenols. Tetrahedron *54*, 15711-15720.

42. Dolhem, E., Barhdadi, R., Folest, J.C., Nedelec, J.Y., and Troupel, M. (2001). Nickel catalysed electrosynthesis of ketones from organic halides and iron pentacarbonyl. Part 2: Unsymmetrical ketones. Tetrahedron *57*, 525-529.

43. Morris, J., Wishka, D.G., and Fang, Y. (1994). A cyclodehydration route to 2-aminochromones. Synth. Commun. *24*, 849-858.

Chapter 5

A pharmacological map of the PI3-K family defines a role for p110α in insulin signaling

5.1 Abstract:

Phosphoinositide 3-kinases (PI3-Ks) are an important emerging class of drug targets, yet the unique roles of PI3-K isoforms remain poorly defined. We describe here an approach to pharmacologically interrogate the PI3-K family. A chemically diverse panel of PI3-K inhibitors was synthesized and their target selectivity was biochemically enumerated, revealing cryptic homologies across targets and chemotypes. Crystal structures of three of these inhibitors bound to p110γ identify a conformationally mobile region that is uniquely exploited by selective compounds. This chemical array was then used define the PI3-K isoforms required for insulin signaling. We find that p110α is required for insulin action in cultured cells, whereas p110β is dispensable, but sets a phenotypic threshold for p110α activity. p110α inhibitors block the effects of acute insulin treatment *in vivo,* whereas a p110β inhibitor has no effect. These results illustrate systematic target validation using a matrix of inhibitors that span a protein family.

5.2 Introduction:

The PI3-K family of lipid kinases catalyze the synthesis of the second messengers phosphatidylinositol-3-phosphate (PI(3)P), phosphatidylinositol-3,4-*bis*phosphate (PI(3,4)P_2) and phosphatidylinositol-3,4,5-*tris*phosphate (PIP_3) [1]. In the appropriate cellular context, these three lipids direct wide array of biology – ranging from cell growth, survival, differentiation and chemotaxis to immune function and glucose homeostasis [2]. It is now appreciated that the PI3-K family comprises 15 kinases with diverse substrate specificities, expression patterns, and modes of regulation [2]. The class I PI3-Ks (p110α, p110β, p110δ, and p110γ) are activated by tyrosine kinases or G-protein coupled receptors to generate PIP_3, which activates downstream effectors that

include the Akt/PDK1 pathway, the Tec family kinases, and the Rho family GTPases. The class II and III PI3-Ks, by contrast, generate mainly PI(3)P or PI(3,4)P_2 and play a key role protein trafficking. A fourth class of PI3-K family members – the PI3-K related kinases (PIKKs) – are protein kinases that control cell growth (mTORC1) or monitor the integrity of nucleic acids (ATM, ATR, DNA-PK, and hSmg-1).

The importance of these enzymes in diverse pathophysiology has made the PI3-K family the focus of intense interest as a new class of drug targets [3]. This interest has been fueled by the recent discovery that p110α is frequently mutated in primary tumors [4] and evidence that the lipid phosphatase PTEN, an inhibitor of PI3-K signaling, is a commonly inactivated tumor suppressor [5]. Efforts are underway to develop small molecule PI3-K inhibitors for the treatment of inflammation and autoimmune disease (p110δ, p110γ, and mTOR), thrombosis (p110β), viral infection (the PIKKs) and cancer (p110α, mTOR, and others). Recently, the first selective inhibitors of these enzymes have been reported [6-11].

A key challenge in targeting the PI3-K family with drugs is to understand how individual PI3-K isoforms control normal physiology, as this defines the therapeutic window for targeting any specific isoform. Genetic efforts to uncouple the action of individual PI3-K isoforms have been frustrated by redundancy, compensation, and kinase-independent activities of these enzymes. Genetic disruption of either p110α or p110β (the two most widely expressed PI3-Ks) leads to embryonic lethality in mice [12, 13]. Knockout of the p85 regulatory subunits of the class I PI3-Ks induces a paradoxical increase in PI3-K signaling [14, 15]. This reflects the fact that p85 both promotes PI3-K activity (by stabilizing the p110 catalytic subunit) and inhibits it (by reducing basal activity and sequestering essential signaling complexes) [16, 17]. Moreover, it is clear that expression levels between and among the p110 and p85 isoforms are tightly coupled,

such that changes in expression of one isoform can induce compensating changes in the expression of others [18, 19]. A similar effect has been observed among the PIKKs, where a deficiency in DNA-PK alters the expression of the closely related proteins ATM and hSmg-1 [20]. Finally, it is increasingly clear that PI3-Ks, like many protein kinases, have kinase-independent signaling activities that can complicate efforts to predict inhibitor phenotypes from knockouts [18, 21]. Mice bearing a p110δ kinase-dead allele have more pronounced proliferative defects among certain lymphocyte populations than p110δ knockout animals [22, 23] – presumably because the kinase-dead p110δ prevents compensation by p110α and p110β [24]. Similarly, p110γ knockout mice suffer from cardiac damage due to chronic pressure overload, whereas mice bearing a p110γ kinase-dead allele have normal heart function [25]. In this case, the discrepancy was traced to the ability of p110γ to regulate PDE3B in a kinase-independent fashion. Moreover, in all cases it remains unclear to what extent genetic inactivation of these kinases prior to development accurately mimics acute inactivation with a small molecule in the adult [26].

Cell permeable, small molecule inhibitors make it possible to directly assess the phenotypic consequences of inhibiting a kinase with a drug in a physiologically relevant model system. The challenge for pharmacological target validation is that few well-characterized, selective kinase inhibitors are known. This has been particularly true for the PI3-Ks, as the two primary pharmacological tools available, wortmannin and LY294002, are broadly active within the family. We report here a set of potent, chemotypically diverse small molecule inhibitors that span the PI3-K family. For each compound, we have biochemically enumerated its target selectivity relative to all PI3-K family members and, in many cases, structurally defined its binding mode by x-ray crystallography. Critically, this panel includes representatives from a large number of

PI3-K inhibitor chemotypes currently in preclinical drug development, and therefore anticipates the biological activities likely to be found in eventual clinical candidates. Using this chemical array, we identify p110α as the key PI3-K activity downstream of the insulin receptor.

5.3 A basis set of isoform-specific PI3-K inhibitors

Representatives from nine chemical classes of isoform-selective PI3-K inhibitors were selected from lead compounds (or derivatives thereof) under development by the pharmaceutical industry. These compounds were synthesized and their activity against the class I PI3-Ks measured *in vitro* (see Experimental Procedures). Based on this initial screen, a subset representing the most potent and selective agents was selected for further characterization. This panel includes one to three representatives from each chemical class (Figure 5.1A and Figure 5.2). For most chemotypes, a negative control compound, inactive against all PI3-Ks tested, was also synthesized that differs from the active inhibitor by a single atom substitution (Figure 5.2).

The extended specificity profile of these compounds was determined by measuring IC_{50} values *in vitro* against purified protein for each PI3-K family member (Figure 5.1B and Tables 5.1 and 5.2). This target panel includes the class I (p110α/p85α, p110β/p85α, p110δ/p85α, and p110γ), class II (PI3KC2α, PI3KC2β, PI3KC2γ) and class III (hVPS34) PI3-Ks, as well as the related PI4-Ks (PI4KIIIα and PI4KIIIβ) and PIKKs (ATM, ATR, mTOR, DNA-PK, mTORC1, and mTORC2). We also tested two families of unrelated lipid kinases, the PIPKs and class II PI4-Ks (Table 5.1), and 30 protein kinases (Table 5.2). As this panel includes almost all proteins with sequence homology to p110α, it is highly enriched for the likely targets of these compounds.

A spectrum of biochemical target selectivities was observed across different inhibitor classes (Figure 5.1B). The most selective compounds include the quinazoline purine inhibitors of p110δ (PIK-23, PIK-39, and IC87114), the morpholino and pyridinyl chromones that target p110β/p110δ (TGX-115, TGX-286, and PIK-108), and the imidazopyridine p110α/p110γ inhibitor PIK-75. At least one compound from each of these chemotypes exhibits >100-fold selectivity between its primary target(s) and other class I PI3-Ks. Other chemical classes (e.g., the benzyloxazonines, pyridinylfuranopyrimidines, phenylthiazoles, and imidazopyridines, Figure 5.1A) were found to inhibit multiple PI3-Ks with varied affinities (Figure 5.1B). These multi-targeted compounds possess overlapping yet distinct target selectivities, and can complement more selective agents by unmasking hidden synergies between targets within the PI3-K family (Z.A.K., W.A.W., and K.M.S., submitted). Indeed, in several cases we identified unique targets for these compounds relative to all other inhibitors in our panel. For example, a phenylthiazole, PIK-93, potently inhibits PI4KIIIβ (IC_{50} = 30 nM at 100 μM ATP). This compound is the first potent, synthetic PI4-kinase inhibitor, and we have used this reagent to dissect the role of PI4-K isoforms in calcium signaling (Z.A.K., P.V., T.B., and K.M.S., unpublished data). Similarly, the pyridinylfuranopyrimidine PI-103 potently inhibits both the rapamycin sensitive (mTORC1, IC_{50} = 20 nM at 100 μM ATP) and rapamycin insensitive (mTORC2, IC_{50} = 120 nM at 100 μM ATP) complexes of the protein kinase mTOR. Thus, PI-103 represents the first reported potent, synthetic inhibitor of mTOR.

5.4 Identification of structure-activity relationship (SAR) and target homology within the PI3-K family

More than a decade of research on protein kinase inhibitors has revealed trends in inhibitor sensitivity among kinases (SAR homology) and target selectivity among chemotypes (target homology) that are critical to predicting off-target effects and interpreting inhibitor induced phenotypes [21]. To better understand the relationships between PI3-K related targets and chemotypes, we subjected family-wide specificity data to principal component analysis (Figure 5.1D). This analysis reduces the multidimensional relationship between inhibitors and their targets to three principal components that can be plotted to depict the relatedness of these elements. Organizing the data in this way can reveal functional similarities between the ATP binding pockets of kinases or between chemotypes of inhibitors that cannot be predicted from the sequence of the kinase or the chemical structure of the inhibitor.

We first compared PI3-K family members according to their sensitivity to different inhibitors (Figure 5.1D, center) and contrasted this with the same analysis based on pairwise sequence homology within the kinase domain (Figure 5.1D, top). Analysis by sequence segregates the PI3-Ks and PI4-Ks into five clusters, essentially recapitulating the original assignment of these enzymes into subfamilies based on sequence similarity [27]. When these kinases are instead clustered by inhibitor sensitivity, several key differences emerge. First, the class I PI3-Ks are more widely distributed by SAR homology than by sequence homology. This reflects the fact that the compounds in our panel, which were designed to be selective among the class I isoforms, do distinguish between these kinases to a greater extent than sequence differences alone. Nonetheless, meaningful SAR homologies persist among the class I PI3-Ks. p110β and p110δ cluster in target space (Figure 5.1D, top), and compounds that inhibit p110β tend to inhibit p110δ more potently than other PI3-Ks (Figure 5.1C, left). Likewise, p110α tends to be inhibited by compounds targeting p110γ, and vice versa (Figure 5.1C, left).

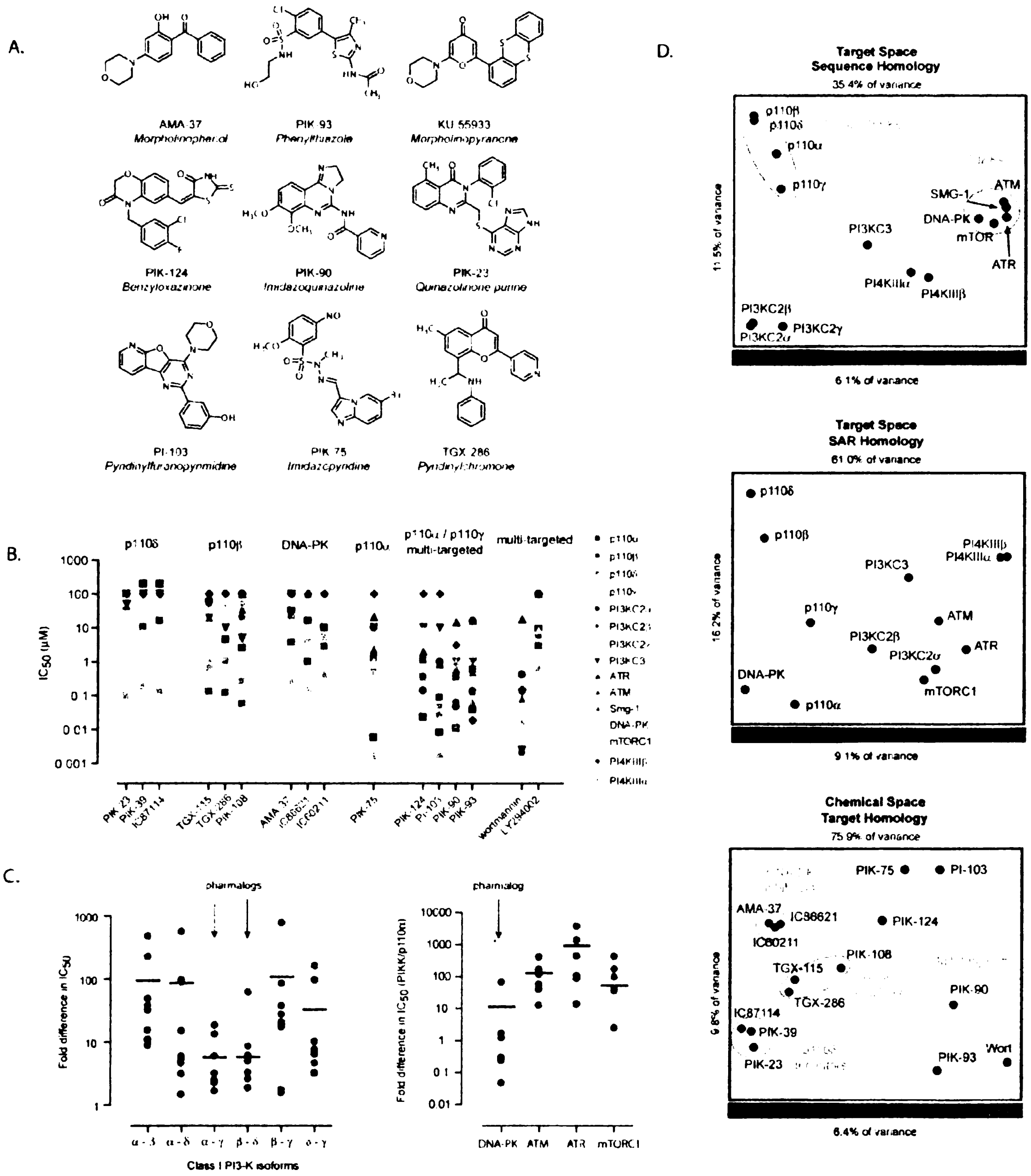

Figure 5.1: Biochemical analysis of selected PI3-K inhibitors. A. Structures of representative compounds from nine chemotypes of isoform-selective PI3-K inhibitors. The core chemotype is colored blue for each inhibitor. B. Top. Distribution of IC_{50} values for inhibitors against the PI3-K family members. Bottom, left. Fold-difference in IC_{50} values between class I PI3-Ks for a representative compound from each chemotype (TGX-115, AMA-37, PIK-39, PIK-75, PIK-90, PIK-93, PI-103, PIK-124). Bottom, right. Fold-difference in IC_{50} value between p110α and PIKKs for potent p110α inhibitors. C. Principal component analysis of PI3-K family members and inhibitors. The percentage of variance explained by each axis is noted. The z-axis is depicted as color as designated in the color bar for each plot.

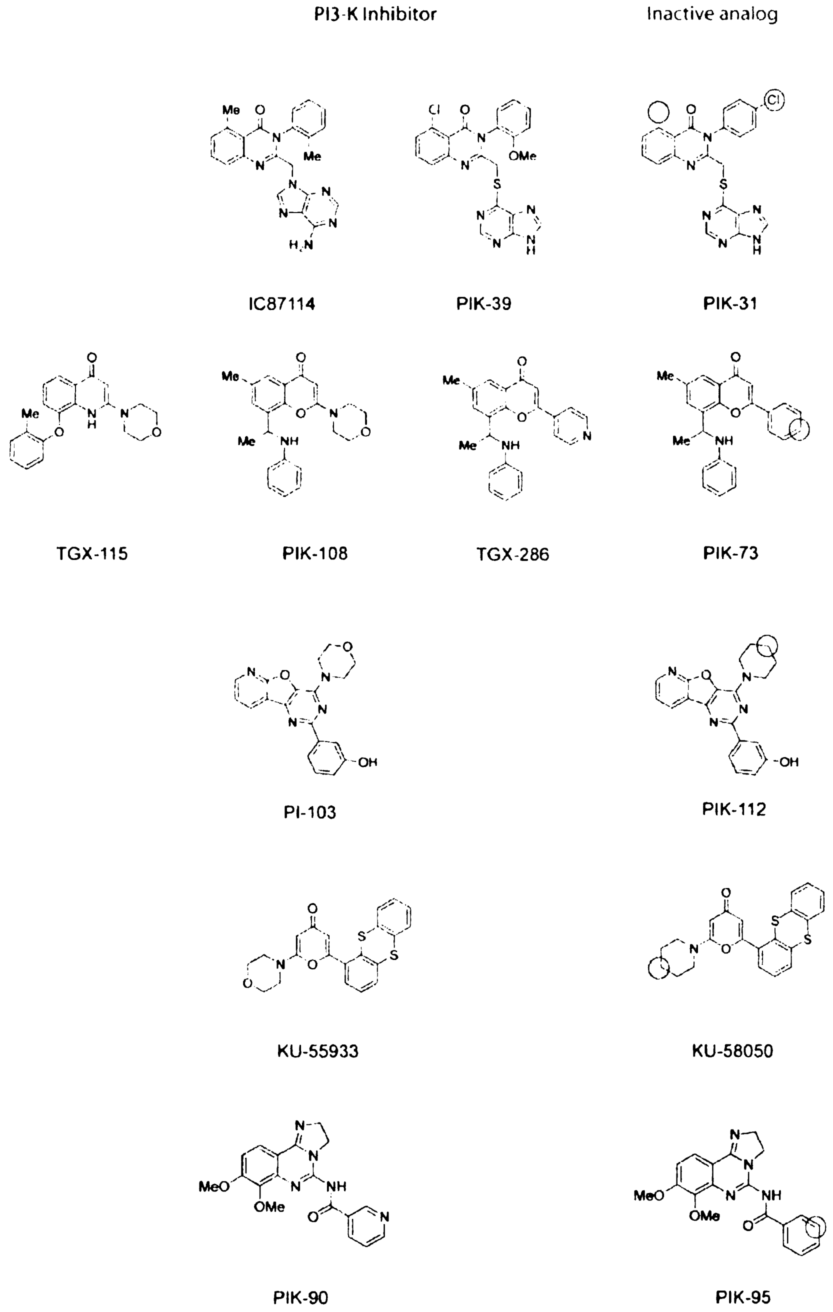
PI3-K Inhibitor
Inactive analog
IC87114
PIK-39
PIK-31
TGX-115
PIK-108
TGX-286
PIK-73
PI-103
PIK-112
KU-55933
KU-58050
PIK-90
PIK-95

Figure 5.2: Structures of active and inactive analogs of PI3-K inhibitors

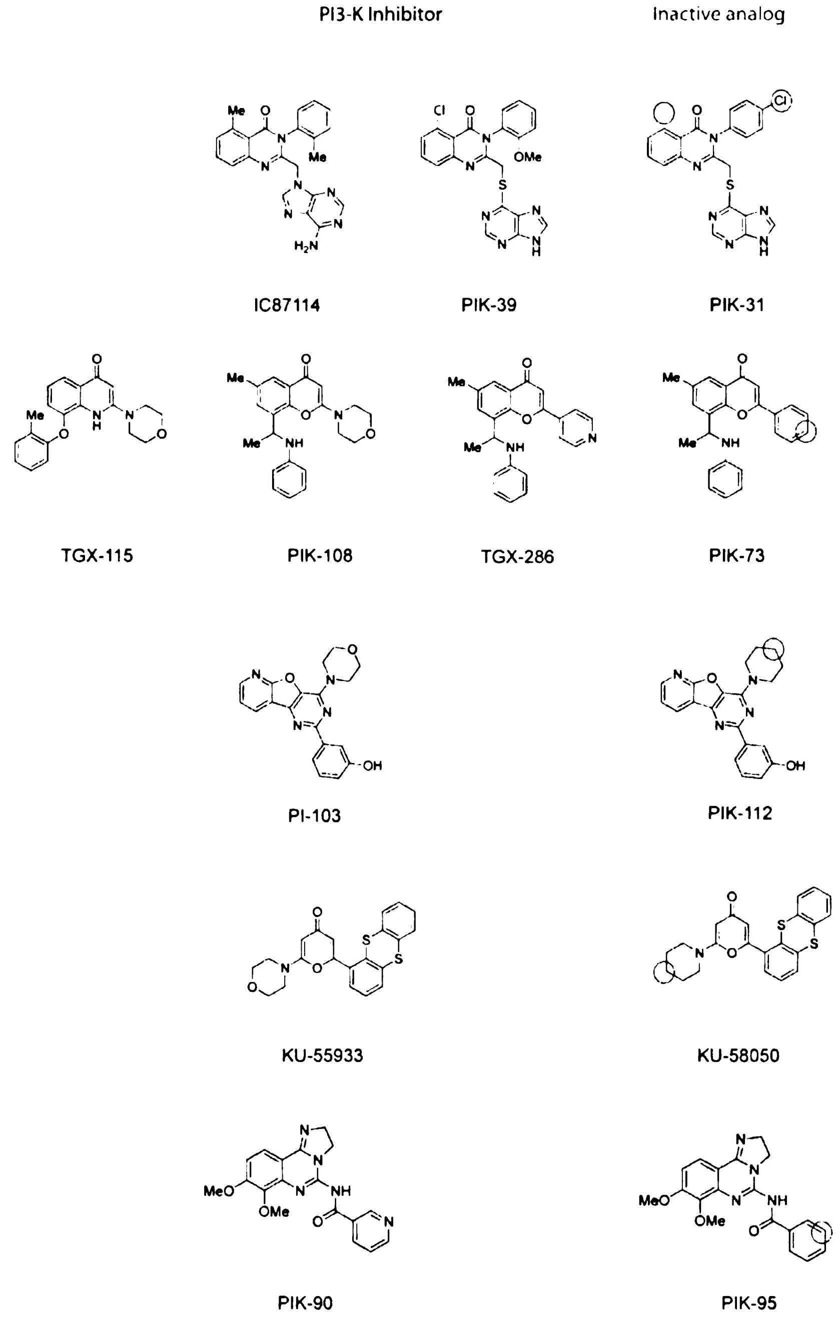
PI3-K Inhibitor
Inactive analog
IC87114
PIK-39
PIK-31
TGX-115
PIK-108
TGX-286
PIK-73
PI-103
PIK-112
KU-55933
KU-58050
PIK-90
PIK-95

Figure 5.2: Structures of active and inactive analogs of PI3-K inhibitors

We refer to the pairs p110β/p110δ and p110α/p110γ as pharmalogs in recognition of this SAR homology, and suggest that it may be more challenging to find inhibitors with high selectivity between these targets. Consistent with this prediction, the recently described p110γ inhibitor AS604850, which was not included in our analysis, has been reported to inhibit p110α more potently than p110β or p110δ [11].

A second unexpected result from this analysis is that p110α clusters in target space with DNA-PK based on SAR homology (Figure 5.1D, center), even though these kinases share limited sequence similarity (Figure 5.1D, top). Indeed, five of the six chemotypes that inhibit p110α with an $IC_{50} < 5$ μM also inhibit DNA-PK in the same concentration range (Figure 5.1C, right). By contrast, the other PIKKs are generally resistant to these same compounds (Figure 5.1C, right). While certain chemotypes can discriminate between these targets (e.g. arylmorpholines such as AMA-37), DNA-PK inhibition is a common feature of p110α inhibitors, and likely reflects a cryptic similarity between the active sites of these two pharmalogs.

We next analyzed compounds according to their target selectivity in order to reveal relationships within and among chemotypes. Compounds from a single chemotype cluster in chemical space based on target homology (Figure 5.1D, bottom), which supports grouping these inhibitors into target classes. To define the region of chemical space occupied by multi-targeted inhibitors, wortmannin was also included in this analysis (Figure 5.1D, bottom). Wortmannin is a widely-used, broad spectrum PI3-K inhibitor, and comparison of the selectivity profile of this compound with our panel highlights the remarkable pan-specificity of this natural product (Figure 5.1B). The compounds classified as most selective (e.g. the isoquinoline purines, arylmorpholines,

	PIK-23	TGX-115	PIK-37	PIK-39	IC87114	TGX-186	PIK-75	PIK-90	PIK-93	PIK-108	PI-103	PIK-124
PI3Ks												
p110α *p*85α	*>200*	*61*	*32*	*>200*	*>200*	4.5	0.0058	0.011	0.039	2.6	0.0082	0.023
p110β *p*85α	*42*	*0.13*	*3.7*	*11*	*16*	0.12	1.3	0.35	0.59	0.057	0.088	1.1
p110δ *p*85α	*0.097*	*0.63*	*22*	*0.18*	*0.13*	1	0.51	0.058	0.12	0.26	0.048	0.34
p110γ	*50*	*100*	*100*	*17*	*61*	10	0.076	0.018	0.016	4.1	0.15	0.054
PI3KC2α	*>100*	*>100*	*>100*	*>100*	*>100*	>100	~10	0.047	~16	~100	~1	0.14
PI3KC2β	*100*	*50*	*>100*	*100*	*>100*	~100	~1	0.064	0.14	~20	0.026	0.37
PI3KC2γ	*>100*	*100*	*50*	*100*	*>100*	ND	ND	ND	ND	ND	ND	ND
PI3KC3	~50	20	>100	>100	>100	10	10	1	1	5	10	10
PI4Ks												
PI4KIIα	>100	>100	>100	>100	>100	>100	>100	>100	>100	>100	>100	>100
PI4KIIIα	>100	>100	>100	>100	>100	>100	>100	0.83	1.1	~50	>100	>100
PI4KIIIβ	>100	>100	>100	>100	>100	>100	>100	3.1	0.019	>100	>100	>100
PIKKs												
ATR	>100	>100	>100	>100	>100	>100	21	15	17	>100	0.85	2
ATM	>100	20	ND	>100	>100	>100	2.3	0.61	0.49	35	0.92	ND
DNA-PK	*>100*	*1.2*	*0.27*	*>100*	*>100*	~50	0.0017	0.013	0.064	0.12	0.0019	1.5
mTORC1	*>100*	*>100*	*>100*	*>100*	*>100*	*>100*	*1*	*1.05*	*1.38*	*ND*	*0.02*	*ND*
mTORC2	*>101*	*ND*	*>100*	*>100*	*>100*	*ND*	*~10*	*ND*	*ND*	*ND*	*0.125*	*ND*
PIPKs												
PI4P5KIα	>100	>100	>100	>100	>100	>100	>100	>100	>100	>100	>100	>100
PI4P5KIβ	>100	>100	>100	>100	>100	>100	>100	>100	>100	>100	>100	>100
PI5P4KIIβ	>100	>100	>100	>100	>100	>100	>100	>100	>100	>100	>100	>100

Table 5.1 IC_{50} values (μM) for inhibition of purified PI3-K family members. Values were determined at either 10 μM ATP or 100 μM ATP (italics).

	TGX115	AMA37	PIK39	IC87114	TGX286	PIK75	PIK90	PIK93	PI103	PIK124	KU55933
Abl	89.0	77.6	90.7	86.4	89.0	68.3	90.5	75.4	95.9	87.3	83.1
Akt1	69.0	84.6	88.9	102.4	69.9	(0.05)	84.5	44.0	78.3	23.7	94.9
Akt2 (dPH)	104.4	94.4	111.3	117.8	117.3	95.0	108.5	110.7	112.6	98.7	100.2
CamKII	111.4	121.9	122.1	115.4	118.8	119.8	116.1	120.4	127.6	135.5	121.8
CDK1/cyc. B	103.0	114.0	115.5	116.0	120.3	61.6	126.6	124.5	142.3	110.7	101.2
CDK2/cyc. A	105.3	99.7	105.6	102.4	103.1	(1.2)	100.9	98.1	98.5	104.9	97.4
Chk1	119.9	104.0	105.2	103.0	104.1	98.4	102.9	99.7	92.3	107.9	81.4
CK1	99.7	99.2	100.1	98.1	91.3	27.9	97.8	100.2	84.8	104.6	94.1
CK2	103.3	106.6	99.6	111.7	111.2	82.2	103.1	113.2	108.1	78.5	105.4
Erk1	96.7	99.3	97.6	93.7	99.0	77.9	98.8	98.6	92.0	97.8	104.6
Erk2	107.7	102.5	109.2	104.7	106.9	94.3	102.0	103.2	98.8	98.0	102.1
FAK	105.5	105.5	106.4	110.1	102.8	34.9	100.0	101.8	101.8	102.8	107.3
Fyn	81.5	118.2	117.7	114.5	115.7	(~10)	108.6	97.9	95.9	110.1	94.2
GSK3B	114.0	107.3	101.5	104.7	96.1	(4.4)	85.6	104.0	105.5	97.6	102.0
Hck	106.5	91.2	84.0	85.8	83.0	(~10)	79.9	86.4	83.8	68.3	82.1
IR	108.4	113.4	113.6	115.7	112.1	99.5	102.8	109.8	106.0	109.9	109.7
JNK1α1	99.9	95.5	92.1	88.5	93.8	97.8	94.2	87.2	83.6	96.9	99.6
JNK2α1	104.8	104.8	116.7	107.1	88.1	88.1	90.5	88.1	81.0	85.7	85.7
JNK2α2	95.4	101.6	90.8	87.7	89.3	86.2	83.1	98.5	76.9	89.3	95.4
IRAK4	112.7	98.9	100.1	93.1	95.0	17.2	94.9	95.9	105.6	175.4	74.2
NEK2	125.2	99.1	98.6	114.3	126.4	106.9	103.4	110.1	120.0	118.5	106.5
PKA	105.4	94.0	108.1	108.6	107.3	(~10)	103.1	105.6	102.5	104.3	104.1
PKCδ	103.9	104.9	103.9	104.6	104.9	114.3	100.7	103.7	101.2	105.5	103.7
PKCε	108.9	111.9	111.9	114.1	111.5	45.0	105.2	103.4	103.4	106.0	104.8
PDK1	111.2	101.9	97.4	113.4	114.4	111.0	110.4	118.7	107.5	109.4	130.7
PLK1	122.7	118.9	117.4	109.6	107.6	93.7	107.6	111.1	106.2	96.0	84.9
p38	101.2	102.8	106.5	104.1	100.9	100.3	98.5	102.9	99.8	102.6	101.4
Src	139.9	119.0	125.6	127.2	101.1	(~10)	113.5	107.3	88.7	98.0	74.8
Src (T338I)	94.5	78.7	75.7	92.6	73.6	(~10)	85.9	79.2	86.2	79.7	81.1
Zap70	123.8	121.1	130.4	110.5	130.0	179.5	115.8	115.4	117.7	100.4	99.3

Table 5.2 Percentage inhibition of PI3-K inhibitors (10 μM) against purified protein kinases in the presence of 200 μM ATP. Values in parentheses are IC_{50} values for kinases that were significantly inhibited.

pyridinyl/morpholinochromones, and imidazopyridines) occupy a region of chemical space most distant from wortmannin (Figure 5.1D, bottom). By contrast, the pan-specific inhibitors PIK-90 and PIK-93 cluster near wortmannin in chemical space, reflecting the target homology of these chemically unrelated compounds (Figure 5.1D, bottom).

5.5 Structures of isoform-specific PI3-K inhibitors

To better understand the selectivity trends observed among these chemically diverse inhibitors, the structural basis for their binding to PI3-K was investigated. Crystal structures of a single PI3-K, p110γ, have been reported, alone and in complex with ATP or pan-specific inhibitors such as LY294002 and wortmannin [28, 29]. It is not known how potent and selective inhibitors such as those we report here achieve their binding. To explore this, the crystal structures of PI3-K inhibitors from three chemotypes bound to human p110γ were determined at 2.5 - 2.6 Å resolution: the quinazoline purine PIK-39, the imidazopyridine PIK-90 and the phenylthiazole PIK-93 (Figure 5.3 and Table 5.3).

Based on these co-crystal structures and a conserved arylmorpholine pharmacophore model, structural models were generated for three additional chemotypes bound to p110γ: the pyridinylfuranopyrimidine PI-103, the morpholinochromone PIK-108, and the morpholinopyranone KU-55933 (Figure 5.3). Model-building for these inhibitors was guided by the observation that each compound contains the key arylmorpholine pharmacophore found in LY294002. The oxygen atom in the morpholine ring of LY294002 makes a critical hydrogen bond to the backbone amide of Val 882 (p110γ numbering) and substitution of this oxygen abolishes LY294002 binding to PI3-K [28]. In a similar fashion, we (Figure 5.2) and others [30] have shown that replacement of the morpholine oxygen atom in these novel

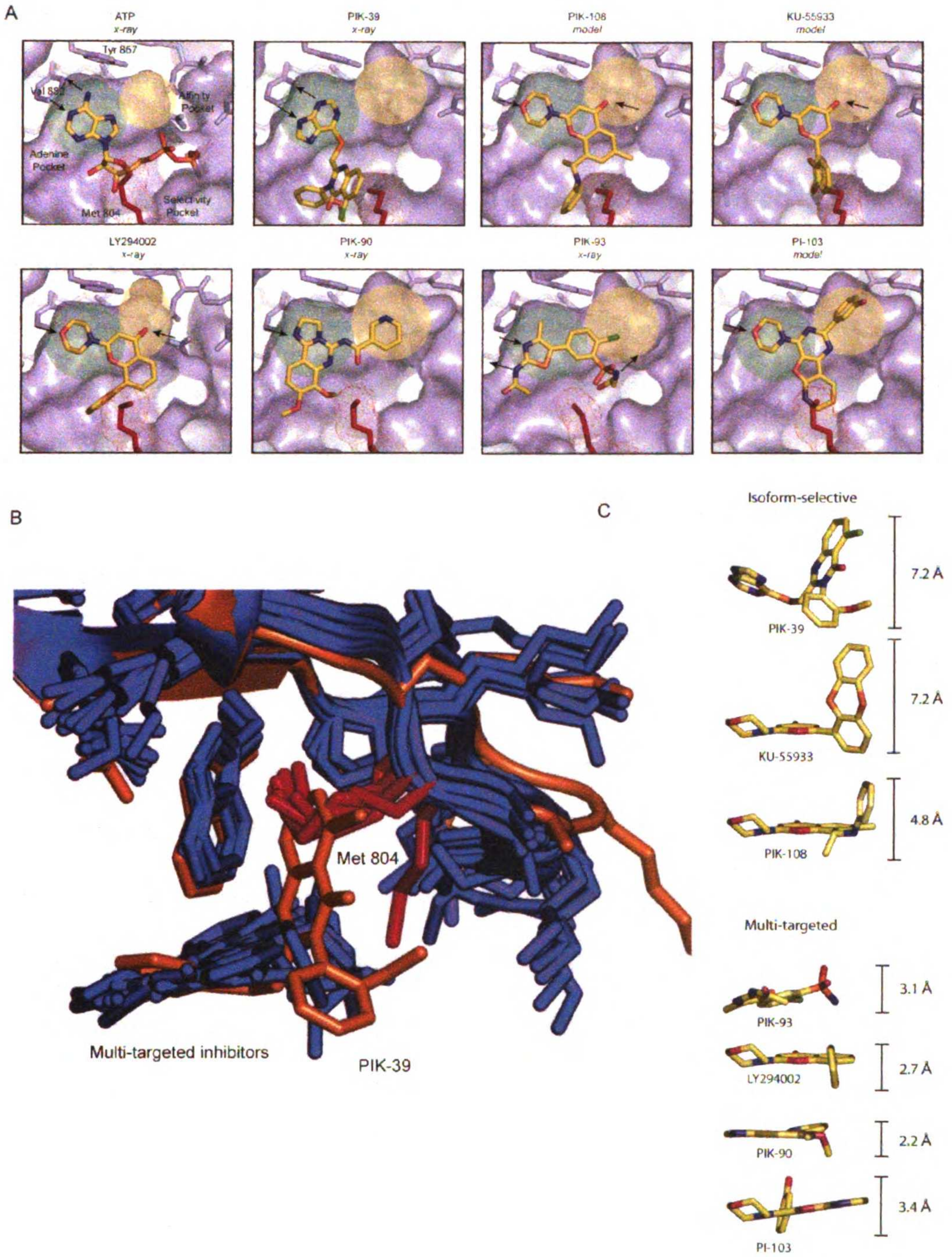
A
ATP
x-ray
Tyr 867
Val 882
Affinity Pocket
Adenine Pocket
Met 804
Selectivity Pocket
PIK-39
x-ray
PIK-108
model
KU-55933
model
LY294002
x-ray
PIK-90
x-ray
PIK-93
x-ray
PI-103
model
B
Met 804
Multi-targeted inhibitors
PIK-39
C
Isoform-selective
7.2 Å
PIK-39
7.2 Å
KU-55933
4.8 Å
PIK-108
Multi-targeted
3.1 Å
PIK-93
2.7 Å
LY294002
2.2 Å
PIK-90
3.4 Å
PI-103

Figure 5.3. Structural basis for isoform selective inhibition of PI3-K. A. Structures of isoform-selective PI3-K inhibitors bound to p110γ. The regions occupied by adenine (green), the affinity pocket (yellow), and the selectivity region surrounding Met 804 (red) are highlighted. **B.** An alignment of all reported PI3-K inhibitor co-crystal structures. PIK-39 is orange and all other inhibitors are blue. Met 804 (red) adopts an up conformation in all structures except PIK-39. **C.** Alignment of PI3-K inhibitors based on their orientation in the p110γ active site reveals that multi-targeted inhibitors are flat, whereas more selective compounds project vertically.

compounds abolishes PI3-K inhibition, supporting a conserved mode of binding for the arylmorpholine moiety in these inhibitors.

5.6 The structure of PIK-39 reveals a conformational switch that controls inhibitor selectivity

The discovery of compounds that can distinguish between closely related isozymes remains a major challenge for kinase inhibitor design. An emerging theme in protein kinase inhibitors is the importance of conformational mobility of the ATP binding pocket, which allows certain kinases, such as Bcr-Abl, to present unique binding surfaces to an inhibitor, such as Imatinib, that are not presented by a closely related homolog [31]. The most selective PI3-K inhibitor reported here, PIK-39, is an isoquinoline purine that inhibits p110δ at mid-nanomolar concentrations, p110γ and p110β at concentrations ~100-fold higher, and shows no activity against any other PI3-K family member, including p110α, at concentrations up to 100 μM (Table 5.1). The remarkable biochemical selectivity of this compound is achieved through an unusual binding mode revealed in its co-crystal structure with p110γ, in which only the mercaptopurine moiety makes contacts within the interior of the ATP binding pocket (Figure 5.3A). The mercaptopurine is rotated ~110º and twisted ~35º out of the plane relative to the adenine of the ATP, and in this orientation, it satisfies hydrogen bonds to the backbone amide nitrogen of Val 882 as well as the backbone carbonyl oxygen of Glu 880 (thereby recapitulating the hydrogen bonds made by N1 and N6 of adenine). To achieve this interaction, the mercaptopurine adopts an unusual N(3)-H tautomer (Figure 5.5).

In contrast to other PI3-K inhibitor structures, PIK-39 does not access the deeper pocket in the active site interior (Figure 5.3A, yellow). Instead, the aryl-isoquinoline

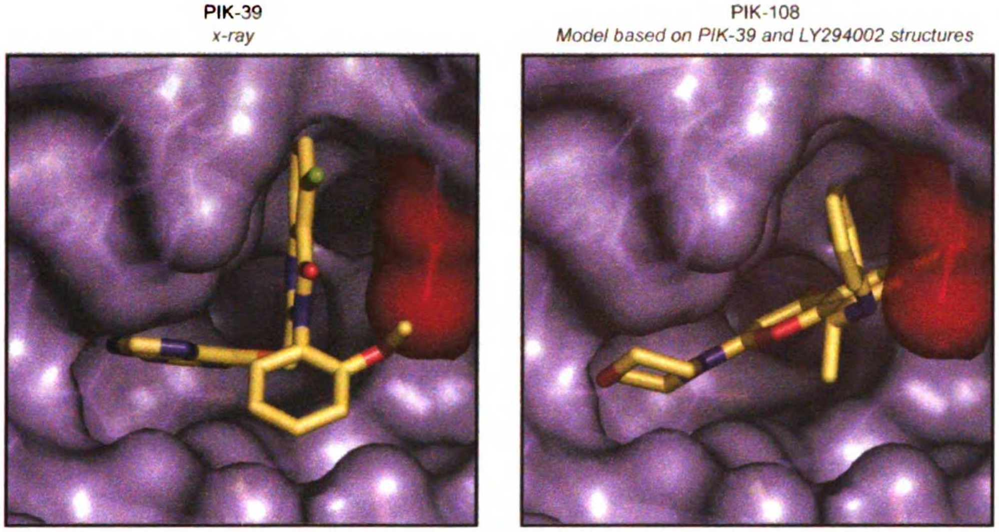
PIK-39
x-ray
PIK-108
Model based on PIK-39 and LY294002 structures

Figure 5.4: Left panel: Structure of PIK-39 bound to p110γ with Met 804 (red) in the down conformation. Right panel: Model of PIK-108 bound to p110γ. In this model, the aniline moiety of PIK-108 accesses the same induced pocket as PIK-39.

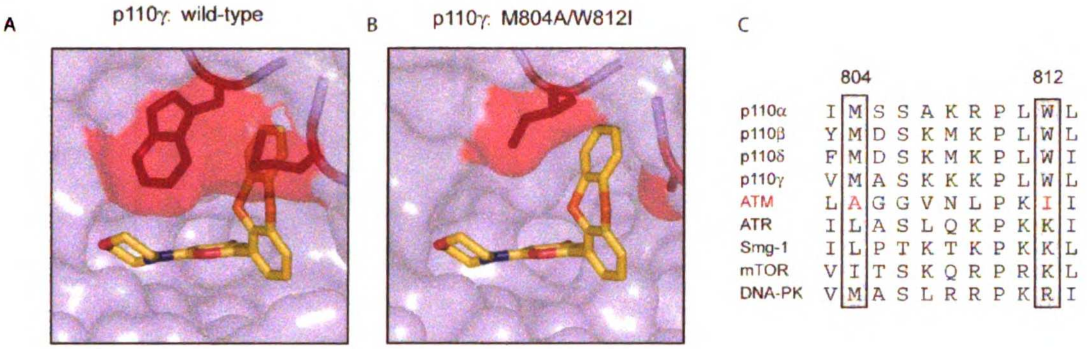

		804								812	
p110α	I	M	S	S	A	K	R	P	L	W	L
p110β	Y	M	D	S	K	M	K	P	L	W	L
p110δ	F	M	D	S	K	M	K	P	L	W	I
p110γ	V	M	A	S	K	K	K	P	L	W	L
ATM	L	A	G	G	V	N	L	P	K	I	I
ATR	I	L	A	S	L	Q	K	P	K	K	I
Smg-1	I	L	P	T	K	T	K	P	K	K	L
mTOR	V	I	T	S	K	Q	R	P	R	K	L
DNA-PK	V	M	A	S	L	R	R	P	K	R	I

Figure 5.5. Structural rationale for selective inhibition of ATM by KU-55933. A. Model of KU-55933 bound to p110γ indicating the steric clash with Met 804. B. A model of KU-55933 in the ATP binding site of p110γ in which Met 804 and Trp 812 have been changed to the corresponding residues from ATM to relieve this steric clash. C. A sequence alignment of the class I PI3-Ks and PIKKs in this region.

A.

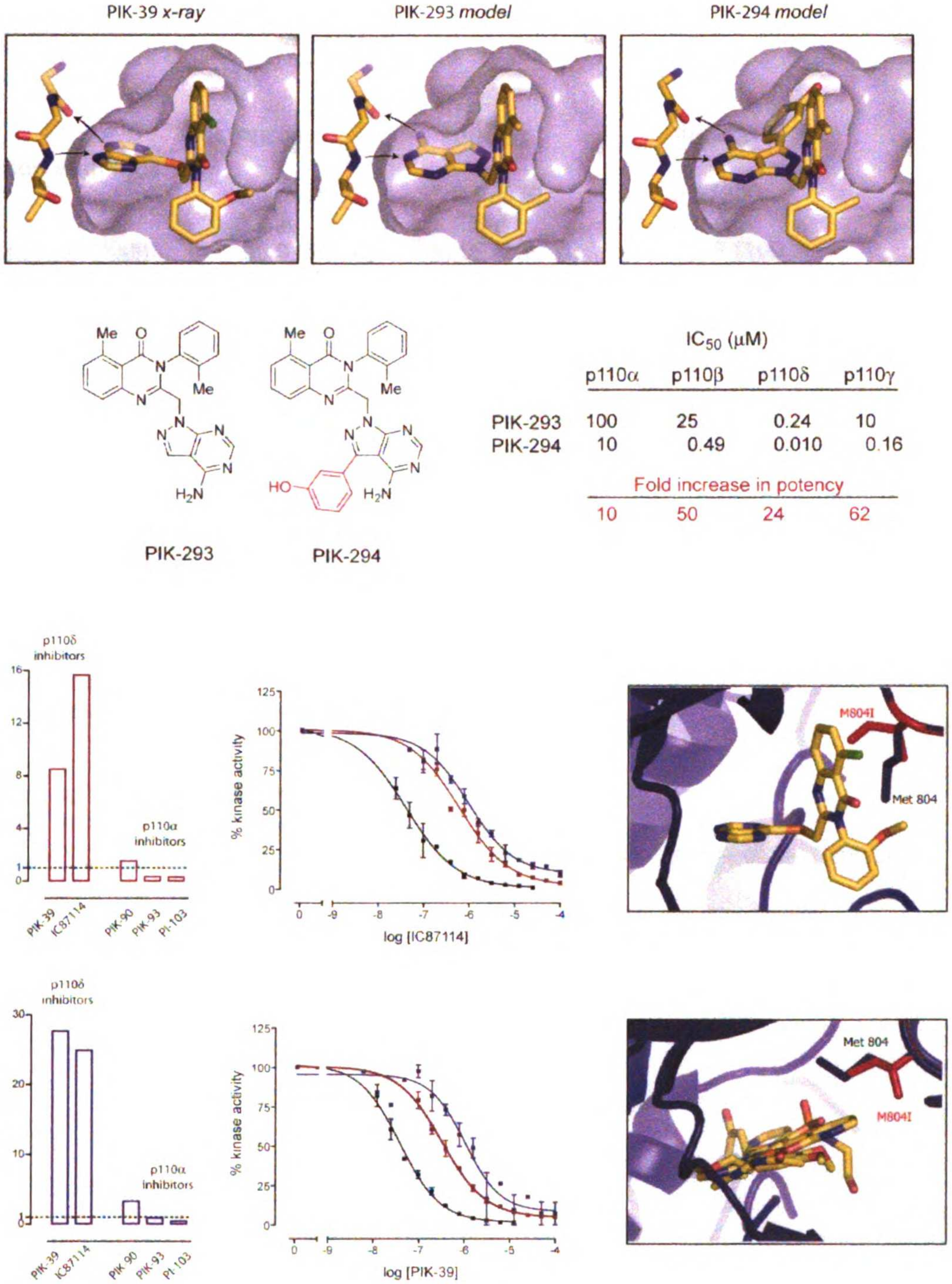

IC$_{50}$ (μM)

	p110α	p110β	p110δ	p110γ
PIK-293	100	25	0.24	10
PIK-294	10	0.49	0.010	0.16
Fold increase in potency	10	50	24	62

B.

Figure 5.6. A. Design of a p110δ selective inhibitor that accesses the affinity pocket. B. Mutation of Met752 in p110d (Met804 in p110γ) to Ile or Val induces selective resistance to p110δ selective inhibitors.

Compound	**PIK-39**	**PIK-90**	**PIK-93**
Data collection statistics			
Wavelength[a]	0.97930	0.97930	0.97930
Resolution	2.6 Å	2.5 Å	2.6 Å
Completeness (last shell)	99.9 (100.0)	99.8 (99.8)	99.8 (100.0)
R_{merge}[b] (last shell)	0.062 (0.446)	0.072 (0.405)	0.066 (0.356)
Multiplicity (last shell)	3.7 (3.7)	3.7 (3.7)	3.7 (3.7)
$<I/\sigma>$ (last shell)	22.4 (2.2)	19.7 (2.0)	22.4 (2.2)
Refinement statistics			
Resolution (Number of reflections, no cutoff)	62.1-2.6 Å (30150)	57.1-2.6 Å (34491)	71.8-2.6 Å (30445)
Protein atoms	6774	6799	6781
Waters	5	0	0
R_{cryst}[c]	0.24	0.23	0.25
R_{free}[c] (% data used)	0.30 (4.1)	0.28 (4.1)	0.30 (4.1)
r.m.s.d. from ideality[d]			
bonds/angles/dihedrals	0.015 Å/1.4°/6.7°	0.017 Å/1.7°/6.9°	0.012 Å/1.2°/5.9°
Average B (Wilson B factor)	63 $Å^2$ (74)	48 $Å^2$ (60)	60 $Å^2$ (70)
RMSD B for bonded main (side) chain atoms	0.6 (1.3)	0.9 (2.0)	0.5 (0.9)

[a] Data sets were collected at ESRF beamline ID14-4

[b] $R_{merge} = \Sigma hkl \Sigma i \, |I_i(hkl) - <I(hkl)>| \, / \, \Sigma hkl \Sigma i \, I_i(hkl)$.

[c] R_{cryst} and $R_{free} = \Sigma \, |F_{obs} - F_{calc}| \, / \, \Sigma \, F_{obs}$; R_{free} calculated with the percentage of the data shown in parentheses.

[d] r.m.s. deviations for bond angles and lengths in regard to Engh and Huber parameters.

Table 5.3: Crystallographic statistics.

moiety of PIK-39 extends out to the entrance of the ATP binding pocket (Figure 5.3). In this region, the kinase accommodates the inhibitor by undergoing a conformational rearrangement in which Met 804 shifts from an "up" position, in which it forms the ceiling of the ATP binding pocket, to a "down" position which it packs against the isoquinoline moiety. The effect of this movement, which is unique to the PIK-39 structure (Figure 5.3B), is to create a novel hydrophobic pocket between Met 804 and Trp 812 at the entrance to the ATP binding site (Figure 5.3). This induced-fit pocket buries ~180 $Å^2$ of solvent accessible inhibitor surface area, explaining how PIK-39 achieves nanomolar affinity despite limited contacts within the active site core.

This structure suggests that Met 804 is responsible for the selective binding of the isoquinoline purines to p110δ, since different PI3-K isoforms may exhibit differential conformational plasticity in the region surrounding Met 804. Met 804 is in a loop in the catalytic domain that is structurally analogous to the glycine-rich loop of protein kinases. In protein kinases [32], this loop is unusually flexible and its dynamics appear to optimally align ATP relative to the peptide substrate. Thus, compounds like PIK-39 may be suited to exploit flexibility in this region that is necessary for phosphate transfer to the lipid substrate. Consistent with this view, movement of Met 804 induces a shift in the protein backbone that propagates through the loop connecting beta strands kβ3 and kβ4 and into the adjacent alpha helix kα2. These two beta strands and the alpha helix possess low sequence homology among the class I PI3-Ks relative to the ATP binding pocket (which is nearly 100% conserved) and this sequence variation may account for differential conformational plasticity among isoforms. This mode of inhibitor binding is reminiscent of selective protein kinase inhibitors that exploit differentially accessible conformational states [31].

We tested the hypothesis that the residue corresponding to Met 804 in p110γ is responsible for the selective binding of the isoquinoline purines to p110δ by mutating this residue in p110δ (Met 752) to a β-branched amino acid. Modelling suggests that this mutation should block binding of the p110δ selective isoquinoline purines, but not multi-targeted inhibitors that do not exploit the conformational mobility of this methionine (Figure 5.6B). Consistent with this prediction, we find that the mutations M752I and M752V reduce the binding affinity of the isoquinoline purines for p110δ by 20-30 fold, yet have little or no effect on the binding of three unrelated chemotypes that do not require the conformational rearrangement of this methionine for binding (Figure 5.5B).

The isoquinoline purine inhibitors of p110δ are unique in that they do not access the deeper affinity pocket in the PI3-K active site that is exploited by other inhibitors in our panel (see section 5.8). Our binding models suggest that an isoquinoline purine inhibitor which occupied this affinity pocket would be more potent than the parent compound, while retaining p110δ selectivity. To test this hypothesis, we designed an isoquinoline purine which accesses both the selectivity and affinity pockets. To this end, we noted that a confounding SAR of the isoquinoline purines is that it is possible to replace the mercaptopurine moiety (connected through S6) with adenine (connected through N9) without significantly altering the potency or selectivity of these compounds, despite the fact that this substitution dramatically alters the shape, orientation, and hydrogen bonding potential of the inhibitor (Figure 5.2; compare PIK-39 and IC87114). To understand how this is possible, we replaced the mercaptopurine in our PIK-39 structure with adenine to yield a model of IC87114 (Figure 5.6A depicts this hydrogen bonding scheme for PIK-293, which is identical to IC87114 except that adenine is replaced by pyrrazolopyrimidine). Remarkably, this substitution places the adenine in an orientation very similar to the adenine ring of ATP, such that the adenine in IC87114 is poised to make the same hydrogen bonds to Glu 880 and Val 882.

Based on this binding model, we reasoned that replacement of the adenine in IC87114 with the isosteric pyrrazolopyrimidine would generate an inhibitor scaffold from which we could project hydrophobic substitutuents into the affinity pocket. We therefore synthesized the pyrrazolopyrimidine analog of IC87114 (PIK-293) as well as a second compound containing a *m*-phenol moiety (PIK-294) which we predicted would access the affinity pocket. (Figure 5.6A) The *m*-phenol was selected based on the observation that the most potent inhibitor in our panel, PI-103, projects a *m*-phenol into the affinity pocket in our binding model. PIK-293 and PIK-294 were tested *in vitro* against all four class IA PI3-K isoforms. Consistent with these structural predictions, we find that introduction of the *m*-phenol moiety in PIK-294 induces a 25-50 fold increase in inhibitor potency relative to the parent compound PIK-293. (Figure 5.6A) This supports our designation of this region as an affinity pocket (Section 5.8) and provides additional evidence that our crystal structures of these inhibitors bound to p110γ, and binding models derived thereof, accurately reflect the binding orientation of the same compounds to p110δ.

5.7 Met 804 is a hot spot for selective inhibitors

The unexpected conformational mobility of Met 804 in the PIK-39 structure prompted us to ask whether other selective inhibitors rely on this same feature. The pyridinyl and morpholino chromones TGX-115, TGX-286 and PIK-108 are derivatives of LY294002 that show selectivity for p110β/p110δ relative to p110α/p110γ (Figure 5.1). These compounds differ from LY294002 by replacement of the 8-phenyl moiety with more extended aryl substituents (Figure 5.2). Models of these compounds bound to p110γ based on the LY294002 structure indicate that the extended aryl substituent in these inhibitors is poised to occupy the same inducible pocket that is created by rearrangement of Met 804 in the PIK-39 structure (Figure 5.4). This is consistent with the observation that these compounds are potent inhibitors of p110δ, and suggests that these two unrelated chemotypes may target the same conformationally mobile residue to achieve selectivity.

The morpholinopyranone inhibitor KU-55933 was recently reported to be a highly selective inhibitor of ATM relative to all other PI3-K family members [30]. Based on an arylmorpholine pharmacophore model, KU-55933 is predicted to bind in the ATP binding pocket, with the morpholinopyranone substituting for the chemically identical fragment from LY294002 (Figure 5.3A and Figure 5.5). The thianthrene moiety of KU-55933 is orientated orthogonal to the pyranone ring in this model in recognition of the steric penalty for placing bi-aryl substituents coplanar (estimated to be ~11 kcal/mol for this ring system using MMFF94 calculations). In this orientation, the sterically cumbersome thianthrene directly clashes with Met 804 in p110γ (Figure 5.5A). As ATM differs significantly from p110γ in sequence, we performed an alignment of the residues surrounding Met 804 for the class I PI3-Ks and PIKKs. Remarkably, this alignment reveals that Met 804 is conserved as a large hydrophobic residue in every PI3-K family member except for ATM, where this residue is instead an alanine (Figure 5.5C). This suggests an immediate structural basis for the selectivity of this compound, since the M804A substitution creates a novel pocket that can accommodate the thianthrene in KU-55933 (Figure 5.5B). A prediction of this model is that p110δ should be inhibited by KU-55933 more potently than other class I PI3-Ks, and this is indeed observed (Table 5.1). Taken together, these data argue that at least three chemotypes of selective PI3-K inhibitors achieve their selectivity by projecting a large substituent vertically toward the roof of the ATP binding pocket, where this moiety either displaces a conformationally mobile residue (PIK-39 and PIK-108) or occupies a unique pocket created by sequence variation (KU-55933).

5.8 Structures of PIK-90 and PIK-93 define features of potent, multi-targeted inhibitors

Several compounds in our panel potently inhibit multiple PI3-K family members, and we sought to understand how these inhibitors achieve high affinity, pan-specific binding. This analysis can help define the unique features of more selective compounds, and may identify general interactions that contribute to inhibitor affinity in this target class. The growing interest in multi-targeted inhibitors of protein kinases, which have shown unexpected clinical efficacy, also motivates a structural investigation of the analogous PI3-K inhibitors [33]. PIK-90 and PIK-93 are the two most potent and multi-targeted synthetic PI3-K inhibitors that have been characterized (Figure 5.1C, bottom), and we therefore determined co-crystal structures of these compounds bound to p110γ.

These structures reveal that both compounds make a hydrogen bond to the backbone amide nitrogen of Val 882, the residue that otherwise hydrogen bonds to N1 of the adenine ring in ATP (Figure 5.3A). This hydrogen bond has been observed in every PI3-K inhibitor co-crystal structure reported [28], and the absolute conservation of this interaction is reminiscent of protein kinase inhibitors, essentially all of which make a hydrogen bond to the structurally equivalent residue in protein kinases (Met 341 in c-Src). In addition to this hydrogen bond, PIK-93 makes a second hydrogen bond to the backbone carbonyl of Val 882 and a third between its sulphonamide moiety and the sidechain of Asp 964. PIK-93 is one of the most polar inhibitors in our panel (clogP = 1.69) and these extended polar interactions may compensate for its limited hydrophobic surface area. Overall, PIK-93 adopts a flat conformation in the ATP binding pocket that is characteristic of pan-specific PI3-K inhibitors (Figure 5.3C).

PIK-90 binds in a mode similar to PIK-93, although this larger compound makes more extensive hydrophobic interactions, burying 327 Å^2 of solvent accessible inhibitor surface area. To achieve this, PIK-90 projects its pyridine ring into a deeper cavity that is partially accessed by PIK-93 but not occupied by ATP (Figure 5.3A, yellow). PI-103, a third multi-targeted PI3K inhibitor, projects a phenol into the same pocket based on an arylmorpholine pharmacophore model (Figure 5.3A) Much of the hydrophobic surface of this deeper pocket is contributed by Ile 879, a residue we have argued is structurally analogous to the gatekeeper in protein kinases (Thr 338 in c-Src) [34]. In lipid kinases, this residue is conserved as a large hydrophobic amino acid, but it is shifted ~2 Å vertically to expose this deeper pocket. In addition to these hydrophobic interactions, the pyridine ring of PIK-90 is poised to make a hydrogen bond to Lys 833, and we find that replacement of this pyridine nitrogen with carbon results in a ~100-fold loss in affinity (PIK-95, Figure 5.2).

Collectively, these data suggest that potent, multi-targeted inhibitors achieve their binding, in part, through hydrophobic and polar interactions with a deeper, affinity pocket that is not accessed by ATP. A striking feature of these compounds is that they bind to the kinase active site in a uniformly flat conformation, whereas more selective compounds project out of the plane occupied by ATP (Figure 5.3C).

5.9 The role of PI3-K isoforms in insulin signaling

Insulin was one of the first stimuli shown to activate PI3-kinase [35] and the broad spectrum PI3-K inhibitors wortmannin and LY294002 block the metabolic effects of insulin in target tissues such as fat and muscle [36, 37]. Overexpression of constitutively active alleles of class I PI3-Ks is sufficient to induce membrane

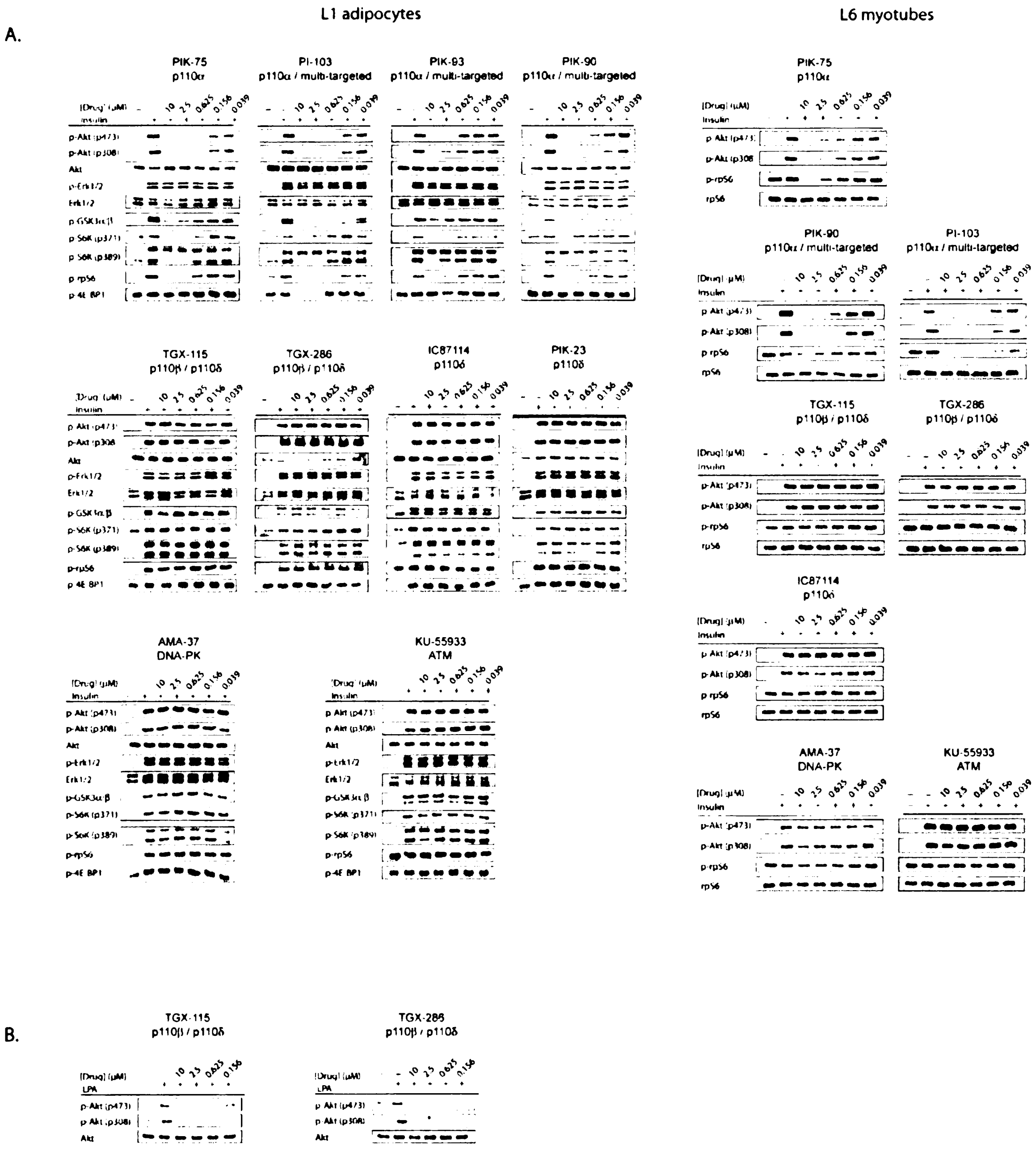
A.
L1 adipocytes
L6 myotubes
PIK-75
p110α
PI-103
p110α / multi-targeted
PIK-93
p110α / multi-targeted
PIK-90
p110α / multi-targeted
TGX-115
p110β / p110δ
TGX-286
p110β / p110δ
IC87114
p110δ
PIK-23
p110δ
AMA-37
DNA-PK
KU-55933
ATM
[Drug] (μM)
10
2.5
0.625
0.156
0.039
Insulin
p-Akt (p473)
p-Akt (p308)
Akt
p-Erk1/2
Erk1/2
p-GSK3α/β
p-S6K (p371)
p-S6K (p389)
p-rpS6
rpS6
p-4E BP1
B.
LPA

Figure 5.7. p110α is required for insulin signaling in adipocytes and myotubes. A. Western blots of lysates from adipocytes or myotubes stimulated with insulin in the presence of indicated PI3-K inhibitors. B. L6 myotubes stimulated with lysophosphatidic acid are sensitive to p110β inhibitors.

translocation of GLUT4, the primary insulin-responsive glucose transporter, and to stimulate glucose uptake in adipocytes [38-40]. In humans, a mutation in Akt2, a downstream effector of PI3-K, causes hereditary insulin resistance [41].

The critical role of PI3-K in insulin signaling raises the possibility that therapeutic use of PI3-K inhibitors may cause insulin resistance and associated morbidity. Broad spectrum pharmacological inhibition of all PI3-Ks would be predicted to block the metabolic effects of insulin, although this has not yet been demonstrated *in vivo*. It may be possible to selectively inhibit individual PI3-K isoforms without impairing glucose homeostasis, but the sensitivity of this process to pharmacological inhibition of each class I PI3-K remains to be defined. Asano and coworkers have argued that p110β is the primary insulin-responsive PI3-K in adipocytes, relying largely on adenoviral overexpression of p110 isoforms and microinjection of isoform-specific inhibitory antibodies [42]. These pioneering studies were among the first to explore signaling by PI3-K isoforms, but it remains unclear to what extent these approaches accurately anticipate the effects of small molecule inhibitors. Brachmann and coworkers have recently shown that p110α +/- or p110β +/- mice exhibit normal insulin sensitivity, whereas p110α +/- p110β +/- animals are mildly glucose intolerant and hyperinsulemic when fasted [43]. This demonstrates that deficiency in a PI3-K catalytic subunit can induce insulin resistance *in vivo*, and suggests that both p110α and p110β contribute to insulin signaling. The extrapolation of these results to pharmacological inhibitors, however, is complicated by the inability to generate viable homozygotes and a compensatory downregulation of the p85 subunit that is observed in heterozygous animals [43]. For these reasons, the key translational question with respect to insulin signaling by PI3-K – the sensitivity of this process to pharmacological inhibition of each

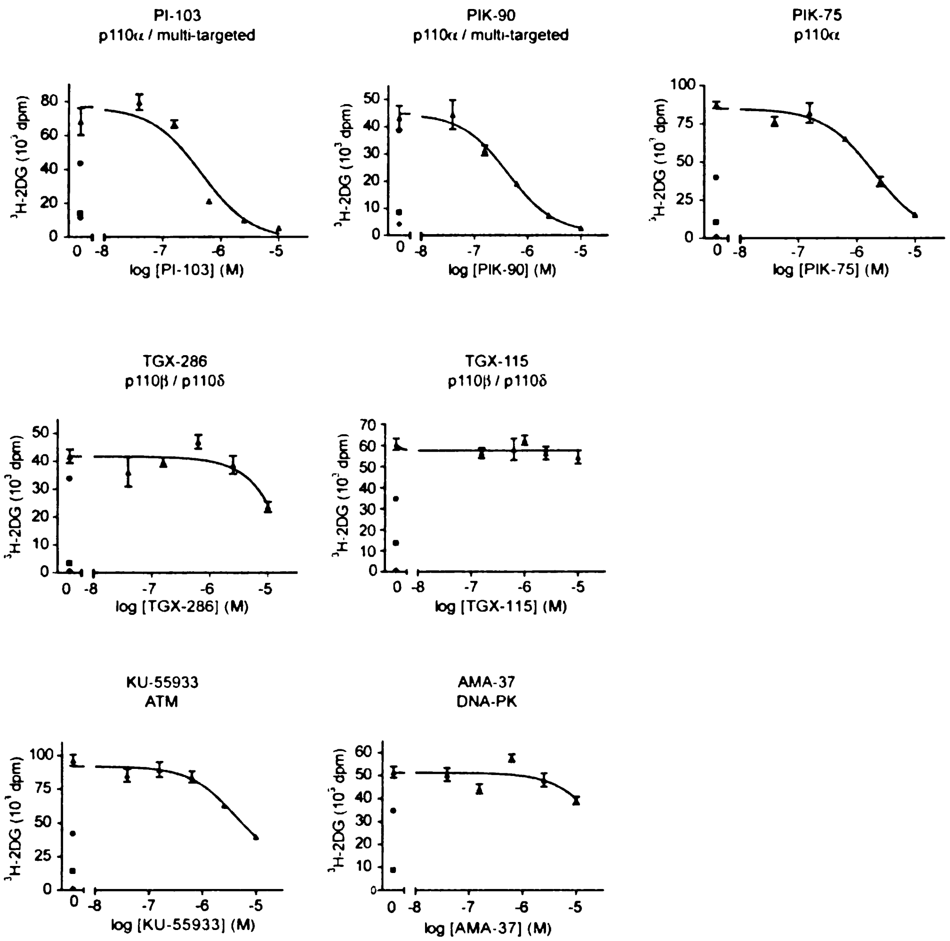

Figure 5.8. p110α is required for glucose uptake in adipocytes. Insulin-stimulated transport of ^{3}H-2-deoxyglucose into adipocytes in the presence of isoform specific PI3-K inhibitors. Triangle, insulin plus inhibitor; square, no insulin; diamond, insulin plus cytochalasin B (20 μM); circle, 1% of input ^{3}H-2-deoxyglucose.

isoform – remains unresolved. We therefore chose to examine this question using isoform-selective PI3-K inhibitors.

5.10 p110α is required for insulin signaling in adipocytes and myotubes

3T3-L1 adipocytes and L6 myotubes are widely-used model systems for studying insulin action in fat and muscle, respectively. We therefore focused initially on exploring the effects of PI3-K inhibitors in these two cell lines (Figures 5.7 and 5.8). Fully differentiated adipocytes were pretreated for thirty minutes with each inhibitor over a 250-fold concentration range (0.039 to 10 μM). These cells were then stimulated with 100 nM insulin, and probed for either the phosphorylation of downstream markers (Figure 5.7) or insulin stimulated glucose uptake (Figure 5.8). Phosphorylation of Akt (Thr 308 and Ser 473) and its putative direct substrate GSK3β (Ser 9) were monitored as proxies for PI3-K activity. Insulin also activates mTORC1, which functions to increase protein synthesis and controls a retrograde pathway leading to PI3-K inactivation [44]. As compounds in our panel may inhibit mTORC1 directly or indirectly (via PI3-K), we followed several markers that report on mTORC1 activity, including phosphorylation of its putative direct substrates 4E-BP1 (Ser 37 and Thr 46) and p70S6K (Ser 371 and Thr 389) as well as the p70S6K substrate ribosomal protein S6 (Ser 235 and Ser 236). Phosphorylation of Erk (Thr 202 and Tyr 204) was monitored as an insulin-dependent signal that typically does not require PI3-K or mTOR activity. Similar experiments focusing on a smaller set of phosphoproteins were performed in differentiated myotubes (Figure 5.7).

All compounds that inhibit p110α *in vitro* also potently block insulin-induced Akt phosphorylation in adipocytes and myotubes (Figure 5.7). This was observed for multi-targeted inhibitors such as PIK-90 and PI-103 (which inhibit p110α most potently, but also target p110β at concentrations 10 to 30-fold higher), as well as the highly selective inhibitor PIK-75, which inhibits p110α >200-fold more potently than p110β. p110α inhibitors blocked phosphorylation of GSK3β as well as the direct mTORC1 substrate p70S6K, and functional inhibition of p70S6K activation was confirmed by potent inhibition of rpS6 phosphorylation (Figure 5.7). 4E-BP1 phosphorylation, by contrast, was not insulin stimulated under these conditions, and consequently was insensitive to p110α inhibitors (Figure 5.7). Phosphorylation of this protein was inhibited only by PI-103, which is consistent with our finding that only this compound potently inhibits purified mTORC1 *in vitro* (Table 5.1), These biochemical results were recapitulated in a functional assay for insulin stimulated glucose uptake. PIK-75, PIK-90, and PI-103 all blocked glucose uptake by adipocytes over the same concentration range that they inhibited Akt phosphorylation (Figure 5.8).

Surprisingly, inhibitors of p110β (TGX-115 and TGX-286) and p110δ (PIK-23 and IC87114) had no effect on the phosphorylation status of any protein in the pathway, indicating that these isoforms are not required for insulin signaling in these two cell types (Figure 5.7). TGX-115 also failed to block glucose uptake by adipocytes, whereas TGX-286 had a small effect at the highest dose (Figure 5.8); we attribute this weak activity of TGX-286 to p110α inhibition at high concentrations, as this compound is less selective than TGX-115 (Table 5.1). TGX-115 and TGX-286 effectively block Akt phosphorylation in several cell types that rely on signaling by p110β or p110δ (Z.A.K. and K.M.S., submitted and unpublished data), indicating that the lack of effect observed here does not reflect a trivial defect in the cell permeability or potency of these inhibitors. Moreover, TGX-115 and TGX-286 potently inhibit Akt phosphorylation in L6 myotubes stimulated with lysophosphatidic acid (LPA), a stimulus which has previously been reported to be dependent on p110β (Figure 5.7B). Taken together, this data argues that

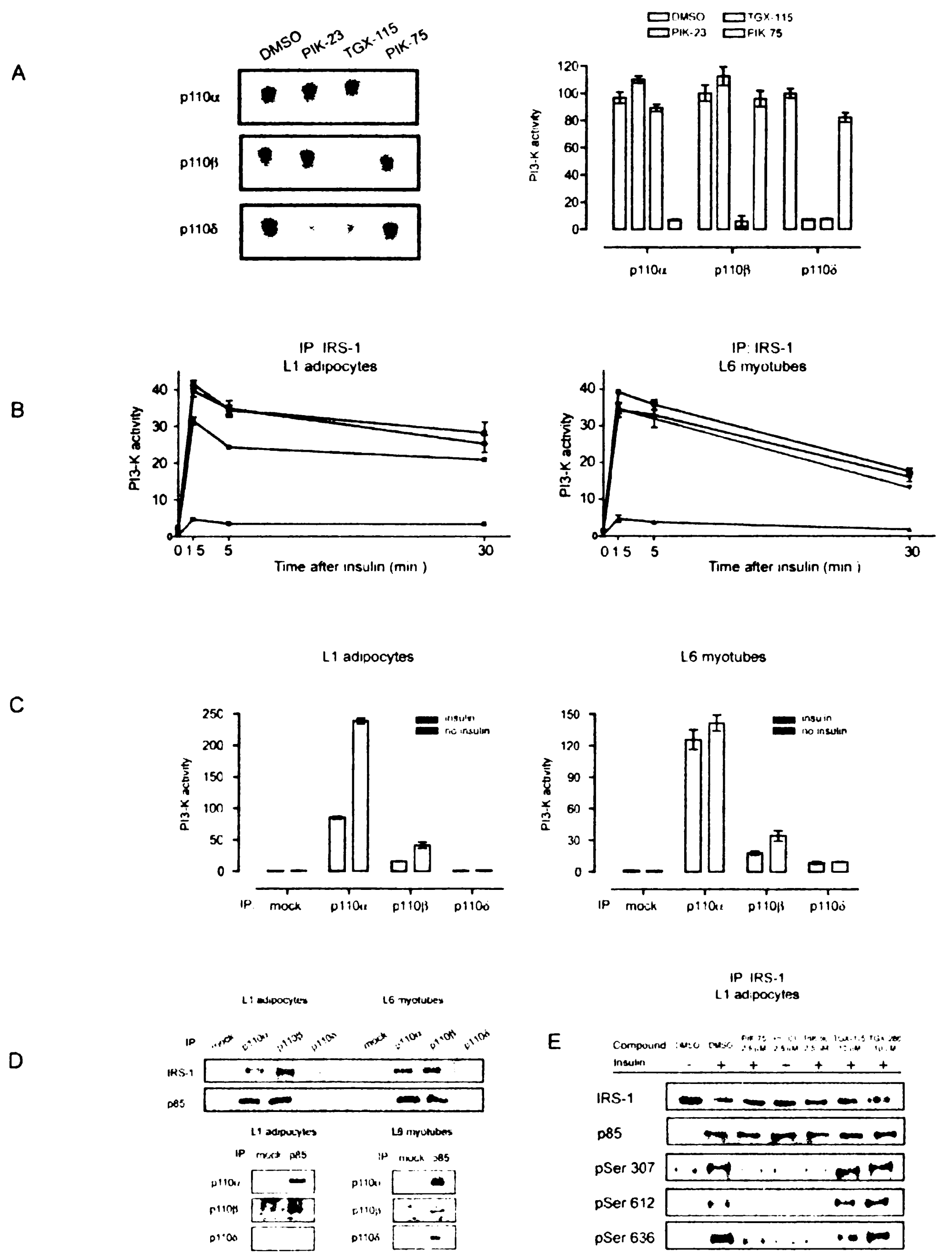

Figure 5.9. p110α is the dominant PI3-K activity associated with the IRS-1 complex. A. Inhibition of recombinant class I PI3-Ks by PIK-23 (1.5 μM), TGX-115 (1.5 μM), and PIK-75 (0.05 μM) *in vitro* in the presence of 10 μM ATP. B. PI3-K activity from IRS-1 immunoprecipitates at 1.5, 5, and 30 minutes after insulin stimulation (100 nM). C. PI3-K activity from immunoprecipitates of class IA enzymes with and without insulin stimulation (100 nM, 90 s). D. Top. Blot for IRS-1 from immunoprecipitates of each class IA PI3-K. Bottom. Blot for class IA PI3-Ks from immunoprecipitates of p85. E. Blot for IRS-1, p85, and phosphorylation of Ser 307, 612, or 636 from IRS-1 immunoprecipitates from adipocytes treated with 100 nM insulin for 30 minutes.

the kinase activity of p110α, but not p110β or p110δ, is required for insulin signaling in adipocytes and myotubes.

5.11 DNA-PK and ATM are dispensable for Akt activation

Several compounds in our panel inhibit PI3-kinase related protein kinases, either as their primary target (KU-55933 and AMA-37) or as a secondary target to PI3-K inhibition. We therefore investigated how inhibition of these kinases affects insulin signaling.

The arylmorpholine AMA-37 is a selective inhibitor of DNA-PK *in vitro* (Table 5.1) and in cells (Z.A.K. and K.M.S., submitted). Treatment of adipocytes or myotubes with this compound had no effect on the insulin-stimulated phosphorylation of any protein monitored (Figure 5.7). Treatment of these cells with the ATM selective inhibitor KU-55933 had a small effect on the phosphorylation of p70S6K at the highest dose, and no effect on the phosphorylation of any other target (Figure 5.7). Inhibition of p70S6K phosphorylation was observed only at 10 μM, which is ~50-fold higher than the concentration required to block ATM-mediated p53 phosphorylation by this compound [30], arguing that this is an off-target effect. These data suggest that inhibition of DNA-PK or ATM is unlikely to contribute to the activity of compounds in our panel, and do not support a recently proposed role for these two kinases in controlling phosphorylation of the Akt hydrophobic motif (Ser 473) in response to insulin [45, 46].

Consistent with its failure to block Akt phosphorylation, AMA-37 had no effect on glucose uptake (Figure 5.8). At higher concentrations, KU-55933 inhibited glucose transport in adipocytes (Figure 5.8) and myotubes (data not shown). Although the mechanistic basis for this activity is unclear, it is intriguing that insulin resistance is a hallmark of A-T (the genetic disease caused by ATM inactivation), and these results may reflect a defect in acute insulin signaling caused by a lack of ATM kinase activity.

5.12 p110α is the primary lipid kinase in the IRS-1 complex

PI3-K is recruited to the insulin receptor and activated by the insulin receptor substrate (IRS) proteins, which present tyrosine phosphorylated docking sites for the p85 regulatory subunit [47]. The IRS-1 complex is critical for insulin stimulated PI3-K activity, and degradation of this protein through a PI3-K dependent retrograde pathway causes insulin resistance [48]. We therefore analyzed the activity of PI3-K isoforms in the IRS-1 complex from adipocytes and myotubes.

An assay was developed to quantitate the contribution of each class I PI3-K isoform to the total PI3-K activity present in protein complexes that may contain multiple lipid kinases (Figure 5). This assays relies on the ability of three compounds in our chemical panel (PIK-23, TGX-115, and PIK-75) to inhibit greater than 90% of the activity of their primary target, with minimal inhibition of the other class I PI3-Ks, at a selected concentration of drug *in vitro* (Figure 5.9A). Adipocytes and myotubes were stimulated with 100 nM insulin for the indicated times, IRS-1 was immunoprecipitated from lysates of these cells, and immunocomplexes were subjected to an *in vitro* PI3-K assay (Figure 5.9B). IRS-1 associated PI3-K activity increased 20 to 40-fold within 90 seconds of insulin stimulation in each cell type, and then gradually declined over 30 minutes (Figure 5.9B, blue). Treatment with the p110α inhibitor PIK-75 dramatically reduced the overall level of PI3-K activity in immunoprecipitates from both cells (Figure 5.9B, green). By contrast, the p110β/p110δ inhibitor TGX-115 reduced IRS-1 associated PI3-K activity in adipocytes by ~25% and in myotubes by ~10% (Figure 5.9B, red line). The p110δ inhibitor PIK-23 had no effect on IRS-1 associated PI3-K activity from adipocytes, and a very small effect on IRS-1 from myotubes (Figure 5.9B, black). Taken together, these data identify p110α as the dominant lipid kinase activity associated with IRS-1, and support our finding that this isoform is the most important for insulin signaling in intact cells.

We next asked how the relative activity of PI3-K isoforms in the IRS-1 complex compares to the total activity of each isoform in these cells. p110α, p110β or p110δ was immunoprecipitated from each cell type, with or without prior insulin stimulation (90 seconds), and these immunoprecipitates were subjected to a lipid kinase assay. PI3-K activity was detected in immunoprecipitates of p110α and p110β from adipocytes, and for all three isoforms from myotubes (Figure 5.9C). Consistent with these results, western blotting confirmed that p110α and p110β are expressed in adipocytes, whereas all three isoforms are expressed in myotubes (Figure 5.9D). The activity of p110α and p110β was increased by insulin treatment in both cells, but the magnitude of this increase was significantly greater in adipocytes than myotubes (Figure 5.9C). Strikingly, the amount of total p110α, p110β, and p110δ activity from each cell type closely mirrors the relative activities of these kinases in the IRS-1 complex, with p110α representing the dominant lipid kinase activity in both cases (Figure 5.9B). As each isoform is immunoprecipitated with different antisera, however, the absolute amounts of PI3-K activity in each immunoprecipitate may not be directly comparable.

PI3-K also controls a retrograde signaling pathway which leads to the phosphorylation of IRS-1 on serine residues that target this protein for degradation [48]. We therefore asked which PI3-K isoform is required for serine phosphorylation of IRS-1. Adipocytes were pretreated with isoform-specific inhibitors and then stimulated with insulin for 30 minutes. IRS-1 was immunoprecipitated from lysates of these cells and blotted for phosphorylation of three key residues (Ser 307, Ser 612, and Ser 632).

Phosphorylation of these serine residues is insulin-stimulated, wortmannin-sensitive, and promotes IRS-1 inactivation, indicating that these are major sites of negative regulation under the control of the PI3-K pathway [48, 49]. We find that inhibitors of p110α, but not inhibitors of p110β/p110δ, abolish the phosphorylation of these residues (Figure 5.9E). This indicates that the kinase activity of p110α, but not p110β or p110δ, is required for the retrograde as well as positive signaling pathways induced by insulin.

5.13 p110β/p110δ sets a phenotypic threshold for p110α activity in myotubes, but not adipocytes

These data demonstrate that p110α is the dominant PI3-K activity driving insulin signaling in L1 adipocytes and L6 myotubes. However, it is clear that p110β and, to a lesser extent, p110δ, are expressed in these cells and activated by insulin (Figure 5.9). In this context, it is surprising that selective inhibition of these isoforms has little effect on insulin signal transduction. One explanation for this finding is that p110β and p110δ perform a subsidiary role to p110α, by contributing a pool of PIP_3 which is not independently required for Akt phosphorylation, but which defines a threshold for the amount of p110α activity necessary to activate the pathway. A prediction of this model is that inhibition of p110β/p110δ should shift the amount of p110α activity required to activate Akt and other downstream effectors.

We tested this hypothesis by measuring the effect of the p110β/p110δ inhibitor TGX-115 on the ability of the p110α inhibitor PIK-75 to block Akt phosphorylation at Thr 308. TGX-115 alone at a concentration of up to 10 μM had no effect on Thr 308 phosphorylation in either adipocytes or myotubes (Figure 5.10, black). PIK-75 alone blocked Thr 308 phosphorylation in these two cell types with IC_{50} values of 1.2 and 1.3 μM, respectively (Figure 5.10, blue). When PIK-75 was tested in the presence of 10 μM

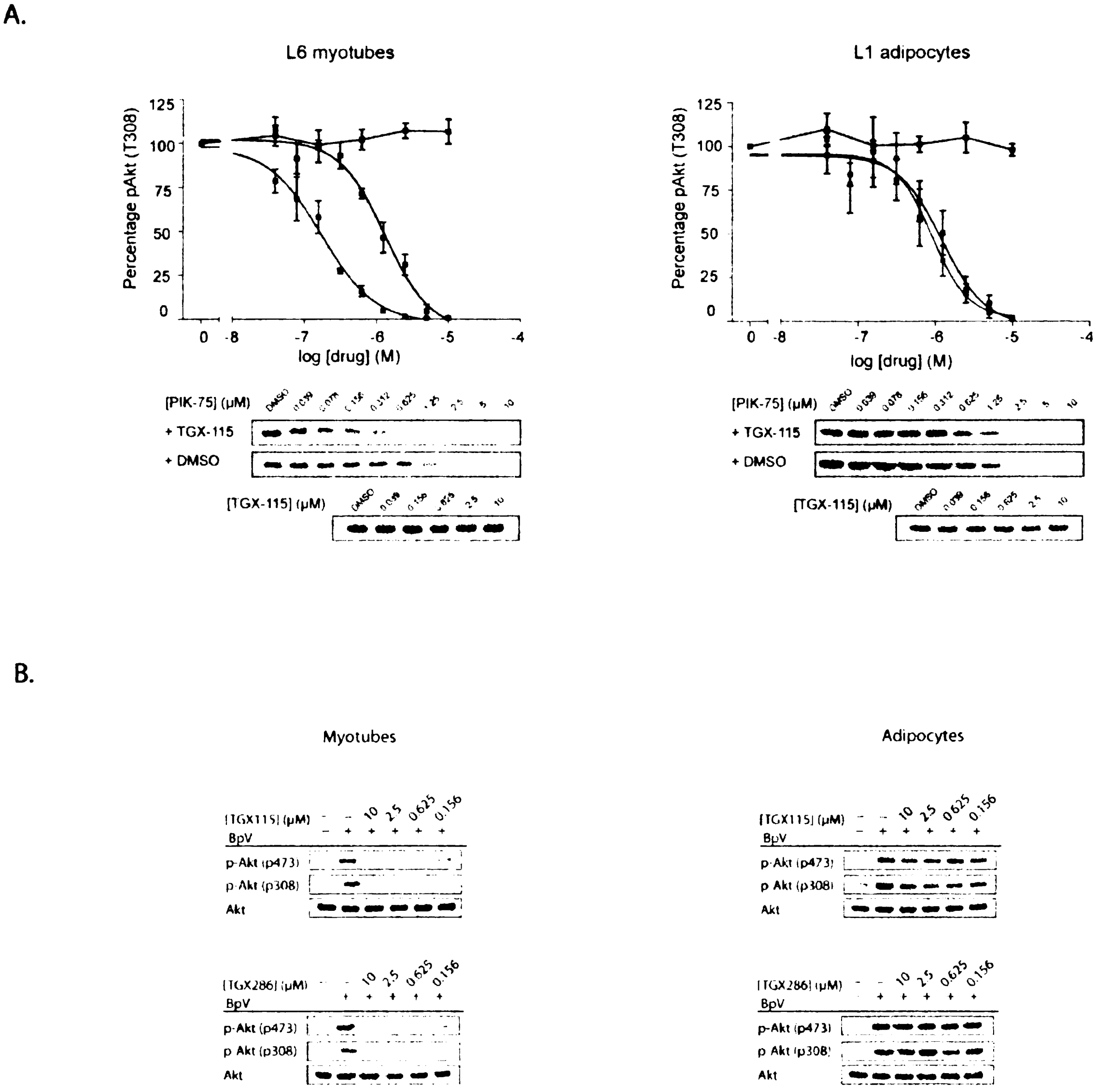

Figure 5.10. p110β sets a threshold for p110α activity in myotubes, but not adipocytes. A. Dose response for inhibition of Akt Thr 308 phosphorylation in response to TGX-115 (black), PIK-75 alone (blue), or PIK-75 + 10 μM TGX-115 (red). B. p110β inhibitors block Akt phosphorylation due to acute inhibition of PTEN in myotubes, but not adipocytes.

TGX-115, the dose response in myotubes shifted to ~8-fold lower concentrations (IC_{50} = 0.17 μM). By contrast, a significant shift was not observed in adipocytes (Figure 5.10A, red). This data supports a model in which inhibition of p110β/p110δ in myotubes increases the amount of p110α activity that is required for Akt phosphorylation. The change in this phenotypic threshold is then detected in our assay as a shift in the dose response curve for the p110α inhibitor PIK-75.

One explanation for the PIK-75 dose shift observed in myotubes in the presence of TGX-115 is that p110β controls the synthesis of a basal pool of PIP_3 that is not growth factor regulated. If this is the case, then it should be possible to unmask this basal PIP_3 synthesis through acute inhibition of the lipid phosphatase PTEN. We tested this hypothesis by treating adipocytes or myotubes with the PTEN inhibitor bis-peroxyvanadium and monitoring the sensitivity of the rapidly induced Akt phosphorylation to p110β inhibitors (Figure 5.10B). This analysis reveals that Akt phosphorylation in myotubes is highly sensitive to p110β inhibitors, whereas Akt phosphorylation in adipocytes is resistant. This supports a model in which p110β contributes to a basal pool of PIP_3 in myotubes, but not adipocytes.

5.14 p110α inhibitors, but not p110β/p110δ inhibitors, block the acute effects of insulin on blood glucose in mice

We next asked whether the critical role for p110α in insulin signaling that we observe in cell culture is recapitulated *in vivo* by testing the insulin tolerance of mice treated with isoform-specific inhibitors. Four month old FVB/N female mice (n=5) were fasted at 9:00 a.m. and injected intravenously at 12:30 p.m. on the same day with either insulin or vehicle (PBS). Immediately following insulin injection animals were treated intraperitoneally with either PI-103 (10 mg/kg), PIK-90 (10 mg/kg), TGX-115 (10 mg/kg),

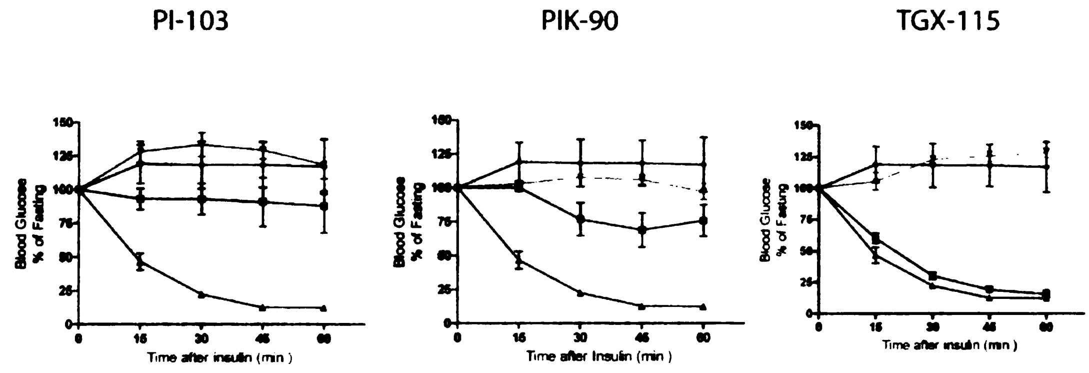
PI-103

PIK-90

TGX-115

Figure 5.11. PI-103 and PIK-90, but not TGX-115, induces acute insulin resistance in mice. Green: drug in 50% DMSO plus insulin vehicle (PBS). Black: drug vehicle (50% DMSO) plus insulin vehicle (PBS). Red: insulin (0.75 U/kg) plus drug vehicle (50% DMSO). Blue: drug in 50% DMSO plus insulin (0.75 U/kg).

or vehicle (50% DMSO), and blood glucose levels were monitored at 15 minute intervals for one hour (Figure 5.11).

Treatment with drug alone (Figure 5.11, green) or vehicle alone (Figure 5.11, black) induced a small increase in blood glucose that likely reflects a stress response to injection. Treatment with insulin plus the drug vehicle caused blood glucose levels to sharply decline by 80% over one hour (Figure 5.11, red). By contrast, treatment with either of the p110α inhibitors (PI-103 or PIK-90) abolished the effects of insulin treatment on blood glucose (Figure 5.11, blue). This is the first demonstration that pharmacological inhibition of PI3-K can induce insulin resistance *in vivo*. In contrast to p110α inhibitors, the p110β inhibitor TGX-115 had no effect on the insulin-induced decrease in blood glucose (Figure 5.11, blue). These data are consistent with our results from cell based experiments which argue that inhibition of p110α, but not p110β and p110δ, is required to block the metabolic effects of insulin.

5.15 Discussion

PI3-K inhibitors are likely to follow protein kinase inhibitors as the next major class of targeted drugs. In contrast to protein kinases, however, the structural basis for potent, selective PI3-K inhibition remains largely unknown. It is likewise an open question which PI3-Ks should be targeted for many diseases, which biomarkers will be predictive of these targets, and to what extent different PI3-K isoforms can be inhibited without impairing normal physiology. These uncertainties reflect the unique challenges facing target validation for this family of enzymes, which are coordinatively regulated and control complex biology. As distinct PI3-K isoforms are often recruited to the same protein complex where they phosphorylate the same substrate, quantitative differences in localization, timing, and thresholds of catalytic activity are likely to be critical in defining the phenotypic consequences of inhibiting different isoforms.

Addressing these questions will require a systematic re-interpretation of PI3-K signaling according to its sensitivity to pharmacological inhibitors with defined isoform-selectivities. Toward this goal, we report here the biochemical and structural analysis of a panel of potent, chemically diverse, and isoform-selective inhibitors of the PI3-K family. This family-wide selectivity analysis provides the first global view of how different PI3-K family members interact with chemically distinct inhibitors and reveals trends in SAR homology that will inform future efforts to target these enzymes with small molecules. As this chemical array includes representatives from a large number of chemotypes currently in preclinical development, these compounds preview the target selectivities, and therefore biological activities, of eventual clinical candidates.

The crystal structure of PIK-39 provides the first structural rationale for selective inhibition of a lipid kinase, based on the identification of an active site residue (Met 804) that undergoes an inhibitor-induced conformational rearrangement to create a novel pocket. Modeling suggests that at least two additional chemotypes of selective PI3-K inhibitors exploit this same residue to distinguish between isoforms. As the first crystal structures of selective protein kinase inhibitors informed efforts to design inhibitors that target the gatekeeper pocket [50] or the inactive conformation [31], it is likely that the structural analysis reported here will guide the design of PI3-K inhibitors that target this conformationally mobile region. Alternative mechanisms of inhibitor selectivity are likely to be important for other family members. As this manuscript was being submitted, the structure of a novel inhibitor with selectivity for p110γ was reported [11]. This crystal structure may assist in the design of selective p110γ inhibitors, although the structural features that control the isoform-selectivity of this compound have not been described.

The key role of PI3-K in insulin signaling is an unresolved concern for the therapeutic development of PI3-K inhibitors, and we therefore used this chemical array to explore the sensitivity of this process to pharmacological inhibition of different PI3-Ks. This analysis identifies p110α as the critical lipid kinase required for insulin signaling in two key cell types, adipocytes and myotubes. By contrast, p110β and p110δ are largely dispensable in these cells. p110β and p110δ are being actively pursued as targets for the treatment of thrombosis and inflammation, respectively, and our results suggest that insulin resistance is less likely to be associated with drugs that inhibit these enzymes. Insulin resistance is a larger concern for p110α inhibitors, although it is important to emphasize that we have focused in this report only on the effects of acute insulin treatment. As glucose homeostasis involves complex and adaptable signaling across tissues, it will be important to investigate the effects of chronic inhibitor treatment *in vivo*, and correlate these effects with the detailed target selectivity, dosing regimen, and pharmacokinetics of different inhibitors. Long term treatment with PI-103 at doses sufficient to block the growth of xenografted tumors does not induce obvious morbidity due to insulin resistance (such as weight loss), although the basis for this observation is still under investigation (Z.A.K, W.A.W. and K.M.S., submitted and unpublished data). Likewise, we have focused on target tissues such as fat and muscle that control glucose clearance from the blood, but insulin-regulated glucose release from hepatic tissue is also a critical metabolic effect of this hormone and the PI3-K inhibitor sensitivity of this process remains unexplored. These questions are beyond the scope of this report, but can begin to be addressed using the chemical array we describe.

Translating our detailed knowledge of signal transduction into effective targeted therapies is a key challenge for biomedical research. Pharmacology will play an important role in meeting this challenge, not least because small molecules often induce emergent phenotypes that cannot be anticipated from the isolated study of their targets [21]. We have described here a novel approach for pharmacological target validation, based on the parallel evaluation of chemically diverse inhibitors whose targets span a protein family, and the correlation of the activity of these compounds with their detailed biochemical target selectivity. This family-wide approach can define new functions for individual proteins, but is also uniquely poised to expose latent antagonism or cooperativity between targets within an enzyme class. Such multiplex activity underlies many of the most clinically successful protein kinase inhibitors [33], and we have observed similar cooperativity within the PI3-K family (Z.A.K., W.A.W., and K.M.S., submitted). The comprehensive elucidation of these types of interactions would yield a pharmacological map of signal transduction, thereby guiding progress toward more effective targeted therapies.

5.16 Summary of experimental procedures

5.16.1 Cell Culture

3T3-L1 fibroblasts were differentiated to adipocytes essentially as described [51]. Adipocytes were used between 5 and 25 days post-differentiation and in all cases >95% of cells were differentiated. L6 myoblasts were differentiated to myotubes by allowing the cells to grow to confluence and then culturing in low serum (2% FBS) containing media for 5 days.

5.16.2 Synthesis and biochemical characterization of PI3-K inhibitors

PI3-K inhibitors were synthesized following published patent specifications (WO 01/53266, 01/81346, 01/083456, 01/83481, 02/20500, 03/072557, 03/070726, 04/052373, 04/029055). See Supplemental Experimental Procedures for details.

Kinases were expressed, purified, and subjected to an *in vitro* kinase assay to determine IC_{50} values for each inhibitor. See Supplementary Experimental Procedures for details.

5.16.3 Determination of p110γ crystal structures

Recombinant human p110γ (residues 144-1102, with a His_6 tag directly fused to the C-terminus) was purified from baculovirus-infected Sf9 cells. Crystals were grown at 17 ºC using sitting-drop vapour-diffusion, and these crystals were soaked with inhibitor. Diffraction data was collected at ESRF ID14-4. Data collection and refinement statistics are summarised in Table 5.3. See Supplementary Experimental Procedures for details of protein purification, crystallization, and structure determination.

5.16.4 PI3-K pathway western blotting

Fully differentiated adipocytes or myotubes were serum starved overnight, and pre-incubated with inhibitor at the indicated concentration for 30 minutes. Cells were then stimulated with insulin (100 nM) for 5 minutes and lysed in RIPA buffer. These lysates were resolved by SDS-PAGE, transferred to nitrocellulose, and analyzed by western blotting.

5.16.5 Glucose Uptake

Glucose uptake in adipocytes was measured essentially as described [51]. Adipocytes in 12-well plates were serum starved for 3 h and then incubated in PBS with compound or vehicle (0.1% DMSO) for 30 min., at which point cells were stimulated with insulin (100 nM). 15 min. following insulin stimulation 100 μM (^{3}H)-2-deoxyglucose (1μCi/mL) was added and uptake was allowed to proceed for 15 min. Adipocytes were then washed three times with ice cold PBS, dissolved in 0.1% SDS, and the internalized radioactivity was measured by scintillation counting.

5.16.6 IRS-1 assays

Differentiated adipocytes or myotubes were serum starved overnight, stimulated with 100 nM insulin for 1.5, 5 or 30 minutes, and then placed on ice. Cells were lysed in RIPA buffer and then immunoprecipitated for 2 hours using protein G loaded with IRS-1 antisera (IM92-7, Upstate). Immunoprecipitates were washed twice with lysis buffer, once with high salt buffer (500 mM NaCl, 50 mM Tris, pH 7.4), and then three times with PBS. 5 μL of protein G beads from each immunoprecipitate were then aliquoted to each of 12 tubes containing kinase buffer (25 mM HEPES, pH 7.4, 10 mM $MgCl_2$), substrate (PI: 0.1 mg/mL), and either inhibitor or DMSO. The final inhibitor concentrations were 1.5 μM (PIK-23 and TGX-115) or 0.05 μM (PIK-75) and the final DMSO concentration was 2%. Kinase reactions were initiated by the addition of (γ–^{32}P)-ATP to a final concentration of 10 μM in a total volume of 50 μL. Reactions were stopped after 20 minutes by the addition 100 μL 1N HCl, followed by 160 μL 1:1 $CHCl_3$:MeOH. The organic phase was extracted and loaded onto TLC plates, which were developed for three hours in 65:35 n-propanol:2M acetic acid and the radiolabelled PI(3)P was quantitated by phosphorimaging.

Immunocomplex kinase assays for the p110 catalytic subunits (Figure 5.9C) were performed essentially as described above, except that antisera against p110α (Santa Cruz), p110β (Upstate) or p110δ (Santa Cruz) was used; cells were stimulated with insulin for only 1.5 min; and no inhibitors were added to the lipid kinase assay.

5.16.7 Insulin tolerance tests

4 month old FVB/N female mice (n=5) were fasted at 9:00 a.m. and injected intravenously at 1:00 p.m. on the same day with human insulin (Sigma - 0.75 U/kg). Immediately following insulin injection mice were treated intraperitoneally with inhibitor in 50% DMSO, and blood glucose level was measured with an Accu-Check Active glucose meter at 0, 15, 30, 45, and 60 min after insulin injection. Data for each time point was averaged and the standard error of the mean was calculated.

5.18 Experimental procedures

5.18.1 Reagents

All antibodies were from Cell Signaling with the following exceptions: antibodies against IRS-1, IRS-1 (p307), p110β (IP), and p110δ (WB) were from Upstate; antibodies against p85α, p110α (IP), p110β (WB) and p110δ (IP) were from Santa Cruz; an ATM antibody was from Calbiochem and an ATR antibody was from Novus Biological.

5.18.2 Principle component analysis

For a general description of principle component analysis, see [52]

An alignment of the catalytic domains of human PI3-kinase family members was obtained from Pfam [53]. Clustal W was used to generate a pairwise distance matrix from the Pfam multiple alignment. Principle components were calculated from the pairwise distance matrix using Matlab's principle component analysis function. The first three principle components were used as the x, y and color axes respectively.

A table of the log IC_{50} values of all compounds against all kinases was input into Matlab's principle component analysis function. To compute principle components describing the relationships between the kinases based on how potently they are inhibited by each compound, the IC_{50} table was oriented with kinases as rows and compounds as columns. The table was transposed in order to locate compounds in principle component space based on how potently they inhibit each kinase.

5.18.3 Expression and assay of p110α/p85α, p110β/p85α, p110δ/p85α, and p110γ

The class I PI3-Ks were either purchased (p110α/p85α, p110β/p85α, p110δ/p85α from Upstate, and p110γ from Sigma) or expressed as previously described [9]. IC_{50} values were measured using either a standard TLC assay for lipid kinase activity (described below) or a high-throughput membrane capture assay (Z.A.K. and K.M.S., manuscript in preparation). Kinase reactions were performed by preparing a reaction mixture containing kinase, inhibitor (2% DMSO final concentration), buffer (25 mM HEPES, pH 7.4, 10 mM $MgCl_2$), and freshly sonicated phosphatidylinositol (100 μg/ml). Reactions were initiated by the addition of ATP containing 10 μCi of γ-32P-ATP to a final concentration 10 or 100 μM, as indicated in Table 5.1, and allowed to proceed for 5 minutes at room temperature. For TLC analysis, reactions were then terminated by the addition of 105 μl 1N HCl followed by 160 μl $CHCl_3$:MeOH (1:1). The biphasic mixture was vortexed, briefly centrifuged, and the organic phase transferred to a new tube using a gel loading pipette tip precoated with $CHCl_3$. This extract was spotted on TLC plates and developed for 3 – 4 hours in a 65:35 solution of n-propanol:1M acetic acid. The TLC plates were then dried, exposed to a phosphorimager screen (Storm, Amersham), and quantitated. For each compound, kinase activity was measured at 10 – 12 inhibitor concentrations representing two-fold dilutions from the highest concentration tested (typically, 200 μM). For compounds showing significant activity, IC_{50} determinations were repeated two to four times, and the reported value is the average of these independent measurements.

5.18.4 Expression and assay of PI3KC2α, PI3KC2β, PI3KC2γ

HEK-293 cells were transiently transfected (Lipofectamine 2000) with plasmids encoding EE-PI3KC2α, EE-PI3KC2β, and V5-PI3KC2γ. 48 hours after transfection, cells were collected by trypsinization and the pellets were stored at -80° C. Cells were lysed in lysis buffer (50 mM Tris (pH 7.4), 300 mM NaCl, 5 mM EDTA, 0.02% NaN_3, 1% Triton X-100, and protease inhibitors) and the kinase immunoprecipitated with the appropriate antibody-protein G complex for 2 – 4 hours at 4º C. Immunoprecipitates were washed twice with wash buffer 1 (PBS, 1 mM EDTA, 1% Triton X-100), twice with wash buffer 2 (100 mM Tris (pH 7.4), 500 mM LiCl, 1 mM EDTA), and twice with wash buffer 3 (50 mM Tris (pH 7.4), 100 mM NaCl). Kinase reactions were performed essentially as described for the class I PI3-Ks.

5.18.5 Expression and assay of hsVPS34

The full-length human Vps34p was cloned into pGEX-6P-3 plasmid with the restriction enzymes *Eco*RI/*Not*I. After IPTG induction (200 μM, 6 h at 18º C) the recombinant fusion protein was isolated from the bacterial lysates using glutathione-agarose chromatography. The untagged enzymes were produced by cleavage of the recombinant protein with either TEV or PreScission protease.

Kinase reactions were performed essentially as described for the class I PI3-Ks except that the following kinase assay buffer was used: 50 mM Tris, pH 8.0, 20 mM $MnCl_2$.

5.18.6 Expression and assay of PI4KIIα PI4KIIIα, and PI4KIIIβ

The full length bovine PI4KIIIβ was cloned into the pGEX-6P-3 plasmid with the restriction enzymes BamHI/NotI. A truncated minimally catalytically active GST-PI4KIIIα (residues 873- 2044 of the bovine protein) and the GST-PI4KIIα (human) were subcloned into a pET23b(+) plasmid using NdeI/NotI restriction enzyme sites. In all GST-constructs a TEV protease site was introduced in addition to the PreScission protease site.

After IPTG induction (30-200 μM, 6 h at 18º C) the recombinant fusion proteins were isolated from the bacterial lysates using glutathione-agarose chromatography. The untagged enzymes were produced by cleavage of the recombinant protein with either TEV or PreScission protease.

Kinase reactions were performed essentially as described for the class I PI3-Ks except that the following kinase assay buffer was used: 50 mM Tris, pH 7.4, 20 mM $MgCl_2$, and 0.4% Triton X-100.

5.18.7 Expression and Assay of ATM and ATR

Pelleted K562a cells (National Cell Culture Center) were stored at -80° C. Cells were thawed, and lysis buffer was added to ~5 mg/mL. For ATM, the lysis buffer was 50mM Tris-Hcl pH 7.4, 100 mM NaCl, 50 mM beta-glycerophosphate, 10% glycerol (w/v), 1% Tween-20 (w/v), 1 mM EDTA. For ATR, the lysis buffer was 25 mM HEPES pH 7.4, 300 mM NaCl 0.5% NP-40, 1.5 mM EGTA, 1 mM $MgCl_2$. Both lysis buffers were supplemented with protease and phosphatase inhibitors.

1.5 mL aliquots of lysates were centrifuged at 16,000 x g for 10 minutes at 4° C. The supernatants were transferred to a new tube, anti-PIKK antibody was added to a concentration of ~2 μg per mg of total lysate protein, and immunoprecipitations was allowed to proceed overnight at 4° C. Antibodies used were Ab-3 (Calbiochem) for ATM and ab2905 (Novus Biological) for ATR.

Protein A agarose beads incubated with 1% BSA in PBS overnight at 4° C. Beads were rinsed two times with 0.75 mL PBS, the immunoprecitates were added to ~100 μL of protein A-agarose slurry, and these were incubated overnight at 4° C. Beads were then rinsed three times with lysis buffer, once with high salt buffer (100 mM Tris-HCl pH 7.4 500 mM LiCl), once with wash buffer (10 mM HEPES pH 7.4, 50 mM NaCl, 50 mM beta-glycerophosphate, 10% glycerol (w/v)), and once with assay buffer (10 mM HEPES pH 7.4 50 mM NaCl, 50 mM beta-glycerophosphate, 10% glycerol (w/v), 10 mM $MnCl_2$, 1 mM DTT). Beads were resuspended in assay buffer, and 30 μL of bead suspension was aliquoted to each tube. 10 μL of a mix of peptide substrate (100 μM final concentration) and inhibitor (2% DMSO final concentration) was then added to each tube. For ATR, the Rad17-derived peptide ASELPASQPQPFSAKKK was used; for ATM, the p53-derived peptide AEPPLSQEAFAGGKKK was used. Reactions were initiated by adding 10 μL of (γ–^{32}P)-ATP to a final concentration of 10 μM. Reactions were terminated by spotting onto phosphocellulose disks and allowing to dry to 5-10 minutes. Disks were rinsed once with 10% acetic acid (5 min), six times with 0.5% phosphoric acid (5 min), and once with acetone (1 min). Disks were then allowed to dry, and the radioactivity was measured by scintillation counting.

5.18.8 Expression and Assay of DNA-PK

DNA-PK was purchased (Promega) and assay according to the manufacturer's instructions using a biotinylated p53 derived peptide.

5.18.9 Expression and Assay of mTORC1 and mTORC2

mTORC1 and mTORC2 were respectively precipitated with anti-raptor and anti-mAVO3 antisera from HEK293T protein extract as described [54]. Kinase assays were performed in a final volume of 30 μL containing 1 μg PHAS-I (Stratagene, mTORC1 assays) or 250 ng of recombinant MmPKBβ (purified from *E. coli*, mTORC2 assays), 120 mM NaCl, 40 mM HEPES pH 7, 0.3% CHAPS, 4 mM $MnCl_2$, 10 mM DTT, 1X Roche inhibitor cocktail – EDTA, 2 μg/mL heparin, 100 μM ATP, 2 μCi γ-^{32}P ATP (mTORC1 assays only), 0.83% DMSO and inhibitors at various concentrations. All assay points were done in triplicate. Assays were started with addition of ATP, maintained at 30°C (mTORC1) or 37°C (mTORC2) for 5 minutes and terminated with the addition of 8 μL of 5X SDS-PAGE sample buffer. Proteins were resolved by SDS-PAGE: relative mTORC1 activity was assessed by determining ^{32}P labeling of PHAS-I; relative mTORC2 activity was assessed after transfer of proteins to nitrocellulose membrane and blotting with monoclonal anti-phospho-AKT (Ser473) antibody (Cell Signaling Technology). Signals were quantified using Quantity One software (BioRad).

5.18.10 Expression and assay of PIPK1α, PIPKIβ, and PIPKIIβ

PIPKIIβ was a kind gift of James Hurley. Constructs encoding GST-PIPK1α or GST-PIPKIβ were transformed into BL21(DE3) cells. A 500 mL culture of these cells was grown to an O.D. of 0.6 at 37° C, and protein expression was induced by adding IPTG to a final concentration of 200 μM. Cells were then grown for an additional 4.5 hours at 37° C. These cells were then collected by centrifugation, and the pellets were stored at - 80° C.

Cell pellets were thawed, resuspended in 20 mL lysis buffer (20 mM Tris, pH 7.4 1 mM EDTA, 150 mM NaCl, 1 mg/ml lysozyme, and 5 mM DTT), and lysed using a probe sonicator. Triton X-100 was added to a final concentration of 1%, and lysates were clarified by centrifugation for 10 minutes at 15,000 rpm. Lysates were further clarified by passing through a 0.45 μm syringe filter. Kinases were then purified by glutathione chromatography using a GST-Trap column (Amersham). Eluents were diluted to 50% glycerol and stored at -80° C.

Kinase reactions were performed essentially as described for the class I PI3-Ks except that the following substrates were used. PIPK1α and PIPKIβ were assayed using PI(4)P and phosphatidylserine, whereas PIPKIIβ was assayed using PI(5)P and phosphatidylserine.

5.18.11 Protein kinase assays

Abl: Inhibitors (final concentration: 10 μM) were assayed in triplicate against recombinant full-length Abl in an assay containing 25 mM HEPES, pH 7.4, 10 mM $MgCl_2$, 200 μM ATP (2.5 μCi of γ-32P-ATP), and 0.5 mg/mL BSA. The optimized Abl peptide substrate EAIYAAPFAKKK was used as phosphoacceptor (200 μM) . Reactions were terminated by spotting onto phosphocellulose sheets, which were washed with 0.5% phosphoric acid (approximately 6 times, 5-10 minutes each). Sheets were dried and the transferred radioactivity quantitated by phosphorimaging.

Akt1: Inhibitors (final concentration: 10 μM) were assayed in triplicate against recombinant full-length Akt (Active Motif Inc.) in an assay containing 25 mM HEPES, pH 7.4, 10 mM $MgCl_2$, 200 μM ATP (2.5 μCi of γ-32P-ATP), and 0.5 mg/mL BSA. Myelin basic protein (0.2 mg/mL) was used as a substrate. Reactions were terminated by spotting onto nitrocellulose, which was washed with 1M NaCl/1% phosphoric acid (approximately 6 times, 5-10 minutes each). Sheets were dried and the transferred radioactivity quantitated by phosphorimaging.

Akt2 (ΔPH): Inhibitors (final concentration: 10 μM) were assayed in triplicate against recombinant Akt2-ΔPH (Upstate) in an assay containing 25 mM HEPES, pH 7.4, 10 mM $MgCl_2$, 200 μM ATP (2.5 μCi of γ-32P-ATP), and 0.5 mg/mL BSA. Myelin basic protein (0.2 mg/mL) was used as a substrate. Reactions were terminated by spotting onto nitrocellulose, which was washed with 1M NaCl/1% phosphoric acid (approximately 6 times, 5-10 minutes each). Sheets were dried and the transferred radioactivity quantitated by phosphorimaging.

CamKII: Inhibitors (final concentration: 10 μM) were assayed in triplicate against CamKII (NEB) in an assay containing 50 mM Tris, pH 7.5, 10 mM $MgCl_2$, 2 mM DTT, 2 mM $CaCl_2$, 1.2 μM calmodulin, 200 μM ATP (2.5 μCi of γ-32P-ATP), and 0.5 mg/mL BSA. Myelin basic protein (0.2 mg/mL) was used as a substrate. Reactions were terminated by spotting onto nitrocellulose, which was washed with 1M NaCl/1% phosphoric acid (approximately 6 times, 5-10 minutes each). Sheets were dried and the transferred radioactivity quantitated by phosphorimaging.

CDK1/cyclin B: Inhibitors (final concentration: 10 μM) were assayed in triplicate against recombinant CDK1/cyclin B (NEB) in an assay containing 25 mM HEPES, pH 7.4, 10 mM $MgCl_2$, 200 μM ATP (2.5 μCi of γ-32P-ATP), and 0.5 mg/mL BSA. Histone H1 (0.8 mg/mL) was used as a substrate. Reactions were terminated by spotting onto nitrocellulose, which was washed with 1M NaCl/1% phosphoric acid (approximately 6 times, 5-10 minutes each). Sheets were dried and the transferred radioactivity quantitated by phosphorimaging.

CDK2/cyclin A: Inhibitors (final concentration: 10 μM) were assayed in triplicate against recombinant CDK2/cyclin A (NEB) in an assay containing 25 mM HEPES, pH 7.4, 10 mM $MgCl_2$, 200 μM ATP (2.5 μCi of γ-32P-ATP), and 0.5 mg/mL BSA. Histone H1 (0.8 mg/mL) was used as a substrate. Reactions were terminated by spotting onto nitrocellulose, which was washed with 1M NaCl/1% phosphoric acid (approximately 6 times, 5-10 minutes each). Sheets were dried and the transferred radioactivity quantitated by phosphorimaging.

Chk1: Inhibitors (final concentration: 10 μM) were assayed in triplicate against recombinant Chk1 (Invitrogen) in an assay containing 25 mM HEPES, pH 7.4, 10 mM $MgCl_2$, 200 μM ATP (2.5 μCi of γ-32P-ATP), and 0.5 mg/mL BSA. The peptide KKKVSRSGLYRSPSMPENLNRPR (CHKtide, Upstate) was used as a substrate. Reactions were terminated by spotting onto phosphocellulose sheets, which were washed with 0.5% phosphoric acid (approximately 6 times, 5-10 minutes each). Sheets were dried and the transferred radioactivity quantitated by phosphorimaging.

CK1: Inhibitors (final concentration: 10 μM) were assayed in triplicate against recombinant CK1 (NEB) in an assay containing 25 mM HEPES, pH 7.4, 10 mM $MgCl_2$, 200 μM ATP (2.5 μCi of γ-32P-ATP), and 0.5 mg/mL BSA. Dephosphorylated casein (1 mg/mL) was used as a substrate. Reactions were terminated by spotting onto nitrocellulose, which was washed with 1M NaCl/1% phosphoric acid (approximately 6 times, 5-10 minutes each). Sheets were dried and the transferred radioactivity quantitated by phosphorimaging.

CK2: Inhibitors (final concentration: 10 μM) were assayed in triplicate against recombinant CK2 (NEB) in an assay containing 25 mM HEPES, pH 7.4, 10 mM $MgCl_2$, 200 μM ATP (2.5 μCi of γ-32P-ATP), and 0.5 mg/mL BSA. Dephosphorylated casein (1 mg/mL) was used as a substrate. Reactions were terminated by spotting onto nitrocellulose, which was washed with 1M NaCl/1% phosphoric acid (approximately 6 times, 5-10 minutes each). Sheets were dried and the transferred radioactivity quantitated by phosphorimaging.

Erk1: Inhibitors (final concentration: 10 μM) were assayed in triplicate against recombinant Erk1 (Upstate) in an assay containing 25 mM HEPES, pH 7.4, 10 mM $MgCl_2$, 200 μM ATP (2.5 μCi of γ-32P-ATP), and 0.5 mg/mL BSA. Myelin basic protein (0.2 mg/mL) was used as a substrate. Reactions were terminated by spotting onto nitrocellulose, which was washed with 1M NaCl/1% phosphoric acid (approximately 6 times, 5-10 minutes each). Sheets were dried and the transferred radioactivity quantitated by phosphorimaging.

Erk2: Inhibitors (final concentration: 10 μM) were assayed in triplicate against recombinant Erk2 (Upstate) in an assay containing 25 mM HEPES, pH 7.4, 10 mM $MgCl_2$, 200 μM ATP (2.5 μCi of γ-32P-ATP), and 0.5 mg/mL BSA. Myelin basic protein (0.2 mg/mL) was used as a substrate. Reactions were terminated by spotting onto nitrocellulose, which was washed with 1M NaCl/1% phosphoric acid (approximately 6 times, 5-10 minutes each). Sheets were dried and the transferred radioactivity quantitated by phosphorimaging.

FAK: Inhibitors (final concentration: 10 μM) were assayed in triplicate against recombinant FAK (Prospec-Tany Technogene) in an assay containing 25 mM HEPES, pH 7.4, 10 mM $MgCl_2$, 200 μM ATP (2.5 μCi of γ-32P-ATP), and 0.5 mg/mL BSA. Poly E-Y (Sigma; 2 mg/mL) was used as a substrate. Reactions were terminated by spotting onto nitrocellulose, which was washed with 1M NaCl/1% phosphoric acid (approximately 6 times, 5-10 minutes each). Sheets were dried and the transferred radioactivity quantitated by phosphorimaging.

Fyn: Inhibitors (final concentration: 10 μM) were assayed in triplicate against recombinant full-length Fyn in an assay containing 25 mM HEPES, pH 7.4, 10 mM $MgCl_2$, 200 μM ATP (2.5 μCi of γ-32P-ATP), and 0.5 mg/mL BSA. The optimized Src family kinase peptide substrate EIYGEFKKK was used as phosphoacceptor (200 μM) . Reactions were terminated by spotting onto phosphocellulose sheets, which were washed with 0.5% phosphoric acid (approximately 6 times, 5-10 minutes each). Sheets were dried and the transferred radioactivity quantitated by phosphorimaging.

Gsk3β: Inhibitors (final concentration: 10 μM) were assayed in triplicate against recombinant Gsk3β (NEB) in an assay containing 25 mM HEPES, pH 7.4, 10 mM $MgCl_2$, 200 μM ATP (2.5 μCi of γ-32P-ATP), and 0.5 mg/mL BSA. Myelin basic protein (0.2 mg/mL) was used as a substrate. Reactions were terminated by spotting onto nitrocellulose, which was washed with 1M NaCl/1% phosphoric acid (approximately 6 times, 5-10 minutes each). Sheets were dried and the transferred radioactivity quantitated by phosphorimaging.

Hck: Inhibitors (final concentration: 10 μM) were assayed in triplicate against recombinant full-length Hck in an assay containing 25 mM HEPES, pH 7.4, 10 mM $MgCl_2$, 200 μM ATP (2.5 μCi of γ-32P-ATP), and 0.5 mg/mL BSA. The optimized Src family kinase peptide substrate EIYGEFKKK was used as phosphoacceptor (200 μM) . Reactions were terminated by spotting onto phosphocellulose sheets, which were washed with 0.5% phosphoric acid (approximately 6 times, 5-10 minutes each). Sheets were dried and the transferred radioactivity quantitated by phosphorimaging.

Insulin receptor: Inhibitors (final concentration: 10 μM) were assayed in triplicate against recombinant insulin receptor kinase domain (Upstate) in an assay containing 25 mM HEPES, pH 7.4, 10 mM $MgCl_2$, 10 mM $MnCl_2$, 200 μM ATP (2.5 μCi of γ-32P-ATP), and 0.5 mg/mL BSA. Poly E-Y (Sigma; 2 mg/mL) was used as a substrate. Reactions were terminated by spotting onto nitrocellulose, which was washed with 1M NaCl/1% phosphoric acid (approximately 6 times, 5-10 minutes each). Sheets were dried and the transferred radioactivity quantitated by phosphorimaging.

JNK1α1: Inhibitors (final concentration: 10 μM) were assayed in triplicate against recombinant JNK1α1 (Upstate) in an assay containing 25 mM HEPES, pH 7.4, 10 mM $MgCl_2$, 200 μM ATP (2.5 μCi of γ-32P-ATP), and 0.5 mg/mL BSA. ATF-2 (0.2 mg/mL) was used as a substrate. Reactions were terminated by spotting onto nitrocellulose, which was washed with 1M NaCl/1% phosphoric acid (approximately 6 times, 5-10 minutes each). Sheets were dried and the transferred radioactivity quantitated by phosphorimaging.

JNK2α1: Inhibitors (final concentration: 10 μM) were assayed in triplicate against recombinant JNK2α1 (Biosource) in an assay containing 25 mM HEPES, pH 7.4, 10 mM $MgCl_2$, 200 μM ATP (2.5 μCi of γ-32P-ATP), and 0.5 mg/mL BSA. ATF-2 (0.2 mg/mL) was used as a substrate. Reactions were terminated by spotting onto nitrocellulose, which was washed with 1M NaCl/1% phosphoric acid (approximately 6 times, 5-10 minutes each). Sheets were dried and the transferred radioactivity quantitated by phosphorimaging.

JNK2α2: Inhibitors (final concentration: 10 μM) were assayed in triplicate against recombinant JNK2α2 (Biosource) in an assay containing 25 mM HEPES, pH 7.4, 10 mM $MgCl_2$, 200 μM ATP (2.5 μCi of γ-32P-ATP), and 0.5 mg/mL BSA. ATF-2 (0.2 mg/mL) was used as a substrate. Reactions were terminated by spotting onto nitrocellulose, which was washed with 1M NaCl/1% phosphoric acid (approximately 6 times, 5-10 minutes each). Sheets were dried and the transferred radioactivity quantitated by phosphorimaging.

IRAK4: Inhibitors (final concentration: 10 μM) were assayed in triplicate against recombinant IRAK4 in an assay containing 25 mM HEPES, pH 7.4, 10 mM $MgCl_2$, 200 μM ATP (2.5 μCi of γ-32P-ATP), and 0.5 mg/mL BSA. Myelin basic protein (0.2 mg/mL) was used as a substrate. Reactions were terminated by spotting onto nitrocellulose, which was washed with 1M NaCl/1% phosphoric acid (approximately 6 times, 5-10 minutes each). Sheets were dried and the transferred radioactivity quantitated by phosphorimaging.

NEK2: Inhibitors (final concentration: 10 μM) were assayed in triplicate against recombinant NEK2 (Upstate) in an assay containing 25 mM HEPES, pH 7.4, 10 mM $MgCl_2$, 200 μM ATP (2.5 μCi of γ-32P-ATP), and 0.5 mg/mL BSA. Myelin basic protein (0.2 mg/mL) was used as a substrate. Reactions were terminated by spotting onto nitrocellulose, which was washed with 1M NaCl/1% phosphoric acid (approximately 6 times, 5-10 minutes each). Sheets were dried and the transferred radioactivity quantitated by phosphorimaging.

PKA: Inhibitors (final concentration: 10 μM) were assayed in triplicate against recombinant PKA (NEB) in an assay containing 25 mM HEPES, pH 7.4, 10 mM $MgCl_2$, 200 μM ATP (2.5 μCi of γ-32P-ATP), and 0.5 mg/mL BSA. Myelin basic protein (0.2 mg/mL) was used as a substrate. Reactions were terminated by spotting onto nitrocellulose, which was washed with 1M NaCl/1% phosphoric acid (approximately 6 times, 5-10 minutes each). Sheets were dried and the transferred radioactivity quantitated by phosphorimaging.

PKCδ: Inhibitors (final concentration: 10 μM) were assayed in triplicate against recombinant PKCδ in an assay containing 25 mM HEPES, pH 7.4, 10 mM $MgCl_2$, phosphatidylserine (0.5 mg/mL), PMA (1 μM), 200 μM ATP (2.5 μCi of γ-32P-ATP), and 0.1 mg/mL BSA. Histone H3 (1 mg/mL) was used as a substrate. Reactions were terminated by spotting onto nitrocellulose, which was washed with 1M NaCl/1% phosphoric acid (approximately 6 times, 5-10 minutes each). Sheets were dried and the transferred radioactivity quantitated by phosphorimaging.

PKCε: Inhibitors (final concentration: 10 μM) were assayed in triplicate against recombinant PKCε in an assay containing 25 mM HEPES, pH 7.4, 10 mM $MgCl_2$, phosphatidylserine (0.5 mg/mL), PMA (1 μM), 200 μM ATP (2.5 μCi of γ-32P-ATP), and 0.1 mg/mL BSA. Histone H3 (1 mg/mL) was used as a substrate. Reactions were terminated by spotting onto nitrocellulose, which was washed with 1M NaCl/1% phosphoric acid (approximately 6 times, 5-10 minutes each). Sheets were dried and the transferred radioactivity quantitated by phosphorimaging.

PDK1: Inhibitors (final concentration: 10 μM) were assayed in triplicate against recombinant PDK1 (Upstate) in an assay containing 25 mM HEPES, pH 7.4, 10 mM $MgCl_2$, 200 μM ATP (2.5 μCi of γ-32P-ATP), and 0.5 mg/mL BSA. The peptide KTFCGTPEYLAPEVRREPRILSEEEQEMFRDFDYIADWC (PDKtide, Upstate) was used as a substrate. Reactions were terminated by spotting onto phosphocellulose sheets, which were washed with 0.5% phosphoric acid (approximately 6 times, 5-10 minutes each). Sheets were dried and the transferred radioactivity quantitated by phosphorimaging.

PLK1: Inhibitors (final concentration: 10 μM) were assayed in triplicate against recombinant PLK1 in an assay containing 25 mM HEPES, pH 7.4, 10 mM $MgCl_2$, 200 μM ATP (2.5 μCi of γ-32P-ATP), and 0.5 mg/mL BSA. Dephosphorylated casein (1 mg/mL) was used as a substrate. Reactions were terminated by spotting onto nitrocellulose, which was washed with 1M NaCl/1% phosphoric acid (approximately 6 times, 5-10 minutes each). Sheets were dried and the transferred radioactivity quantitated by phosphorimaging.

p38: Inhibitors (final concentration: 10 μM) were assayed in triplicate against recombinant p38 in an assay containing 25 mM HEPES, pH 7.4, 10 mM $MgCl_2$, 200 μM ATP (2.5 μCi of γ-32P-ATP), and 0.5 mg/mL BSA. Myelin basic protein (0.2 mg/mL) was used as a substrate. Reactions were terminated by spotting onto nitrocellulose, which was washed with 1M NaCl/1% phosphoric acid (approximately 6 times, 5-10 minutes each). Sheets were dried and the transferred radioactivity quantitated by phosphorimaging.

Src: Inhibitors (final concentration: 10 μM) were assayed in triplicate against recombinant full-length Src in an assay containing 25 mM HEPES, pH 7.4, 10 mM $MgCl_2$, 200 μM ATP (2.5 μCi of γ-32P-ATP), and 0.5 mg/mL BSA. The optimized Src family kinase peptide substrate EIYGEFKKK was used as phosphoacceptor (200 μM) . Reactions were terminated by spotting onto phosphocellulose sheets, which were washed with 0.5% phosphoric acid (approximately 6 times, 5-10 minutes each). Sheets were dried and the transferred radioactivity quantitated by phosphorimaging.

Src (T338I): Inhibitors (final concentration: 10 μM) were assayed in triplicate against recombinant full-length Src (T338II) in an assay containing 25 mM HEPES, pH 7.4, 10 mM $MgCl_2$, 200 μM ATP (2.5 μCi of γ-32P-ATP), and 0.5 mg/mL BSA. The optimized Src family kinase peptide substrate EIYGEFKKK was used as phosphoacceptor (200 μM) . Reactions were terminated by spotting onto phosphocellulose sheets, which were washed with 0.5% phosphoric acid (approximately 6 times, 5-10 minutes each). Sheets were dried and the transferred radioactivity quantitated by phosphorimaging.

Zap70: Inhibitors (final concentration: 10 μM) were assayed in triplicate against recombinant Zap70 (Upstate) in an assay containing 25 mM HEPES, pH 7.4, 10 mM $MgCl_2$, 10 mM $MnCl_2$, 200 μM ATP (2.5 μCi of γ-32P-ATP), and 0.5 mg/mL BSA. Poly E-Y (Sigma; 2 mg/mL) was used as a substrate. Reactions were terminated by spotting onto nitrocellulose, which was washed with 1M NaCl/1% phosphoric acid (approximately 6 times, 5-10 minutes each). Sheets were dried and the transferred radioactivity quantitated by phosphorimaging.

5.18.12 Determination of p110γ crystal structures

Protein expression and purification

Recombinant human p110γ (residues 144-1102, with a His_6 tag directly fused to the C-terminus) was purified from baculovirus-infected Sf9 cells. Cells were sonicated in buffer A (0.1M NaCl, 0.005M potassium phosphate pH 8 (4°C), 10 mM Tris-Hcl pH 8 4°C) and 1 mM $MgCl_2$) and the supernatant from a 1 hr ultracentrifugation was purified by heparin affinity, metal chelate affinity and gel filtration. The protein in gel filtration buffer (20 mM Tris pH 7.2 (4°C), 0.5 mM ammonium sulfate, 1% ethylene glycol, 0.02% CHAPS and 5 mM DTT) was concentrated to approximately 6 mg/ml.

Crystallisation of p110γ and soaking with inhibitors

Crystals were grown at 17 ºC using sitting-drop vapour-diffusion by mixing 1 μl p110γ sample (4 mg/ml in a buffer containing 0.5 mM $(NH_4)_2SO_4$, 20 mM Tris pH 7.2, 1% ethylene glycol, 0.02% Chaps and 5 mM DTT) and 1 μl of a reservoir solution (16-17% PEG 4000, 250 mM $(NH_4)_2SO_4$ and 100mM Tris pH 7.5). Crystal seeds were introduced in the drops by hair seeding with a cat whisker. The crystals grow over 1-2 weeks reaching a maximum size of 0.2 mm x 0.1 mm x 0.1 mm.

Inhibitor stocks were diluted in freezing solution (23% PEG 4000, 250 mM $(NH_4)_2SO_4$, 100mM Tris pH 7.5 and 14% glycerol) to final concentrations of 0.01 mM, 0.1 mM and 1 mM. Aliquots of increasing inhibitor concentration in freezing solution were added to the drops in which the crystals were grown. The additions were of 0.5 µl and drops were incubated for 30-60 minutes between additions. Finally, 1 µl was taken out of the drop and 1 µl of 1 mM inhibitor in freezing solution was added, and the crystals were soaked in this solution for three hours. After soaking, the crystals were transferred to a fresh drop containing 1mM inhibitor in freezing solution then immediately frozen by dunking the crystals in liquid nitrogen.

Diffraction data collection and structure refinement

Diffraction data were collected at ESRF ID14-4. Data were integrated with MOSFLM and scaled using SCALA. Human p110γ was used as an initial model for molecular replacement using AMORE. The model was refined using REFMAC, starting with rigid-body refinement then using restrained maximum-likelihood refinement with individual isotropic B factors alternated with restrained refinement using TLS parameters. Cycles of REFMAC refinement were alternated with manual rebuilding. The data collection and refinement statistics are summarised in Table 5.3

5.18.13 Chemical Synthesis

The synthesis of a representative compound from each chemotype is described below. Refer to synthetic schemes in Figure 5.12 for nomenclature and structures of intermediates. The synthesis of the morpholinophenols (e.g., AMA-37) has been described previously [9], and the following syntheses are based on patent specifications as described below.

Scheme 1: Synthesis of the pyridinylfuranopyrimidine PI-103

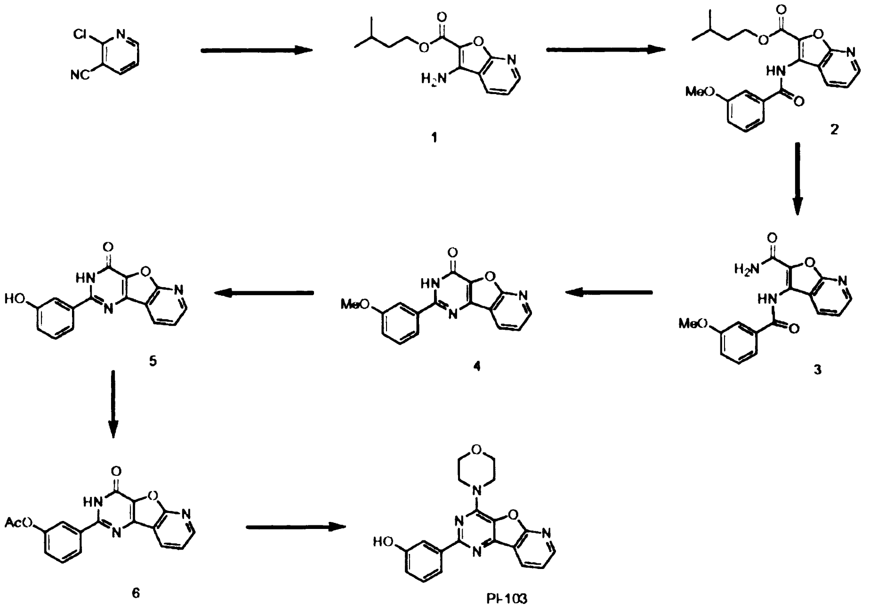
1
2
3
4
5
6
PI-103

Scheme 2: Synthesis of the phenylthiazole PIK-93

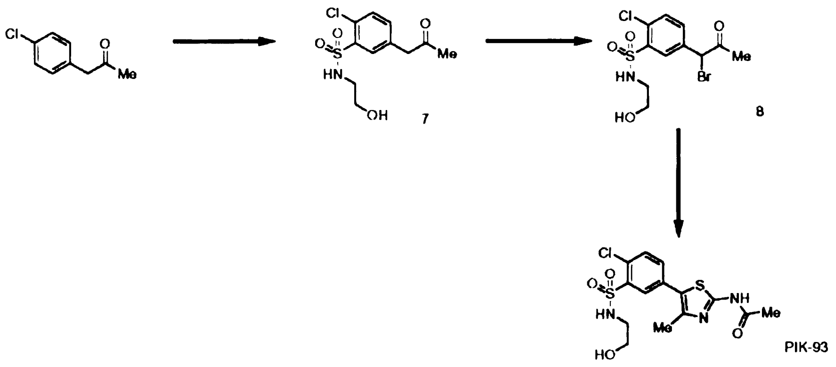

Scheme 3: Synthesis of the benzyloxazinone PIK-124

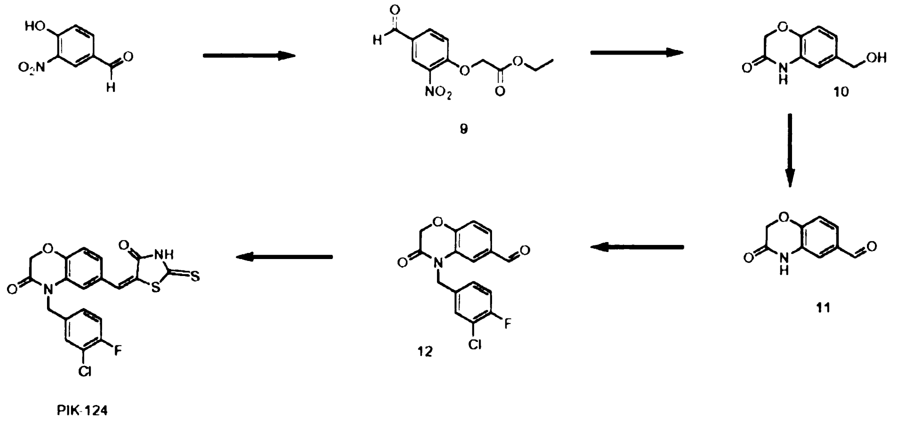
9
10
11
12
PIK 124

Scheme 4: Synthesis of the imidazoquinazoline PIK-90

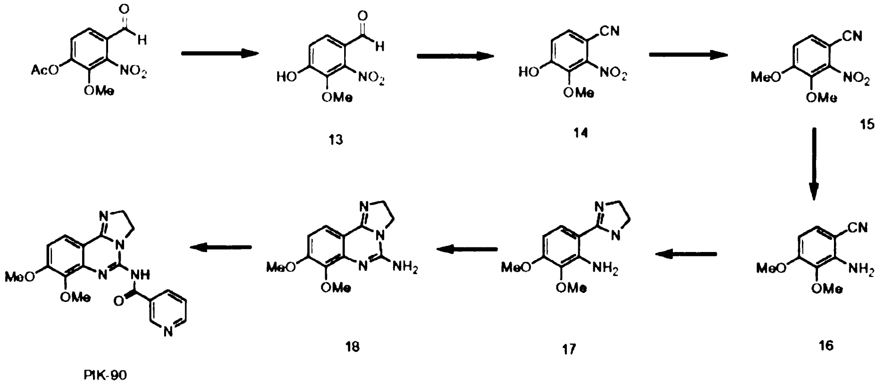
13
14
15
16
17
18
PIK-90

Scheme 5: Synthesis of the morpholinochromone PIK-108

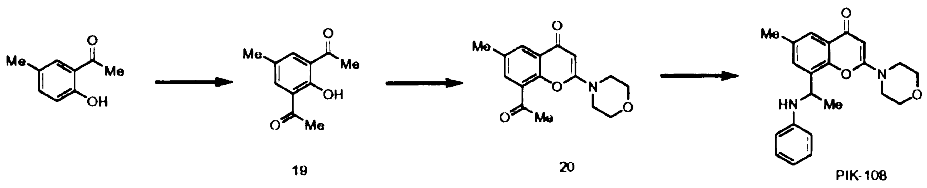
Me
O
Me
OH
19
20
HN
N
O
PIK-108

Scheme 6: Synthesis of the morpholinopyranone KU-55933

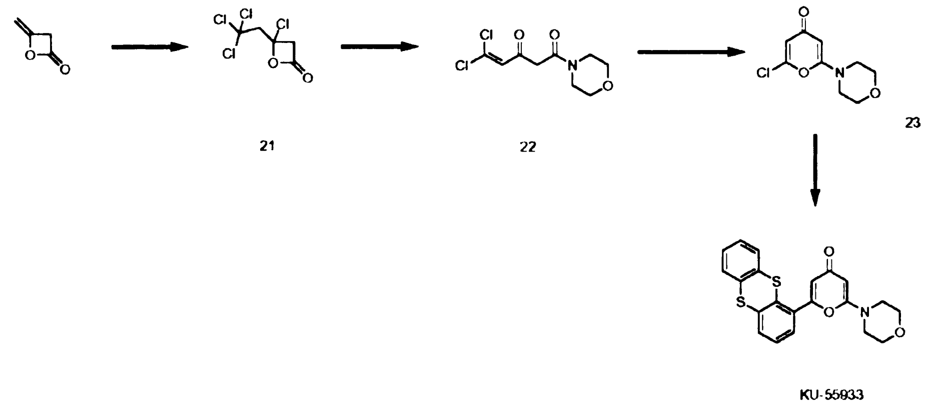
Cl
O
N
21
22
23
S
KU-55933

Scheme 7: Synthesis of the quinazoline purine PIK-39

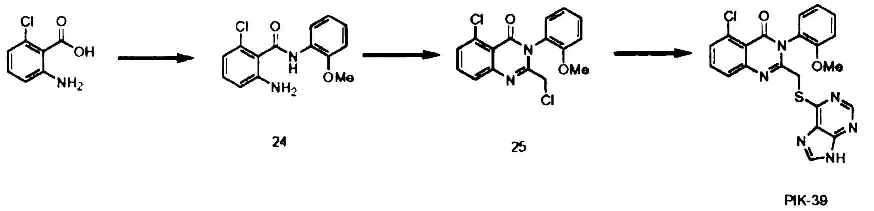
Cl
O
OH
NH2
N
H
OMe
S
NH
24
25
PIK-39

Scheme 8: Synthesis of imidazopyridine PIK-75

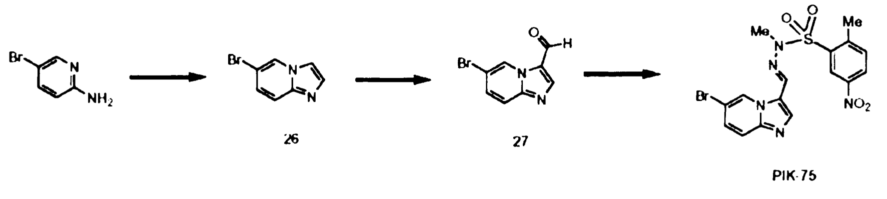
Br
N
NH2
Br
N
N
26
Br
O
H
N
N
27
Me
N
N
O
O
S
Me
NO2
Br
N
N
PIK-75

Figure 5.12. Synthetic schemes for the synthesis of a representative PI3-K inhibitor from each chemotype.

Synthesis of the pyridinylfuranopyrimidine PI-103 (Scheme 1)

Synthesis of isopentyl 3-aminofuro[2,3-b]pyridine-2-carboxylate (1): The following is based on the procedures described in WO 01/083456 unless otherwise noted. 2-chloropyridine-3-carbonitrile (25 g, 180 mmol), ethyl glycolate (18.8 mL, 198 mmol), and sodium carbonate (38 g, 360 mmol) were dissolved in 3-methylbutanol (200 mL) and heated to reflux for 72 hours. The reaction was cooled to room temperature, water was added, and the product extracted into CH_2Cl_2. The organic extract was purified by silica gel flash chromatography in 10% EtOAc/Hexanes to yield 11.3 g (25% yield). LC-ESI-MS $[MH]^+$ m/z calcd for $C_{13}H_{17}N_2O_3$, 249.12; found, 249.29.

Synthesis of isopentyl 3-(3-methoxybenzamido)furo[2,3-b]pyridine-2-carboxylate (2): Product 1 (11.3 g, 45.5 mmol) was dissolved in CH_2Cl_2 (60 mL). Triethylamine (6.7 mL, 50 mmol) was added, followed by m-anisoyl chloride (6.8 mL, 50 mmol), and the reaction was allowed to proceed overnight at room temperature. The reaction was then diluted into water, the product extracted into CH_2Cl_2, and purified by silica gel flash chromatography in 10% EtOAc/Hexanes to yield 17.45 g (89% yield). LC-ESI-MS $[MH]^+$ m/z calcd for $C_{21}H_{23}N_2O_5$, 383.15; found, 383.21.

Synthesis of 3-(3-methoxybenzamido)furo[2,3-b]pyridine-2-carboxamide (3): Product 2 (17.45 g, 45.6 mmol) was taken up in methanolic ammonia (7N, 2 L) and stirred at room temperature overnight. The following day the solvent was removed *in vacuo* and the product was taken onto the next step without further purification. LC-ESI-MS $[MH]^+$ m/z calcd for $C_{16}H_{14}N_3O_4$, 312.09; found, 312.29.

Synthesis of (4): The crude product 3 (~12 g) was taken up in 300 mL aqueous NaOH (5%) and 150 mL ethanol [55]. The reaction was heated to reflux for 1 hour, at

which point it was allowed to cool to room temperature. The product was then precipitated by adding 30 mL concentrated HCl, and a white solid was collected by filtration. This was taken onto the next step without further purification. LC-ESI-MS $[MH]^+$ m/z calcd for $C_{16}H_{12}N_3O_3$, 294.08; found, 294.28.

Synthesis of (5): The crude product 4 (~6 g) was taken up in a solution of 20 mL glacial acetic acid and 90 mL concentrated HBr. This solution was heated to reflux for 8 hours, at which point it was cooled to room temperature and the solvent removed *in vacuo.* Diethylether was added and removed *in vacuo* two times to yield a tan solid. This was taken onto the next step without further purification. LC-ESI-MS $[MH]^+$ m/z calcd for $C_{15}H_{10}N_3O_3$, 280.06; found, 280.29.

Synthesis of (6): The crude product 5 (~6 g) was dissolved in acetic anhydride (200 mL) and triethylamine (5 mL) was added. The reaction was heated to reflux for one hour, at which point it was cooled to room temperature and the solvent was removed *in vacuo*. CH_2Cl_2 was added and removed *in vacuo* two times to yield a green/grey solid. This was taken onto the next step without further purification. LC-ESI-MS $[MH]^+$ m/z calcd for $C_{17}H_{12}N_3O_4$, 322.07; found, 322.25.

Synthesis of PI-103: The crude product 6 (~6 g) was taken up in $POCl_3$ (200 mL) and heated to reflux for 45-10 minutes. The reaction was then cooled to room temperature and solvent removed *in vacuo.* The solid residue was dissolved in morpholine (100 mL) and heated to reflux for 4 hours. The reaction was then cooled to room temperature and the morpholine removed *in vacuo.* Water was added, and the aqueous phase was extracted with $CHCl_3$ followed by EtOAc. The organic phases were then combined, concentrated *in vacuo,* and the product purified by silica gel flash

chromatography in 2% MeOH/ CH_2Cl_2 to yield an off-white solid. The product containing fractions from this column were combined, solvent removed *in vacuo,* and the product was subjected to a second purification by reverse phase HPLC using a $MeCN/H_2O$/0.1% TFA solvent system to yield an off-white solid. LC-ESI-MS $[MH]^+$ m/z calcd for $C_{19}H_{17}N_4O_3$, 349.12; found, 349.23.

Synthesis of the phenylthiazole PIK-93 (Scheme 2)

Synthesis of (7): The following is based on the procedures described in WO 03/072557 unless otherwise noted. 1-(4-chlorophenyl)propan-2-one (1 mL, 14.8 mmol) was added dropwise to SO_3ClH (5 mL) in an ice bath, and the reaction was then heated to 40º C for 2 hours. The reaction was stopped by transfer dropwise to 200 mL ice. The aqueous phase was then extracted 3 times with EtOAc, the combined organic dried with Na_2SO_4, filtered, and then concentrated *in vacuo* to give a brown oil. This oil was dissolved in THF (10 mL), ethanolamine was added (~1.5 mL), and the reaction was allowed to stir overnight at room temperature. The following day the reaction was concentrated *in vacuo*, water was added, and the aqueous phase was extracted three times with EtOAc. The combined organic phase was concentrated, and the product purified by silica gel flash chromatography using a gradient of 2% - 10% MeOH in CH_2Cl_2. The product containing fractions from this column were combined, solvent removed *in vacuo,* and the product was subjected to a second purification by reverse phase HPLC using a $MeCN/H_2O$/0.1% TFA solvent system. Product containing fractions were lyophilized to yield 414 mg (24% yield) of product. LC-ESI-MS $[MH]^+$ m/z calcd for $C_{11}H_{15}ClNO_4S$, 292.03; found, 292.17.

Synthesis of (8): $Ph_3PCH_2CH_2COOH\ Br_3$ (900 mg, 1.5 mmol) was dissolved in THF (15 mL) [56]. Product 7 (414 mg, 1.42 mmol) was dissolved in THF (10 mL) and

this was added dropwise to the first solution at room temperature. The reaction was allowed to proceed one hour at room temperature, at which point the solvent was removed *in vacuo* and the product purified by silica gel flash chromatography to yield 377 mg (72% yield) of product. LC-ESI-MS $[MH]^+$ m/z calcd for $C_{11}H_{14}BrClNO_4S$, 369.94; found, 369.83.

Synthesis of PIK-93: Product 8 (377 mg, 1.02 mmol) was dissolved in ethanol (6 mL), and N-acetylthiourea (130 mg, 1.1 mmol) was added at room temperature. The reaction was heated to reflux for 30 minutes, then cooled to room temperature, and the product purified by silica gel flash chromatography using a gradient of 0% - 10% MeOH in CH_2Cl_2 to yield 167 mg (42% yield) of PIK-93. LC-ESI-MS $[MH]^+$ m/z calcd for $C_{14}H_{17}ClN_3O_4S_2$, 390.03; found, 390.14.

Synthesis of the benzyloxazinone PIK-124 (Scheme 3)

Synthesis of ethyl 2-(4-formyl-2-nitrophenoxy)acetate (9): The following is based on the procedures described in WO 04/052373 unless otherwise noted. 4-hydroxy-3-nitrobenzaldehyde (7.1 g, 42.5 mmol), methyl 2-bromoacetate (4.4 mL, 46.7 mmol) and sodium hydride (1.12 g, 46.7 mmol) were dissolved in a solution of 420 mL THF and 170 mL DMF. The reactions was then heated to 90º C for 48 hours. When the reaction was complete, it was cooled to room temperature, concentrated in vacuo, and EtOAc (400 mL) was added. The organic phase was extracted twice with sodium bicarbonate, and twice with brine. The organic phase was then dried with Na_2SO_4, filtered, and the solvent removed *in vacuo*. The resultant dark brown oil was carried onto the next step without further characterization.

Synthesis of 6-(hydroxymethyl)-2H-benzo[b][1,4]oxazin-3(4H)-one (10): Product 9 (~ 5 mL) was dissolved in methanol (50 mL) and rainey nickel in water was added. The reaction was placed in a Parr bomb and subjected to 48 psi H_2 (g) for 24 hours. The reaction was then filtered through celite, and solvent removed *in vacuo* to yield an off-white solid. The resultant dark brown oil was carried onto the next step without further characterization.

Synthesis of 3,4-dihydro-3-oxo-2H-benzo[b][1,4]oxazine-6-carbaldehyde (11): Product 10 (2.75 g, 15.4 mmol) was dissolved in CH_2Cl_2, pyridinium dichromate (8.7 g, 23.1 mmol) was added, and the reaction was allowed to proceed overnight at room temperature. The reaction was then filtered through celite, and the solvent removed *in vacuo* to give a red solid. The product was purified by silica gel flash chromatography using 2% MeOH in CH_2Cl_2 to yield 400 mg (15%) and taken onto the next step without further characterization.

Synthesis of 4-(3-chloro-4-fluorobenzyl)-3,4-dihydro-3-oxo-2H-benzo[b][1,4]oxazine-6-carbaldehyde (12): Product 11 (400 mg, 2.26 mmol), 4-(bromomethyl)-2-chloro-1-fluorobenzene (0.37 mL, 2.5 mmol) and BEMP resin (1.5 g) were added to DMF (30 mL) and stirred at room temperature for 2 hours. The reaction was then filtered and the solvent removed *in vacuo*. The product was taken onto the next step without further characterization.

Synthesis of PIK-124: The crude product 13 (600 mg, 1.88 mmol) was dissolved in methanol (100 mL). Ethylene diamine (336 mg, 5.6 mmol) and rhodadine (249 mg, 1.9 mmol) were added the reaction was stirred at room temperature. Within 30 minutes, a yellow precipitate appeared, and the reaction was allowed to go overnight.

The next day, the product was collected by filtration and triturated with methanol and diethyl ether to yield 549 mg (67%) of a yellow solid. ^{1}H NMR (400 MHz, DMSO) δ 7.55 (1H, d, J = 6 Hz), 7.49 (1H, s), 7.30 – 7.36 (3H, m), 7.21 – 7.23 (1H, m), 7.12 – 7.14 (1H, m), 7.07 (1H, s), 5.13 (2H, s), 4.90 (2H, s)

Synthesis of the imidazoquinazoline PIK-90 (Scheme 4)

Synthesis of 4-hydroxy-3-methoxy-2-nitrobenzaldehyde (13): The following is based on the procedures described in WO 04/029055 unless otherwise noted. 4-formyl-2-methoxy-3-nitrophenyl acetate (2.5 g, 10.5 mmol) was dissolved in methanol (20 mL), K_2CO_3 (2.9 g, 21 mmol) was added, and the reaction was stirred overnight. The reaction was then added to water (100 mL), 1N HCl (20 mL) was added to yield a yellow precipitate. EtOAc was added, and the aqueous phase extraced three times. The organic phases were combined, dried with Na_2SO_4, and concentrated *in vacuo* to yield a yellow solid that was taken onto the next step without further characterization.

Synthesis of 4-hydroxy-3-methoxy-2-nitrobenzonitrile (14): The crude product 13 (~2 g, 10.5 mmol) was dissolved in aqueous ammonia (28%, 20 mL) and THF (2 mL). Iodine (3.2 g, 12.6 mmol) was added and the reaction was stirred at room temperature overnight. The reaction was concentrated *in vacuo*, and 1N HCl was added to yield a brown precipitate. EtOAc was added and the aqueous phase was extracted five times. The organic phases were combined, dried with Na_2SO_4, and concentrated *in vacuo*. The product was purified by silica gel flash chromatography in 25% EtOAc:Hexanes to yield an off-white solid (~2 g), which was taken onto the next step without further characterization.

Synthesis of 3,4-dimethoxy-2-nitrobenzonitrile (15): The crude product 14 (~2 g, 10 mmol) was dissolved in DMF (20 mL), Na_2CO_3 (1.42 g, 13.4 mmol) and dimethylsulphate (1.55 g, 12.3 mmol) were added and the reaction was heated to reflux for 4 hours. The reaction was then cooled to room temperature, and poured into water (200 mL). The aqueous phase was extracted five times with EtOAc, and the combined organic was washed once with brine and dried with Na_2SO_4. The solvent was removed *in vacuo*, and then chromatographed through a silica plug to yield a white solid (~2 g) which was taken onto the next step without further characterization.

Synthesis of 2-amino-3,4-dimethoxybenzonitrile (16): The crude product 15 (~2 g, 10 mmol), was dissolved in a solution of ethanol (150 mL) and methanol (2 mL) and palladium on carbon was added (2.0 g). The reaction was stirred at room temperature for 24 hours under a hydrogen atmosphere, at which point the reaction was filtered through celite. The product was purified by silica gel flash chromatography in 25% EtOAc:Hexanes to yield 704 mg of a clear oil (38% yield over 4 steps). LC-ESI-MS $[MH]^+$ m/z calcd for $C_9H_{11}N_2O_2$, 179.07; found, 179.32.

Synthesis of (17): Product 16 (704 mg, 3.9 mmol) was added to ethylenediamine (5.3 mL, 79.9 mmol) in a 25 mL round bottom flask. The reaction was heated to 40º C, at which point P_2S_5 (89 mg, 0.2 mmol) was added. The reaction turned green upon P_2S_5 addition, and was heated overnight to 100º C. The following day, the reaction was stopped by adding to ice water (200 mL). The aqueous phase was extracted three times each wih CH_2Cl_2, $CHCl_3$, and EtOAc, the organic phases combined, and the solvent removed *in vacuo* to give a 874 mg (85% yield) of a yellow soild. LC-ESI-MS $[MH]^+$ m/z calcd for $C_{11}H_{15}N_3O_2$, 222.12; found, 222.32.

Synthesis of 2,3-dihydro-7,8-dimethoxyimidazo[1,2-c]quinazolin-5-amine (18): Product 17 (500 mg, 2.3 mmol) was dissolved in a solution of methanol (5 mL) and water (1 mL) at 0º C. Cyanogen bromide (264 mg, 2.5 mmol) was added and the reaction was allowed to stir at room temperature overnight. The aqueous phase was then extracted with CH_2Cl_2 four times, the organic phases combined and the solvent removed *in vacuo*. The product was purified by silica gel flash chromatography in 5% MeOH:CH_2Cl_2 to yield 160 mg of a white solid (29% yield). LC-ESI-MS $[MH]^+$ m/z calcd for $C_{12}H_{15}N_4O_2$, 247.11; found, 247.17.

Synthesis of N-(2,3-dihydro-7,8-dimethoxyimidazo[1,2-c]quinazolin-5-yl)nicotinamide (PIK-90): Product 18 (80 mg, 0.33 mmol), triethylamine (0.17 mL, 1.3 mmol) and nicotinoyl chloride HCl (116 mg, 0.7 mmol) were dissolved in $CHCl_3$ (20 mL) and stirred at room temperature for 1 hour. The solvent was removed *in vacuo* and the product was purified by silica gel flash chromatography using a gradient of 0 - 10% MeOH:CH_2Cl_2 to yield 53 mg (46% yield) of a white solid. LC-ESI-MS $[MH]^+$ m/z calcd for $C_{18}H_{18}N_5O_3$, 352.13; found, 352.08.

Synthesis of the morpholinochromone PIK-108 (Scheme 5)

Synthesis of (19): The following is based on the procedures described in WO 03/004177 unless otherwise noted. 1-(2-hydroxy-5-methylphenyl)ethanone (15 g, 100 mmol) was dissolved in CH_2Cl_2 (100 mL). Acetic anhydride (11 mL, 116 mmol), triethylamine (13.9 mL, 106 mmol), and DMAP (1.22 g, 10 mmol) were added, and the reaction was stirred overnight at room temperature. The reaction was diluted with water (300 mL) and then extracted three times with CH_2Cl_2. The organic phases were combined, washed with saturated Na_2CO_3, and filtered. The solvent was then removed *in vacuo* to yield an orange solid. This solid was then dissolved in CH_2Cl_2 (250 mL), cooled to 0º C, $AlCl_3$ (19.5 g, 146 mmol) was added and the reaction was allowed to stir at room temperature for four days. After this period, the reaction was stopped by adding ice (50 mL) followed by 1N HCl (50 mL) and then stirring for 1 hour at room temperature. This was extracted three times with CH_2Cl_2, the organic phases combined, washed with brine once, and then dried with Na_2SO_4. The solvent was then removed *in vacuo* and the product purified by silica gel flash chromatography in 25% EtOAc:Hexanes to obtain a yellow solid (7.29 g, 38% yield). ^1H NMR (400 MHz, $CDCl_3$) δ 13.1 (1H, s), 7.73 (2H, s), 2.62 (6H, s), 2.28 (3H, s).

Synthesis of 8-acetyl-6-methyl-2-morpholino-4H-chromen-4-one (20):

Product 19 (800 mg, 4.16 mmol) was dissolved in THF (40 mL), cooled to -78º C, and lithium bis(trimethylsilyl)amide (12.9 mL of 1.0 M THF solution, 12.9 mmol) was added [57]. The reaction was stirred at 0º C for one hour, then cooled to -78º C, morpholino acetylchloride (0.48 mL, 4.2 mmol) was added, and the reaction was transferred to an ice bath and allowed to warm to room temperature overnight. The reaction was then added to water (100 mL) and extracted six times with CH_2Cl_2. The organic phases were combined, the solvent removed *in vacuo*, and the product purified by silica gel flash chromatography in 50% EtOAc:Hexanes to yield a yellow solid. This product was then dissolved in CH_2Cl_2 (20 mL), triflic anhydride (1.5 mL, 9 mmol) was added, and the reaction stirred at room temperature overnight. The next day, the solvent was removed *in vacuo*, methanol (20 mL) was added, and the reaction was stirred for 5 hours. The solvent was then removed *in vacuo* and the product was purified by silica gel flash chromatography using a 0 – 10% MeOH:CH_2Cl_2 to yield 77 mg product (6.5% yield over two steps). LC-ESI-MS $[MH]^+$ m/z calcd for $C_{16}H_{18}NO_4$, 288.12; found, 288.27.

Synthesis of PIK-108: Product 20 (77 mg, 0.27 mmol), sodium cyanoborohydride (17 mg, 0.27 mmol), aniline (0.6 mL), and acetic acid (0.6 mL) were dissolved in methanol (7.5 mL) and heated to reflux overnight. The solvent was then removed *in vacuo* and the product purified by silica gel flash chromatography in 5% MeOH:CH_2Cl_2 to yield 79 mg of a white solid (81% yield). LC-ESI-MS $[MH]^+$ m/z calcd for $C_{22}H_{25}N_2O_3$, 365.18; found, 365.33.

Synthesis of the morpholinopyranone KU-55933 (Scheme 6)

Synthesis of 4-chloro-4-(2,2,2-trichloroethyl)oxetan-2-one (21): The following is based on the procedures described in WO 03/070726 unless otherwise noted. 4-methyleneoxetan-2-one (21 mL, 290 mmol) and benzoyl peroxide (1 g, 7.2 mmol) were dissolved in CCl_4 (81 mL). Separately, CCl_4 (400 mL) was added to 1 L three-neck flask and heated to reflux. The first solution was added to the refluxing CCl_4 over 4 hours using an addition funnel. The reaction was allowed to proceed for an additional hour, at which point it was cooled to room temperature and the solvent was removed *in vacuo*. CH_2Cl_2 was added once and then removed *in vacuo*. The product was taken up in CH_2Cl_2, filtered through celite, and then the solvent removed *in vacuo* to yield ~12 g of a red oil (20% yield) that was taken onto the next step without further characterization.

Synthesis of 5,5-dichloro-1-morpholinopent-4-ene-1,3-dione (22): Product 21 (~12 g, 50 mmol) was dissolved in CH_2Cl_2 (25 mL). Separately, morpholine (4.6 mL, 53 mmol) was dissolved in CH_2Cl_2 (25 mL). Separately, sodium bicarbonate (10 g, 120 mmol) was added to CH_2Cl_2 (50 mL) in a three-neck flask and cooled to 0º C. Solutions 1 and 2 were then added to this flask by addition funnel and the reaction was allowed to proceed at room temperature for three hours. The product was purified by a chromatography through a short plug of slica gel and taken onto the next step without further characterization.

Synthesis of 2-chloro-6-morpholino-4H-pyran-4-one (23):

Product 22 (~10 g, 40 mmol) was dissolved in dioxane, perchloric acid (10 mL) was added, and the reaction was heated to 90º C for one hour. The reaction was then cooled to room temperature, neutralized with 2N NaOH, and then extracted with CH_2Cl_2. The product was purified by silica gel flash chromatography in EtOAc:Hexanes to yield 4.015 g of a brown solid. LC-ESI-MS $[MH]^+$ m/z calcd for $C_9H_{11}ClNO_3$, 216.03; found, 216.08.

2-morpholino-6-(thianthren-1-yl)-4H-pyran-4-one (KU-55933): Product 23 (863 mg, 4.0 mmol), 1-thianthrenyl boronic acid (1.185 g, 4.6 mmol), and K_2CO_3 (1.1 g, 8.0 mmol) were added to dioxane (15 mL). The reaction was heated to 100º C and $Pd(PPh_3)$ (250 mg, 0.2 mmol) was added and the reaction was allowed to proceed overnight. The next day CH_2Cl_2 was added and the organic phase was washed with saturated $NaHCO_3$. The solvent was removed *in vacuo* and the product was purified by silica gel flash chromatography using a gradient of 0 – 5% MeOH:CH_2Cl_2. The product containing fractions were combined, the solvent was removed *in vacuo* and the product was subjected to a second purification by reverse phase HPLC using a MeCN/H_2O/0.1% TFA solvent system to yield 278 mg of an off-white solid (17.5% yield). LC-ESI-MS $[MH]^+$ m/z calcd for $C_{21}H_{18}NO_3S_2$, 396.06; found, 396.04.

Synthesis of the quinazoline purine PIK-39 (Scheme 7)

Synthesis of 2-amino-6-chloro-N-(2-methoxyphenyl)benzamide (24): The following is based on the procedures described in WO 01/81346 unless otherwise noted.

2-amino-6-chlorobenzoic acid (2.00 g, 11.6 mmol) was dissolved in anhydrous benzene (30 mL), thionyl chloride (2.5 mL, 35 mmol) was added, and the reaction was heated to reflux overnight. The following day, the solvent was removed *in vacuo*, and benzene was added and then removed *in vacuo* three times. The resultant brown oil was dissolved in $CHCl_3$ (60 mL) and *o*-anisidine (2.6 mL, 23 mmol) was added. The reaction was heated to reflux for four hours, then cooled to room temperature and filtered. The filtrate was concentrated in vacuo and then purified by silica gel flash chromatography in CH_2Cl_2 to yield 2.36 g (73% yield) of a brown solid. HR-EI-MS $[M]^+$ m/z calcd for $C_{14}H_{13}ClN_2O_2$, 276.0666; found, 276.0658.

Synthesis of 5-chloro-2-(chloromethyl)-3-(2-methoxyphenyl)quinazolin-4(3H)-one (25): Product 24 (1.5 g, 5.4 mmol) was dissolved in glacial acetic acid (25 mL) and chloroacetyl chloride (1.3 mL, 16.2 mmol) was added. The reaction was heated to reflux for 3 hours, concentrated *in vacuo*, and then purified by silica gel flash chromatography in CH_2Cl_2 to yield 469 mg of product (25.8 % yield). HR-EI-MS $[M]^+$ m/z calcd for $C_{16}H_{12}Cl_2N_2O_2$, 334.0276; found, 334.0262.

Synthesis of 2-((9H-purin-6-ylthio)methyl)-5-chloro-3-(2-methoxyphenyl)quinazolin-4(3H)-one (PIK-39): Product 25 (200 mg, 0.6 mmol) was dissolved in DMF (4 mL) and K_2CO_3 (99 mg, 0.72 mmol) and mercaptopurine (122 mg, 0.72 mmol) were added. The reaction was stirred at room temperature for two days, and then stored overnight at 4º C. The following day the product was filtered to yield 179 mg (66% yield) of a white solid. HR-EI-MS $[M]^+$ m/z calcd for $C_{21}H_{15}ClN_6O_2S$, 450.0666; found, 450.0669.

Synthesis of the imidazopyridine PIK-75 (Scheme 8)

Synthesis of 6-bromoH-imidazo[1,2-a]pyridine (26): The following is based on the procedures described in WO 01/083481 unless otherwise noted. 5-bromopyridin-2-amine (25 g, 144 mmol) was dissolved in a solution of water (34 mL) and ethanol (114 mL). $NaHCO_3$ (14.6 g, 174 mmol) and chloroacetylchloride (34 mL, 173 mmol) were added and the reaction was heated to reflux for 3 hours [58]. The reaction was concentrated *in vacuo*, and the aqueous phase then extracted ten times with diethylether. The organic phases were combined, concentrated *in vacuo*, and purified by silica gel flash chromatography in 50% EtOAc:Hexanes to yield 19.5 g (68.6 % yield) of a brown solid. LC-ESI-MS $[MH]^+$ m/z calcd for $C_7H_6BrN_2$, 196.96; found, 197.19.

Synthesis of 6-bromoH-imidazo[1,2-a]pyridine-3-carbaldehyde (27): Product 26 (10 g, 51 mmol) was dissolved in DMF (15 mL) [59]. Separately, $POCl_3$ (12 mL, 130 mmol) was dissolved in DMF (34 mL). This solution was added dropwise to the first solution, and the combined reaction was then heated to reflux for one hour, followed by four hours at 90º C. The reaction was then cooled to room temperature, added to water, and neutralized with 5M NaOH. The aqueous phase was then extracted six times with CH_2Cl_2, concentrated *in vacuo*, and purified by silica gel flash chromatography in EtOAc. LC-ESI-MS $[MH]^+$ m/z calcd for $C_8H_6BrN_2O$, 224.96; found, 225.15.

Synthesis of PIK-75: Product 27 (1.0 g, 4.4 mmol) was dissolved in ethanol (10 mL), methylhydrazine (205 mg, 4.4 mmol) was added, and the reaction was heated to reflux for 2 hours. The reaction was then concentrated *in vacuo*, and redissolved in pyridine (10 mL). 2-methyl-5-nitrobenzene-1-sulfonyl chloride (1.0 g, 4.4 mmol) was added and the reaction was stirred at room temperature for three hours. The product was purified by silica gel flash chromatography in 25% EtOAc:Hexanes followed by reverse phase HPLC using a $MeCN/H_2O/0.1\%$ TFA solvent system to yield 172 mg

(8.5% yield over two steps) of a white solid. LC-ESI-MS $[MH]^+$ m/z calcd for $C_{16}H_{15}BrN_5O_4S$, 451.99; found, 452.03.

5.19 References for experimental procedures

Almirante, L., Mugnaini, A., De Toma, N., Gamba, A., and Murmann, W. (1970). Imidazole Derivatives. IV. Synthesis and Pharmacological Activity of Oxygenated Derivatives of Imidazo[1,2-a]pyridine. Journal of Medicinal Chemistry *13*, 1048-1051.

Armstrong, V. W., N.H., C., and Ramage, R. (1975). A new brominating reagent: 2-carboxyethyltriphenylphosphonium perbromide. Tetrahedron Letters *6*, 373-376.

Bateman, A., Birney, E., Durbin, R., Eddy, S. R., Howe, K. L., and Sonnhammer, E. L. (2000). The Pfam protein families database. Nucleic Acids Res *28*, 263-266.

Jacinto, E., Loewith, R., Schmidt, A., Lin, S., Ruegg, M. A., Hall, A., and Hall, M. N. (2004). Mammalian TOR complex 2 controls the actin cytoskeleton and is rapamycin insensitive. Nat Cell Biol *6*, 1122-1128.

Jolliffe, I. T. (2002). Principal component analysis, 2nd edn (New York: Springer).

Knight, Z. A., Chiang, G. G., Alaimo, P. J., Kenski, D. M., Ho, C. B., Coan, K., Abraham, R. T., and Shokat, K. M. (2004). Isoform-specific phosphoinositide 3-kinase inhibitors from an arylmorpholine scaffold. Bioorg Med Chem *12*, 4749-4759.

Lombardino, J. G. (1965). Preparation and new reactions of imidazo[1,2-a]pyridines. Journal of Organic Chemistry *30*, 2403-2407.

Mhaske, S. B., and Argade, N. P. (2004). Regioselective quinazolinone-directed ortho lithiation of quinazolinoylquinoline: practical synthesis of naturally occurring human DNA topoisomerase I poison luotonin a and luotonins B and E. J Org Chem *69*, 4563-4566.

Morris, J., Wishka, D. G., and Fang, Y. (1994). A cyclodehydration route to 2-aminochromones. Synthetic Communications *24*, 849-858.

5.20 References

1. Fruman, D.A., Meyers, R.E., and Cantley, L.C. (1998). Phosphoinositide kinases. Annu Rev Biochem *67*, 481-507.
2. Katso, R., Okkenhaug, K., Ahmadi, K., White, S., Timms, J., and Waterfield, M.D. (2001). Cellular function of phosphoinositide 3-kinases: implications for development, homeostasis, and cancer. Annu Rev Cell Dev Biol *17*, 615-675.
3. Ward, S., Sotsios, Y., Dowden, J., Bruce, I., and Finan, P. (2003). Therapeutic potential of phosphoinositide 3-kinase inhibitors. Chem Biol *10*, 207-213.

4. Samuels, Y., Wang, Z., Bardelli, A., Silliman, N., Ptak, J., Szabo, S., Yan, H., Gazdar, A., Powell, S.M., Riggins, G.J., Willson, J.K., Markowitz, S., Kinzler, K.W., Vogelstein, B., and Velculescu, V.E. (2004). High frequency of mutations of the PIK3CA gene in human cancers. Science *304*, 554.

5. Cantley, L.C., and Neel, B.G. (1999). New insights into tumor suppression: PTEN suppresses tumor formation by restraining the phosphoinositide 3-kinase/AKT pathway. Proc Natl Acad Sci U S A *96*, 4240-4245.

6. Lau, A., Swinbank, K.M., Ahmed, P.S., Taylor, D.L., Jackson, S.P., Smith, G.C., and O'Connor, M.J. (2005). Suppression of HIV-1 infection by a small molecule inhibitor of the ATM kinase. Nat Cell Biol *7*, 493-500.

7. Sadhu, C., Masinovsky, B., Dick, K., Sowell, C.G., and Staunton, D.E. (2003). Essential role of phosphoinositide 3-kinase delta in neutrophil directional movement. J Immunol *170*, 2647-2654.

8. Jackson, S.P., Schoenwaelder, S.M., Goncalves, I., Nesbitt, W.S., Yap, C.L., Wright, C.E., Kenche, V., Anderson, K.E., Dopheide, S.M., Yuan, Y., Sturgeon, S.A., Prabaharan, H., Thompson, P.E., Smith, G.D., Shepherd, P.R., Daniele, N., Kulkarni, S., Abbott, B., Saylik, D., Jones, C., Lu, L., Giuliano, S., Hughan, S.C., Angus, J.A., Robertson, A.D., and Salem, H.H. (2005). PI 3-kinase p110beta: a new target for antithrombotic therapy. Nat Med *11*, 507-514.

9. Knight, Z.A., Chiang, G.G., Alaimo, P.J., Kenski, D.M., Ho, C.B., Coan, K., Abraham, R.T., and Shokat, K.M. (2004). Isoform-specific phosphoinositide 3-kinase inhibitors from an arylmorpholine scaffold. Bioorg Med Chem *12*, 4749-4759.

10. Condliffe, A.M., Davidson, K., Anderson, K.E., Ellson, C.D., Crabbe, T., Okkenhaug, K., Vanhaesebroeck, B., Turner, M., Webb, L., Wymann, M.P., Hirsch, E., Ruckle, T., Camps, M., Rommel, C., Jackson, S.P., Chilvers, E.R., Stephens, L.R., and Hawkins, P.T. (2005). Sequential activation of class IB and class IA PI3K is important for the primed respiratory burst of human but not murine neutrophils. Blood *106*, 1432-1440.

11. Camps, M., Ruckle, T., Ji, H., Ardissone, V., Rintelen, F., Shaw, J., Ferrandi, C., Chabert, C., Gillieron, C., Francon, B., Martin, T., Gretener, D., Perrin, D., Leroy, D., Vitte, P.A., Hirsch, E., Wymann, M.P., Cirillo, R., Schwarz, M.K., and Rommel, C. (2005). Blockade of PI3Kgamma suppresses joint inflammation and damage in mouse models of rheumatoid arthritis. Nat Med.

12. Bi, L., Okabe, I., Bernard, D.J., and Nussbaum, R.L. (2002). Early embryonic lethality in mice deficient in the p110beta catalytic subunit of PI 3-kinase. Mamm Genome *13*, 169-172.

13. Bi, L., Okabe, I., Bernard, D.J., Wynshaw-Boris, A., and Nussbaum, R.L. (1999). Proliferative defect and embryonic lethality in mice homozygous for a deletion in the p110alpha subunit of phosphoinositide 3-kinase. J Biol Chem *274*, 10963-10968.

14. Ueki, K., Fruman, D.A., Yballe, C.M., Fasshauer, M., Klein, J., Asano, T., Cantley, L.C., and Kahn, C.R. (2003). Positive and negative roles of p85 alpha and p85 beta regulatory subunits of phosphoinositide 3-kinase in insulin signaling. J Biol Chem *278*, 48453-48466.

15. Ueki, K., Yballe, C.M., Brachmann, S.M., Vicent, D., Watt, J.M., Kahn, C.R., and Cantley, L.C. (2002). Increased insulin sensitivity in mice lacking p85beta subunit of phosphoinositide 3-kinase. Proc Natl Acad Sci U S A *99*, 419-424.

16. Yu, J., Zhang, Y., McIlroy, J., Rordorf-Nikolic, T., Orr, G.A., and Backer, J.M. (1998). Regulation of the p85/p110 phosphatidylinositol 3'-kinase: stabilization and inhibition of the p110alpha catalytic subunit by the p85 regulatory subunit. Mol Cell Biol *18*, 1379-1387.

17. Luo, J., Field, S.J., Lee, J.Y., Engelman, J.A., and Cantley, L.C. (2005). The p85 regulatory subunit of phosphoinositide 3-kinase down-regulates IRS-1 signaling via the formation of a sequestration complex. J Cell Biol *170*, 455-464.

18. Vanhaesebroeck, B., Ali, K., Bilancio, A., Geering, B., and Foukas, L.C. (2005). Signalling by PI3K isoforms: insights from gene-targeted mice. Trends Biochem Sci *30*, 194-204.

19. Fruman, D.A., Mauvais-Jarvis, F., Pollard, D.A., Yballe, C.M., Brazil, D., Bronson, R.T., Kahn, C.R., and Cantley, L.C. (2000). Hypoglycaemia, liver necrosis and perinatal death in mice lacking all isoforms of phosphoinositide 3-kinase p85 alpha. Nat Genet *26*, 379-382.

20. Peng, Y., Woods, R.G., Beamish, H., Ye, R., Lees-Miller, S.P., Lavin, M.F., and Bedford, J.S. (2005). Deficiency in the catalytic subunit of DNA-dependent protein kinase causes down-regulation of ATM. Cancer Res *65*, 1670-1677.

21. Knight, Z.A., and Shokat, K.M. (2005). Features of selective kinase inhibitors. Chem Biol *12*, 621-637.

22. Okkenhaug, K., Bilancio, A., Farjot, G., Priddle, H., Sancho, S., Peskett, E., Pearce, W., Meek, S.E., Salpekar, A., Waterfield, M.D., Smith, A.J., and Vanhaesebroeck, B. (2002). Impaired B and T cell antigen receptor signaling in p110delta PI 3-kinase mutant mice. Science *297*, 1031-1034.

23. Jou, S.T., Carpino, N., Takahashi, Y., Piekorz, R., Chao, J.R., Carpino, N., Wang, D., and Ihle, J.N. (2002). Essential, nonredundant role for the phosphoinositide 3-kinase p110delta in signaling by the B-cell receptor complex. Mol Cell Biol *22*, 8580-8591.

24. Okkenhaug, K., and Vanhaesebroeck, B. (2003). PI3K-signalling in B- and T-cells: insights from gene-targeted mice. Biochem Soc Trans *31*, 270-274.

25. Patrucco, E., Notte, A., Barberis, L., Selvetella, G., Maffei, A., Brancaccio, M., Marengo, S., Russo, G., Azzolino, O., Rybalkin, S.D., Silengo, L., Altruda, F., Wetzker, R., Wymann, M.P., Lembo, G., and Hirsch, E. (2004). PI3Kgamma

modulates the cardiac response to chronic pressure overload by distinct kinase-dependent and -independent effects. Cell *118*, 375-387.

26. Vanhaesebroeck, B., Rohn, J.L., and Waterfield, M.D. (2004). Gene targeting: attention to detail. Cell *118*, 274-276.

27. Domin, J., and Waterfield, M.D. (1997). Using structure to define the function of phosphoinositide 3-kinase family members. FEBS Lett *410*, 91-95.

28. Walker, E.H., Pacold, M.E., Perisic, O., Stephens, L., Hawkins, P.T., Wymann, M.P., and Williams, R.L. (2000). Structural determinants of phosphoinositide 3-kinase inhibition by wortmannin, LY294002, quercetin, myricetin, and staurosporine. Mol Cell *6*, 909-919.

29. Walker, E.H., Perisic, O., Ried, C., Stephens, L., and Williams, R.L. (1999). Structural insights into phosphoinositide 3-kinase catalysis and signalling. Nature *402*, 313-320.

30. Hickson, I., Zhao, Y., Richardson, C.J., Green, S.J., Martin, N.M., Orr, A.I., Reaper, P.M., Jackson, S.P., Curtin, N.J., and Smith, G.C. (2004). Identification and characterization of a novel and specific inhibitor of the ataxia-telangiectasia mutated kinase ATM. Cancer Res *64*, 9152-9159.

31. Schindler, T., Bornmann, W., Pellicena, P., Miller, W.T., Clarkson, B., and Kuriyan, J. (2000). Structural mechanism for STI-571 inhibition of abelson tyrosine kinase. Science *289*, 1938-1942.

32. Madhusudan, Trafny, E.A., Xuong, N.H., Adams, J.A., Teneyck, L.F., Taylor, S.S., and Sowadski, J.M. (1994). cAMP-Dependent Protein-Kinase - Crystallographic Insights Into Substrate Recognition and Phosphotransfer. Protein Science *3*, 176-187.

33. Branca, M.A. (2005). Multi-kinase inhibitors create buzz at ASCO. Nat Biotechnol *23*, 639.

34. Alaimo, P.J., Knight, Z.A., and Shokat, K.M. (2005). Targeting the gatekeeper residue in phosphoinositide 3-kinases. Bioorg Med Chem *13*, 2825-2836.

35. Ruderman, N.B., Kapeller, R., White, M.F., and Cantley, L.C. (1990). Activation of phosphatidylinositol 3-kinase by insulin. Proc Natl Acad Sci U S A *87*, 1411-1415.

36. Cheatham, B., Vlahos, C.J., Cheatham, L., Wang, L., Blenis, J., and Kahn, C.R. (1994). Phosphatidylinositol 3-kinase activation is required for insulin stimulation of pp70 S6 kinase, DNA synthesis, and glucose transporter translocation. Mol Cell Biol *14*, 4902-4911.

37. Okada, T., Kawano, Y., Sakakibara, T., Hazeki, O., and Ui, M. (1994). Essential role of phosphatidylinositol 3-kinase in insulin-induced glucose transport and antilipolysis in rat adipocytes. Studies with a selective inhibitor wortmannin. J Biol Chem *269*, 3568-3573.

38. Katagiri, H., Asano, T., Ishihara, H., Inukai, K., Shibasaki, Y., Kikuchi, M., Yazaki, Y., and Oka, Y. (1996). Overexpression of catalytic subunit p110alpha of phosphatidylinositol 3-kinase increases glucose transport activity with translocation of glucose transporters in 3T3-L1 adipocytes. J Biol Chem *271*, 16987-16990.

39. Frevert, E.U., and Kahn, B.B. (1997). Differential effects of constitutively active phosphatidylinositol 3-kinase on glucose transport, glycogen synthase activity, and DNA synthesis in 3T3-L1 adipocytes. Mol Cell Biol *17*, 190-198.

40. Egawa, K., Sharma, P.M., Nakashima, N., Huang, Y., Huver, E., Boss, G.R., and Olefsky, J.M. (1999). Membrane-targeted phosphatidylinositol 3-kinase mimics insulin actions and induces a state of cellular insulin resistance. J Biol Chem *274*, 14306-14314.

41. George, S., Rochford, J.J., Wolfrum, C., Gray, S.L., Schinner, S., Wilson, J.C., Soos, M.A., Murgatroyd, P.R., Williams, R.M., Acerini, C.L., Dunger, D.B., Barford, D., Umpleby, A.M., Wareham, N.J., Davies, H.A., Schafer, A.J., Stoffel, M., O'Rahilly, S., and Barroso, I. (2004). A family with severe insulin resistance and diabetes due to a mutation in AKT2. Science *304*, 1325-1328.

42. Asano, T., Kanda, A., Katagiri, H., Nawano, M., Ogihara, T., Inukai, K., Anai, M., Fukushima, Y., Yazaki, Y., Kikuchi, M., Hooshmand-Rad, R., Heldin, C.H., Oka, Y., and Funaki, M. (2000). p110beta is up-regulated during differentiation of 3T3-L1 cells and contributes to the highly insulin-responsive glucose transport activity. J Biol Chem *275*, 17671-17676.

43. Brachmann, S.M., Ueki, K., Engelman, J.A., Kahn, R.C., and Cantley, L.C. (2005). Phosphoinositide 3-kinase catalytic subunit deletion and regulatory subunit deletion have opposite effects on insulin sensitivity in mice. Mol Cell Biol *25*, 1596-1607.

44. Harrington, L.S., Findlay, G.M., and Lamb, R.F. (2005). Restraining PI3K: mTOR signalling goes back to the membrane. Trends Biochem Sci *30*, 35-42.

45. Viniegra, J.G., Martinez, N., Modirassari, P., Losa, J.H., Parada Cobo, C., Lobo, V.J., Luquero, C.I., Alvarez-Vallina, L., Ramon y Cajal, S., Rojas, J.M., and Sanchez-Prieto, R. (2005). Full activation of PKB/Akt in response to insulin or ionizing radiation is mediated through ATM. J Biol Chem *280*, 4029-4036.

46. Feng, J., Park, J., Cron, P., Hess, D., and Hemmings, B.A. (2004). Identification of a PKB/Akt hydrophobic motif Ser-473 kinase as DNA-dependent protein kinase. J Biol Chem *279*, 41189-41196.

47. Sun, X.J., Rothenberg, P., Kahn, C.R., Backer, J.M., Araki, E., Wilden, P.A., Cahill, D.A., Goldstein, B.J., and White, M.F. (1991). Structure of the insulin receptor substrate IRS-1 defines a unique signal transduction protein. Nature *352*, 73-77.

48. Gual, P., Le Marchand-Brustel, Y., and Tanti, J.F. (2005). Positive and negative regulation of insulin signaling through IRS-1 phosphorylation. Biochimie *87*, 99-109.

49. Gual, P., Gremeaux, T., Gonzalez, T., Le Marchand-Brustel, Y., and Tanti, J.F. (2003). MAP kinases and mTOR mediate insulin-induced phosphorylation of insulin receptor substrate-1 on serine residues 307, 612 and 632. Diabetologia *46*, 1532-1542.

50. Schindler, T., Sicheri, F., Pico, A., Gazit, A., Levitzki, A., and Kuriyan, J. (1999). Crystal structure of Hck in complex with a Src family-selective tyrosine kinase inhibitor. Mol Cell *3*, 639-648.

51. Lakshmanan, J., Elmendorf, J.S., and Ozcan, S. (2003). Analysis of insulin-stimulated glucose uptake in differentiated 3T3-L1 adipocytes. Methods Mol Med *83*, 97-103.

52. Jolliffe, I.T. (2002). Principal component analysis, 2nd Edition (New York: Springer).

53. Bateman, A., Birney, E., Durbin, R., Eddy, S.R., Howe, K.L., and Sonnhammer, E.L. (2000). The Pfam protein families database. Nucleic Acids Res *28*, 263-266.

54. Jacinto, E., Loewith, R., Schmidt, A., Lin, S., Ruegg, M.A., Hall, A., and Hall, M.N. (2004). Mammalian TOR complex 2 controls the actin cytoskeleton and is rapamycin insensitive. Nat Cell Biol *6*, 1122-1128.

55. Mhaske, S.B., and Argade, N.P. (2004). Regioselective quinazolinone-directed ortho lithiation of quinazolinoylquinoline: practical synthesis of naturally occurring human DNA topoisomerase I poison luotonin a and luotonins B and E. J Org Chem *69*, 4563-4566.

56. Armstrong, V.W., N.H., C., and Ramage, R. (1975). A new brominating reagent: 2-carboxyethyltriphenylphosphonium perbromide. Tetrahedron Letters *6*, 373-376.

57. Morris, J., Wishka, D.G., and Fang, Y. (1994). A cyclodehydration route to 2-aminochromones. Synthetic Communications *24*, 849-858.

58. Lombardino, J.G. (1965). Preparation and new reactions of imidazo[1,2-a]pyridines. Journal of Organic Chemistry *30*, 2403-2407.

59. Almirante, L., Mugnaini, A., De Toma, N., Gamba, A., and Murmann, W. (1970). Imidazole Derivatives. IV. Synthesis and Pharmacological Activity of Oxygenated Derivatives of Imidazo[1,2-a]pyridine. Journal of Medicinal Chemistry *13*, 1048-1051.

c-Abl[1] (peptide)	12
v-Abl[2] (peptide)	14
v-Abl[2] (casein)	18
v-Abl[3] (peptide)	21
Akt[4] (peptide)	43
Akt1[5] (peptide)	132
Akt1-cat[5] (peptide)	26
Akt1	470
Akt2[5] (peptide)	254
Akt2-cat[5] (peptide)	36
ATM[6] (Mn) (PHAS-1)	29
ATM[6] (Mn) (PHAS-1+DNA)	15
Aurora 2[7] (peptide)	34
Aurora 2[8] (peptide)	50
Aurora 2-cat[8] (peptide)	50
Btk	29
Cak1-*Sc*[9] (CDK2)	5.0
Cak1-*Pb*[9] (CDK2)	8.5
Cak1-*Ca*[9] (CDK2)	1.8
Cak1-*At*[9] (CDK2)	60
CaMKI[10] (peptide)	110
CaMKIIα[11] (auto)	19
CaMKII[12] (auto)	7.5
CaMKIV[13] (peptide)	27
CaMKKα[14] (CamKI)	33
CaMKKβ[14] (CamKI)	33
CDK1/cyclin B[15]	2.3
CDK2/cyclin A[16] (Rb-C)	23
CDK2/cyclin E[17] (peptide)	3.6
CDK4/cyclin D1[16] (Rb-C)	418
CDK4/cyclin D2[18]	200
CDK4/cyclin D	18
CDK5/p25[17] (peptide)	3.2
Chk1[19] (peptide)	1.4
Chk2[19] (peptide)	3.3
CK1α-*Ze*[20] (casein)	33
CK-p45[21] (casein)	3.5
CK-A[22] (casein)	19
CK2α[22] (casein)	12
CK2α	10
CK2α[23]	13.9
CK2β[23]	8.8
CLK1[24] (Mn) (MBP)	80
Csk[25] (peptide)	195
Csk[25] (Mn) (peptide)	12
Csk[26] (peptide)	120
Csk[27] (peptide)	160
Csk[28] (Mn) (casein)	46
Csk[29] (Mn) (peptide)	8.9
Csk[30] (Mn) (Lck)	4.9
Csk[31] (Mn) (peptide)	12
Csk[30] (Lck)	15
Csk	11.5
CTR1-*Ar*[32] (Mn) (MBP)	9.1
DAPK[33] (peptide)	2.4
DMPK[34] (MBS)	2.3
DNA-PK[35] (peptide)	228
EGFR[36] (Mn) (peptide)	18
EGFR[37] (Mn) (peptide)	11.2
EGFR[38] (Mn) (peptide)	5
EGFR[39] (Mn) (peptide)	4.5
EGFR[38] (peptide)	17
EphA7[40] (peptide)	30
EphB3[41] (Mn) (peptide)	2.7
ErbB-2[38] (peptide)	27
ErbB-2[38] (Mn) (peptide)	13
ErbB-4[38] (peptide)	37
ErbB-4[38] (Mn) (peptide)	21
Erk2[42] (peptide)	76
Erk2[43] (Elk1)	16
Erk2[44] (MBP)	47
Erk2[45] (Ets-1)	140
Erk2[46] (TAL2)	220
Erk2[46] (peptide)	350
Erk2[46] (MBP)	190
FAK[47] (Mn) (peptide)	4.3
FAK[47] (Mn) (p) (peptide)	6.7
FER[40] (peptide)	7
FER[48] (peptide)	7.1
c-Fgr[49] (peptide)	20
FGFR1[50] (Mn) (peptide)	4.6
FGFR1[27] (peptide)	70
Fyn[51] (peptide)	70
GRK1[52] (rhodopsin)	2
GRK2[53] (rhodopsin)	60.8
GRK3[53] (rhodopsin)	88.8
GRK5[54] (rhodopsin)	23.8
GRK6[54] (rhodopsin)	111
GSK3β[55] (peptide)	50.2
IGFR[56] (0p) (peptide)	720
IGFR[56] (1p) (peptide)	527
IGFR[56] (2p) (peptide)	148
IGFR[56] (3p) (peptide)	107
IGFR[56] (3p) (peptide)	90.1
IKK[57] (peptide)	10
IKK-i[58] (Mn) (IκB)	3.1
IKK-α[59] (Mn) (IκB)	0.126
IKK-β[59] (Mn) (IκB)	0.136
IKK-β[60] (Mn) (IκB)	0.1
IKK-β[60] (Mn) (IκB)	0.11
IKK-1/IKK-2[61] (IκB)	13
IKK-2/IKK-2[61] (IκB)	18
IKK-1/IKK-1[58] (Mn) (IκB)	0.9
IKK-2/IKK-2[58] (Mn) (IκB)	0.6

IKK-1/IKK-2[58] (Mn) (IκB)	0.6	PDGFRβ[91] (Mn) (0p) (peptide)	80
IKK-1/IKK-1[62] (Mn) (IκB)	0.63	PDGFRβ[91] (Mn) (p) (peptide)	320
IKK-2/IKK-2[62] (Mn) (IκB)	0.56	PI3KC2α[92] (PI)	32
IKK-1/IKK-1[63] (Mn) (IκB)	0.9	PI3KC2α[92] (PI4P)	54
IKK-2/IKK-2[63] (Mn) (IκB)	0.65	PI3KC2β[93] (PI)	120
IKK-1/IKK-2[63] (Mn) (IκB)	0.63	PI4KIIα[94] (PI)	28
InsR[64] (0p) (peptide)	800	PI4KII[95] (PI)	120
InsR[65] (0p) (peptide)	900	PI4KIIIα[96] (PI)	300
InsR[64] (3p) (peptide)	130	PI4KIIIβ[97] (PI)	1000
InsR[65] (3p) (peptide)	40	PI4KIIIβ[95] (PI)	422
InsR[66] (Mn) (auto)	208	PI4KIIIα/β[98] (PI)	410
ITK[67] (SAM68)	36	PI(4)P(5)KI[99] (PIP)	25
ITK[40] (peptide)	40	PI(4)P(5)KIα[100] (PI4P)	27
ITK-cat[68] (peptide)	61.8	PI(4)P(5)KIβ[100] (PI4P)	33
ITK[68] (peptide)	7.8	PI(4)P(5)KIγ[100] (PI4P)	39
IRAK4[69] (peptide)	600	PI(5)P(4)KII[99] (PIP)	5
JAK1[40] (peptide)	15	PAK2[101] (ATPase)	150
JAK3[70] (peptide)	6	PAK2[101] (MBP)	71
JNK2[43] (c-Jun)	39	PhK[102] (phosphorylase)	200
JNK2[71] (ATF2)	1.9	PKA-α[103] (peptide)	41.7
JNK3α1[71] (ATF2)	1.9	PKA-α[104] (histone)	25
c-Kit[72] (peptide)	53.6	PKA-α[104] (peptide)	25
Lck[73] (Mn) (peptide)	2	PKA-γ[104] (histone)	9.1
Lck[73] (Mn) (peptide)	3	PKA-γ[104] (peptide)	10
Lck[74] (Mn) (peptide)	4	PKA-βI[103] (peptide)	44.7
Lck[75] (Mn) (enolase)	10	PKC[105] (auto)	1.5
Lyn	35	PKC[105] (histone)	15
MAPKAPK2[76] (peptide)	43	PKC-α	20
MEK1[77] (ERK1)	5.6	PKC-α[106] (histone)	24.3
MER[40] (peptide)	40	PKC-βI[106] (histone)	37.2
mTOR[78] (S6K1)	1000	PKC-βII	20
MuSK[79] (0p)	3400	PKC-γ[106] (histone)	36
MuSK[79] (3p)	380	PKC-ε[107] (peptide)	14.5
NIMA-*As*[80] (casein)	69	PKC-θ[108] (peptide)	49
p38α[81] (ATF-2)	25	PKG[109]	5.1
p38α[82] (MK2a)	27	PLK1[110]	2.6
p38α[83] (ATF-2)	20	Raf-1[111] (MAPKK)	11.6
p38α[43] (ATF-2)	240	Raf-1	3.3
p38α[42] (peptide)	260	ROCK-I	4.5
p38α[84] (peptide)	200	ROCK-II[112] (peptide)	21
p38α[85] (peptide)	100	ROCK-II[113] (peptide)	20
p38γ[86] (ATPase)	37	ROCK-II[34] (MBS)	4.5
p38γ[86] (EGFR)	54	Sky1p-*Sc*[114] (Npl3)	235
p38γ[86] (ATF-2)	27	smMLCK[115] (myosin)	71
p38-2[87] (ATF-2)	5.8	smMLCK[116] (myosin)	50
p90Rsk-B[88] (peptide)	35	skMLCK[117] (myosin) (0p)	101
p110α/p85α[89] (PI)	62	skMLCK[117] (myosin) (p)	135
p110α/p85α[89] (PIP_2)	230	skMLCK[115] (myosin)	340
p110γ[35] (PI)	7.5	c-Src[118] (peptide)	80
p110γ[90] (PI)	7.3	c-Src[119] (peptide)	90
PDGFRβ[50] (Mn) (auto)	2.2	c-Src[119] (peptide)	90
PDGFRβ[40] (peptide)	15	c-Src[120] (ATPase,pY)	169

c-Src[120] (ATPase, pY)	147
c-Src[120] (ATPase)	147
c-Src[120] (ATPase)	127
c-Src[119] (peptide)	137
c-Src[121] (peptide)	160
c-Src[121] (peptide)	150
c-Src[121] (peptide)	130
c-Src[122] (peptide) (pY419)	148
c-Src[122] (peptide) (pY419)	134
c-Src[122] (peptide) (pY530)	97
c-Src[122] (peptide) (pY530)	76
c-Src[123] (Mn) (peptide)	30
c-Src[124] (Mn) (peptide)	54
c-Src[123] (Mn) (peptide)	51
v-Src-cat[125] (peptide)	11.5
v-Src-cat[51] (peptide)	12
Syk[126] (peptide)	10
c-Tak1[19] (peptide)	3.3
Tie-2[127] (auto)	712
Tie-2[127] (histone) (0p)	366
Tie-2[127] (histone) (2p)	73.9
TBK-1[58] (Mn) (IκB)	5.9
TrkA[128] (Mn) (PLCγ)	9
VEGFR2[50] (Mn) (peptide)	0.53
VEGFR2[129] (5p) (peptide)	130
VEGFR2[130] (5p) (peptide)	150
VEGFR2[130] (0p) (peptide)	600
VEGFR2[129] (0p) (peptide)	900
c-Yes[123] (Mn) (peptide)	23
c-Yes[123] (Mn) (peptide)	16
Zap-70[131] (Mn) (cfb3)	3

1. Liu, Y., Witucki, L.A., Shah, K., Bishop, A.C., and Shokat, K.M. (2000). Src-Abl tyrosine kinase chimeras: replacement of the adenine binding pocket of c-Abl with v-Src to swap nucleotide and inhibitor specificities. Biochemistry *39*, 14400-14408.

2. Pritchard, M.L., Rieman, D., Feild, J., Kruse, C., Rosenberg, M., Poste, G., Greig, R.G., and Ferguson, B.Q. (1989). A truncated v-abl-derived tyrosine-specific tyrosine kinase expressed in Escherichia coli. Biochem J *257*, 321-329.

3. Lydon, N.B., Adams, B., Poschet, J.F., Gutzwiller, A., and Matter, A. (1990). An E. coli expression system for the rapid purification and characterization of a v-abl tyrosine protein kinase. Oncogene Res *5*, 161-173.

4. Turek, T.C., Small, E.C., Bryant, R.W., and Hill, W.A. (2001). Development and validation of a competitive AKT serine/threonine kinase fluorescence polarization assay using a product-specific anti-phospho-serine antibody. Anal Biochem *299*, 45-53.

5. Barnett, S.F., Defeo-Jones, D., Fu, S., Hancock, P.J., Haskell, K.M., Jones, R.E., Kahana, J.A., Kral, A.M., Leander, K., Lee, L.L., Malinowski, J., McAvoy, E.M., Nahas, D.D., Robinson, R.G., and Huber, H.E. (2004). Identification and characterization of pleckstrin homology domain dependent and isozyme specific Akt inhibitors. Biochem J *Pt*.

6. Goodarzi, A.A., and Lees-Miller, S.P. (2004). Biochemical characterization of the ataxia-telangiectasia mutated (ATM) protein from human cells. DNA Repair (Amst) *3*, 753-767.

7. Sun, C., Newbatt, Y., Douglas, L., Workman, P., Aherne, W., and Linardopoulos, S. (2004). High-throughput screening assay for identification of small molecule inhibitors of Aurora2/STK15 kinase. J Biomol Screen *9*, 391-397.

8. Cheetham, G.M., Knegtel, R.M., Coll, J.T., Renwick, S.B., Swenson, L., Weber, P., Lippke, J.A., and Austen, D.A. (2002). Crystal structure of aurora-2, an oncogenic serine/threonine kinase. J Biol Chem *277*, 42419-42422.

9. Tsakraklides, V., and Solomon, M.J. (2002). Comparison of Cak1p-like cyclin-dependent kinase-activating kinases. J Biol Chem *277*, 33482-33489.

10. Chin, D., Winkler, K.E., and Means, A.R. (1997). Characterization of substrate phosphorylation and use of calmodulin mutants to address implications from the enzyme crystal structure of calmodulin-dependent protein kinase I. J Biol Chem *272*, 31235-31240.

11. Colbran, R.J. (1993). Inactivation of Ca2+/calmodulin-dependent protein kinase II by basal autophosphorylation. J Biol Chem *268*, 7163-7170.

12. Brickey, D.A., Bann, J.G., Fong, Y.L., Perrino, L., Brennan, R.G., and Soderling, T.R. (1994). Mutational analysis of the autoinhibitory domain of calmodulin kinase II. J Biol Chem *269*, 29047-29054.

13. Cruzalegui, F.H., and Means, A.R. (1993). Biochemical characterization of the multifunctional Ca2+/calmodulin-dependent protein kinase type IV expressed in insect cells. J Biol Chem *268*, 26171-26178.

14. Tokumitsu, H., Inuzuka, H., Ishikawa, Y., Ikeda, M., Saji, I., and Kobayashi, R. (2002). STO-609, a specific inhibitor of the Ca(2+)/calmodulin-dependent protein kinase kinase. J Biol Chem *277*, 15813-15818.

15. MBL Cyclex cdc2/cyclinB Kinase Assay/Inhibitor Screening Kit.

16. Kim, D.M., Yang, K., and Yang, B.S. (2003). Biochemical characterizations reveal different properties between CDK4/cyclin D1 and CDK2/cyclin A. Exp Mol Med *35*, 421-430.

17. Clare, P.M., Poorman, R.A., Kelley, L.C., Watenpaugh, K.D., Bannow, C.A., and Leach, K.L. (2001). The cyclin-dependent kinases cdk2 and cdk5 act by a random, anticooperative kinetic mechanism. J Biol Chem *276*, 48292-48299.

18. Koresawa, M., and Okabe, T. (2004). High-throughput screening with quantitation of ATP consumption: a universal non-radioisotope, homogeneous assay for protein kinase. Assay Drug Dev Technol *2*, 153-160.

19. MBL. Cyclex Checkpoint Kinase Assay/Inhibitor Screening Kit.

20. Burzio, V., Antonelli, M., Allende, C.C., and Allende, J.E. (2002). Biochemical and cellular characteristics of the four splice variants of protein kinase CK1alpha from zebrafish (Danio rerio). J Cell Biochem *86*, 805-814.

21. Angelov, I. (1994). Characterization of a proline-directed casein kinase from bovine brain. Arch Biochem Biophys *310*, 97-107.

22. Ruzzene, M., Vianello, F., Donella-Deana, A., and Deana, R. (1992). Purification and characterization of two casein kinases from ejaculated bovine spermatozoa. J Biochem (Tokyo) *112*, 768-774.

23. Mitev, V., Pauloin, A., and Houdebine, L.M. (1994). Purification and characterization of two casein kinase type II isozymes from bovine brain gray matter. J Neurochem *63*, 717-726.

24. Menegay, H.J., Myers, M.P., Moeslein, F.M., and Landreth, G.E. (2000). Biochemical characterization and localization of the dual specificity kinase CLK1. J Cell Sci *113 (Pt 18)*, 3241-3253.

25. Grace, M.R., Walsh, C.T., and Cole, P.A. (1997). Divalent ion effects and insights into the catalytic mechanism of protein tyrosine kinase Csk. Biochemistry *36*, 1874-1881.

26. Sun, G., and Budde, R.J. (1999). Mutations in the N-terminal regulatory region reduce the catalytic activity of Csk, but do not affect its recognition of Src. Arch Biochem Biophys *367*, 167-172.

27. Sun, G., and Budde, R.J. (1997). Requirement for an additional divalent metal cation to activate protein tyrosine kinases. Biochemistry *36,* 2139-2146.

28. Amrein, K.E., Takacs, B., Stieger, M., Molnos, J., Flint, N.A., and Burn, P. (1995). Purification and characterization of recombinant human p50csk protein-tyrosine kinase from an Escherichia coli expression system overproducing the bacterial chaperones GroES and GroEL. Proc Natl Acad Sci U S A *92,* 1048-1052.

29. Cole, P.A., Burn, P., Takacs, B., and Walsh, C.T. (1994). Evaluation of the catalytic mechanism of recombinant human Csk (C-terminal Src kinase) using nucleotide analogs and viscosity effects. J Biol Chem *269,* 30880-30887.

30. Sondhi, D., Xu, W., Songyang, Z., Eck, M.J., and Cole, P.A. (1998). Peptide and protein phosphorylation by protein tyrosine kinase Csk: insights into specificity and mechanism. Biochemistry *37,* 165-172.

31. Cole, P.A., Grace, M.R., Phillips, R.S., Burn, P., and Walsh, C.T. (1995). The role of the catalytic base in the protein tyrosine kinase Csk. J Biol Chem *270,* 22105-22108.

32. Huang, Y., Li, H., Hutchison, C.E., Laskey, J., and Kieber, J.J. (2003). Biochemical and functional analysis of CTR1, a protein kinase that negatively regulates ethylene signaling in Arabidopsis. Plant J *33,* 221-233.

33. Velentza, A.V., Schumacher, A.M., Weiss, C., Egli, M., and Watterson, D.M. (2001). A protein kinase associated with apoptosis and tumor suppression: structure, activity, and discovery of peptide substrates. J Biol Chem *276,* 38956-38965.

34. MBL Cyclex Rho Kinase Assay/Inhibitor Screening Kit.

35. Knight, Z.A., Chiang, G.G., Alaimo, P.J., Kenski, D.M., Ho, C.B., Coan, K., Abraham, R.T., and Shokat, K.M. (2004). Isoform-specific phosphoinositide 3-kinase inhibitors from an arylmorpholine scaffold. Bioorg Med Chem *12,* 4749-4759.

36. Gronowski, A.M., and Bertics, P.J. (1995). Modulation of epidermal growth factor receptor interaction with the detergent-insoluble cytoskeleton and its effects on receptor tyrosine kinase activity. Endocrinology *136,* 2198-2205.

37. Wedegaertner, P.B., and Gill, G.N. (1989). Activation of the purified protein tyrosine kinase domain of the epidermal growth factor receptor. J Biol Chem *264,* 11346-11353.

38. Brignola, P.S., Lackey, K., Kadwell, S.H., Hoffman, C., Horne, E., Carter, H.L., Stuart, J.D., Blackburn, K., Moyer, M.B., Alligood, K.J., Knight, W.B., and Wood, E.R. (2002). Comparison of the biochemical and kinetic properties of the type 1 receptor tyrosine kinase intracellular domains. Demonstration of differential sensitivity to kinase inhibitors. J Biol Chem *277,* 1576-1585.

39. McGlynn, E., Becker, M., Mett, H., Reutener, S., Cozens, R., and Lydon, N.B. (1992). Large-scale purification and characterisation of a recombinant epidermal growth-factor receptor protein-tyrosine kinase. Modulation of activity by multiple factors. Eur J Biochem *207*, 265-275.

40. Kawase, Y., OHmoto, H., Kirii, Y., Inoue, Y., and Ishiguro, H. Comprehensive Protein Kinase Profiling Panels for Inhibitor Selectivity Screening. Poster from Carna Biosciences.

41. Bembenek, M.E., Schmidt, S., Li, P., Morawiak, J., Prack, A., Jain, S., Roy, R., Parsons, T., and Chee, L. (2003). Characterization of the kinase domain of the ephrin-B3 receptor tyrosine kinase using a scintillation proximity assay. Assay Drug Dev Technol *1*, 555-563.

42. Fox, T., Coll, J.T., Xie, X., Ford, P.J., Germann, U.A., Porter, M.D., Pazhanisamy, S., Fleming, M.A., Galullo, V., Su, M.S., and Wilson, K.P. (1998). A single amino acid substitution makes ERK2 susceptible to pyridinyl imidazole inhibitors of p38 MAP kinase. Protein Sci *7*, 2249-2255.

43. Forrer, P., Tamaskovic, R., and Jaussi, R. (1998). Enzyme-linked immunosorbent assay for measurement of JNK, ERK, and p38 kinase activities. Biol Chem *379*, 1101-1111.

44. Prowse, C.N., Hagopian, J.C., Cobb, M.H., Ahn, N.G., and Lew, J. (2000). Catalytic reaction pathway for the mitogen-activated protein kinase ERK2. Biochemistry *39*, 6258-6266.

45. Waas, W.F., and Dalby, K.N. (2001). Purification of a model substrate for transcription factor phosphorylation by ERK2. Protein Expr Purif *23*, 191-197.

46. Robinson, M.J., Harkins, P.C., Zhang, J., Baer, R., Haycock, J.W., Cobb, M.H., and Goldsmith, E.J. (1996). Mutation of position 52 in ERK2 creates a nonproductive binding mode for adenosine 5'-triphosphate. Biochemistry *35*, 5641-5646.

47. Withers, B.E., Keller, P.R., and Fry, D.W. (1996). Expression, purification and characterization of focal adhesion kinase using a baculovirus system. Protein Expr Purif *7*, 12-18.

48. Feller, S.M., and Wong, T.W. (1992). Identification and characterization of a cytosolic protein tyrosine kinase of HeLa cells. Biochemistry *31*, 3044-3051.

49. Ruzzene, M., Brunati, A.M., Donella-Deana, A., Marin, O., and Pinna, L.A. (1997). Specific stimulation of c-Fgr kinase by tyrosine-phosphorylated (poly)peptides--possible implication in the sequential mode of protein phosphorylation. Eur J Biochem *245*, 701-707.

50. Laird, A.D., Vajkoczy, P., Shawver, L.K., Thurnher, A., Liang, C., Mohammadi, M., Schlessinger, J., Ullrich, A., Hubbard, S.R., Blake, R.A., Fong, T.A., Strawn, L.M., Sun, L., Tang, C., Hawtin, R., Tang, F., Shenoy, N., Hirth, K.P., McMahon,

G., and Cherrington (2000). SU6668 is a potent antiangiogenic and antitumor agent that induces regression of established tumors. Cancer Res *60,* 4152-4160.

51. Liu, Y., Shah, K., Yang, F., Witucki, L., and Shokat, K.M. (1998). Engineering Src family protein kinases with unnatural nucleotide specificity. Chem Biol *5,* 91-101.

52. Palczewski, K., McDowell, J.H., and Hargrave, P.A. (1988). Purification and characterization of rhodopsin kinase. J Biol Chem *263,* 14067-14073.

53. Kim, C.M., Dion, S.B., Onorato, J.J., and Benovic, J.L. (1993). Expression and characterization of two beta-adrenergic receptor kinase isoforms using the baculovirus expression system. Receptor *3,* 39-55.

54. Kunapuli, P., Onorato, J.J., Hosey, M.M., and Benovic, J.L. (1994). Expression, purification, and characterization of the G protein-coupled receptor kinase GRK5. J Biol Chem *269,* 1099-1105.

55. Ryves, W.J., and Harwood, A.J. (2001). Lithium inhibits glycogen synthase kinase-3 by competition for magnesium. Biochem Biophys Res Commun *280,* 720-725.

56. Favelyukis, S., Till, J.H., Hubbard, S.R., and Miller, W.T. (2001). Structure and autoregulation of the insulin-like growth factor 1 receptor kinase. Nat Struct Biol *8,* 1058-1063.

57. Hideshima, T., Chauhan, D., Richardson, P., Mitsiades, C., Mitsiades, N., Hayashi, T., Munshi, N., Dang, L., Castro, A., Palombella, V., Adams, J., and Anderson, K.C. (2002). NF-kappa B as a therapeutic target in multiple myeloma. J Biol Chem *277,* 16639-16647.

58. Kishore, N., Huynh, Q.K., Mathialagan, S., Hall, T., Rouw, S., Creely, D., Lange, G., Caroll, J., Reitz, B., Donnelly, A., Boddupalli, H., Combs, R.G., Kretzmer, K., and Tripp, C.S. (2002). IKK-i and TBK-1 are enzymatically distinct from the homologous enzyme IKK-2: comparative analysis of recombinant human IKK-i, TBK-1, and IKK-2. J Biol Chem *277,* 13840-13847.

59. Li, J., Peet, G.W., Pullen, S.S., Schembri-King, J., Warren, T.C., Marcu, K.B., Kehry, M.R., Barton, R., and Jakes, S. (1998). Recombinant IkappaB kinases alpha and beta are direct kinases of Ikappa Balpha. J Biol Chem *273,* 30736-30741.

60. Sadler, T.M., Achilleos, M., Ragunathan, S., Pitkin, A., LaRocque, J., Morin, J., Annable, R., Greenberger, L.M., Frost, P., and Zhang, Y. (2004). Development and comparison of two nonradioactive kinase assays for I kappa B kinase. Anal Biochem *326,* 106-113.

61. Wisniewski, D., LoGrasso, P., Calaycay, J., and Marcy, A. (1999). Assay for IkappaB kinases using an in vivo biotinylated IkappaB protein substrate. Anal Biochem *274,* 220-228.

62. Mercurio, F., Murray, B.W., Shevchenko, A., Bennett, B.L., Young, D.B., Li, J.W., Pascual, G., Motiwala, A., Zhu, H., Mann, M., and Manning, A.M. (1999). IkappaB kinase (IKK)-associated protein 1, a common component of the heterogeneous IKK complex. Mol Cell Biol *19*, 1526-1538.

63. Huynh, Q.K., Boddupalli, H., Rouw, S.A., Koboldt, C.M., Hall, T., Sommers, C., Hauser, S.D., Pierce, J.L., Combs, R.G., Reitz, B.A., Diaz-Collier, J.A., Weinberg, R.A., Hood, B.L., Kilpatrick, B.F., and Tripp, C.S. (2000). Characterization of the recombinant IKK1/IKK2 heterodimer. Mechanisms regulating kinase activity. J Biol Chem *275*, 25883-25891.

64. Li, S., Covino, N.D., Stein, E.G., Till, J.H., and Hubbard, S.R. (2003). Structural and biochemical evidence for an autoinhibitory role for tyrosine 984 in the juxtamembrane region of the insulin receptor. J Biol Chem *278*, 26007-26014.

65. Frankel, M., Ablooglu, A.J., Leone, J.W., Rusinova, E., Ross, J.B., Heinrikson, R.L., and Kohanski, R.A. (2001). Intrasteric inhibition of ATP binding is not required to prevent unregulated autophosphorylation or signaling by the insulin receptor. Mol Cell Biol *21*, 4197-4207.

66. Ridge, K.D., Hofmann, K., and Finn, F.M. (1988). ATP sensitizes the insulin receptor to insulin. Proc Natl Acad Sci U S A *85*, 9489-9493.

67. Hawkins, J., and Marcy, A. (2001). Characterization of Itk tyrosine kinase: contribution of noncatalytic domains to enzymatic activity. Protein Expr Purif *22*, 211-219.

68. Brown, K., Long, J.M., Vial, S.C., Dedi, N., Dunster, N.J., Renwick, S.B., Tanner, A.J., Frantz, J.D., Fleming, M.A., and Cheetham, G.M. (2004). Crystal structures of interleukin-2 tyrosine kinase and their implications for the design of selective inhibitors. J Biol Chem *279*, 18727-18732.

69. Maly, D.J. personal communication.

70. Wang, R., Griffin, P.R., Small, E.C., and Thompson, J.E. (2003). Mechanism of Janus kinase 3-catalyzed phosphorylation of a Janus kinase 1 activation loop peptide. Arch Biochem Biophys *410*, 7-15.

71. Lisnock, J., Griffin, P., Calaycay, J., Frantz, B., Parsons, J., O'Keefe, S.J., and LoGrasso, P. (2000). Activation of JNK3 alpha 1 requires both MKK4 and MKK7: kinetic characterization of in vitro phosphorylated JNK3 alpha 1. Biochemistry *39*, 3141-3148.

72. Chan, P.M., Ilangumaran, S., La Rose, J., Chakrabartty, A., and Rottapel, R. (2003). Autoinhibition of the kit receptor tyrosine kinase by the cytosolic juxtamembrane region. Mol Cell Biol *23*, 3067-3078.

73. Seethala, R. (2000). Fluorescence polarization competition immunoassay for tyrosine kinases. Methods *22*, 61-70.

74. Snow, R.J., Cardozo, M.G., Morwick, T.M., Busacca, C.A., Dong, Y., Eckner, R.J., Jacober, S., Jakes, S., Kapadia, S., Lukas, S., Panzenbeck, M., Peet, G.W., Peterson, J.D., Prokopowicz, A.S., 3rd, Sellati, R., Tolbert, R.M., Tschantz, M.A., and Moss, N. (2002). Discovery of 2-phenylamino-imidazo[4,5-h]isoquinolin-9-ones: a new class of inhibitors of lck kinase. J Med Chem *45*, 3394-3405.

75. Flint, N.A., Amrein, K.E., Jascur, T., and Burn, P. (1994). Purification and characterization of an activated form of the protein tyrosine kinase Lck from an Escherichia coli expression system. J Cell Biochem *55*, 389-397.

76. Schindler, J.F., Godbey, A., Hood, W.F., Bolten, S.L., Broadus, R.M., Kasten, T.P., Cassely, A.J., Hirsch, J.L., Merwood, M.A., Nagy, M.A., Fok, K.F., Saabye, M.J., Morgan, H.M., Compton, R.P., Mourey, R.J., Wittwer, A.J., and Monahan, J.B. (2002). Examination of the kinetic mechanism of mitogen-activated protein kinase activated protein kinase-2. Biochim Biophys Acta *1598*, 88-97.

77. Horiuchi, K.Y., Scherle, P.A., Trzaskos, J.M., and Copeland, R.A. (1998). Competitive inhibition of MAP kinase activation by a peptide representing the alpha C helix of ERK. Biochemistry *37*, 8879-8885.

78. Dennis, P.B., Jaeschke, A., Saitoh, M., Fowler, B., Kozma, S.C., and Thomas, G. (2001). Mammalian TOR: a homeostatic ATP sensor. Science *294*, 1102-1105.

79. Till, J.H., Becerra, M., Watty, A., Lu, Y., Ma, Y., Neubert, T.A., Burden, S.J., and Hubbard, S.R. (2002). Crystal structure of the MuSK tyrosine kinase: insights into receptor autoregulation. Structure (Camb) *10*, 1187-1196.

80. Lu, K.P., Osmani, S.A., and Means, A.R. (1993). Properties and regulation of the cell cycle-specific NIMA protein kinase of Aspergillus nidulans. J Biol Chem *268*, 8769-8776.

81. Frantz, B., Klatt, T., Pang, M., Parsons, J., Rolando, A., Williams, H., Tocci, M.J., O'Keefe, S.J., and O'Neill, E.A. (1998). The activation state of p38 mitogen-activated protein kinase determines the efficiency of ATP competition for pyridinylimidazole inhibitor binding. Biochemistry *37*, 13846-13853.

82. Davidson, W., Frego, L., Peet, G.W., Kroe, R.R., Labadia, M.E., Lukas, S.M., Snow, R.J., Jakes, S., Grygon, C.A., Pargellis, C., and Werneburg, B.G. (2004). Discovery and characterization of a substrate selective p38alpha inhibitor. Biochemistry *43*, 11658-11671.

83. LoGrasso, P.V., Frantz, B., Rolando, A.M., O'Keefe, S.J., Hermes, J.D., and O'Neill, E.A. (1997). Kinetic mechanism for p38 MAP kinase. Biochemistry *36*, 10422-10427.

84. McLaughlin, M.M., Kumar, S., McDonnell, P.C., Van Horn, S., Lee, J.C., Livi, G.P., and Young, P.R. (1996). Identification of mitogen-activated protein (MAP) kinase-activated protein kinase-3, a novel substrate of CSBP p38 MAP kinase. J Biol Chem *271*, 8488-8492.

85. Chen, G., Porter, M.D., Bristol, J.R., Fitzgibbon, M.J., and Pazhanisamy, S. (2000). Kinetic mechanism of the p38-alpha MAP kinase: phosphoryl transfer to synthetic peptides. Biochemistry *39*, 2079-2087.

86. Fox, T., Fitzgibbon, M.J., Fleming, M.A., Hsiao, H.M., Brummel, C.L., and Su, M.S. (1999). Kinetic mechanism and ATP-binding site reactivity of p38gamma MAP kinase. FEBS Lett *461*, 323-328.

87. Stein, B., Yang, M.X., Young, D.B., Janknecht, R., Hunter, T., Murray, B.W., and Barbosa, M.S. (1997). p38-2, a novel mitogen-activated protein kinase with distinct properties. J Biol Chem *272*, 19509-19517.

88. Pierrat, B., Correia, J.S., Mary, J.L., Tomas-Zuber, M., and Lesslauer, W. (1998). RSK-B, a novel ribosomal S6 kinase family member, is a CREB kinase under dominant control of p38alpha mitogen-activated protein kinase (p38alphaMAPK). J Biol Chem *273*, 29661-29671.

89. Woscholski, R., Dhand, R., Fry, M.J., Waterfield, M.D., and Parker, P.J. (1994). Biochemical characterization of the free catalytic p110 alpha and the complexed heterodimeric p110 alpha.p85 alpha forms of the mammalian phosphatidylinositol 3-kinase. J Biol Chem *269*, 25067-25072.

90. Fuchikami, K., Togame, H., Sagara, A., Satoh, T., Gantner, F., Bacon, K.B., and Reinemer, P. (2002). A versatile high-throughput screen for inhibitors of lipid kinase activity: development of an immobilized phospholipid plate assay for phosphoinositide 3-kinase gamma. J Biomol Screen *7*, 441-450.

91. Kovalenko, M., Ronnstrand, L., Heldin, C.H., Loubtchenkov, M., Gazit, A., Levitzki, A., and Bohmer, F.D. (1997). Phosphorylation site-specific inhibition of platelet-derived growth factor beta-receptor autophosphorylation by the receptor blocking tyrphostin AG1296. Biochemistry *36*, 6260-6269.

92. Domin, J., Pages, F., Volinia, S., Rittenhouse, S.E., Zvelebil, M.J., Stein, R.C., and Waterfield, M.D. (1997). Cloning of a human phosphoinositide 3-kinase with a C2 domain that displays reduced sensitivity to the inhibitor wortmannin. Biochem J *326 (Pt 1)*, 139-147.

93. Arcaro, A., Volinia, S., Zvelebil, M.J., Stein, R., Watton, S.J., Layton, M.J., Gout, I., Ahmadi, K., Downward, J., and Waterfield, M.D. (1998). Human phosphoinositide 3-kinase C2beta, the role of calcium and the C2 domain in enzyme activity. J Biol Chem *273*, 33082-33090.

94. Minogue, S., Anderson, J.S., Waugh, M.G., dos Santos, M., Corless, S., Cramer, R., and Hsuan, J.J. (2001). Cloning of a human type II phosphatidylinositol 4-kinase reveals a novel lipid kinase family. J Biol Chem *276*, 16635-16640.

95. Zhao, X.H., Bondeva, T., and Balla, T. (2000). Characterization of recombinant phosphatidylinositol 4-kinase beta reveals auto- and heterophosphorylation of the enzyme. J Biol Chem *275*, 14642-14648.

96. Gehrmann, T., Gulkan, H., Suer, S., Herberg, F.W., Balla, A., Vereb, G., Mayr, G.W., and Heilmeyer, L.M., Jr. (1999). Functional expression and characterisation of a new human phosphatidylinositol 4-kinase PI4K230. Biochim Biophys Acta *1437*, 341-356.

97. Suer, S., Sickmann, A., Meyer, H.E., Herberg, F.W., and Heilmeyer, L.M., Jr. (2001). Human phosphatidylinositol 4-kinase isoform PI4K92. Expression of the recombinant enzyme and determination of multiple phosphorylation sites. Eur J Biochem *268*, 2099-2106.

98. Downing, G.J., Kim, S., Nakanishi, S., Catt, K.J., and Balla, T. (1996). Characterization of a soluble adrenal phosphatidylinositol 4-kinase reveals wortmannin sensitivity of type III phosphatidylinositol kinases. Biochemistry *35*, 3587-3594.

99. Bazenet, C.E., Ruano, A.R., Brockman, J.L., and Anderson, R.A. (1990). The human erythrocyte contains two forms of phosphatidylinositol-4-phosphate 5-kinase which are differentially active toward membranes. J Biol Chem *265*, 18012-18022.

100. Ishihara, H., Shibasaki, Y., Kizuki, N., Wada, T., Yazaki, Y., Asano, T., and Oka, Y. (1998). Type I phosphatidylinositol-4-phosphate 5-kinases. Cloning of the third isoform and deletion/substitution analysis of members of this novel lipid kinase family. J Biol Chem *273*, 8741-8748.

101. Wu, H., Zheng, Y., and Wang, Z.X. (2003). Evaluation of the catalytic mechanism of the p21-activated protein kinase PAK2. Biochemistry *42*, 1129-1139.

102. Tabatabai, L.B., and Graves, D.J. (1978). Kinetic mechanism and specificity of the phosphorylase kinase reaction. J Biol Chem *253*, 2196-2202.

103. Gamm, D.M., Baude, E.J., and Uhler, M.D. (1996). The major catalytic subunit isoforms of cAMP-dependent protein kinase have distinct biochemical properties in vitro and in vivo. J Biol Chem *271*, 15736-15742.

104. Zhang, W., Morris, G.Z., and Beebe, S.J. (2004). Characterization of the cAMP-dependent protein kinase catalytic subunit Cgamma expressed and purified from sf9 cells. Protein Expr Purif *35*, 156-169.

105. Huang, K.P., Chan, K.F., Singh, T.J., Nakabayashi, H., and Huang, F.L. (1986). Autophosphorylation of rat brain Ca2+-activated and phospholipid-dependent protein kinase. J Biol Chem *261*, 12134-12140.

106. Marais, R.M., and Parker, P.J. (1989). Purification and characterisation of bovine brain protein kinase C isotypes alpha, beta and gamma. Eur J Biochem *182*, 129-137.

107. Schaap, D., and Parker, P.J. (1990). Expression, purification, and characterization of protein kinase C-epsilon. J Biol Chem *265*, 7301-7307.

108. Xu, Z.B., Chaudhary, D., Olland, S., Wolfrom, S., Czerwinski, R., Malakian, K., Lin, L., Stahl, M.L., Joseph-McCarthy, D., Benander, C., Fitz, L., Greco, R., Somers, W.S., and Mosyak, L. (2004). Catalytic domain crystal structure of protein kinase C-theta (PKCtheta). J Biol Chem *279*, 50401-50409.

109. MBL Cyclex cyclic GMP Dependent Kinase Assay/Inhibitor Screening Kit.

110. MBL Cyclex Polo-like Kinase Assay/Inhibitor Screening Kit.

111. Force, T., Bonventre, J.V., Heidecker, G., Rapp, U., Avruch, J., and Kyriakis, J.M. (1994). Enzymatic characteristics of the c-Raf-1 protein kinase. Proc Natl Acad Sci U S A *91*, 1270-1274.

112. Trauger, J.W., Lin, F.F., Turner, M.S., Stephens, J., and LoGrasso, P.V. (2002). Kinetic mechanism for human Rho-Kinase II (ROCK-II). Biochemistry *41*, 8948-8953.

113. Turner, M.S., Fen Fen, L., Trauger, J.W., Stephens, J., and LoGrasso, P. (2002). Characterization and purification of truncated human Rho-kinase II expressed in Sf-21 cells. Arch Biochem Biophys *405*, 13-20.

114. Aubol, B.E., Nolen, B., Vu, D., Ghosh, G., and Adams, J.A. (2002). Mechanistic insights into Sky1p, a yeast homologue of the mammalian SR protein kinases. Biochemistry *41*, 10002-10009.

115. Gallagher, P.J., Herring, B.P., Trafny, A., Sowadski, J., and Stull, J.T. (1993). A molecular mechanism for autoinhibition of myosin light chain kinases. J Biol Chem *268*, 26578-26582.

116. Adelstein, R.S., and Klee, C.B. (1981). Purification and characterization of smooth muscle myosin light chain kinase. J Biol Chem *256*, 7501-7509.

117. Gao, Z.H., Moomaw, C.R., Hsu, J., Slaughter, C.A., and Stull, J.T. (1992). Autophosphorylation of skeletal muscle myosin light chain kinase. Biochemistry *31*, 6126-6133.

118. Boerner, R.J., Barker, S.C., and Knight, W.B. (1995). Kinetic mechanisms of the forward and reverse pp60c-src tyrosine kinase reactions. Biochemistry *34*, 16419-16423.

119. Edison, A.M., Barker, S.C., Kassel, D.B., Luther, M.A., and Knight, W.B. (1995). Exploration of the sequence specificity of pp60c-src tyrosine kinase. Minimal peptide sequence required for maximal activity. J Biol Chem *270*, 27112-27115.

120. Boerner, R.J., Kassel, D.B., Edison, A.M., and Knight, W.B. (1995). Examination of the dephosphorylation reactions catalyzed by pp60c-src tyrosine kinase explores the roles of autophosphorylation and SH2 ligand binding. Biochemistry *34*, 14852-14860.

121. Barker, S.C., Kassel, D.B., Weigl, D., Huang, X., Luther, M.A., and Knight, W.B. (1995). Characterization of pp60c-src tyrosine kinase activities using a

continuous assay: autoactivation of the enzyme is an intermolecular autophosphorylation process. Biochemistry *34*, 14843-14851.

122. Boerner, R.J., Kassel, D.B., Barker, S.C., Ellis, B., DeLacy, P., and Knight, W.B. (1996). Correlation of the phosphorylation states of pp60c-src with tyrosine kinase activity: the intramolecular pY530-SH2 complex retains significant activity if Y419 is phosphorylated. Biochemistry *35*, 9519-9525.

123. Susa, M., Luong-Nguyen, N.H., Crespo, J., Maier, R., Missbach, M., and McMaster, G. (2000). Active recombinant human tyrosine kinase c-Yes: expression in baculovirus system, purification, comparison to c-Src, and inhibition by a c-Src inhibitor. Protein Expr Purif *19*, 99-106.

124. Sun, G., Ramdas, L., Wang, W., Vinci, J., McMurray, J., and Budde, R.J. (2002). Effect of autophosphorylation on the catalytic and regulatory properties of protein tyrosine kinase Src. Arch Biochem Biophys *397*, 11-17.

125. Witucki, L.A., Huang, X., Shah, K., Liu, Y., Kyin, S., Eck, M.J., and Shokat, K.M. (2002). Mutant tyrosine kinases with unnatural nucleotide specificity retain the structure and phospho-acceptor specificity of the wild-type enzyme. Chem Biol *9*, 25-33.

126. Baldock, D., Graham, B., Akhlaq, M., Graff, P., Jones, C.E., and Menear, K. (2000). Purification and characterization of human Syk produced using a baculovirus expression system. Protein Expr Purif *18*, 86-94.

127. Murray, B.W., Padrique, E.S., Pinko, C., and McTigue, M.A. (2001). Mechanistic effects of autophosphorylation on receptor tyrosine kinase catalysis: enzymatic characterization of Tie2 and phospho-Tie2. Biochemistry *40*, 10243-10253.

128. Angeles, T.S., Yang, S.X., Steffler, C., and Dionne, C.A. (1998). Kinetics of trkA tyrosine kinase activity and inhibition by K-252a. Arch Biochem Biophys *349*, 267-274.

129. Kendall, R.L., Rutledge, R.Z., Mao, X., Tebben, A.J., Hungate, R.W., and Thomas, K.A. (1999). Vascular endothelial growth factor receptor KDR tyrosine kinase activity is increased by autophosphorylation of two activation loop tyrosine residues. J Biol Chem *274*, 6453-6460.

130. Parast, C.V., Mroczkowski, B., Pinko, C., Misialek, S., Khambatta, G., and Appelt, K. (1998). Characterization and kinetic mechanism of catalytic domain of human vascular endothelial growth factor receptor-2 tyrosine kinase (VEGFR2 TK), a key enzyme in angiogenesis. Biochemistry *37*, 16788-16801.

131. Isakov, N., Wange, R.L., Watts, J.D., Aebersold, R., and Samelson, L.E. (1996). Purification and characterization of human ZAP-70 protein-tyrosine kinase from a baculovirus expression system. J Biol Chem *271*, 15753-15761.

UNIVERSITY OF CALIFORNIA
UC
San Francisco
LIBRARY

7486825
3 1378 00748 6825

For reference
Not to be taken from the room.

UC
San Francisco
LIBRARY
UNIVERSITY OF CALIFORNIA